Fractional Order and Inverse Problem Solutions for Plate Temperature Control

by

Bilal Jarrah

Thesis submitted to the University of Ottawa
in partial Fulfillment of the requirements for the
Doctorate in Philosophy degree in Mechanical Engineering

Department of Mechanical Engineering
Faculty of Engineering
University of Ottawa

Abstract

Surface temperature control of a thin plate is investigated. Temperature is controlled on one side of the plate using the other side temperature measurements. This is a decades-old problem, reactivated more recently by the awareness that this is a fractional-order problem that justifies the investigation of the use of fractional order calculus. The approach is based on a transfer function obtained from the one-dimensional heat conduction equation solution that results in a fractional-order s-domain representation.

Both the inverse problem approach and the fractional controller approach are studied here to control the surface temperature, the first one using inverse problem plus a Proportional only controller, and the second one using only the fractional controller.

The direct problem defined as the ratio of the output to the input, while the inverse problem defined as the ratio of the input to the output. transfer functions are obtained and the resulting fractional-order transfer functions were approximated using Taylor expansion and Zero-Pole expansion. The finite number of terms transfer functions were used to form an open-loop control scheme and a closed-loop control scheme. Simulation studies were done for both control schemes and experiments were carried out for closed-loop control schemes.

For the fractional controller approach, the fractional controller was designed and used in a closed-loop scheme. Simulations were done for fractional-order-integral, fractional-order-derivative and fractional-integral-derivative controller designs. The experimental study focussed on the fractional-order-integral-derivative controller design.

The Fractional-order controller results are compared to integer-order controller's results. The advantages of using fractional order controllers were evaluated. Both Zero-Pole and Taylor expansions are used to approximate the plant transfer functions and both expansions results are compared.

The results show that the use of fractional order controller performs better, in particular concerning the overshoot.

Acknowledgments

I would like to take a chance to thank and appreciate all people who have been always supporting me and push me forward during my Doctoral study.

First and most I would like to offer my great thanks to my supervisor professor Dan Necsulescu for his supervision, support, guidance, and patience with me during this study. He is always available and ready to help which always pushes me to progress in my research.

I would like to thank Dr. Spinello and Dr. Sasiadek for their help and ideas they provide me during Proposal defense to improve my research, I am also would like to thank all my colleagues who help in my research especially Abdelfattah, Osama and Moayed.

I would like to show my deep grateful and special thanks to my wife Lana for here patience and support, I also would like to mention my children Rama, Mohammad, Omar, and Sara support. I would like to thank my parent and my wife parent for their prayer and support

Finally, I would like to thank everybody who was helping to make this research study possible and successful, I would like to express my apology for everyone who helps and I miss their names.

Table of Contents

Fractional order rational complex functions cannot be computed as such and approximations by integer-order functions are required, as is extensively shown in publications [2, 39-71,

List of Figures

Nomenclature

L: Plate thickness[m].

G_1: Direct problem transfer function.

G_2: Inverse problem transfer function.

θ_1: The input temperature of the direct problem [^{0}C].

θ_2: The output temperature of the direct problem [^{0}C].

θ_{2d}: The desired temperature [^{0}C].

G_c: The Controller transfer function.

k: The thermal conductivity [$\frac{m^2}{sec}$].

A: The amplitude of input temperature [^{0}C].

$\emptyset$: The heat flux [W/m^2].

α: The thermal diffusivity [$\frac{W}{m.K}$].

s: The complex variable.

A_s: The area of the plane isothermal that is considered for the

x-transfer [m^2].

ω: The frequency [rad/sec].

λ: Fractional integral order.

μ: Fractional derivative order.

FOPI: Fractional-order proportional-integral controller.

FOPD: Fractional-order proportional derivative controller.

FOPID: Fractional-order proportional integral derivative controller.

PID: Proportional integral derivative controller.

K_P: Proportional gain.

K_I: Integral gain.

K_D: Derivative gain.

IOPID: Integer order proportional integral derivative controller.

IHCP: Inverse Heat conduction problem.

N: Number of terms for the direct problem.

M: Number of terms for the inverse problem.

PC: Personal computer.

$G_{dir} = G_1$: Direct problem transfer function.

$G_{inv} = G_2$: Inverse problem transfer function.

Chapter One: Problem Description

1.1 Introduction

The fractional-order systems control became an active research issue recently. To have good control of such systems, it needs to be investigated. Thermal systems have been studied with the lumped parameter approach for a long time. The investigation of Fractional calculus to solve the engineering problem is a recent trend. This is mentioned in a review paper by A. Dastjerdi et al. [1] in 2019, "Today, there is a great tendency toward using fractional calculus to solve an engineering problem. Control is one of the fields in which fractional calculus has attracted a lot of attention." This encouraged us to do this study, where we introduce two new approaches to investigate this kind of problem. The first approach is using an inverse problem solution with an integer order controller, and the second approach is the fractional order controller.

Metallic components are widely used in industry, and most of these applications involve heat transfer. Consequently, the need exists to have the desired temperature at least on one metal surface or sometimes on both faces, but most frequently, we have the heat source on one side and we have to achieve a desired temperature on the other side. Thus, the inverse problem must be solved to get a temperature distribution through the plate thickness, as appears in Figure 1.
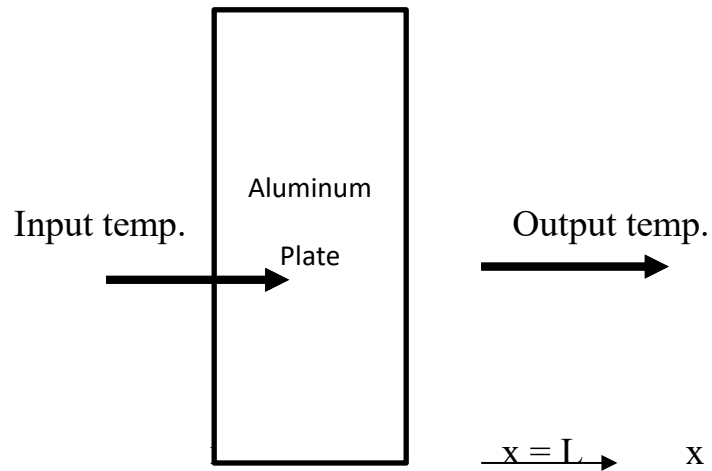
Figure 1: Thin plate diagram.

1.2 The Problem

This study involves an estimation of the temperature on one side of a plate from a measurement on the other side of the plate, control of the temperature output of a plate after heating one side of the plate, and control of the temperature output on the edother side. The investigation, using a thin aluminum plate, consists of applying a sinusoidal heat input of various values on one side and evaluating the effect of the frequency on the temperature amplitude on the other side. Also, to open-loop control the temperature output to the desired value, the study consists of a two-stage problem: the first is the inverse problem where the inverse problem defined in s-domain is the ratio of the output divided by the desired input of the direct problem, and the second is the direct problem (the direct problem defined here as the division of its output by the input) as it appears in Figure 2:
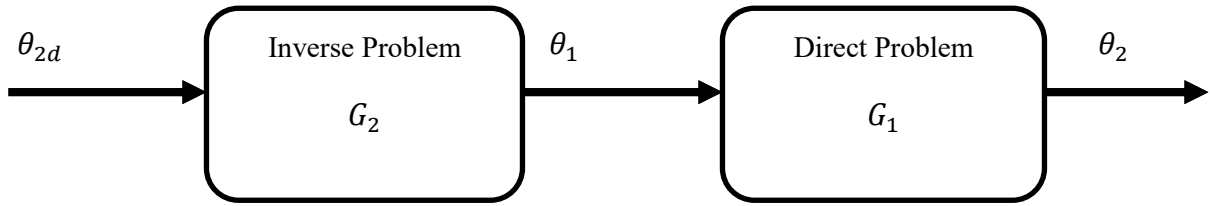
Figure 2: Open loop control block diagram.

Where:

G_1 is the transfer function of the direct problem?

G_2 is the transfer function of the inverse problem?

θ_1 is the input temperature of the direct problem?

θ_2 is the output temperature of the direct problem?

θ_{2d} is the input temperature of the inverse problem?

The direct problem is defined as the ratio of the output temperature θ_2 on the non-heated side to the temperature input θ_1 on the heated side.

The inverse problem is the inverted direct problem, i.e. the ratio of input temperature θ_1 on the heated side to the output temperature on the non-heated side θ_2.

In the open-loop control from Figure 2, the desired temperature θ_{2d} to the loop is the desired value of the output temperature θ_2 on the non-heated side. In Figure 2 are included the transfer functions G_1 of the Direct problem and the transfer function $G_2 = G_1^{-1}$ of the Inverse Problem.

From Figure 2, we get the equation (1.1) as follows:

$$\theta_2 = G_2 G_1 \, \theta_{2d} \qquad\qquad (1.1)$$

Equation (1.1) gives us the transfer function relating the desired input to the actual output. This open-loop transfer function resulted in a product of inverse problem transfer function multiply by the direct problem transfer function.

For the closed-loop case, feedback is added to control the output temperature, using a controller G_C, as is shown in Figure 3:
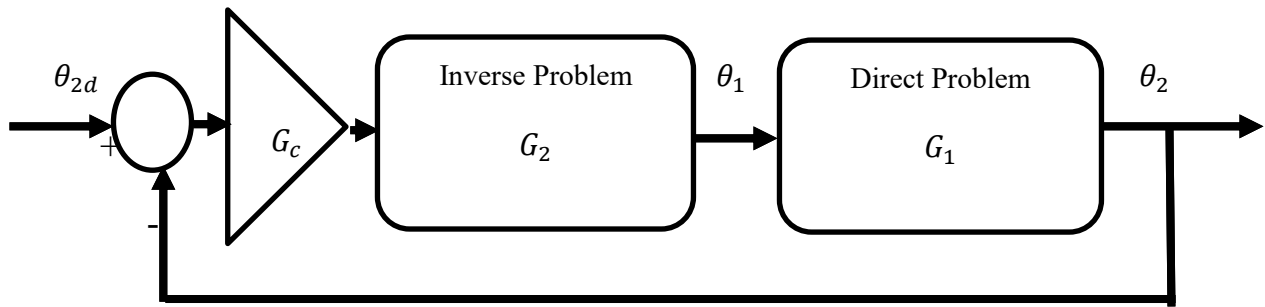
Figure 3: Closed loop control block diagram.

The direct problem is defined as the ratio of the output temperature θ_2 on the non-heated side to the temperature input θ_1 on the heated side.

The inverse problem is the inverted direct problem, i.e. the ratio of input temperature θ_1 on the heated side to the output temperature on the non-heated side θ_2.

In the closed-loop control from Figure 3, the desired temperature θ_{2d} to the loop is the desired value of the output temperature θ_2 on the non-heated side. In Figure 3 are included

the transfer function G_1 of the Direct problem and the transfer function $G_2 = G_1^{-1}$ of the Inverse problem and the transfer function G_C of the controller.

1.3 Why the Focus is on 1-D Temperature Control

To investigate the controller effect for the heat conduction problems, we need an analytical solution for the problem under investigation to obtain the transfer functions for this study, and these solutions are mostly available for the 1-D heat conduction equation, while the solutions for 2-D and 3-D cases are mostly in numerical form. Also, it is very difficult to see the controller effect in the 3-D case; it is easier and clearer in the 1-D case. Most research papers were published for the 1-D case. Finally, in this case, the propagation is in a 1-D direction, and a semi-infinite body is investigated for this purpose.

Transfer functions for fractional-order systems have to be approximated by integer-order equations for actual computations. Taylor series and pole-zero expansions are good candidates and are analyzed next.

1.4 Taylor Expansion

The Taylor series expansion for a hyperbolic sine function is [2]:

$$\text{sech}(x) = \sum_{n=0}^{\infty} \left(\frac{E_n}{n!}\right) x^n, \quad \text{for } |x| < \pi/2 \tag{1.2}$$

isWhere Euler numbers E_n zero for odd-indexed numbers, while even indexed numbers are

$E_0 = 1$

E_2=-1

E_4=5

E_6=-61

E_8=1385

E_{10}=-50521

E_{12}=2702765

E_{14}=-199360981

E_{16}=19391512145

E_{18}=-2404879675441   etc.

The Taylor series expansion for a hyperbolic cosine is the inverse problem result:

$$\cosh(x) = \sum_{n=0}^{\infty} \left(\frac{1}{(2n)!}\right) x^{2n}, \quad \text{for} -\infty < x < \infty \tag{1.3}$$

From the above expansion, we see that there is a limitation of $\text{sech}(x)$ to $|x| < \pi/2$, the alternative form $\text{sech}(x) = 1/\cosh(x)$ is used knowing that there are no domain limitations for $\cosh(x)$.

1.5 Zero-Pole Expansion

The Zero-Pole series expansion for the hyperbolic secant is:

$$\text{sech}(\sqrt{x}) = \frac{1}{\cosh(\sqrt{x})} \approx \frac{p_1 p_2 p_3 p_4 p_5 p_6 \dots}{(x-p_1)(x-p_2)(x-p_3)(x-p_4)(x-p_5)(x-p_6)\dots} \tag{1.4}$$

Where:

$$p_k = -\left[\frac{(2k-1)\pi}{2}\right]^2, \quad k = 1,2,3, \dots$$

The Zero-Pole series expansion for hyperbolic cosine is:

$$\cosh(\sqrt{x}) \approx \frac{(x-z_1)(x-z_2)(x-z_3)(x-z_4)\dots}{z_1 z_2 z_3 z_4 \dots} \tag{1.5}$$

Where:

$$z_k = -\left[\frac{(2k-1)\pi}{2}\right]^2, \quad k = 1,2,3,\dots$$

1.6 Fractional Calculus

The history of fractional calculus started in the 17th century in a letter from L'Hopital to Leibniz asking what if the order of the derivative were (0.5); this letter later led to the birth of fractional order derivatives and integrals. To understand and to compute the fractional-order (FO) derivative and integral better, some definitions are needed. The most important are:

A. Riemann-Liouville definition of FO integration[3].

The Riemann-Liouville definition of fractional order integration is:

$$_0D_t^{-\alpha}f(t) = \frac{1}{\Gamma(\alpha)}\int_0^t \frac{f(\tau)}{(t-\tau)^{1-\alpha}}d\tau \tag{1.6}$$

where $0 < \alpha < 1$, and $\Gamma(x)$ is the Gamma function.

$$\Gamma(x) = \int_0^\infty e^{-u}u^{x-1}du$$

When the initial integral limit changes from (0) to (a), the FO definition is generalized to the Weyl Definition

$$_aD_t^{-\alpha}f(t) = \frac{1}{\Gamma(\alpha)}\int_a^t \frac{f(\tau)}{(t-\tau)^{1-\alpha}}d\tau \tag{1.7}$$

B.   Riemann-Liouville definition of FO differentiation[3].

The Riemann-Liouville definition of fractional order differentiation is:

7

$$_0D_t^\alpha f(t) = \frac{d}{dt}\left[{}_0D_t^{-(1-\alpha)}f(t)\right] \tag{1.8}$$

There are left and right R-L definitions for FO differentiation:

$$_bD_t^\alpha f(t) = \frac{1}{\Gamma(n-\alpha)}\left(-\frac{d}{dt}\right)^n \int_b^t f(\tau)\,(t-\tau)^{n-\alpha-1}d\tau \tag{1.9}$$

$$_aD_t^\alpha f(t) = \frac{1}{\Gamma(n-\alpha)}\left(\frac{d}{dt}\right)^n \int_a^t f(\tau)\,(t-\tau)^{n-\alpha-1}d\tau \tag{1.10}$$

C. Caputo's definition of FO differentiation[3].

The Caputo definition of the fractional order differentiation is:

$$_0^C D_t^\alpha f(t) = \frac{1}{\Gamma(1-\alpha)}\int_0^t \frac{f'(\tau)}{(t-\tau)^\alpha}\,d\tau \tag{1.11}$$

D. Grunwald-Letnikov definition[3].

The Grunwald-Letnikov (G-L) definition introduces a unified definition for both fractional integration and differentiation:

$$_aD_t^\alpha f(t) = \lim_{h\to 0}\frac{1}{h^\alpha}\sum_{j=0}^{[\frac{t-a}{h}]}(-1)^j\binom{\alpha}{j}f(t-jh) \tag{1.12}$$

1.7 Oustaloup approximation

Oustaloup provides a filter approximation to the fractional-order differentiator (s^α) as follows:

$$G_t(s) \;=\; K\prod_{i=1}^{N}\frac{s+\omega_i'}{s+\omega_i} \tag{1.13}$$

Where

$$w_i' = \omega_b\omega_u^{(2i-1-\alpha)/n}$$

$$w_i = \omega_b\omega_u^{(2i-1+\alpha)/n}$$

$$K = \omega_h^{\alpha}$$

$$\omega_u = \sqrt{\frac{\omega_h}{\omega_b}}$$

N is the order of approximation.

Chapter Two: Literature Review

2.1 Introduction

Solving inverse problems are important in industry, science, and engineering applications, as they are very common in these fields. To solve temperature control problems, we have to first try to determine the methods for solving inverse heat problems for both linear and non-linear cases, as follows:

- Integral equation approach,

- Integral transform techniques,

- Series solution approach,

- Polynomial approach,

- Hyperbolization of the heat conduction equation,

- Numerical methods such as finite difference, finite elements, and boundary elements,

- Space marching techniques together with filtering of the noisy input data, such as the mollification method,

- Iterative filtering techniques,

- Steady-state techniques,

- Beck's sequential function specification method,

- Levenberg-Marquardt method for minimization of the least square norm,

- Tikhonov's regularization approach,

- Iterative regularization methods for parameter and function estimations,

- Genetic algorithms.

It is important to know that analytical solutions are only available for linear inverse problems; they are not available for most of the non-linear inverse problems cases.

Having mentioned some of the solution methods for inverse heat problems, we now focus our attention on the Inverse Heat Conduction Problem (IHCP), which we will deal with through our research. Those types of inverse problems can be classified depending on the variable to be estimated:

IHCP of boundary conditions,

IHCP of thermophysical properties,

IHCP of the initial condition,

IHCP of the source term,

IHCP of geometric characteristics of a heated body.

In our research we will focus on the second type, which is the estimation of temperature.

2.2 Reviews of Inverse Problem approach

The effect of heat on any process in the industry, due to power consumption in industrial processes, causes a temperature control issue. That is why surface temperature control of a metal part is essential for most industrial processes these days. In this study, we focus on solving IHCP due to its importance in industrial applications.

One of the first solutions for the inverse heat problems was proposed by Stolz [4]. He formulated the inverse problem in terms of numerical inversion of the related direct problem. The Stolz solution appeared, however, to be unstable in case of small time steps. Miller et al. [4] and Tikhonov et al. [5] were the first to introduce regularizer methods[5] [6]. Murio

developed a technique, known as Mollification, which was able to smooth the temperature estimate at a plate the surface [7]. Beck solved the problem of future time-temperatures in a least-square sequential method. His approach stabilizes the inverse problem and allows small time steps [8].

Scarpa and Milano solved the heat flux at one boundary of a one-dimensional system using the Kalman smoothing technique [9]. Yang and Chen developed a direct method to estimate the boundary conditions in two-dimensional heat conduction by first discretizing the problem using finite difference, then using the least-squares method [10]. Monde used the Laplace transform to develop an analytical solution for an inverse heat conduction problem knowing the temperature at two points for a finite body or the temperature at one point for a semi-finite body [11]. Dul'kin and Garas'ko obtained an analytical solution for a 1-D heat conduction problem for a single straight fin [12]. Shenefelt et al. obtained a solution for a linear inverse heat conduction problem by directly applying the singular value decomposition to the matrix from Duhamel's principle [13].

Necsulescu, Woodbury, Özışık, and Beck introduced several solution methods for inverse heat conduction problems with different boundary condition types [14][15][16][17]. Maillet published a book regarding the use of the Thermal Quadrupoles method to solve the heat equation through integral transforms [18].

Lüttich et al. solved the linear inverse heat conduction problem for the reconstruction of unknown heat flux on the boundary for 2D and 3D problems; their method is based on the interpretation of IHCP in a frequency domain [19]. Lu and Tervola have introduced an analytical approach of heat conduction in a composite slab when it is exposed to periodic temperature changes [20]. Woodfield et al. solved analytically the inverse heat conduction problems when it has a given far-field boundary condition using the Laplace transform [21].

12

Pourgholi and Rostamian provided a numerical solution for the 1D inverse heat conduction problems using the Tikhonov regularization method [22]. Feng et al. provided an approach for temperature control of functionally graded plates using the inverse solution and the proportional-differential controller [23]. Zhou et al. used the Laplace transform technique to solve the problem of heat conduction over a finite slab [24]. Feng et al. presented a new method for solving the 3D inverse heat conduction problem for the special geometry of a thin sheet. They simplified the equation from 3D to 1D using modal expansion then used the Laplace transform to determine the front surface temperature and heat flux in terms of those on the back surface [25]. Zhou et al. proposed a new method to recover the front surface temperature of a finite slab using fine grids based on the back surface temperature measured with coarse grids for 3D inverse heat conduction problems [26]. Pailhes et al. proposed a new method based on the thermal quadrupoles method for heat transfer modelling in a multilayered slab; they used a new formulation based on an exponential function with a negative argument, while the classical Quadrupole method used hyperbolic functions [27]. Krapez and Dohou proposed an extension to the thermal quadrupole method, which allows computing temperature and heat fluxes anywhere inside a multilayer material [28]. Najafi et al. estimated the multiple unknown heat flux at the boundary, using the temperature measurements at the other side of the 2D plate, applying Tikhonov regularization to overcome the ill-posedness of the problem [29]. Kukla and Siedlecka used the Laplace transform for solving the problem of fractional heat conduction in a two-layered slab [30]. Fan et al. obtained the temperature distribution on one surface of a flat plate by solving the inverse problem based on the temperature measurement on the opposite surface of the plate; a modified one-dimensional correction and the finite volume methods were used for both the two- and three-dimensional inverse problems [31]. Feng et al. solved the heat conduction problem for a finite slab using the Laplace transform.

13

A transfer functions link for the temperature and heat flux on the two surfaces of a slab was obtained. These relationships can be used to calculate the front surface heat input (temperature and heat flux) from the back surface measurements (temperature and/or heat flux) when the front surface measurements are not feasible [32].

The solution of the inverse one-dimensional heat conduction problem was presented by Danaila and Chira; they aim to estimate the right-side unsteady boundary condition. They used two techniques to do this estimation: first, conjugate the gradient method with an adjoint problem for the gradient function estimation and second, Tikhonov regularization for Hyperbolization of the heat conduction equation. Both approaches were tested, and the inverse problem was solved for different boundary condition function forms. They include functions containing sharp corners; the mathematical and numerical formulations are presented [33].

The inverse problem in a rectangle was considered by Ivanchov and Kinash: the heat-conduction equation with an unknown coefficient as a function of time and space variables. They used the Green function to reduce the problem to one equation. Schauder's theorem was used to prove the existence of the solution to this equation, and Volterra integral equations theory was used to prove the uniqueness of the solution [34]. Chen et al. used the one-dimensional inverse heat conduction problem to estimate the surface temperature; they used a nonlinear calibration integral equation method. The parameter-free nature of the nonlinear calibration method permits them to introduce the first kind of Volterra integral equation containing the thermophysical properties as a function of temperature. They proposed a temperature-dependent property transform, represented by a Chebyshev expansion to linearize the nonlinear heat equation. The expansion coefficients were estimated using two tests: the time-sequential investigation and the balance verification. The future-time method is used to

regularize the ill-posed problem, and the optimal regularization parameter was estimated using a phase plane and the cross-correlation phase plane analysis. Numerical simulation provides encouraging results for surface temperature predictions [35].

Chang et al., in their review paper on the computation methods used for the inverse heat conduction problems, divided them into two major solving categories: mesh methods and the meshless algorithms. Finite difference discretization methods are the famous mesh methods, while the Tikhonov regularization method and the Singular value decomposition (SVD) are good examples of the meshless algorithms. Based on their literature studies, they realized that the development of meshless methods is the trend [36].

2.3 Reviews of Fractional controller approach

Recently, fractional order controllers have been put in use to obtain better performance of the system.

Gebhart presented a heat conduction model for both steady-state and unsteady-state using periodic boundary conditions [37]. Ogata et al. provided the phase angle and the magnitude of transfer functions of a different order [38]. Maillet et al. presented several solution methods for inverse heat transfer problems [39]. Monje et al. formulated detailed methods for the design of FOPI, FOPD, and FOPID controllers [40]. The heat flux and the temperature control on a front surface were estimated using the measurement on the back surface of a finite slab, which is a standard problem, was estimated. The Laplace transform was used to get a solution of the resulting heat conduction equation to obtain the transfer functions and then was expanded using Zero-Pole expansion [23].

Shekher et al. designed a controller for gain and phase margin criteria to satisfy the robustness property for a PID controller for the case of a ceramic infrared heater [41]. Zheng et al. proposed a detailed design of fractional order PID (FOPID) controller, and the parameters of the controller were obtained according to the model characteristics and design specifications [42]. Cokmez et al. proposed a detailed fractional order PI controller design algorithm based on control error optimized using ITSE criteria; the fractional order of integration fraction will vary according to the sign of the control error [43]. Li, Chen, and Lou proposed a new tuning method of typical classes of second-order systems, which can ensure given gain crossover frequency and phase margin [44] [45]. Batlle et al. proposed the Smith predictor combined with a fractional order controller to control the temperature of a steel slab reheating furnace; they introduced simulation results for a fractional order proportional-integral controller [46].

Muresan et al. introduced an approach to design a fractional order PI controller to control a DC motor speed, and experimental results proved the efficiency of using such a controller [47]. Flores et al. proposed a fractional order controller that can deal with non-modeled dynamics for a cooperative cruise control [48]. Tan et al. used interactive tools like Matlab and Labiew to teach fractional order control methods and how they can be introduced in a classical control course [49]. Maurya and Bhandari proposed a hybrid fractional order PID controller tuned using the Ziegler-Nichols and Astrom-Hagglund methods; the parameters of the FOPID used were proportional constant and integral constant from Ziegler-Nichols and derivative constant from the Astrom-Hagglund method. To obtain solutions for the fractional-order of the integral term and derivative term, two non-linear equations are obtained and solved [50].

Saptarshi et al. examined time and frequency domain tuning strategies for a fractional PID controller to handle higher-order processes. They used reduced parameter modeling [51]. Jesus Isabel and Machado Tenreiro studied the heat diffusion systems based on the fractional calculus concept; several control strategies were investigated and compared [52]. Rapaic and Jelicic presented a generalized fractional-order heat conduction equation solution procedure in which the first step is to represent the fractional distributed parameter model by an equivalent system of fractional-order ordinary differential equations; they then obtained a classical, infinite-dimensional state-space form through suitable transformation to avoid the necessity of solving Euler-Lagrange equations [53].

El-khazali introduced a new design method for both fractional proportional-derivative and fractional proportional-integral-derivative controllers; these were done using a biquadratic approximation to introduce a new structure of finite-order fractional-order PID controllers [54]. Zheng et al. proposed a control strategy based on analytical calculation and a differential evolution algorithm for a permanent magnet motor; the frequency-domain specifications guarantee the system stability and the system robustness while the time-domain specifications ensure the desired step response, constrained overshoot, and proper power consumption [55].

Tavakoli-Kakhki and Haeri used the fractionalized differentiating method to reduce fractional-order models' complexity. The main advantages of this method are simplicity and guaranteed stability of a specific class of fractional-order models. In simplifying the complicated fractional controller to a fractional order PID controller, the reduction proposed tuning rules for parameter adjustment [56]. Jesus et al. studied heat diffusion systems based on concepts of fractional calculus, and several control methodologies were investigated. The Smith predictor structure was adopted for its better control of systems developments [57]. Mehra et al. studied a DC motor speed control using fractional order control, the FOPID

17

parameters were optimally obtained using a genetic algorithm, and the integral of the absolute error (IAE) was chosen for optimization. They showed that a FOPID controller performs better than an IOPID [58].

Ranjan et al. used the method of dominant pole placement, and the settling time and peak overshoot were used as the performance specifications, where constraints have been put on the complementary sensitivity function to handle the high-frequency noise rejection. Then, they extended the method for a fractional-order system and fractional order controller. Since there is no direct method for dominant poles for fractional-order systems, they started the method with the assumption of dominant poles [59]. Al-Saggaf et al. used Bede's ideal transfer function as a reference model to investigate fractional-order controller designs for integer-order first order plus time delay systems; based on this, they proposed a new structure of the fractional-order controller. They used the internal model control principle in designing the controller [60]. Bongulwar and Patre designed a Fractional Order Proportional Integral Derivative Controller (FOPID) for a first non-integer order plus a time-delay system; the model for the system was obtained from a reduced higher-order continuous-time model. The stability boundary locus method was used for designing the controller; the method satisfies frequency domain specifications, phase margin, and gain crossover frequency. They achieved a flat phase condition by designing a robust control system to work against gain variations [61].

Mettu et al. designed a Fractional Order Proportional Integral Derivative (FOPID) controller to control the liquid level of a spherical tank; the tank was modeled as a fractional-order system. They designed the controller following a set of imposed tuning constraints to

guarantee the desired control performance and robustness to the loop gain variations. They showed that the fractional-order controller improved the performance compared with an integer order controller [62]. Jesus et al. studied heat diffusion systems described by the fractional operator ($s^{0.5}$); a nonlinear controller with the fractional order model was investigated, and the tuning follows the optimization of performance control indices [63]. Viola et al. proposed a new method, the quantitative robustness evaluation of PID controllers employed in a DC motor. Robustness analyses were done for a fractional order proportional integral and derivative controller (FOPID), Integer Order Proportional Integral and Derivative controller (IOPID), and the Skogestad Internal Model Control controller (SIMC) PID controller to control the speed of a motor-generator set. A factorial experimental design 2^3 is used as a tool for the robustness analysis [64].

Edet and Katebi designed a fractional order PID controller, tuned based on the frequency domain design method. They developed a new algorithm to tune the FOPID controller based on a single frequency point. Controller parameters were calculated from critical measurements to meet the design specifications [65]. Caponetto et al. proposed a new procedure to define the fractional order PID controller parameters to stabilize a first-order plant plus time delay. The procedure is done using the Hermite–Biehler theorem applied for the quasipolynomials in the field of fractional-order systems [66]. Dormido et al. presented two interactive tools for the design of the Fractional Order Proportional Integral Derivative (FOPID) controller. The time and frequency domain design of the FOPID controller was presented in tool one, while the second tool allows the user to automatically determine the controller parameters by imposing a loop shaping technique. The current technique, which is a computer-aided control system design tool believed to be very useful from an educational

point of view leads to the widespread use of FOPID controllers in the industry [67]. Zhang et al. transformed the FOPID controller adjustment problem to a nonconvex optimization problem. A new State Transition Algorithm (STA) was introduced to select the optimal controller parameters. They found that the Integral Time of Absolute Error (ITAE) has excellent tracking performance compared to other objective criteria; different objective criteria and sample sizes were studied to see the effect on the performance of FOPID controller design [68].

Temperature control of a slab of the long rod was investigated under given boundary conditions by Vajta, and the distributed parameter process model was described. An internal model controller (IMC) scheme was introduced based on an exact process model; this scheme leads to a fractional order controller which was tuned by minimizing the infinity norm of the robust performance index [69]. The fractional proportional-integral controller design for a closed-loop system plant with time was studied by Yüce and Tan. They used a relay autotuning test to find the ultimate frequency to estimate the PI controller parameters in the Ziegler-Nichols method. The estimated parameters that are used in the FOPI controller and the step response of the closed-loop were examined for various values of the fractional integrator order. The fractional-order was chosen from the resulting response based on desired specifications [70]. The direct fractional-order closed-loop bias-eliminated least square method was used for process model identification. The fractional-order controller is designed to improve robustness using the numerical optimization of frequency-domain criteria [71]. A fractional-order PI controller was designed to control the integration process with time delay for a specified gain and phase margin. The stability regions were obtained by assuming the value of integral

20

fractional-order to be between 0.1 and 0.7 using Real Root Boundary and Complex root Boundary [72].

Yin et al. designed the sliding mode control method to control chaos in a class of fractional-order chaotic systems. Based on the used method, the state of the fractional-order systems have been stabilized [73]. Different types of controller designs, implementation, and robustness analysis were introduced by Viola and Angel to control the speed of a motor-generator system. The controllers used are the PID, FOPID, and Skogestad internal model control (SIMC) PID. The MATLAB STATEFLOW toolbox used to implement the system, and the factorial experimental design was used for robustness analysis. Results show that the fractional-order PID controller has better stability and robustness performance [74]. A new version of the particle swarm optimization was introduced by Aghababa. He introduced two modifications to improve the performance of the algorithm. The two modifications make it simple to implement, fast, and reliable; he applied the modified approach to design optimal fractional order PID controllers for some benchmark transfer functions. The modified approach was applied to tune the parameters of a FOPID controller for a five-bar linkage robot. Simulations reveal that the modified approach can optimally tune the FOPID controllers [75]. A fractional order PID controller is used based on the Gases Brownian Motion Optimization algorithm to control load-frequency in the power system; the order of derivation and integration was determined by the designer. This algorithm was introduced as a search method with suitable accuracy and convergence rate; the computations will be higher than the conventional controllers due to the complex design procedure. The proposed controller performance is verified by comparing it with the PI controller and GBMO based fuzzy controller [76].

Ouhsaine et al. used the fractional-order differentiator for a result of dynamics thermal modeling; they tried to provide the possibility to model the system in state-space form. To do that, they characterized the system by heterogeneous media due to multilayers that can be described by fractional order partial differential equations. Their objective was to introduce a new mathematical model for the "hybrid PVT" system and their fractional-order observers in the time domain. They considered modelling of heat conduction with time-fractional order derivative; the asymptotic stability of the estimations error following the fractional-order value (α= 0.5) is investigated [77]. Bongulwar and Patre presented a robust stabilizing method for the controller design of global power control of a Pressurized Heavy Water Reactor (PHWR). They used a Fractional Order Proportional Integral Derivative ($PI^{\lambda}D^{\mu}$) controller and applied the method to design a controller for a One Non-Integer Order Plus Time Delay (NIOPTD-I) plant, which satisfies design specifications such as phase margin and gain crossover frequency. By satisfying a flat phase condition at gain crossover frequency in which phase is almost constant, the robust performance was obtained, and the designed controller provides active step-back control to the insertion of the rod without undershooting for a wide range of gain variations [78]. Swain et al. introduced a design of One Degree of Freedom (1-DOF) and Two Degrees of Freedom (2-DOF) Fractional Order PID (FOPID) controllers for a magnetic levitation (Maglev) plant. The number of feed-forward control loops in a closed-loop system represents the degree of freedom. They formulated an optimization problem with a cost function obtained from the characteristic equation of the closed-loop system at the dominant poles. The controller parameters were obtained through nonlinear interior-point optimization using Matlab^{TM}. They showed that the closed-loop response of the 2-DOF FOPID controller has a good response and robustness compared to an integer order controller [79].

Gherfi et al. introduced a design approach for a proportional integral-fractional filter controller for a first-order plus time delay (FOPTD) system. The controller design method used depends on the transfer function of the overall closed-loop system, which is equivalent to the transfer function of the general fractional Bagley–Torvik reference model. They derived the tuning parameters of the proportional integral-fractional filter controller analytically from the FOPTD process model and the general fractional Bagley–Torvik reference model parameters [80]. The fractional-order proportional integral derivative controller optimal design was proposed for a system with a time delay. The proposed design method was called IWLQR, in which Invasive Weed Optimization (IWO) and Linear Quadratic Regulator (LQR) are joined together. The fractional-order proportional integral derivative (FOPID) regulator is modified to a high order time-delay scheme. The proposed methodology tune the gain of the FOPID controller using LQR theory with the assistance of the IWO technique. The main advantage of this technique is to reduce the fault in a PID controller among the higher-order time delay by the aid of the increased limits of the regulator [81]. Zhan and Ma studied the stabilization problem of singular fractional-order linear systems based on a new admissible condition; they used a fractional order of $0 < \alpha < 1$. They presented a new sufficient and necessary condition that guarantees that the closed-loop system is admissible, then the pseudo-state and static output feedback controllers design was obtained [82].

Maddahi et al. introduced a fractional order proportional integral derivative (FOPID) controller design procedure for the position control of hydraulic actuators; to do that, they used the Oustaloup recursive method. They tuned the controller parameters experimentally using the Iterative Feedback Tuning (IFT) technique. The quality of the proposed controller is tested

23

by comparing the experimental results with those from a quantitative feedback theory (QFT) based controller. The comparisons show that the FOPID controller produces better results in settling time [83]. Chevalier et al. proposed a new reduced-parameters method for fractional order proportional integral derivative (FOPID) controller parameters tuning based on reducing the controller parameters from five to three. The idea of reducing parameters depends on using coincident zeros in the controller. The proposed methods were compared with the CRONE controller; the comparison shows that the proposed method gives a fractional performance similar to other methods, which make it easier to tune the controller due to reduced tuned parameters, which will lead to the wide use of fractional controllers in the industry [84]. Jain et al. presented a two degree of freedom fractional order integral (FOPI) controller for the temperature control of a real-time Heat Flow Experiment (HFE); using the fractional calculus and the two degrees of freedom to PI controller enhances its flexibility. They used an algorithm called a Water Cycle Algorithm (WCA), which leads to a WCA tuned two degrees of freedom fractional order PI (W2FPI) controller that is shown to be an effective controller tuning technique. The convergence analysis of this technique justifies its effectiveness with respect to other optimizers [85]. Liu et al. proposed a numerical inverse Laplace transform algorithm for an oscillatory fractional-order time-delay system. They used the ITAE as an objective function to search for the optimal controller parameters. They performed step unit tracking and load-disturbance response simulations for the proposed optimal ($PI^\lambda D^\mu$) controller and the optimal PID controller for three typical kinds of fractional time-delay systems. The results show that the closed-loop system with a FOPID controller has faster and smoother time responses and robustness [86].

Fractional order systems controlled by a fractional order proportional integral differentiation (FOPID) controller tuning method was introduced by Chunyang et al. The method introduced depends on the phase margin, crossover frequency, and robustness specifications of the system. They used their method to design a FOPI controller and a FOPID controller. The resulting controllers show good performance but the FOPID controller was better [87]. Elmetennani et al. studied the performance of a fractional-order proportional integral derivative (FOPID) controller designed for parabolic distributed solar collectors. They proposed a FOPID controller for the current system due to its tuning flexibility. The controller parameters were obtained by solving a nonlinear optimization problem based on robustness design specifications. The controller was then tested in a closed-loop under different working conditions, and the results show robustness, tracking precision, and time response [88]. The stability control problem for a rotary inverted pendulum was investigated by Wang et al., using two closed-loop schemes in which the first is the controller in the feed-forward loop and the second is the controller in the feedback loop. The inverted pendulum was modeled using the Euler-Lagrange equation, and the fractional order controller is designed based on the Bode ideal transfer function. The resulting fractional order controller and the IOPD controller were compared based on the Quanser company loop simulation experiment platform. The results show that the FOPID controller is better than the FOPD and IOPD controllers [89]. Machado et al. used fractional calculus in the study of dynamic systems; using fractional calculus has been investigated in different fields like controller tuning, legged robots, redundant robots, and heat diffusion. They published the paper to simulate the use of fractional calculus and contribute toward research in the field of fractional calculus. Still in a preliminary stage, they believe their paper shows the advantages of using fractional calculus for dynamic systems [90].

Shah and Agashe introduced a review paper for FOPID controllers; in their review, they talk about almost all progress since it was used in a control system. First, they start the review by introducing the fractional calculus history: "in a letter dated September 30, 1695, L'Hopital wrote to Leibniz asking him for a particular notation that he had used in his publication for the n-th derivative of a function in the case when $n = 1 / 2$. Leibniz's response was, **"this will be equal to $\frac{d^{0.5}x}{dt^{0.5}}$ an apparent paradox from which one day useful consequences will be drawn";** with these words, fractional calculus was born." Then, they proceed by naming different definitions used for fractional calculus, such as *Grunwald-Letnikov definition, Riemann-Liouville definition,* and *M. Caputo definition,* and they stated that Caputo definition is more relevant in the case of engineering applications over all other definitions. They mention why the FOPID works better than a conventional controller by stating the following:

1- Five designing criteria can be achieved due to the five parameters of a FOPID controller.

2- The damping property can be attained easily using a FOPID controller.

3- A fractional-order controller gives better results in higher-order systems.

4- A fractional-order controller gives better results for long time-delay systems.

5- A fractional-order controller is more robust and stable.

6- A fractional-order controller performs better with nonlinear systems.

7- A fractional-order controller achieves a better response for a non-minimum phase system.

8-   Non-linear systems are linearized for different operating points and controllers are designed for different operating points, while one fractional PID controller is mostly sufficient for a non-linear system.

Bode was the first to use fractional calculus in control systems in 1945. In 1958, Tustin proposed a design for position control of massive objects using a fractional-order control. Fractional-order controllers were first used to control dynamic systems beginning with Oustaloup, who developed the so-called CRONE (Non-integer-order Robust Control) controller for easy application. Machado introduced a time-domain algorithm to implement the fractional-order controller; the approach was found suitable for digital implementations and Z-transform analysis in 1995, and 1997. The fractional-order first report published in 1994 by Podlubny showed that the fractional-order controller is a suitable way to control fractional-order systems. Petras investigated the stability of the fractional LTI system based on the Riemann surface. "The fractional-order PD^{μ} controller stability was carried out for the range of differentiation between 0 and 2 in for delay systems. The stability was calculated based on poles located on quasi-polynomial on the right hand of the s-plane and D-partition characterization of stability boundaries. They concluded that for $\mu > 1$, the system would be more unstable than $\mu < = 1$ in most of the cases." Four representations of fractional order controllers were presented in 2002 by Xue and Chen. These are the Tilted Proportional and Integral controller, CRONE controller, Fractional order PID controller, and fractional lead-lag compensator. In 2004, Agrawal introduced a new solution scheme for a class of fractional optimal control problems. Barbosa et al. designed a fractional order PID controller for nonlinear systems. They used the discrete-time approximation to implement the fractional order controller. In 2011, Merrikh-Bayat and Mirebrahimi introduced a nonlinear version of

the fractional-order PID controller. The showed a controller can improve the tracking properties for a feedback system. A sliding mode controller (SMC) was designed using a fractional PID controller; it was shown that SMC using fractional PID controllers were less sensitive to step disturbance. Cao designed in 2006 a fractional order controller using the Particle Swarm Optimization method; the results were compared with an optimization approach, and they claimed that the PSO method provides a better solution and faster search speed. Monje et al. published a well presented and practical book in 2010 that provides the current knowledge regarding fractional-order control. The book provides the necessary tools to understand the use of fractional calculus in control, and it focuses on the most requirements to understand and design fractional-order controllers. The controller design in this thesis was developed following the approach presented in this book.

Fractional order controller tuning is always hard to achieve due to the need to tune five parameters. Valerio and Costa divided tuning methods into rule-based methods like the Ziegler-Nichols method, analytical methods like the frequency domain method, and numerical methods like the genetic algorithm and the PSO algorithm. Simulations and implementation of fractional order systems become easier through the many tools available like Ninteger by Valerio and Costa, FOPID toolbox by Lachhab et al., FOMCON toolbox by Tepljakov et al., Sysquake interactive software tool by Pisoni et al, CRONE by Oustaloup et al., and FOTF toolbox by Xue et al. In the end, it was clear that a fractional order controller achieved a better robust performance [91].

Junyi and Binggang presented a fractional-order control strategy for a pneumatic position servosystem. They were the first to investigate this problem by expressing the relation between the pressure in the cylinder and the mass flow rate into the cylinder. The dynamic model was established, and the fractional-order proportional integral derivative controller was designed. Due to detailed modeling of the current system, they obtained the controller parameters by a trial and error method based on experiments [92]. Kumar et al. used a comparison between a PID controller and a FOPID controller to control a DC servo motor based on different tuning techniques. The comparison showed that FOPID is always better in all criteria like the rise time, settling time, and peak overshoot. They found that a genetic algorithm gives the best FOPID controller results compared to other methods like FMINCON. They also show that simulated annealing produces better results than a PID controller but still worse than a genetic algorithm. However, since the simulated annealing takes a large number of iterations and more time to converge, it is better to use a genetic algorithm [93]. Panteleev et al. proposed an average optimal FOPID controller parametric design method; the method starts over a given system initial state and a given input signal. They formulate the problem as a multidimensional optimization problem with object function $J(K_P, K_I, K_D, \alpha, \beta)$. They suggested a solution approach that minimizes the function J; the solution approach was implemented in the C language, and the design approach has been applied for pitch control of an aircraft in the horizontal flight mode [94]. Ranjbaran and Tabatabaei introduced a generalized Bode's integrals-based PID controller to design FOPI, FOPD, and FOPID controllers. They used the gain crossover frequency, the phase margin, the Nyquist plot slope adjustment, the measurement noise rejection, and minimizing an ITAE as the design conditions. They showed that the proposed controller provides better results compared with the ordinary Bode's integral method [95]. Tang et al. proposed a Fractional Sliding Mode

Controller (FOSMC) to regulate the slip to the desired value; the proposed method used the sliding mode controller and the fractional-order dynamics; the FOPD sliding surface is adopted. They proposed this approach to deal with the Antilock braking system (ABS) nonlinearity. Results show that the FOSMC tracks the desired slip faster than the integer controller [96].

The current investigated problem starts as a theoretical investigation of new control approaches to a problem that was previously investigated at a preliminary level in current publications. Our contribution focuses on how to control the surface temperature of a semi-infinite thin plate exposed to periodic heating at the other surface. To do this, we will use the inverse problem approach and the fractional-order controller approach. We will use this to form closed-loop control and open-loop control schemes used for surface temperature control. The fractional-order controller will be designed and experimentally verified. Also, the inverse problem approach with a proportional only controller will be studied and verified experimentally. This problem became to be of interest recently due to a fractional order plant resulting from solving the one-dimensional heat conduction equation.

Chapter Three: Problem Formulation

In this chapter, we will focus on the problem formulations, and the problem starts.

3.1 Introduction

      Temperature control is necessary for numerous industrial applications. Industrial installations are normally very complex, and novel temperature control solutions have to be first tested on simpler structures. This motivates our research to find suitable solutions for the problem of closed-loop control and open-loop control of a one-dimensional thin plate using the Laplace transform.

 3.2 Single Layer

      This section will focus on the types of expansions used and what are the formulas used.

3.2.1 Zero-Pole Expansion

      The heat equation for a finite plate of a single layer can be written as a 1D heat conduction equation:

$$\frac{\partial^2 T}{\partial x^2} = \frac{1}{\propto}\frac{\partial T}{\partial t} \qquad\qquad (3.1)$$

 Where heat flux $\emptyset$ is:

$$\emptyset = -k\frac{\partial T}{\partial x} \qquad\qquad (3.2)$$

      The Boundary conditions for sinusoidal temperature on sides 1 and 2 are represented by θ and $\emptyset$ where:

$$\theta_1(0, t) = A \sin\omega t \qquad \theta_2(L, t) = free \qquad (3.3)$$

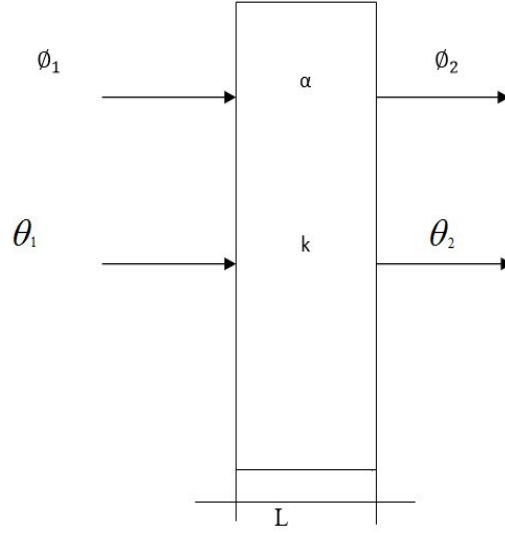$$\emptyset_1(0, t) = free \qquad \emptyset_2(L, t) = 0 \qquad (3.4)$$

Figure 4: Single layer material description.

The direct and inverse problem solutions were obtained as presented in references [13] [16][17].

In the complex domain:

$$\frac{\partial^2\theta}{\partial z^2} = \frac{s}{\alpha}\,\theta(z, s) \qquad (3.5)$$

With the boundary conditions:

$$\theta_1(0, s) = A\,\frac{w}{s^2 + w^2} \qquad \theta_2(L, s) = free \qquad (3.6)$$

$$\emptyset_1(0, s) = free \qquad \emptyset_2(L, s) = 0 \qquad (3.7)$$

The case in Figure 4 can be modeled using the Quadrupole approach as follows [18]:

$$\begin{pmatrix} \theta_1 \\ \emptyset_1 \end{pmatrix} = M \begin{pmatrix} \theta_2 \\ \emptyset_2 \end{pmatrix} \tag{3.8}$$

Where:

$$M = \begin{bmatrix} A & B \\ C & D \end{bmatrix} \tag{3.9}$$

And:

$$A = D = \cosh(K(s)L); \quad B = \frac{1}{k*K*A_s} \sinh(K(s)\,L)$$

$$C = (K*k*A_s)\sinh(K(s)L); \quad K(s) = \sqrt{\frac{s}{\alpha}}$$

A_s : The area of the plane isothermal surface that is considered for the x-transfer.

From equations (3-8) and (3-9) we get:

$$\theta_1 = A*\theta_2 + B*\emptyset_2 \tag{3.10}$$

Applying the boundary conditions, we get:

$$\frac{\theta_2}{\theta_1} = \frac{1}{A} = \frac{1}{\cosh(K(s)L)} = G_1 \tag{3.11}$$

This is the Direct Problem Transfer Function.

The transfer function of the inverse problem is:

$$G_2 = \frac{1}{G_1} = \cosh(K(s)L) \tag{3.12}$$

Equation (3-5) has the solution for the position variable z:

$$\theta(z, s) = A_1 \cosh(K(s)z) + A_2 \sinh(K(s)z) \tag{3.13}$$

The heat flux is given by

$$\emptyset(z, s) = -ks \frac{d\,\theta}{dz} \tag{3.14}$$

Where

$$K(s) = \sqrt{\frac{s}{\alpha}} \tag{3.15}$$

Applying the boundary conditions:

$$A_1 = A\frac{\omega}{S^2+\omega^2}, \qquad A_2 = -A\frac{\omega}{S^2+\omega^2}\tanh(K(s)L) \qquad (3.16)$$

For the above A_1 and A_2, the solution becomes:

$$\theta(z,s) = A\frac{\omega}{S^2+\omega^2}[\cosh(K(s)z) - \tanh(K(s)L)\sinh(K(s)z)] \qquad (3.17)$$

$$\emptyset(z,s) = -KskA\frac{\omega}{S^2+\omega^2}[\tanh(K(s)L)] \qquad (3.18)$$

The dynamics of boundary temperatures θ_1 and θ_2 are:

$$\theta_1 = \theta(0,s) = A\frac{\omega}{S^2+\omega^2} \qquad (3.19)$$

$$\theta_2 = \theta(L,s) = A\frac{w}{S^2+\omega^2}[\cosh(K(s)L) - \tanh(K(s)L)\sinh(K(s0L)]$$
$$= A\frac{\omega}{S^2+\omega^2}[1/\cosh(K(s)L)] \qquad (3.20)$$

The transfer function of the direct problem linking θ_2 to θ_1 is:

$$G_1 = \frac{\theta_2}{\theta_1} = \left[\frac{1}{\cosh(K(s)L)}\right] \qquad (3.21)$$

The transfer function for the inverse problem is:

$$G_2 = \frac{1}{G_1} = \cosh(K(s)L) \qquad (3.22)$$

Solving equations (3-21) and (3-22), we obtain the poles of the direct problem (G_1) and the zeros of the inverse problem (G_2) as the following expansions [23]:

$$\frac{1}{\cosh(KL)} = \frac{p_1 p_2 p_3 p_4 p_5 p_6\cdots}{(s-p_1)(s-p_2)(s-p_3)(s-p_4)(s-p_5)(s-p_6)\cdots} \qquad (3.23)$$

Where:

$$p_k = -[\frac{(2k-1)\pi}{2} * \frac{sqrt(\alpha)}{L}]^2, \quad k = 1,2,3,\dots$$

And

$$\cosh(KL) = \frac{(s-z_1)(s-z_2)(s-z_3)(s-z_4)\ldots}{z_1 z_2 z_3 z_4 \ldots} \tag{3.24}$$

Where:

$$z_k = -\left[\frac{(2k-1)\pi}{2} * \frac{sqrt(\alpha)}{L}\right]^2, \quad k = 1,2,3,\ldots$$

As we see from Equation (1.1), we have the transfer functions resulted from equations (3.23) and (3.24) multiplied with each other. This explains the need for a different number of terms in both functions for the simulation study, which will be later verified by experiments.

3.2.2 Taylor Expansion

Transfer functions for both direct and inverse problems are the same as in the previous section, but here we used different expansions for obtaining both transfer functions as a function of (s).

To simulate the open-loop control problem, we need the transfer function as a dependent of integer powers of (s). The transfer functions are shown above as the hyperbolic cosine and hyperbolic secant containing the square root of the variable (s) and this cannot be simulated directly. To solve this problem, we have to write both transfer functions G_1 and G_2 as a form of a Taylor series expansion as follows:

$$G_1 = \text{sech}(x) = \sum_{n=0}^{\infty} \left(\frac{E_n}{n!}\right) x^n, \quad \text{for } |x| < \pi/2 \tag{3.25}$$

Where Euler numbers E_n is zero for odd-indexed numbers, and even indexed numbers are:

$E_0 = 1$

$E_2 = -1$

$E_4 = 5$

$E_6 = -61$

$E_8 = 1385$

$E_{10} = -50521$

$E_{12} = 2702765$

$E_{14} = -199360981$

$E_{16} = 19391512145$

$E_{18} = -2404879675441$ etc.

For the inverse problem

$$G_2 = \cosh(x) = \sum_{n=0}^{\infty} \left(\frac{1}{(2n)!}\right) x^{2n}, \quad \text{for } -\infty < x < \infty \tag{3.26}$$

From the above expansion, we see that there is a limitation of $\text{sech}(x) = |x| < \frac{\pi}{2}$, the alternative form $\text{sech}(x) = \frac{1}{\cosh(x)}$ is used knowing that there are no domain limitations for $\cosh(x)$.

For the simulation, Taylor's expansion of G_1, the direct problem transfer function will be limited to N terms, and G_2, inverse problem transfer function, is limited to M terms. For the transfer function $(G_1 G_2)$, N and M are chosen such that $N > M$, the reason for this condition is that for the inverse problem, when the number of terms M increase the ill-posedness of the problem increases. In the simulated case here, a thin aluminum plate has the thickness $L = 0.03$ [m] and thermal diffusivity $\alpha = 9.715\text{e-}5$ [m²/sec], such that

36

$$x = K(s)L = \sqrt{\frac{s}{\alpha}} L = \sqrt{\frac{s}{9.715*10-5}} \, 0.03 \qquad (3.27)$$

For the simulations, N and M were chosen to be for M=4 and N=8, such that N >M. The resulting transfer functions for direct and inverse problems are:

$$G_2(s) = 1 + 4.632s + 3.576s^2 + 1.104s^3 \qquad (3.28)$$

$$G_1(s) = \frac{1}{\cosh(KL)} = 1/(1 + 4.632s + 3.576s^2 + 1.104s^3 + 0.1827s^4 + 0.0188s^5$$
$$+ 0.00132s^6 + 6.717e^{-5}s^7) \qquad (3.29)$$

For the system in Figure 2, an open-loop block diagram, we compute the resultant transfer function for the open-loop which is $(G_1 * G_2)$. MATLAB™ and Simulink™ are used for simulation. Simulations were done for the open-loop control for different values of input frequency and the desired sinusoidal temperature amplitude of 20^0 above the original temperature; i.e., for $(20\sin(\omega t))$ as input temperature.

3.3 Two-Layer Plate Formulation

The temperature transfer through a wall of multilayer material can be formulated using the thermal quadrupoles approach for each layer, assuming that the contact between layers is perfect. The 1D heat conduction equation is

$$\frac{\partial^2 T}{\partial x^2} = \frac{1}{\propto} \frac{\partial T}{\partial t} \qquad (3.30)$$

Where the heat flux Ø is:

$$\emptyset = -k\frac{\partial T}{\partial x} \tag{3.31}$$

In the complex domain:

$$\frac{\partial^2 \theta}{\partial z^2} = \frac{s}{\alpha}\,\theta(z,s) \tag{3.32}$$

We consider two layers of thickness, L_1 and L_2, diffusivity α_1, and α_2.
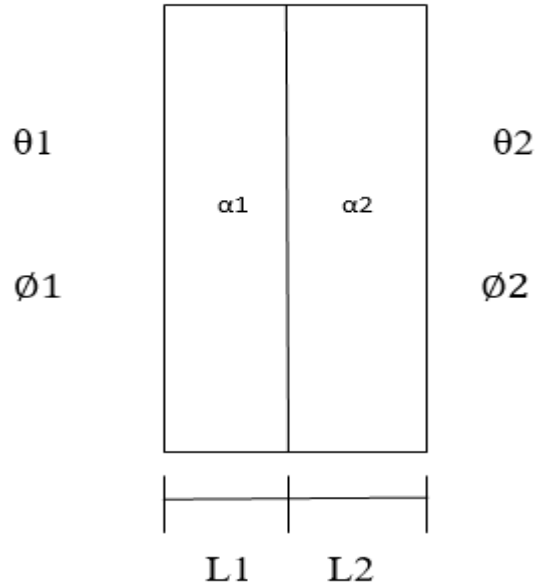

Figure 5: Two-layer material description.

The model for two layers can be obtained using the quadrupole approach as follows:

$$\begin{pmatrix} \theta_1 \\ \emptyset_1 \end{pmatrix} = M_1 M_2 \begin{pmatrix} \theta_2 \\ \emptyset_2 \end{pmatrix} \tag{3.33}$$

Where:

$$M_1 = \begin{bmatrix} A_1 & B_1 \\ C_1 & D_1 \end{bmatrix}$$

$$M_2 = \begin{bmatrix} A_2 & B_2 \\ C_2 & D_2 \end{bmatrix}$$

And:

$$A_1 = D_1 = \cosh(K_1 L_1); \quad B_1 = \frac{1}{k_1 * K_1 * A_s} \sinh(K_1\, L_1)$$

$$C_1 = (K_1 * k_1 * A_s)\sinh(K_1 L_1); \quad K_1 = \sqrt{\frac{s}{\propto_1}}$$

Where

A_s is the area of the plane isothermal surface that considered for the x-transfer?

And:

$$A_2 = D_2 = \cosh(K_2 L_2); \quad B_2 = \frac{1}{k_2 * K_2 * A_s} \sinh(K_2\, L_2)$$

$$C_2 = (K_2 * k_2 * A_s)\sinh(K_2 L_2); \quad K_2 = \sqrt{\frac{s}{\propto_2}}$$

We compute (M) Matrix which is:

$$M = M_1 * M_2 = \begin{bmatrix} A & B \\ C & D \end{bmatrix} \tag{3.34}$$

Where:

$$A = A_1 * A_2 + B_1 * C_2; \quad B = A_1 * B_2 + B_1 * D_2$$

$$C = C_1 * A_2 + D_1 * C_2; \quad D = C_1 * B_2 + D_1 * D_2$$

This product will show that:

$$A = \cosh(K_1 L_1) \cosh(K_2 L_2) + \frac{K_2 k_2}{K_1 k_1} \sinh(K_1 L_1) \sinh(K_2 L_2)$$

$$B = \frac{1}{K_2 k_2 A_s} \cosh(K_1 L_1) \sinh(K_2 L_2) \frac{1}{K_1 k_1 A_s} \sinh(K1L1) \cosh(K_2 L_2)$$

$$C = K_1 k_1 A_s cosh(K_2 L_2) \sinh K_1 L_1 + K_2 k_2 A_s cosh(K_1 L_1) \sinh(K_2 L_2)$$

$$D = \frac{K_1 k_1}{K_2 k_2} \sinh(K_1 L_1) \sinh(K_2 L_2) + \cosh(K_1 L_1) \cosh(K_2 L_2)$$

From these we get:

$$\theta_1 = A * \theta_2 + B * \emptyset_2 \qquad (3.35)$$

$$\emptyset_1 = C * \theta_2 + D * \emptyset_2 \qquad (3.36)$$

We want to solve these two equations to get $G(s) = \frac{\theta_2}{\theta_1}$ as the transfer function related

to input temperature and output temperature.

The boundary conditions were considered in the following:

$$\theta_1(0,t) = A\ sin\omega t \qquad \theta_2(L,t) = free \qquad (3.37)$$

$$\emptyset_1(0,t) = free \qquad \emptyset_2(L,t) = 0 \qquad (3.38)$$

After we apply the boundary conditions, we get:

$$\frac{\theta_2}{\theta_1} = \frac{1}{A} \qquad (3.39)$$

Where:

$$A = \cosh(K_1 L_1)\cosh(K_2 L_2) + \frac{K_2 k_2}{K_1 k_1}\sinh(K_1 L_1)\sinh(K_2 L_2) \qquad (3.40)$$

We further develop A as follows:

$$\cosh(x)\cosh(y) = \frac{1}{2}[\cosh(x+y) + \cosh(x-y)]$$

$$sinh(x)sinh(y) = \frac{1}{2}[\cosh(x+y) - \cosh(x-y)]$$

Where:

$$x = K_1 L_1\ and\ y = K_2 L_2$$

Then A becomes:

$$A = \frac{1}{2}[\cosh(x+y) + \cosh(x-y) + b\{\cosh(x+y) - \cosh(x-y)\}] \qquad (3.41)$$

Where:

$$b = \frac{K_2 k_2}{K_1 k_1}$$

Case 1: Plates of the same material and the same thickness.

Now, when we want to use the same material, this will give that:

$$b = 1$$

We substitute b=1 in equation (3.41), and we get:

$$A = \frac{1}{2}[\cosh(x + y) + \cosh(x + y)] \tag{3.42}$$

Now, we will use the same thickness for the two layers:

$$L_1 = L_2 = \frac{L}{2} \tag{3.43}$$

Where L represents the plate thickness.

From this we get:

$$x = y = K\frac{L}{2}$$

Substituting for x and y in equation (3.42), we get:

$$A = \frac{1}{2}\left[\cosh\left(K(s)\frac{L}{2} + K(s)\frac{L}{2}\right) + \cosh\left(K(s)\frac{L}{2} + K(s)\frac{L}{2}\right)\right] \tag{3.44}$$

Simplifying (A), we get:

$$A = \cosh(K(s)L) \tag{3.45}$$

When we use two layers of the same thickness $(\frac{L}{2})$ and the same material, we verify

that we obtain the same transfer function for a single layer material of thickness (L) and the

same material properties.

Case 2: Using a different material and the same thickness of $(\frac{L}{2})$.

When:

41

$$L_1 = L_2 = \frac{L}{2} \tag{3.46}$$

We get:

$$x - y = \sqrt{s}\left[\frac{L(\sqrt{\alpha_2} - \sqrt{\alpha_1})}{2\sqrt{\alpha_1\alpha_2}}\right] \tag{3.47}$$

$$x + y = \sqrt{s}\left[\frac{L(\sqrt{\alpha_2} + \sqrt{\alpha_1})}{2\sqrt{\alpha_1\alpha_2}}\right] \tag{3.48}$$

From equation (3.41):

$$A = \left[\frac{1}{2} + \frac{b}{2}\right][\cosh(x+y)] + \left[\frac{1}{2} - \frac{b}{2}\right][\cosh(x-y)] \tag{3.49}$$

Where:

$$b = \frac{\sqrt{\alpha_1}\, k_2}{\sqrt{\alpha_2}\, k_1} \tag{3.50}$$

$$A = \left[\frac{1}{2} + \frac{b}{2}\right]\left[\cosh\left(h\sqrt{s}\right)\right] + \left[\frac{1}{2} - \frac{b}{2}\right]\left[\cosh\left(g\sqrt{s}\right)\right] \tag{3.51}$$

Where:

$$h = \frac{x+y}{\sqrt{s}}$$

$$g = \frac{x-y}{\sqrt{s}}$$

From equation (3.45), we have:

$$G_1 = \frac{1}{A} \tag{3.52}$$

Which is the direct problem transfer function?

The inverse problem transfer function is:

$$G_2 = \frac{1}{G_1} = A \tag{3.53}$$

Solving equations (3-52) and (3-53), we obtain the poles of the direct problem (G_1)

and the zeros of the inverse problem (G_2), as follows:

$$G_1 = 1/\left\{\left[\frac{1}{2} + \frac{b}{2}\right]\frac{(s-p_1)(s-p_2)(s-p_3)(s-p_4)(s-p_5)(s-p_6)\cdots}{p_1 p_2 p_3 p_4 p_5 p_6 \cdots} + \right.$$

$$\left.\left[\frac{1}{2} - \frac{b}{2}\right]\quad \frac{(s-f_1)(s-f_2)(s-f_3)(s-f_4)(s-f_5)(s-f_6)\cdots}{f_1 f_2 f_3 f_4 f_5 f_6 \cdots}\right\} \tag{3.54}$$

Where:

$$p_n = -\left[\frac{(2k-1)\pi}{2} * \frac{1}{h}\right]^2, \quad n = 1,2,3,\dots$$

$$f_n = -\left[\frac{(2k-1)\pi}{2} * \frac{1}{g}\right]^2, \quad n = 1,2,3,\dots$$

And

$$G_2 = \left[\frac{1}{2} + \frac{b}{2}\right]\frac{(s-z_1)(s-z_2)(s-z_3)(s-z_4)\cdots}{z_1 z_2 z_3 z_4 \cdots} + \left[\frac{1}{2} - \frac{b}{2}\right]\frac{(s-y_1)(s-y_2)(s-y_3)(s-y_4)\cdots}{y_1 y_2 y_3 y_4 \cdots} \tag{3.55}$$

Where:

$$z_n = -\left[\frac{(2k-1)\pi}{2} * \frac{1}{h}\right]^2, \quad n = 1,2,3,\dots$$

$$y_n = -\left[\frac{(2k-1)\pi}{2} * \frac{1}{g}\right]^2, \quad n = 1,2,3,\dots$$

Chapter Four: Simulations Results

In the current chapter, we will present the simulation results for both open-loop and closed-loop schemes.

4.1 Open Loop Results

Fractional order rational complex functions cannot be computed as such and approximations by integer-order functions are required, as is extensively shown in publications [2, 39-71, 73-95]. In the current section, we will present the simulations' results for both Taylor expansion and Zero-Pole expansion.

4.1.1 Taylor Expansion

Simulations were carried out for open-loop control for different values of input frequency, and the desired sinusoidal temperature amplitude of 20^0 above the original temperature; i.e., for $20\sin(\omega t)$.

To achieve the simulation study, we have to verify first that the number of terms used in the approximation is suitable and gives a good approximation for the transfer function. Figure 6 shows that for only high frequency the magnitude and phase diagrams start to deviate from each other. While for low frequency, which is the case for our study, the magnitude and phase diagrams are identical regardless of the number of terms used in the approximation.
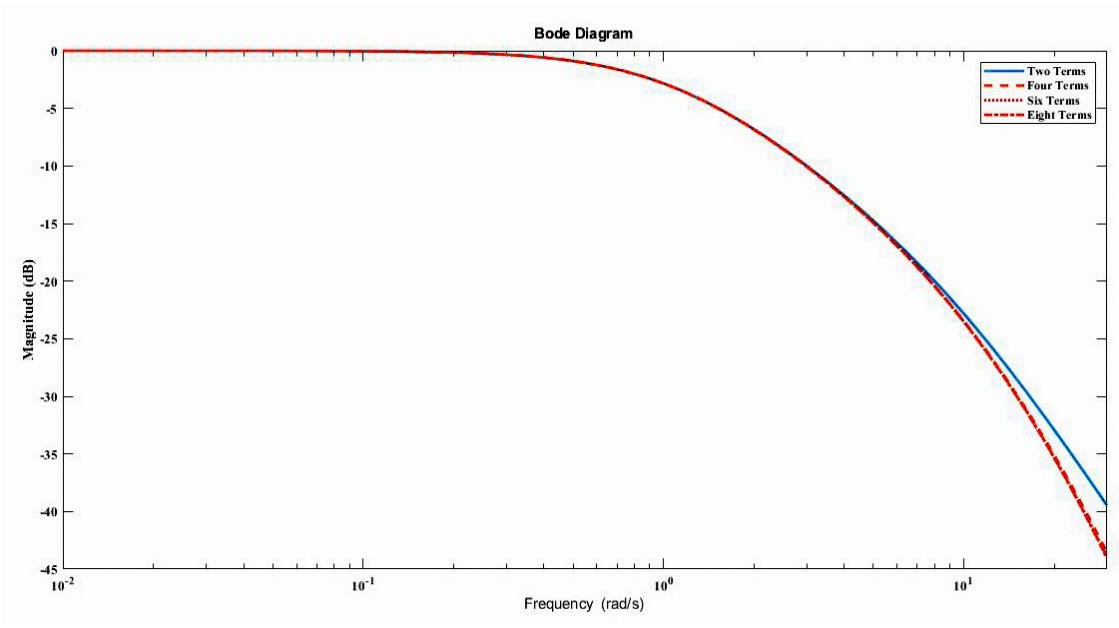
a
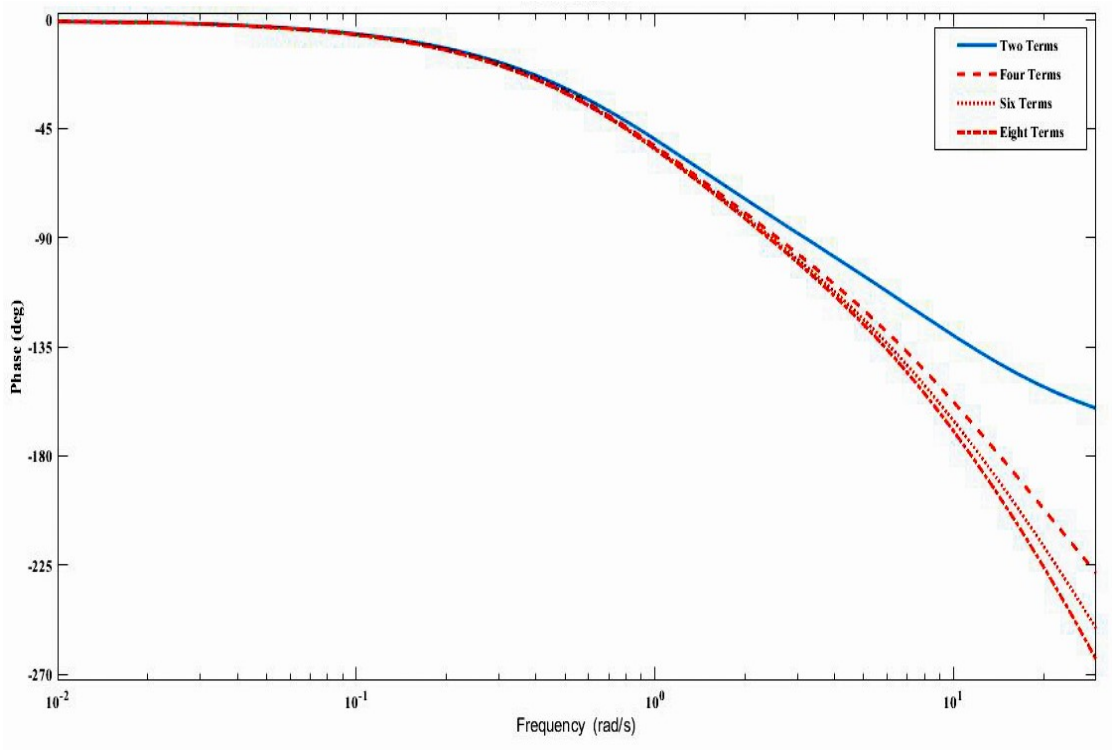
b

Figure (6): Bode plot diagram comparison for a different number of terms used in the approximation, a) Magnitude diagram, b) Phase diagram.

Simulations were carried for the direct problem (G_1) for N=8 while for the inverse problem (G_2) for M= 4. The input was $\theta_2^d = 20\sin(\omega t)$ above the environment temperature. Simulation results for ω =0.1, 1, 5, and 10 (rad/sec) are shown in Figure (7-11), which shows a sine variation of temperature around 0^0C. The results show the sine variation of about 20^0 C above the original (environmental) temperature. The variation of temperature is shown as the relative temperature with regard to the environmental temperature or, alternatively, the environmental temperature assumed to be zero. In all figures of simulation results shows the variations of the temperature due to the sine input temperature.
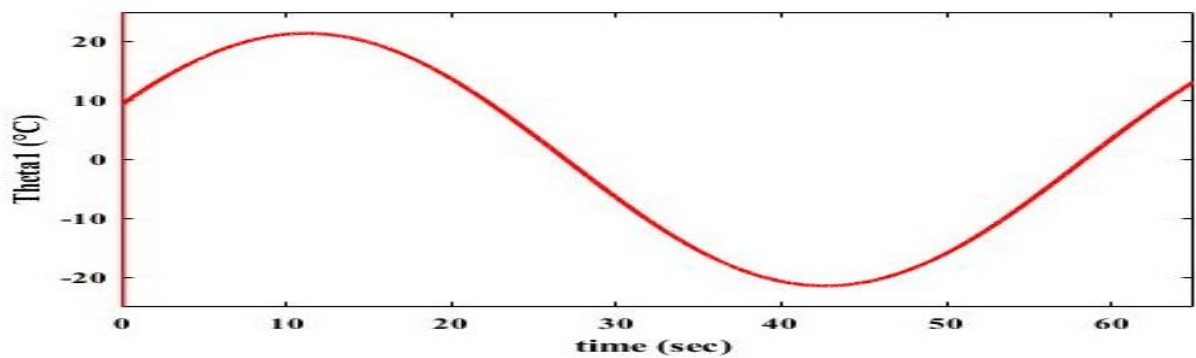
(a)
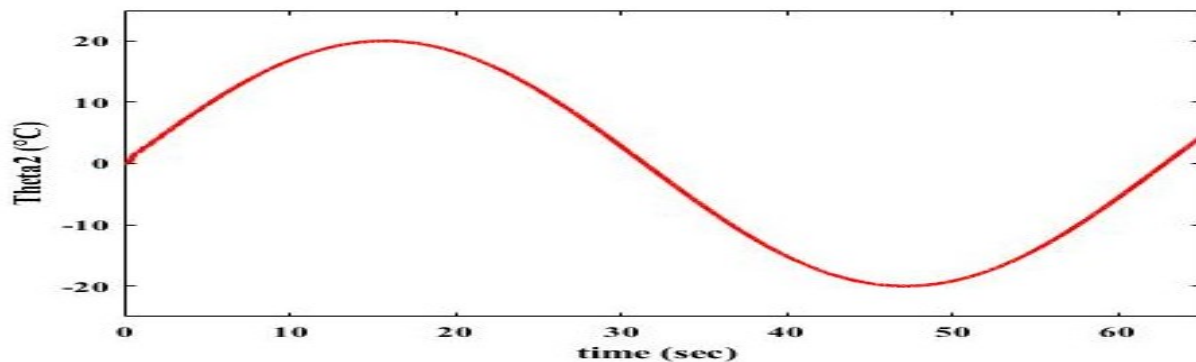
(b)

Figure 7: The relative output temperatures (a) of the inverse problem θ_1 and of (b) the open loop control θ_2 for ω= 0.1 rad/sec.

46
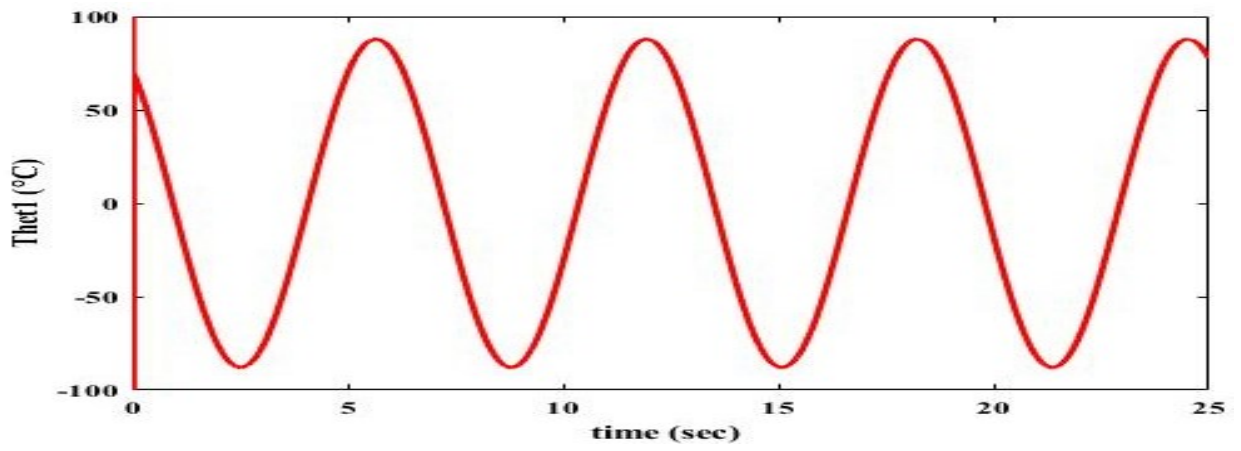
(a)
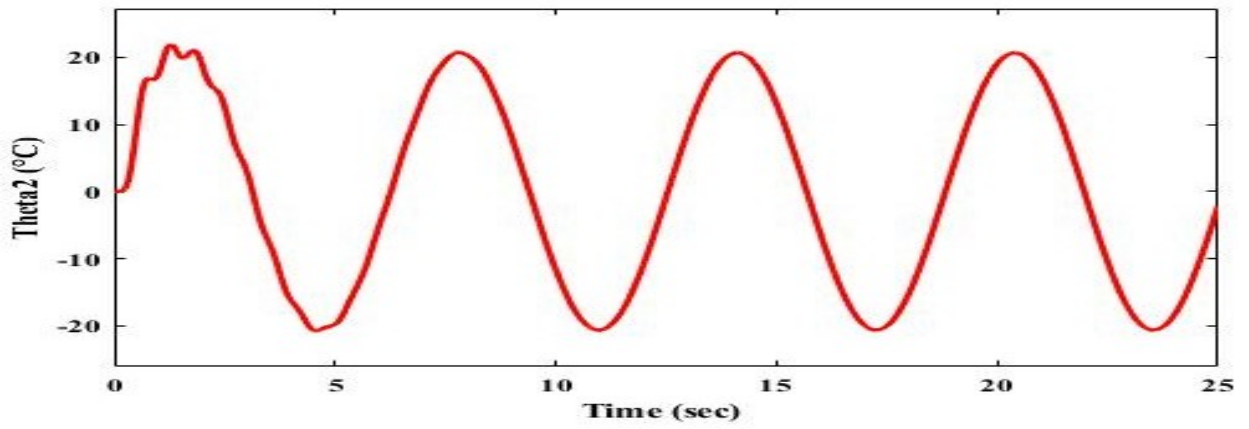
(b)

Figure 8: The relative output temperatures (a) of the inverse problem θ_1 and (b) of the open loop control θ_2 for $\omega = 1$ rad/sec.
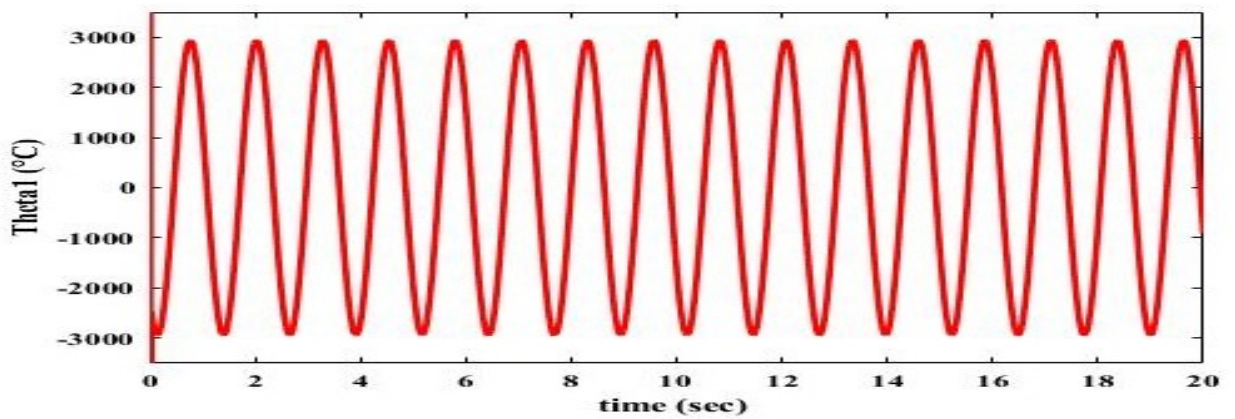
(a)
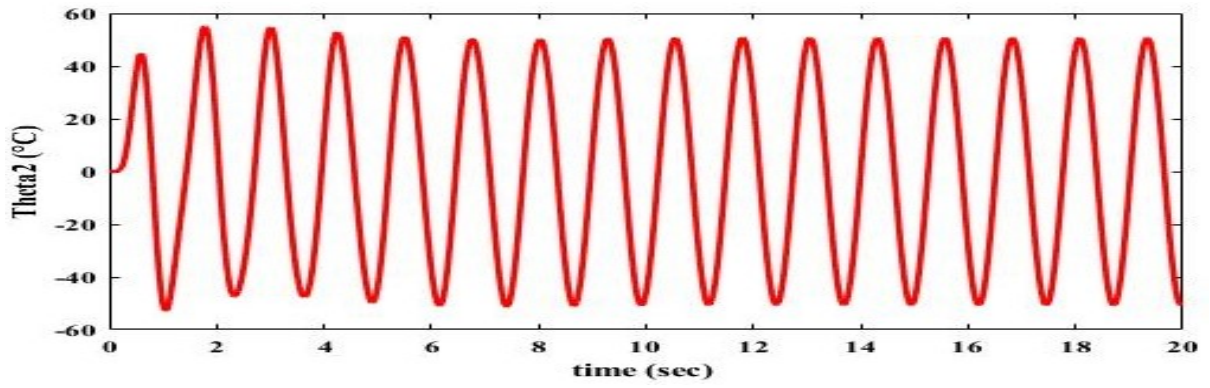
(b)

Figure 9: The relative output temperatures (a) of the inverse problem θ_1 and (b) of the open loop control θ_2 for $\omega = 5$ rad/sec.
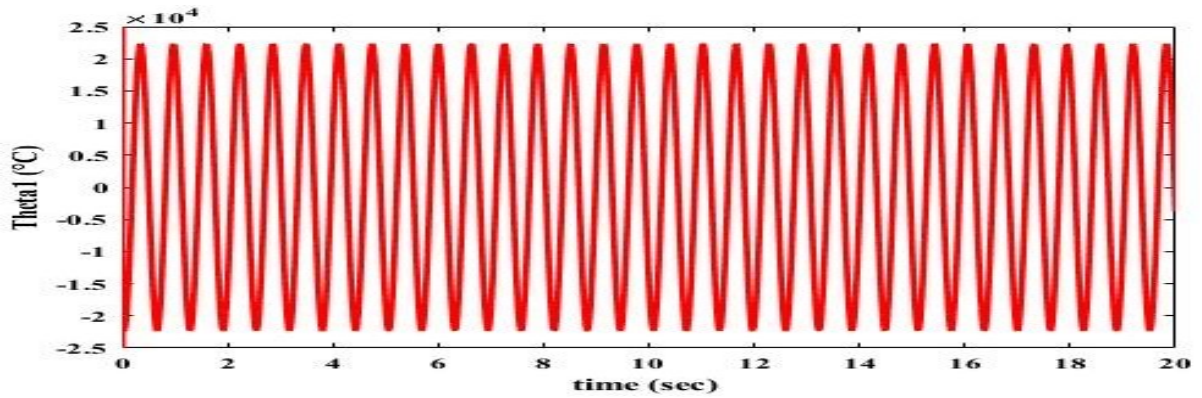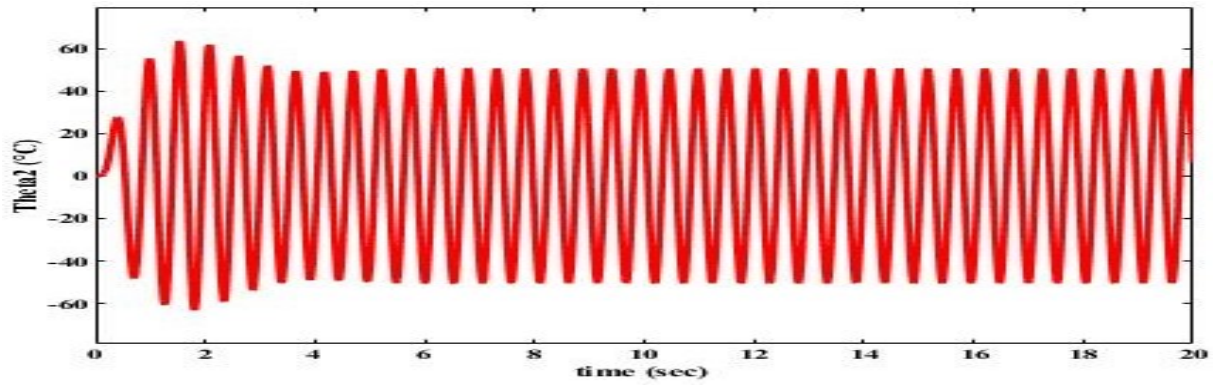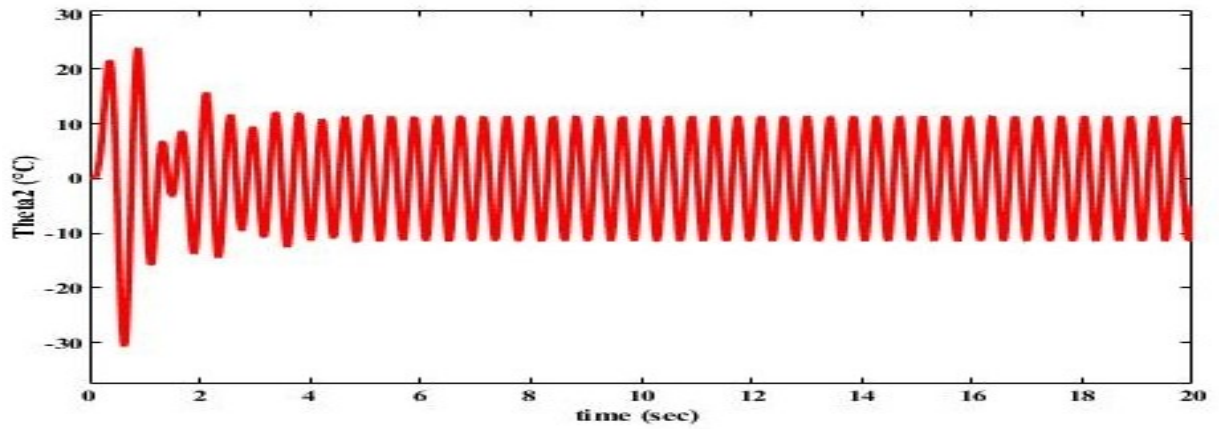

(a)
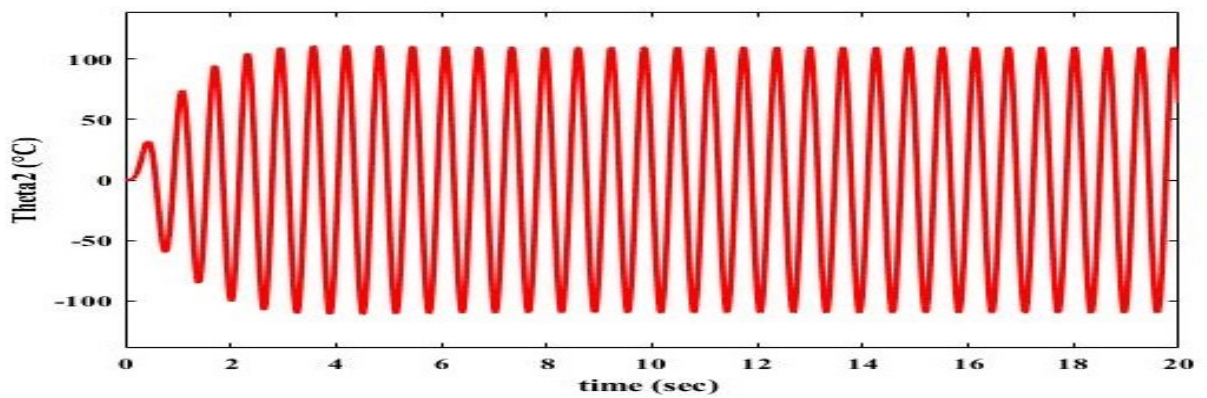
(b)

Figure 10: The relative output temperatures (a) of the inverse problem θ_1 and (b) of the open loop control θ_2 for $\omega = 10$ rad/sec.

(a)

(b)

Figure 11: The relative output temperature of the open-loop control with N=8, M=4 for (a), ω= 12and (b) 15 rad/sec.

The results in Figures (8 – 10) show higher amplitudes of θ_1 for higher frequencies,

i.e. the effect of inverse problem ill-posedness nature on the results for different frequencies.
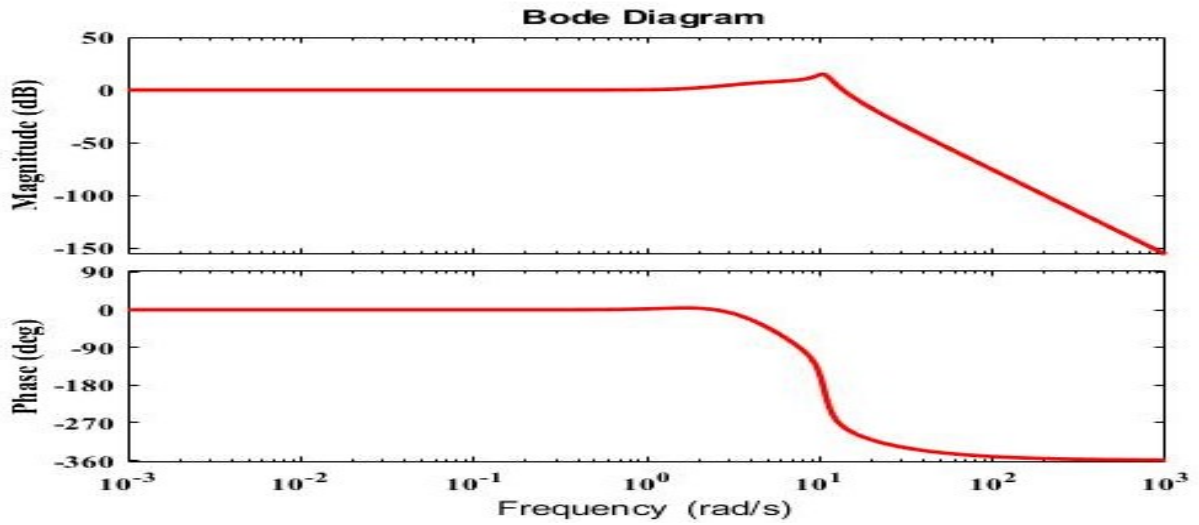
Figure 12: Bode diagram of the open-loop control transfer function G_1*G_2 for N=8 and M=4.

The results in Figures (7-10) are the output temperature deviations about 20^0 for the inverse problem θ_1 (a) and the output of the open-loop control θ_2 (b) with N=8, M=4 for $\omega =$ 0.1, 1, 5 and 10 (rad/sec). The output temperature θ_2 in Figures (7-8) (b) with lower frequencies of 0.1 and 1 rad/sec, compared to the desired one $\theta_2^d = 20\sin\omega t$, are very close. The results in Figures (9-10) (b), for output temperature θ_2, with higher frequencies of 5 and 10 (rad/sec) (compared to the desired deviation of about 20^0 of $\theta_2^d = 20\sin\omega t$) are significantly different. This can be explained by the very high amplitudes of the output of the inverse problem in Figures (9-10) (a), which leads eventually to an ill-posed inverse problem. For $\omega = 12$ and $\omega = 15$ (rad/sec) in Figure 11 (a, and b), we start to see a decrease in the amplitude with increasing the frequency. The Bode diagram of the open-loop control transfer function in Figure 12 explains this by indicating significantly lower magnitudes for $\omega > 11$ rad/sec. the Bode diagram in Fig 12 shows that beyond bandwidth frequency of about 11 rad/sec at -3 dB, the amplitude decreases for 20 rad/sec at cca – 35 dB and for 40 rad/sec at cca – 50 dB. This requires huge values for inverse problem output temperatures θ_1(not

50

displayed in diagrams, illustrating ill-posedness, to achieve the output temperatures θ_2. In fact, for 20 rad/sec and for 40 rad/sec, the resulting θ_1 from simulations is so high that in experiments could not be realized because it would melt the metal plates. These results explain the effect of fractional order systems on the degree of ill-posedness of the inverse problem, which leads to severe ill-posedness of the inverse problem.
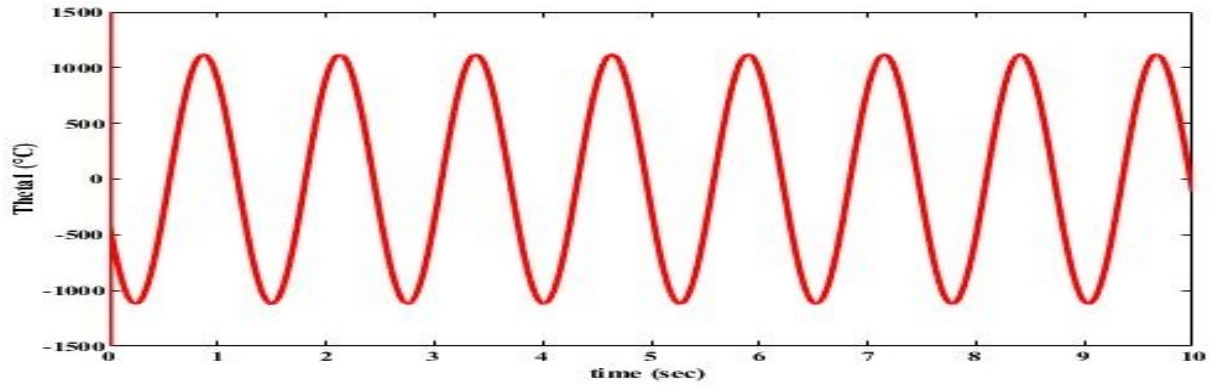
4.1.2 Zero-Pole expansion

Simulations were done for a thin aluminum plate which has the thickness L = 0.03 [m] and thermal diffusivity α= 9.715e-5 [m^2/sec]. For the open-loop scheme, we use M=4 and N=8 terms where M is the number of terms for the inverse problem, while N is the number of terms for the direct problem.
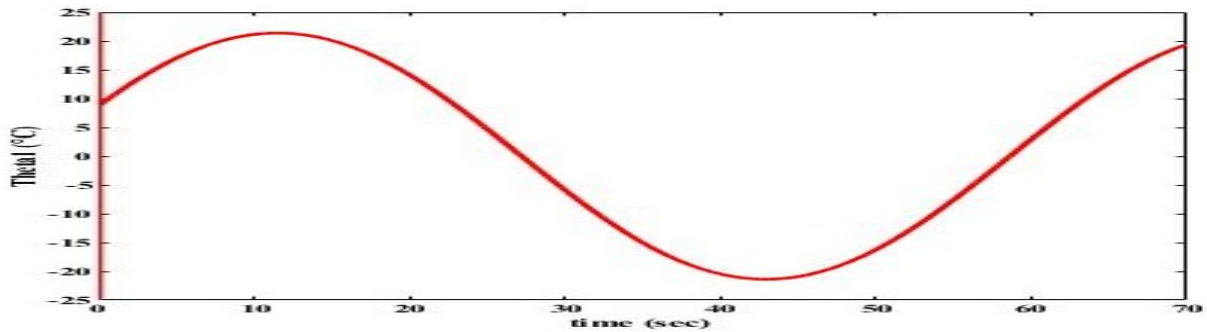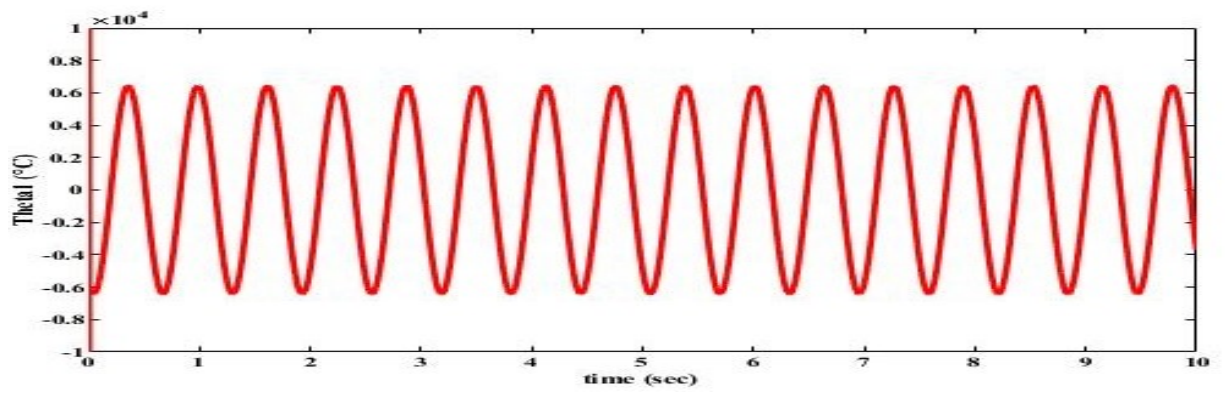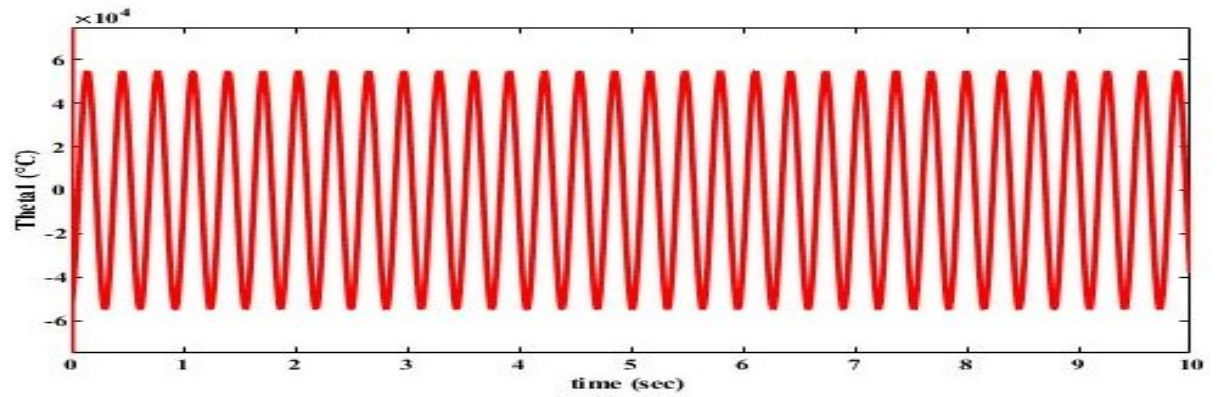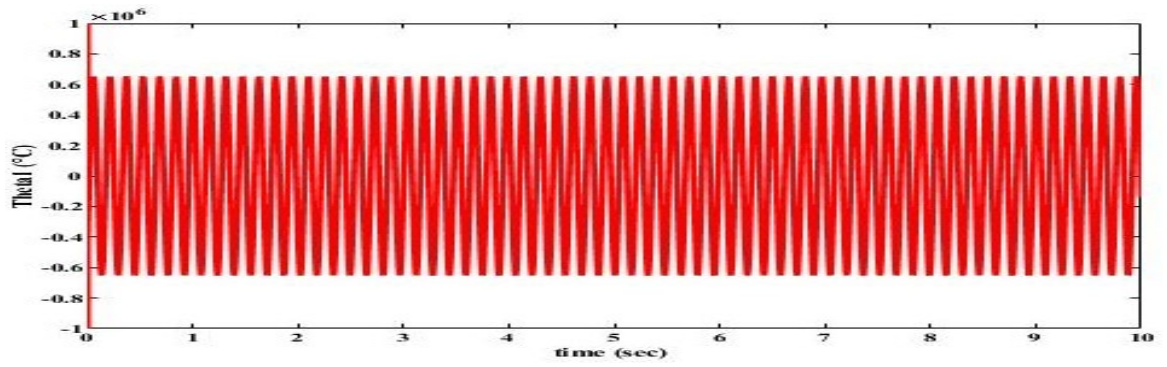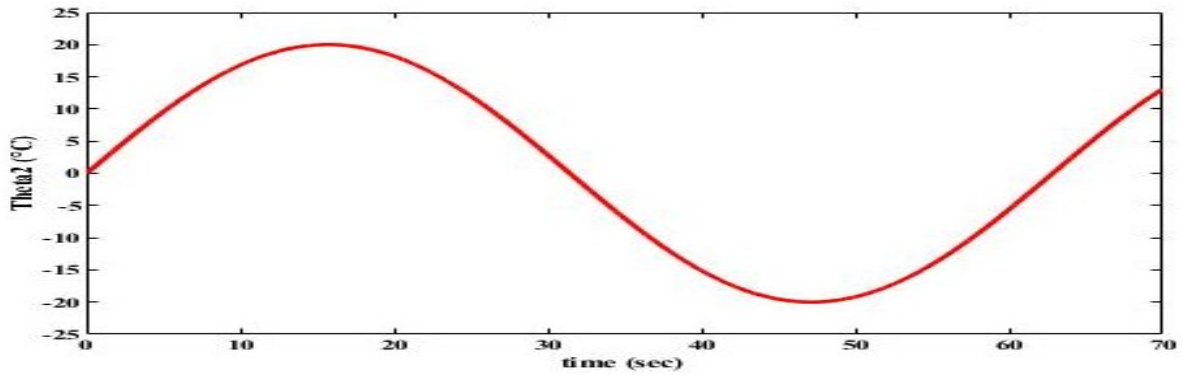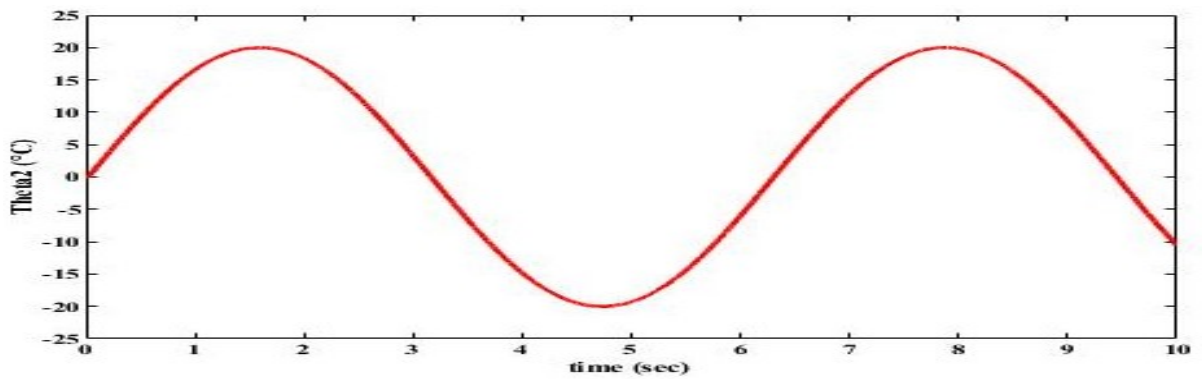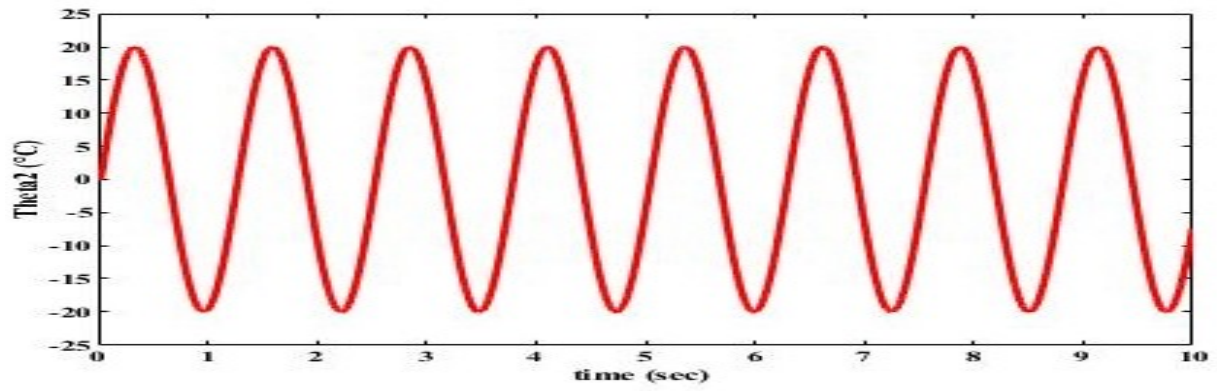

a
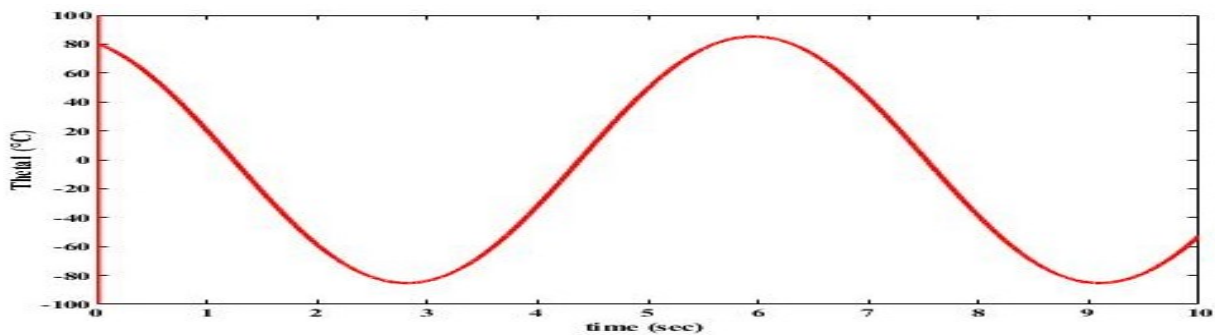
b

c

d

e

f

Figure 13: The open loop control relative temperature response (θ_1) for M=4, N=8 and ω = (a) 0.1 , (b) 1 , (c) 5 , (d) 10 , (e) 20, (f) 40 rad/sec.
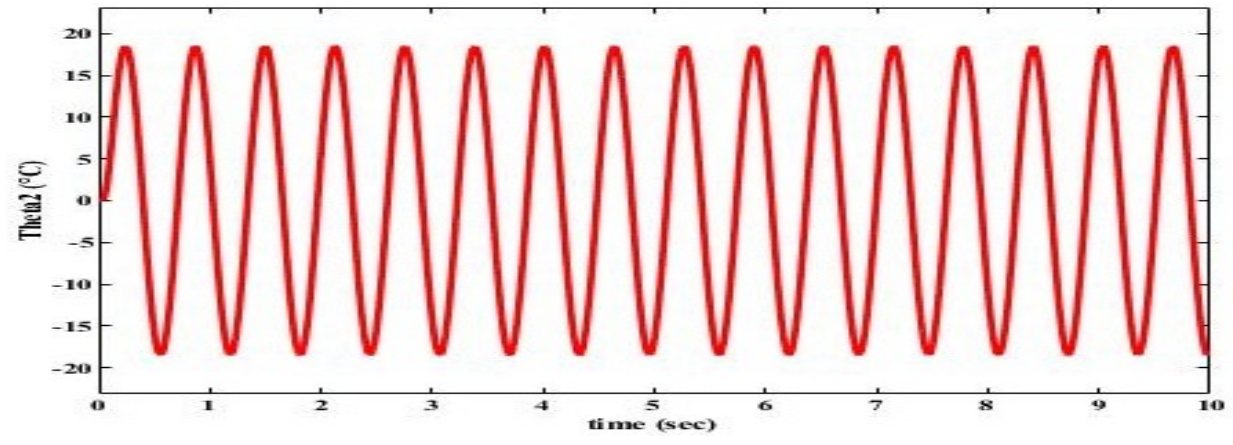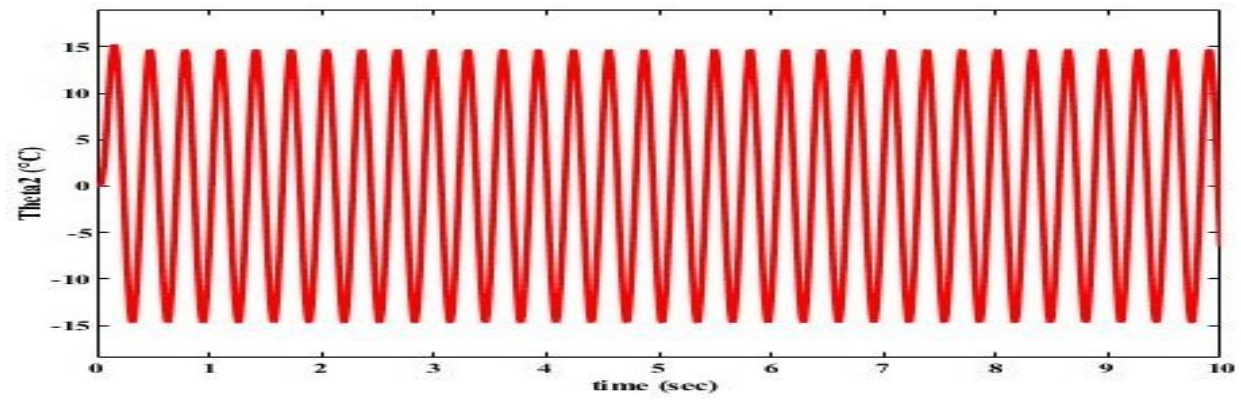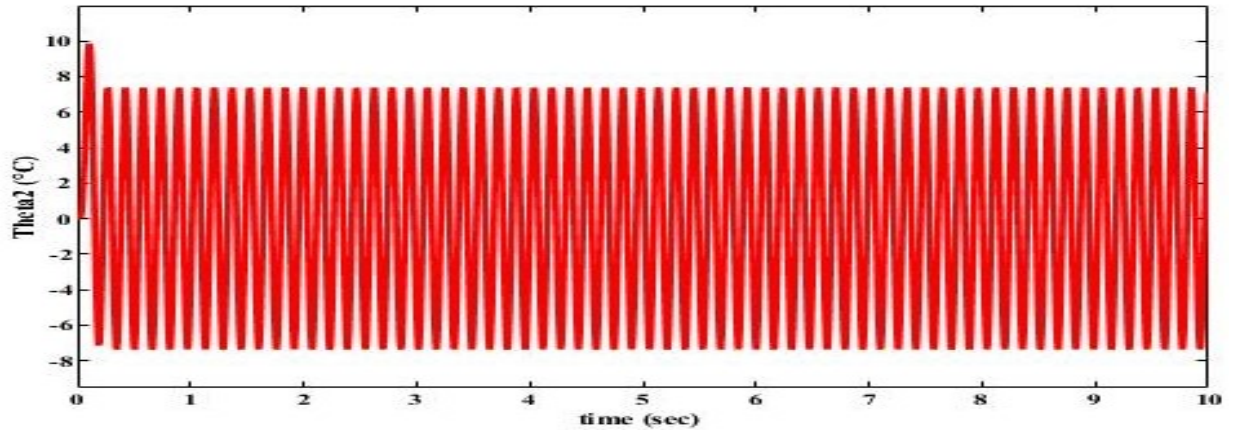

a

b

c

d

e

f

Figure 14: The open loop control relative temperature response (θ_2) for M=4, N=8 and ω = (a) 0.1 , (b) 1 , (c) 5 , (d) 10 , (e) 20, (f) 40 rad/sec.

From Figures 13 (a-f) we see that as frequency increases, the inverse problem output increases rapidly, while from Figures 14 (a-c), the response is almost the same as the desired value, and from Figure 14 (d-f), we see that as frequency increases, the response decreases and starts to be significantly smaller than the desired value.

4.2 Closed Loop Results

In this section, we will present the closed-loop scheme simulations results for both Taylor expansion and Zero-Pole expansion.

4.2.1 Taylor Expansion

Simulations were carried out for the closed-loop control for different values of input frequency and the desired sinusoidal temperature amplitude of 20^0 above the original temperature of 20^0C.

Simulations were carried out for the direct problem G_1 for N=6 while for the inverse problem G_2 for M= 4, these two values for the number of terms for the direct and inverse problems were chosen from the stability results shown in Table 1. The input was $\theta_1(0, t) = 20\sin(\omega t)$. Simulations results for $\omega = 0.1, 1, 5, 10$ and 20 rad/sec are shown in Figure 15 for k=10.

Table 1: Stability results for closed loop control.

Direct	N = 5			N = 6			N = 7			N = 8		
Gain	1	5	10	1	5	10	1	5	10	1	5	10
Inverse												
M = 3	Stable	Stable	Stable	Stable	Unstable		Unstable			Unstable	Unstable	Unstable
M = 4	Unstabl			Stable	Stable	Stable	Unstabl			Unstabl	Unstabl	Unstabl
M = 5	Unstable			Unstable			Stable	Stable	Stable	Unstable		
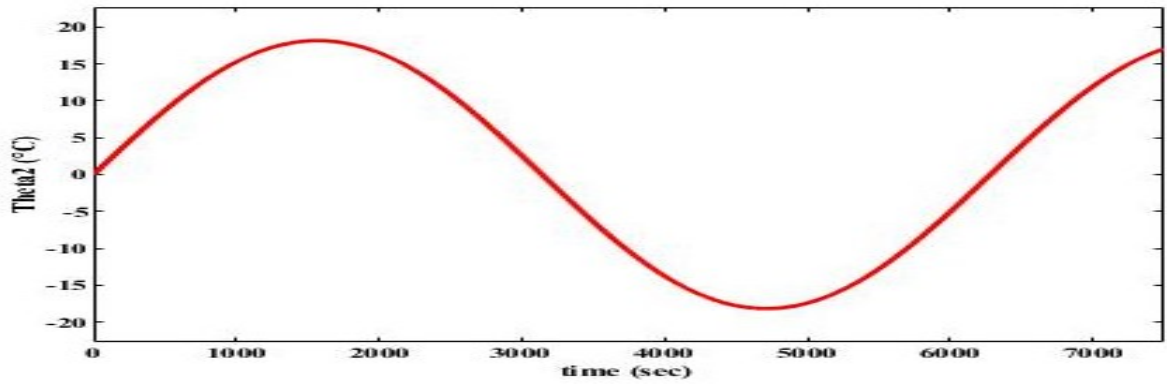
(a)
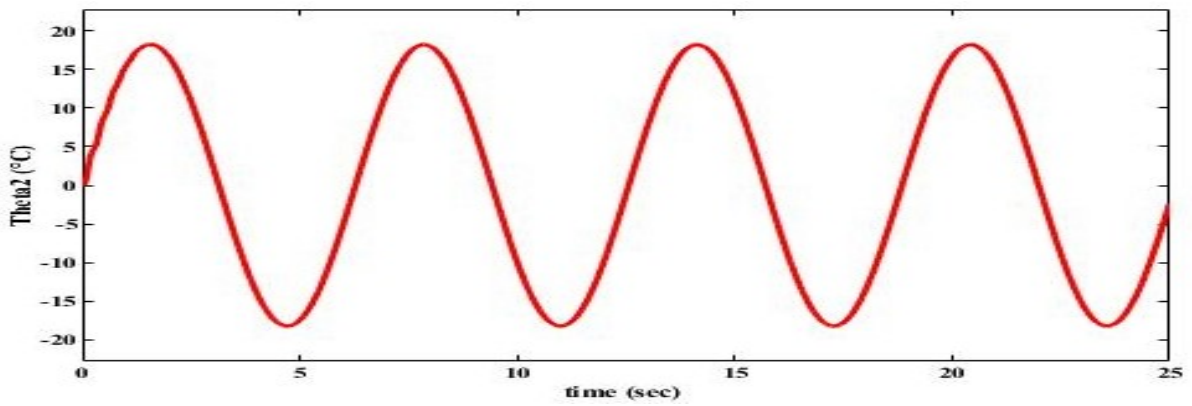
(b)
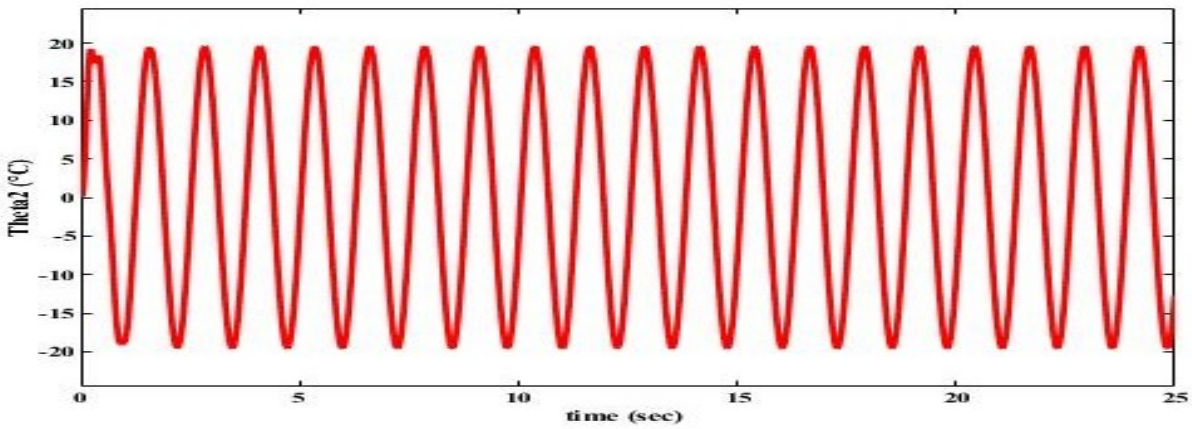
(c)

(d)
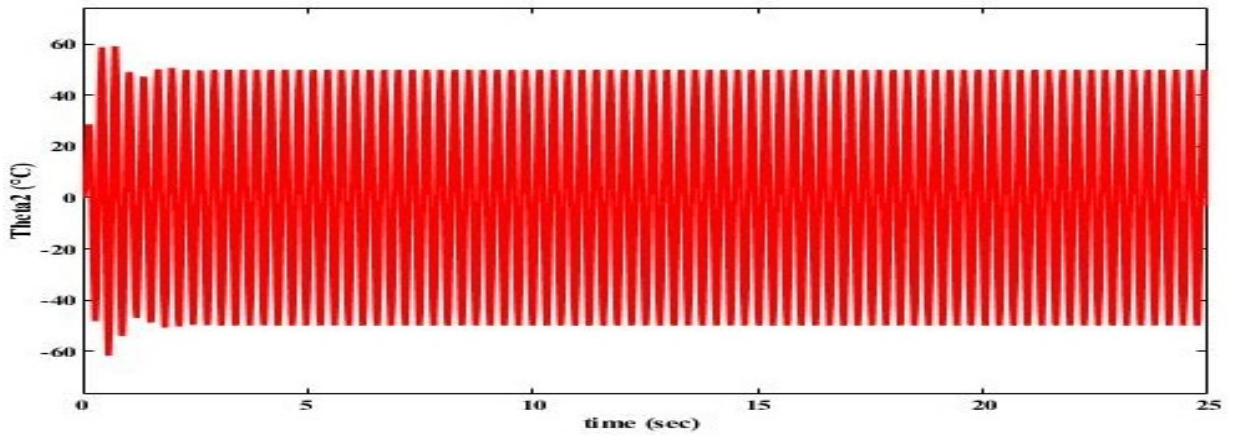
(e)

Figure 15: The closed loop control relative temperature response (θ_2) for M=4, N=6 k=10 and ω = (a) 0.1, (b) 1, (c) 5, (d) 10, (e) 20 rad/sec.
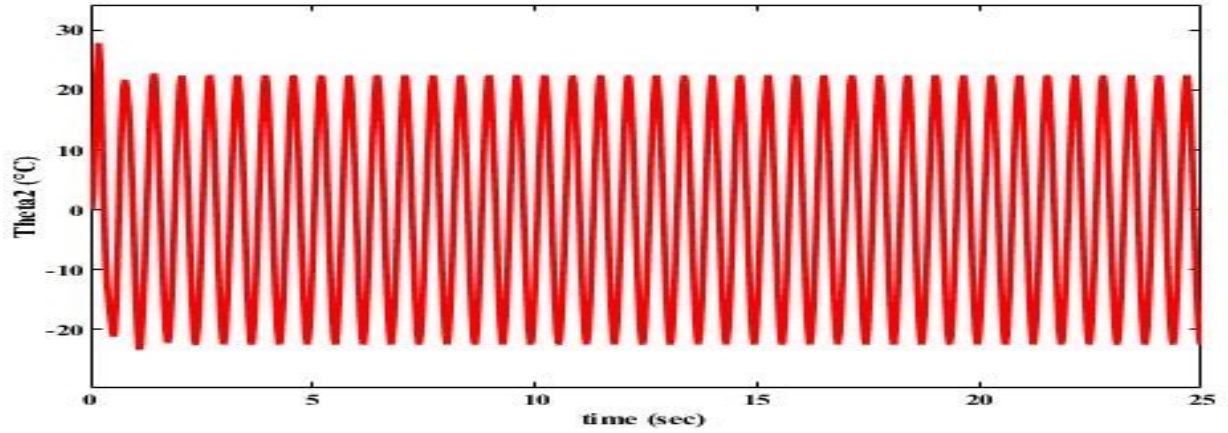
The simulation results in Figure 15, for k=10 represent the relative output temperatures of the closed-loop control θ_2 with N=6, M=4 terms for ω = 0.1, 1, 5, 10 and 20 (rad/sec). The output temperature θ_2 results in Figure 15, for lower frequencies of 0.1 and 1 rad/sec, compared to the desired one, 20 sin(ωt), are very close. The results for output temperature θ_2, for higher frequencies of 5 and 10 rad/sec, compared to the desired one, 20 sinωt, and of the command temperature θ_1, are significantly different. This can be again explained by the very high amplitudes of the output of the inverse problem, shown in Figure 16, which leads

58

eventually to an ill-posed inverse problem at higher frequencies, particularly with regards to

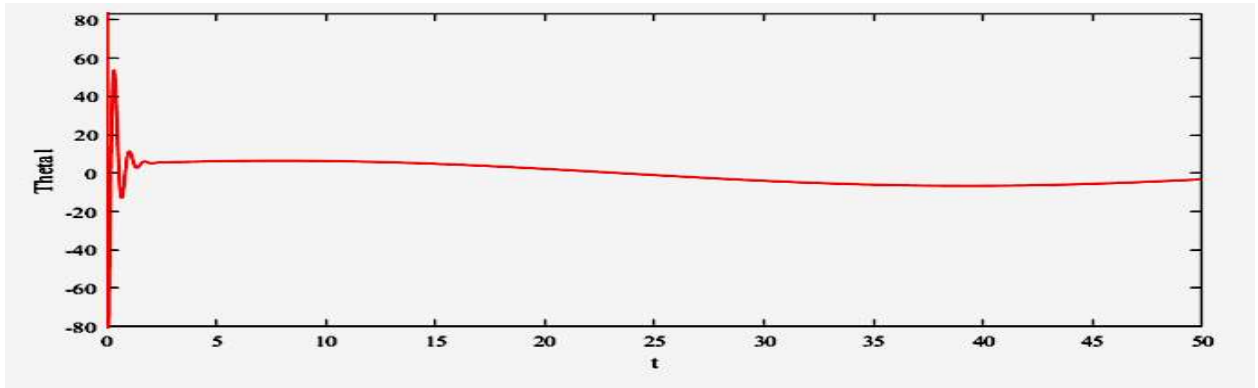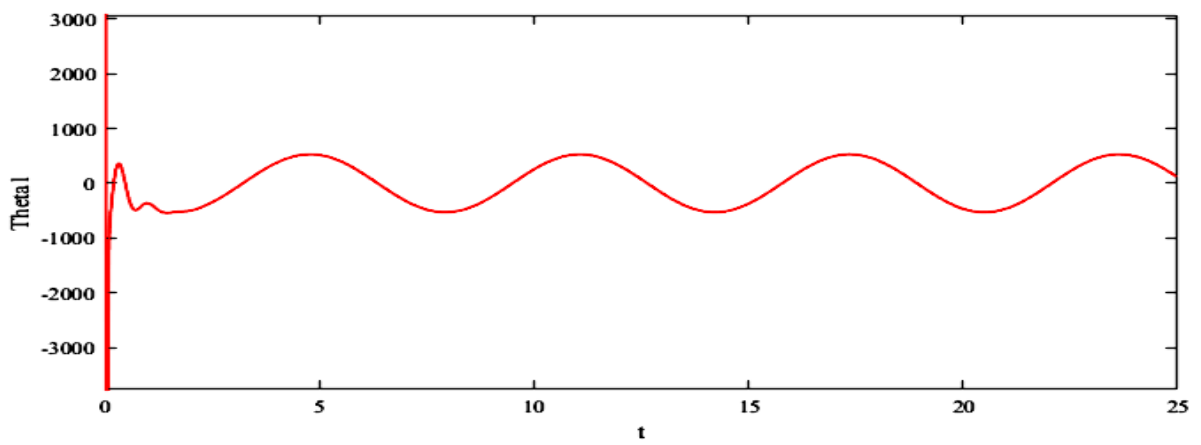parameters L and α uncertainty.

(a)

(b)

(c)

59
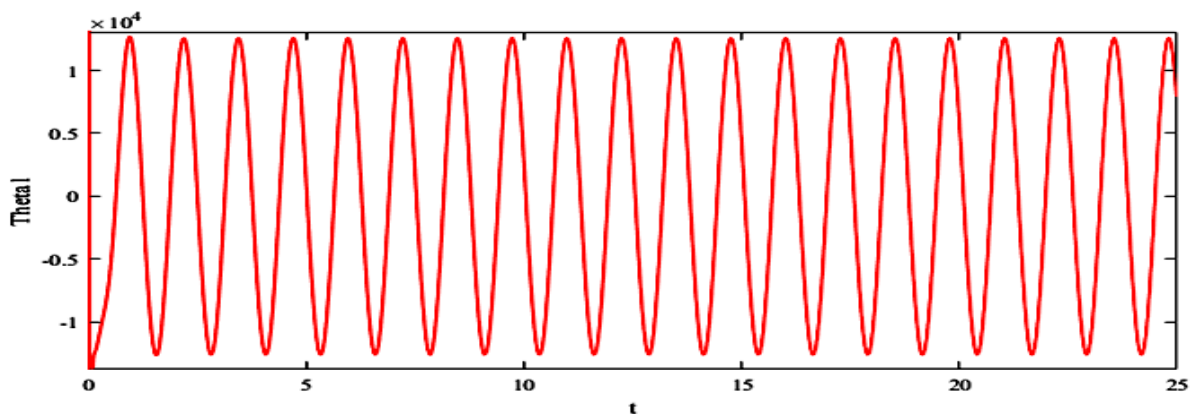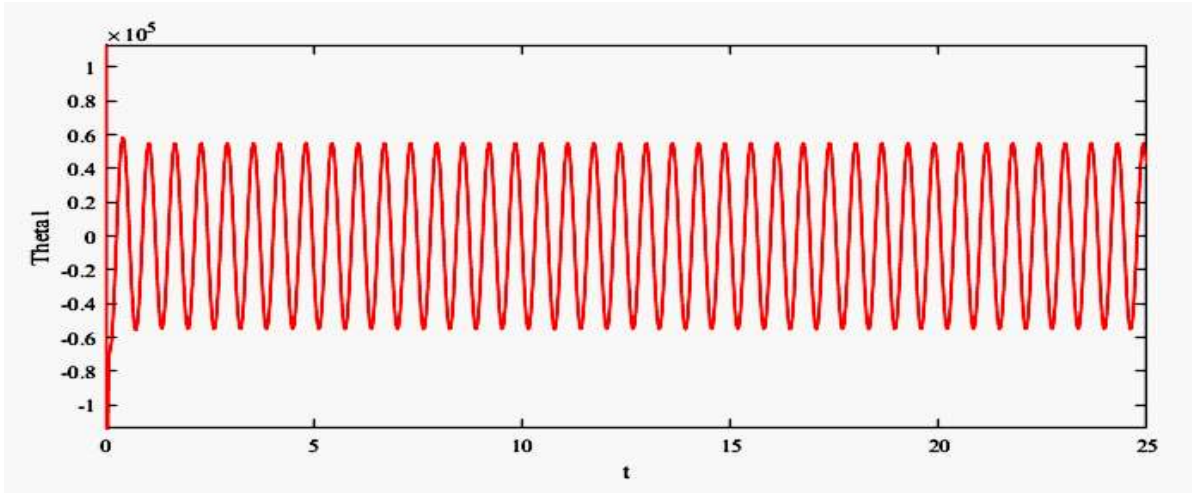
(d)
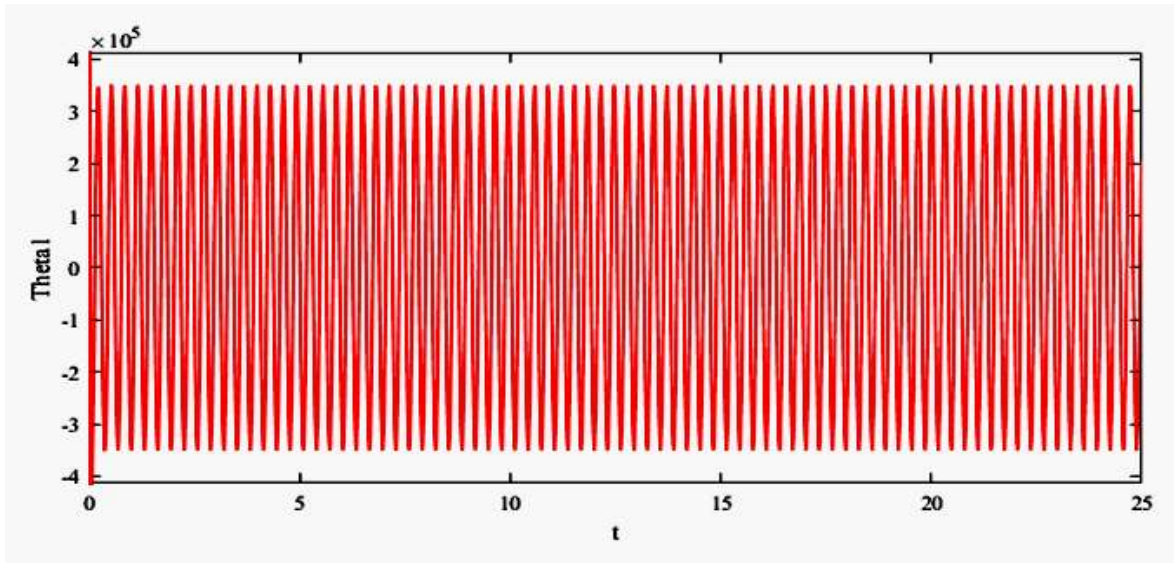
(e)

Figure 16: The inverse problem relative temperature response (θ_1) for M=4, N=6 k=1 and ω = (a) 0.1, (b) 1, (c) 5, (d) 10, (e) 20 rad/sec.

From Figure 16, where the relative temperature response is shown, we see that due to the sudden change of reference temperature from 0 to $20\sin(\omega t)$, there is an initial transient response of temperature that rapidly disappears, which is an unavoidable transient behavior. The high relative temperature shown in results explains the ill-posedness effect of the inverse

60

problem when high frequencies were used. This results in an inverse problem relative temperature response (θ_1) for10 and 20 rad/sec of over 10 000^0 C, obviously unachievable in any experimental study. This makes the results in Figure 15 for 10, and 20 rad/sec equally impossible to verify in experiments. For our simulations and experiments study, we focus on a frequency input in the range of 3 (rad/sec) or less.

Bode diagrams of open-loop control transfer function in Figure 17 explain this by indicating significantly lower magnitudes for $\omega > 11$ rad/sec in Figure (17) (a) for k=1 and for $\omega >20$ rad/sec in Figure 17 (b) for k=10. In the case of the open-loop control, since there is no feedback from the output, parameter uncertainty and disturbance effects cannot be reduced. Figure 17 shows the Bode diagram of the closed-loop control transfer function for N=6 and M=4 and k=1 in (a) and k=10 in (b).
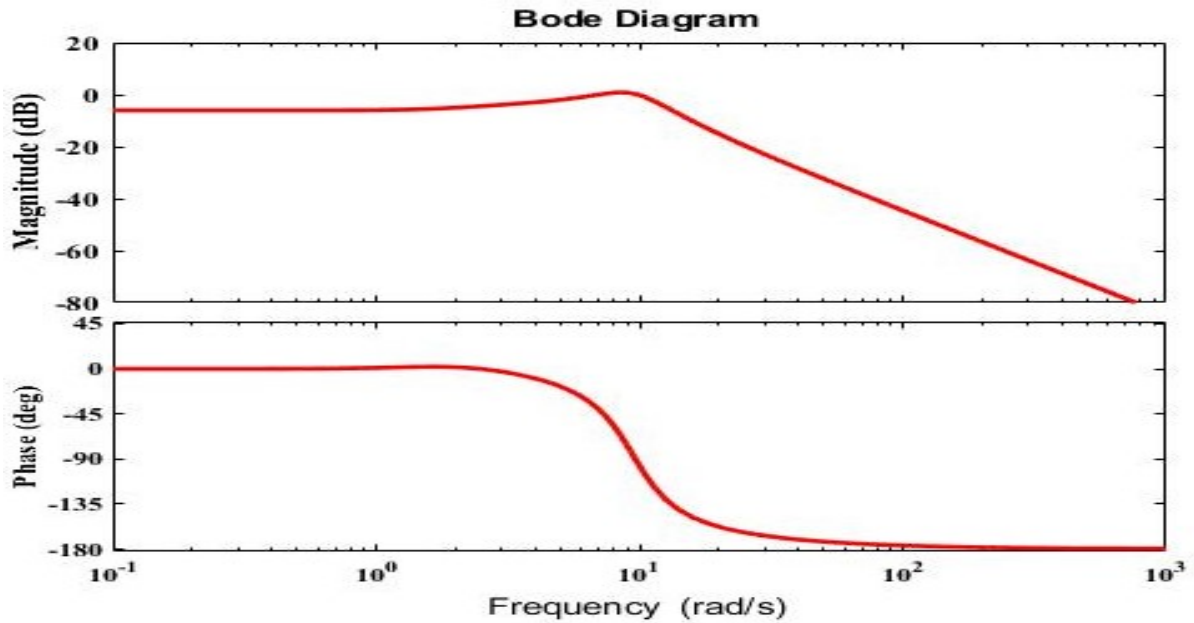
(a)
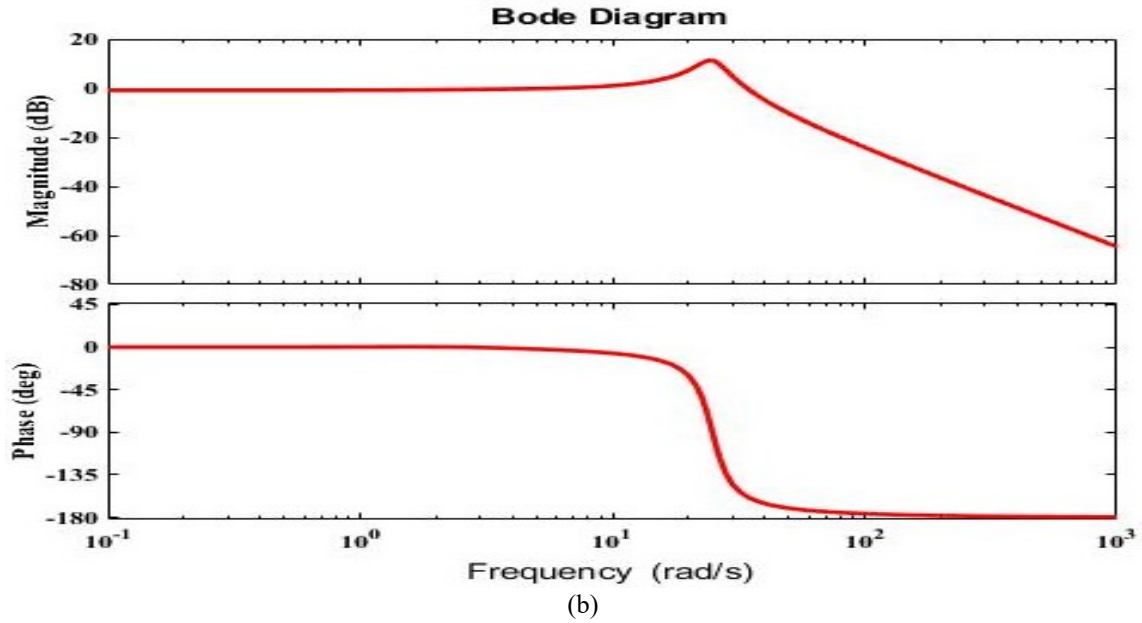
Figure 17: Bode diagram of the closed loop control transfer function for N=6 and M=4.and (a) k=1and (b) k=10.

Bode diagram of the closed-loop control transfer function shows the bandwidth increases from cca 10 to cca 20 rad/s when k changes from 1 to 10.

4.2.2 Zero-Pole Expansion

For a controller with gain $G_c = 1$, Figure 18 (a - f) shows the inverse problem response, which starts a rapid increase while increasing the frequency.

In fact, for an ideal inverse problem

$$G_2^{-1} = G_1$$

And $G_c = 1$, the feedforward transfer function is 1 and the closed-loop output is $\frac{1}{1+1} = 0$.

The amplitude of the output is half the desired one. From Figure 19 (a - f), the closed-loop response for a controller with gain $G_C = 10$ is almost the same as the desired value. Figures 18 and 19 introduced here to show the effect of controller gain on the relative temperature response, the simulations were carried out for different frequencies, to show that the controller works regardless of the frequency input. The simulations used here just for controller verification, given that we know that the high frequency cannot be physically achievable due to the slow rate of heat transfer in a plate.
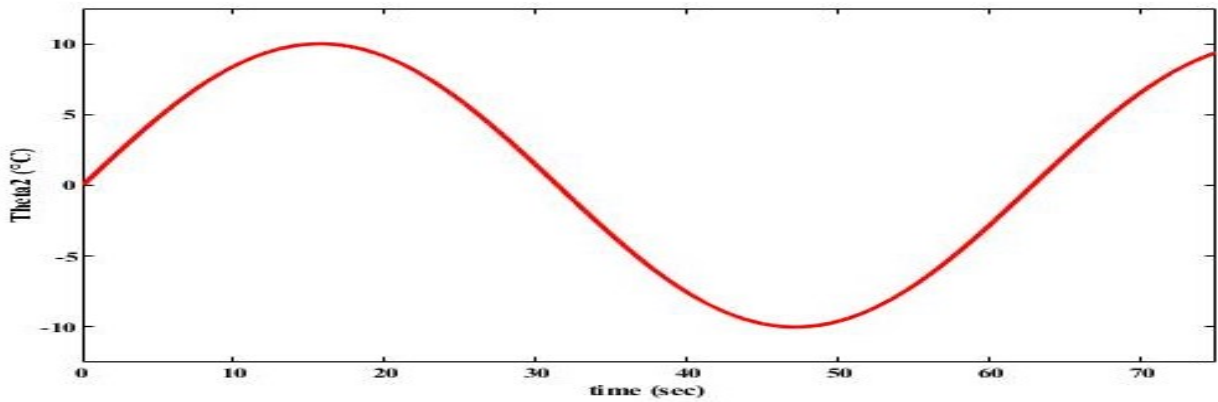
a
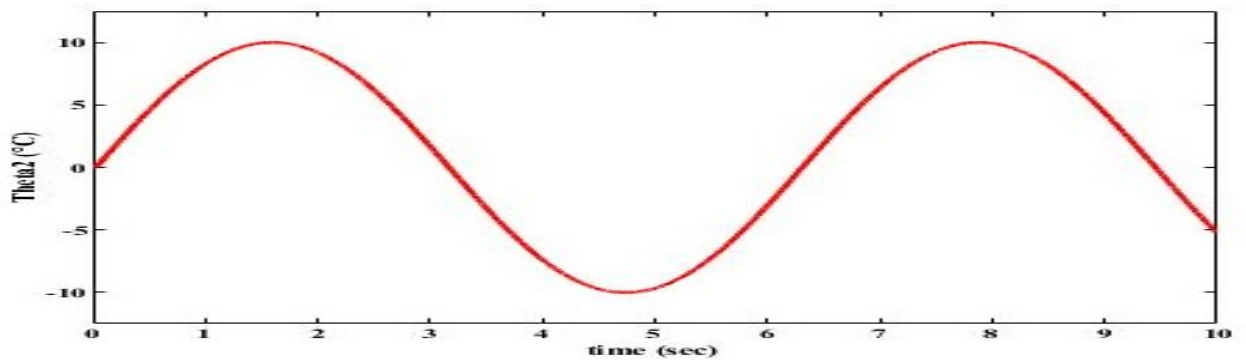
b
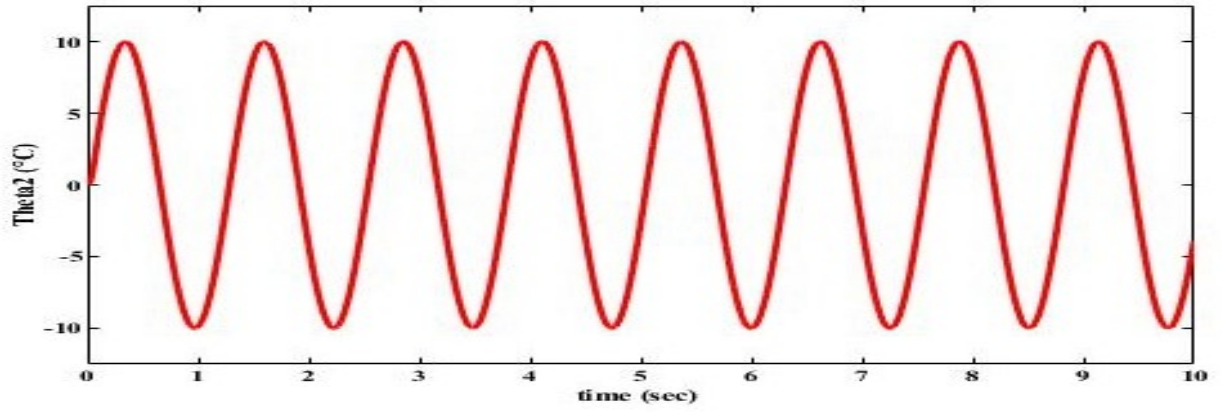
c
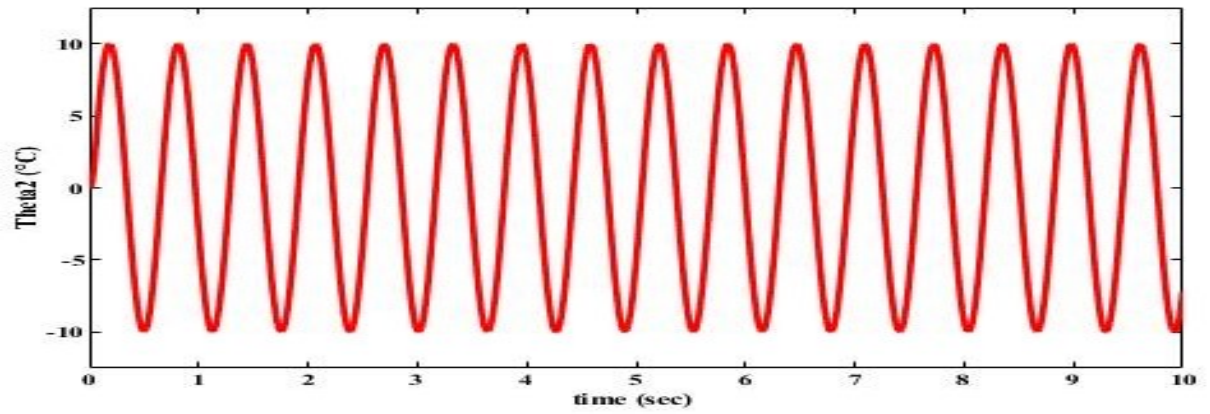
d
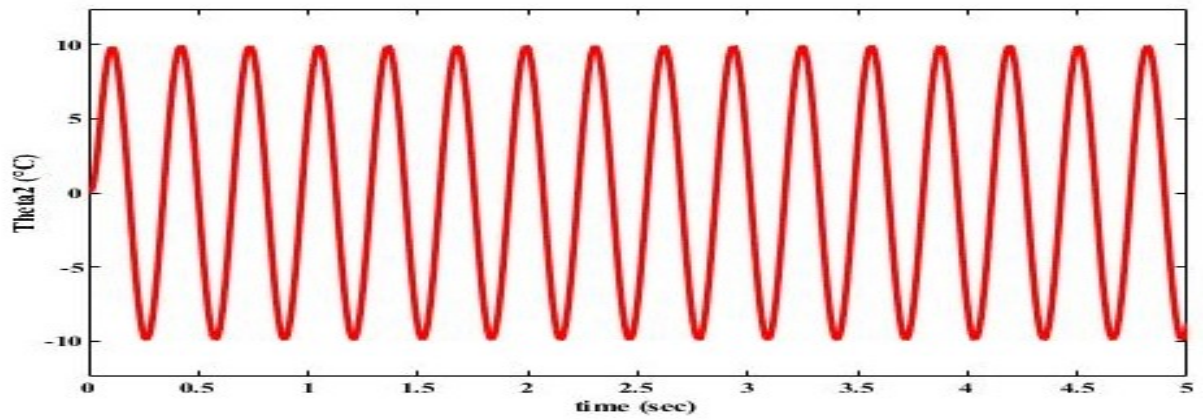
e
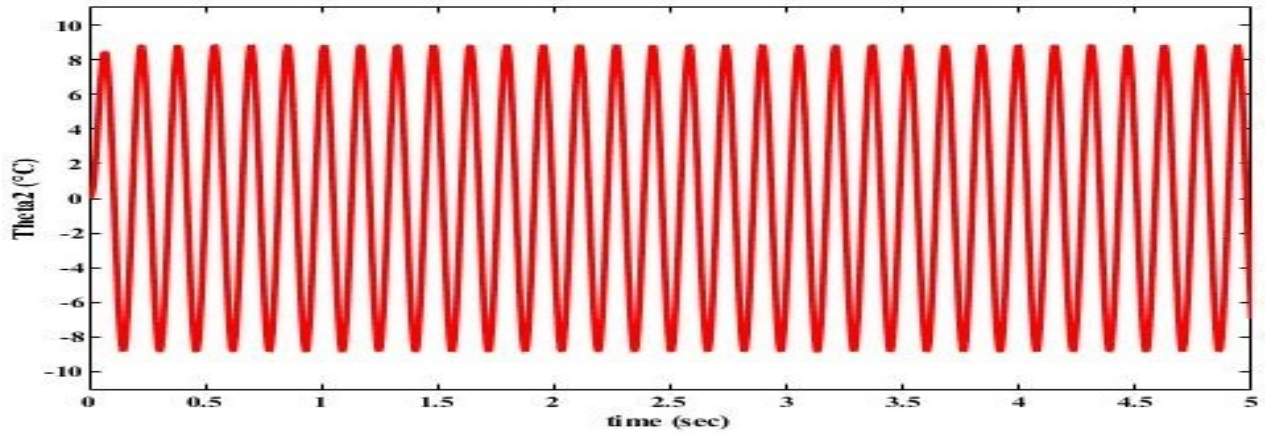
f

Figure 18: The closed loop control relative temperature response (θ_2) for M=4, N=6, gain=1, and ω = (a) 0.1, (b) 1, (c) 5, (d) 10, (e) 20, (f) 40 rad/sec.

a

b

65
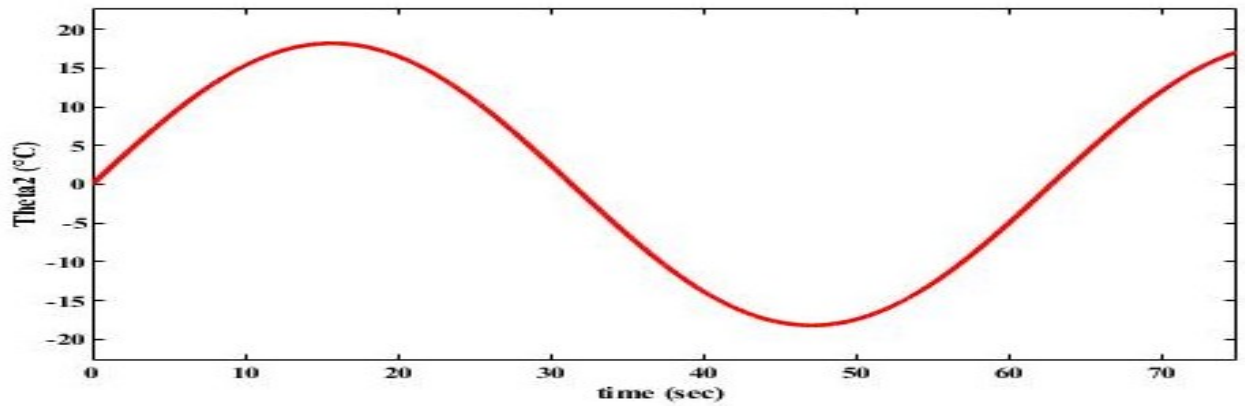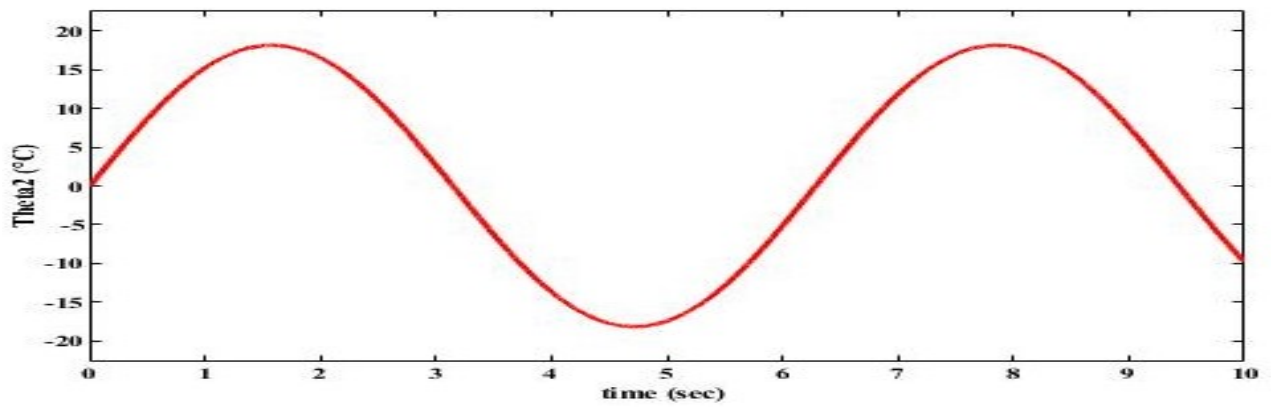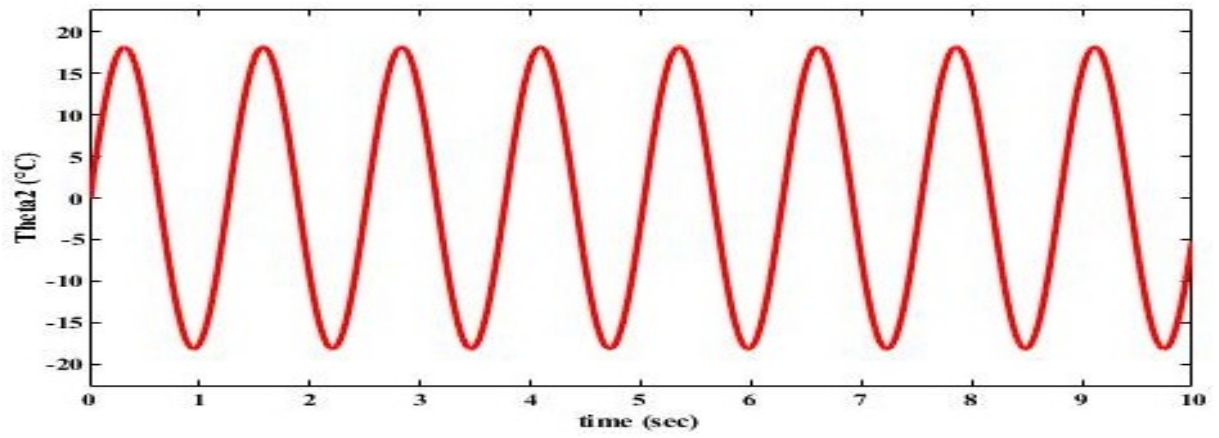
c
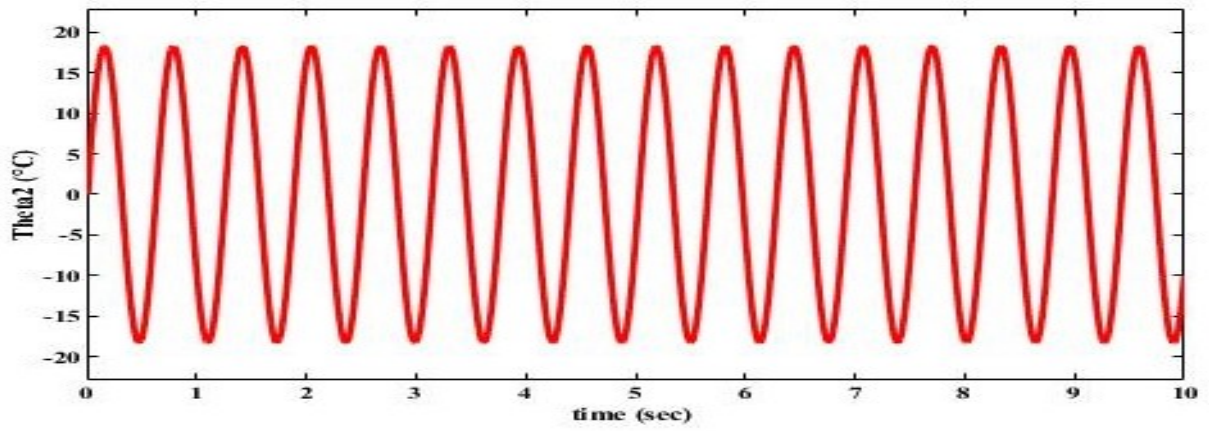
d
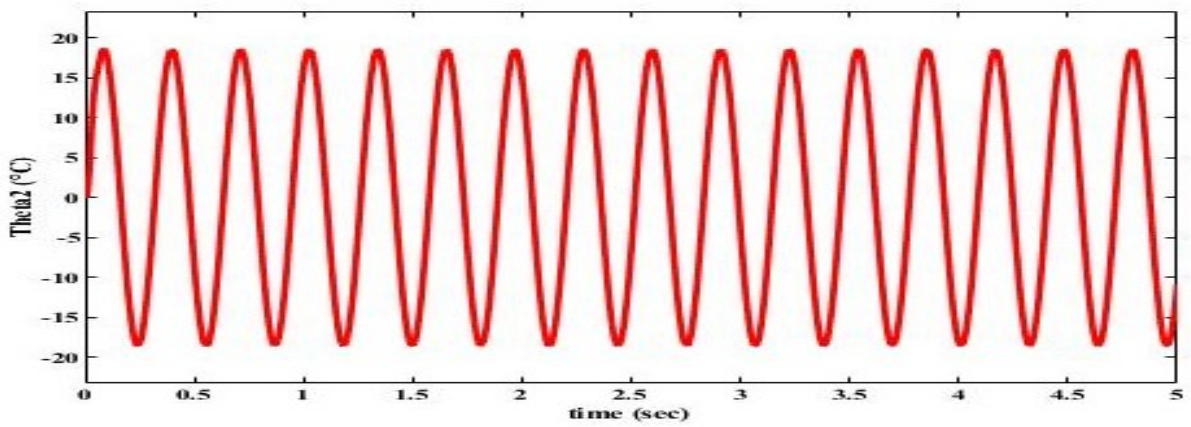
e
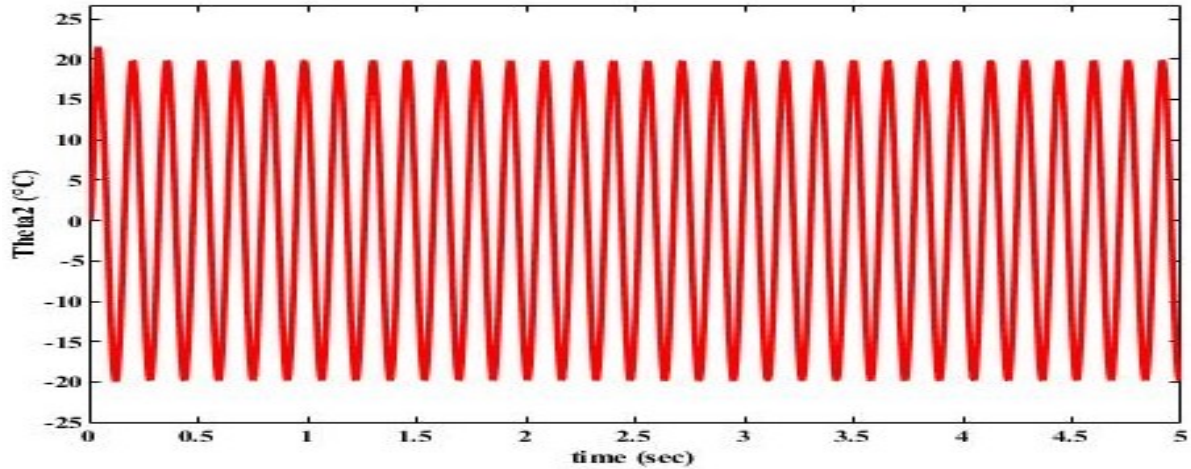
f

Figure 19: The closed loop control relative temperature response (θ_2) for M=4, N=6, gain=10, and ω = (a) 0.1, (b) 1, (c) 5, (d) 10, (e) 20, (f) 40 rad/sec.

The closed-loop control relative temperature response (θ_2) for k=1 and for ω = 0.1, 1, 5, 10, 20 rad/sec is shown in Figure 18, and the amplitude is approximately 0.5 of the desired amplitude. This is explained by the closed-loop output for $G_2^{-1} = G_1$ such that the output is $\frac{1}{1+1}$ = 0.5. The closed-loop control relative temperature response (θ_2) for k=10 and for ω = 0.1, 1, 5, 10, 20 (rad/sec) in Figure 19 shows that the amplitude is about the same as the desired amplitude, including for 40 (rad/sec).

4.3 Comparison of Zero-Pole Expansion and Taylor Expansion

The goal in this comparison of the two expansions is to determine which expansion serves better for the current research problem. Root locus plots for the inverse problem transfer function using both Zero-Pole and Taylor expansion, for a different number of terms, were

67

obtained using Matlab^TM. The results are shown in Figures 20, 21, 22, and 23 for three, four, five, and six terms respectively:
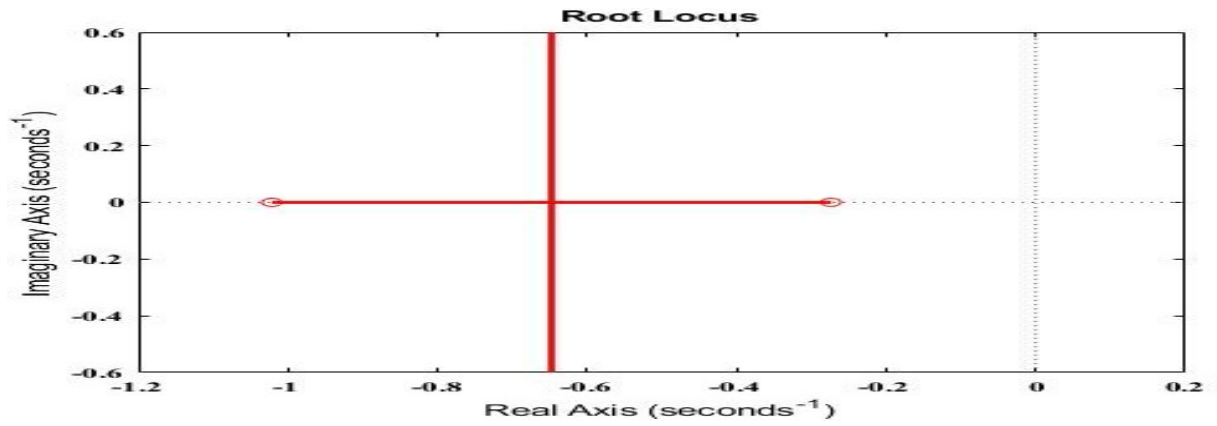
(a)
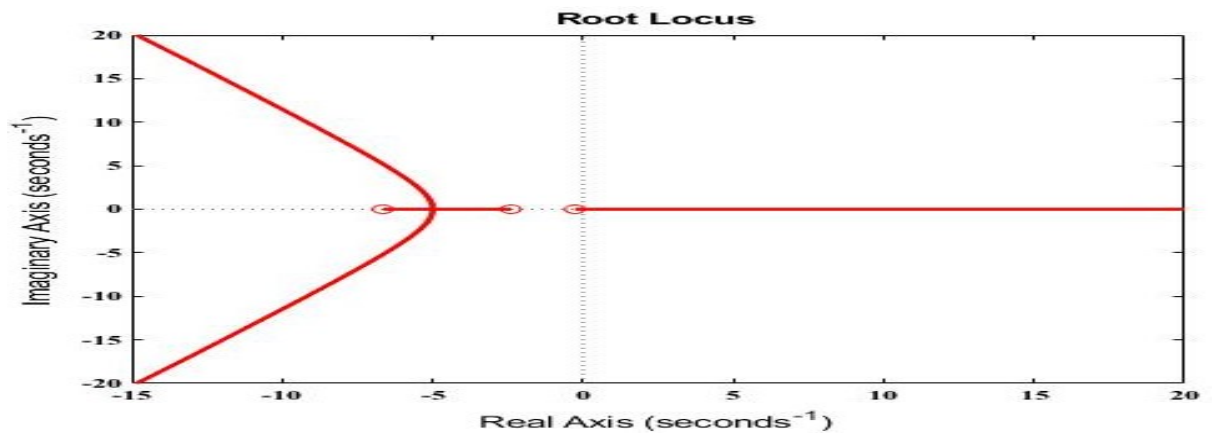
(b)

Figure 20: Root locus plots for the inverse problem with three terms transfer function: (a) Taylor expansion, (b) Zero-Pole expansion.
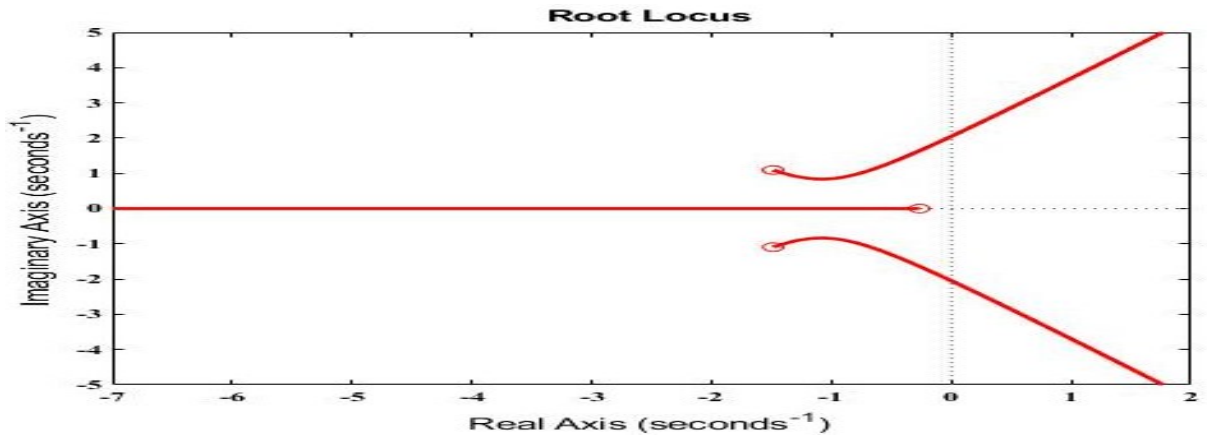
(a)
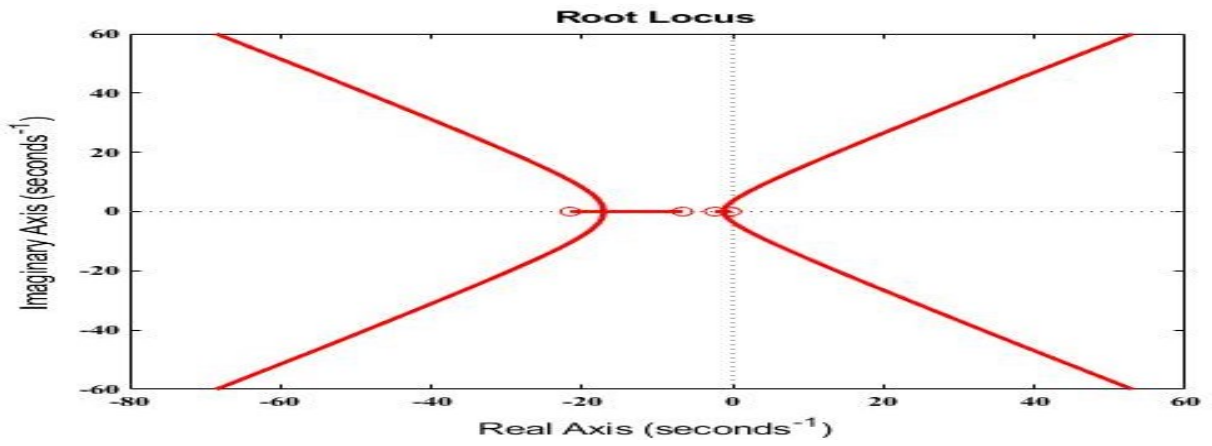
(b)

Figure 21: Root locus plots for the inverse problem with four terms transfer function: a) Taylor expansion, b) Zero-Pole expansion.
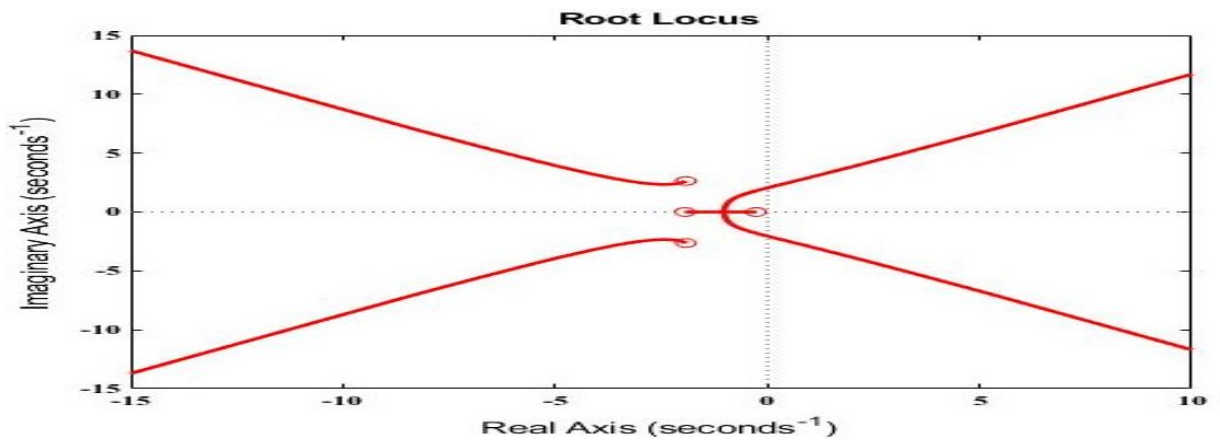
(a)
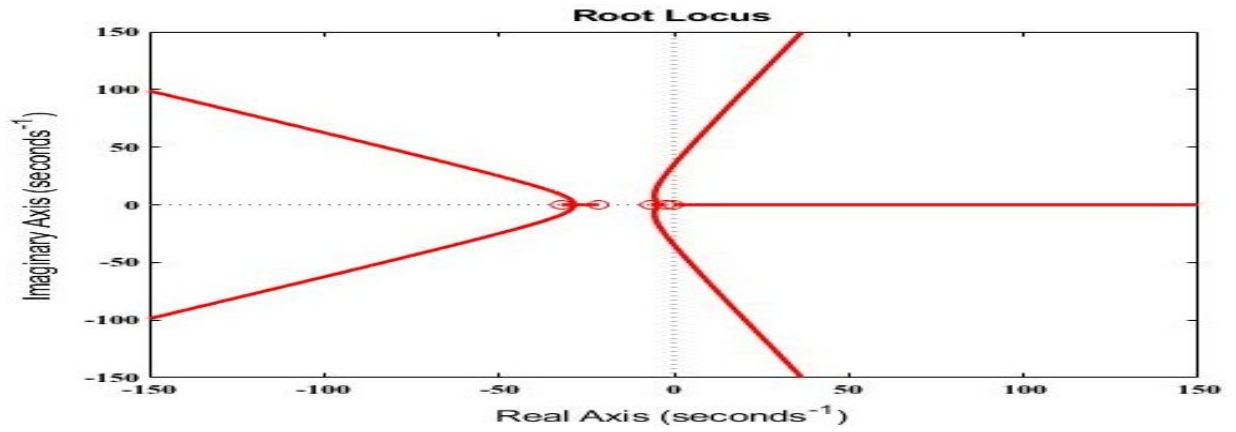
(b)

Figure 22: Root locus plots for the inverse problem with five terms transfer function: (a) Taylor expansion, (b) Zero-Pole expansion.
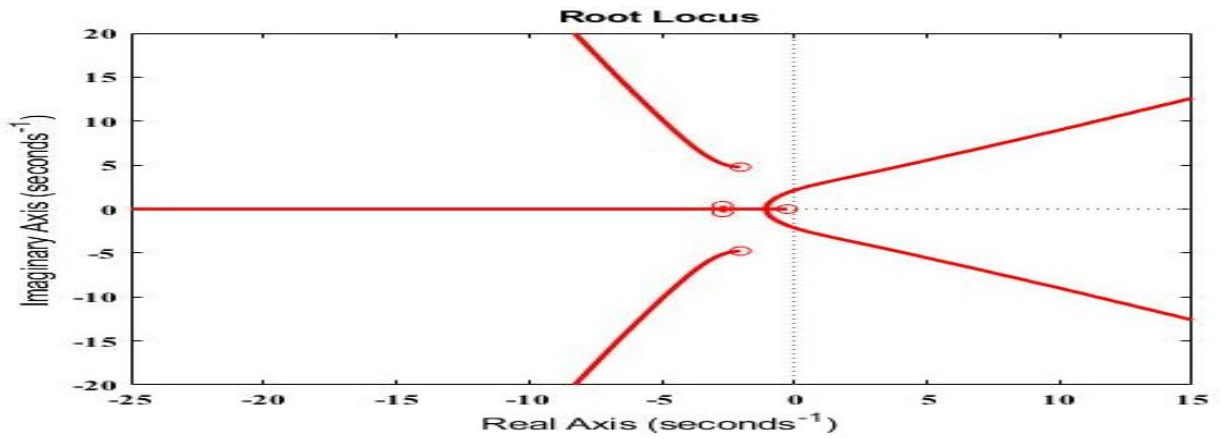
(a)
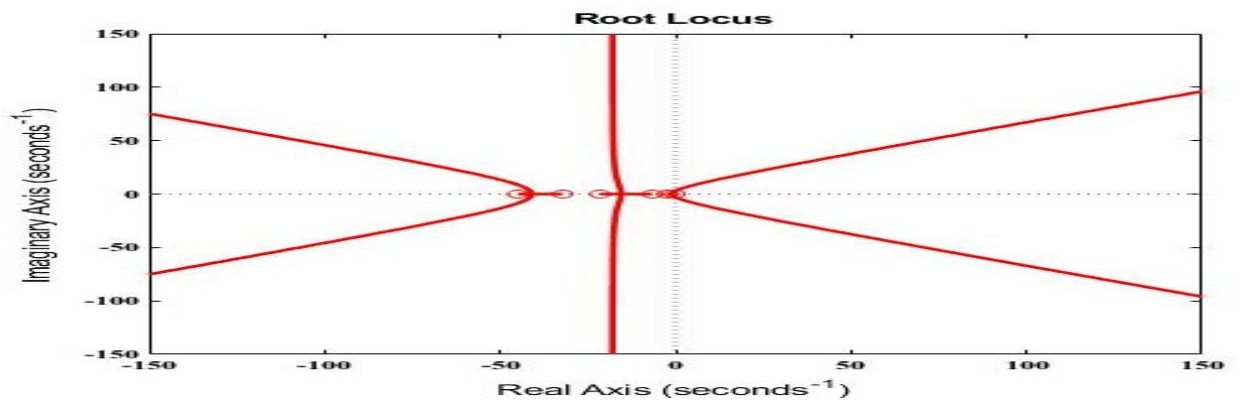
(b)

Figure 23: Root locus plots for the inverse problem with six terms transfer function: (a) Taylor expansion, (b) Zero-Pole expansion.

Figure (20-a) to Figure (23-a) shows that for Taylor expansion, the plots are much closer to the imaginary axis than the plots for Zero-Pole expansion in Figure (20-b) to Figure (23-b). This indicates that Zero-Pole expansion is much more stable than the use of a Taylor expansion.

The second investigation to do is to see the effect of the number of terms used in the transfer function expansion to represent the inverse problem over the ill-posedness of the inverse problem. Bode plots for the inverse problem transfer function using a different number of terms are shown in Figure 24.

(a)

(b)

(c)

(d)

72
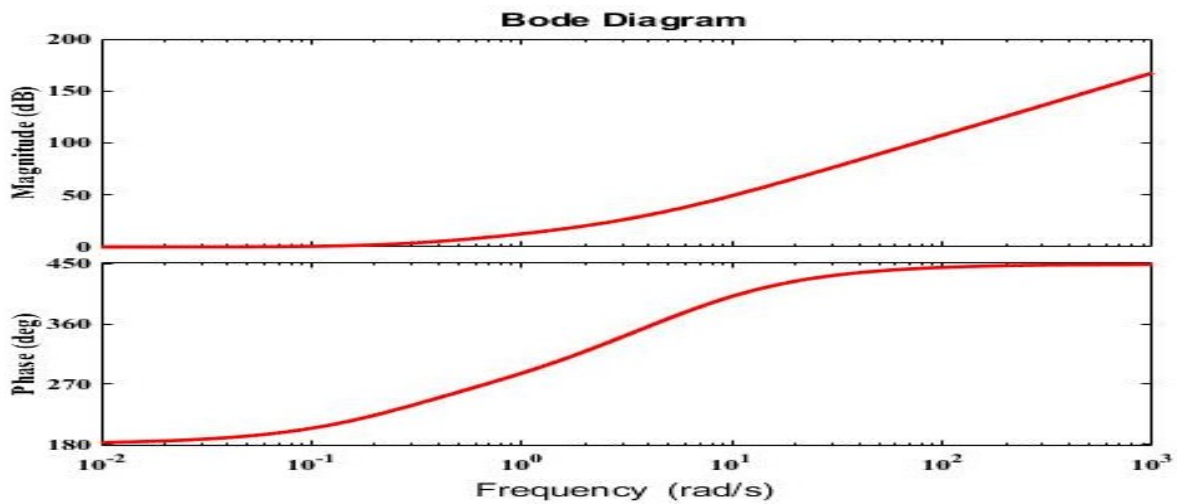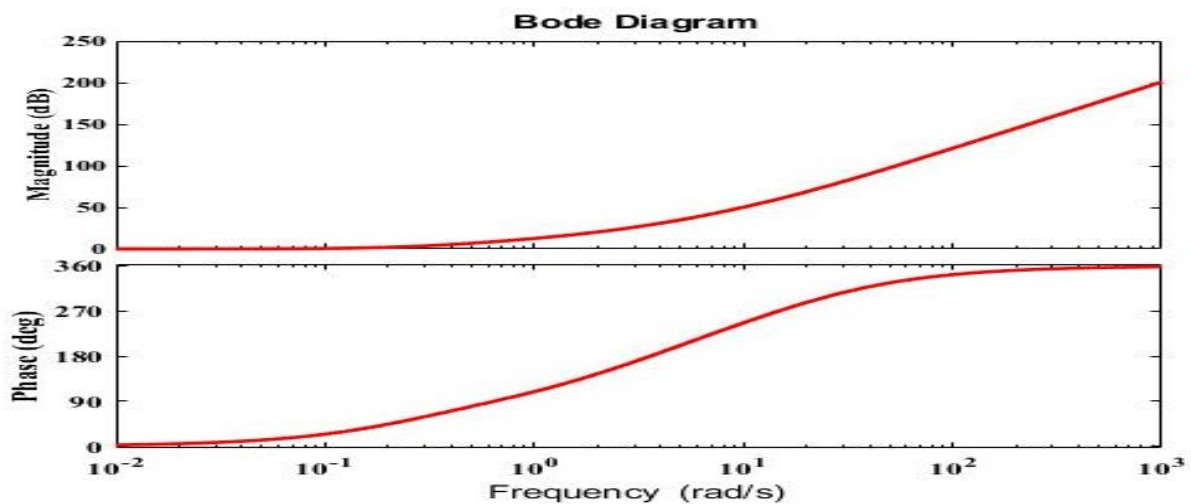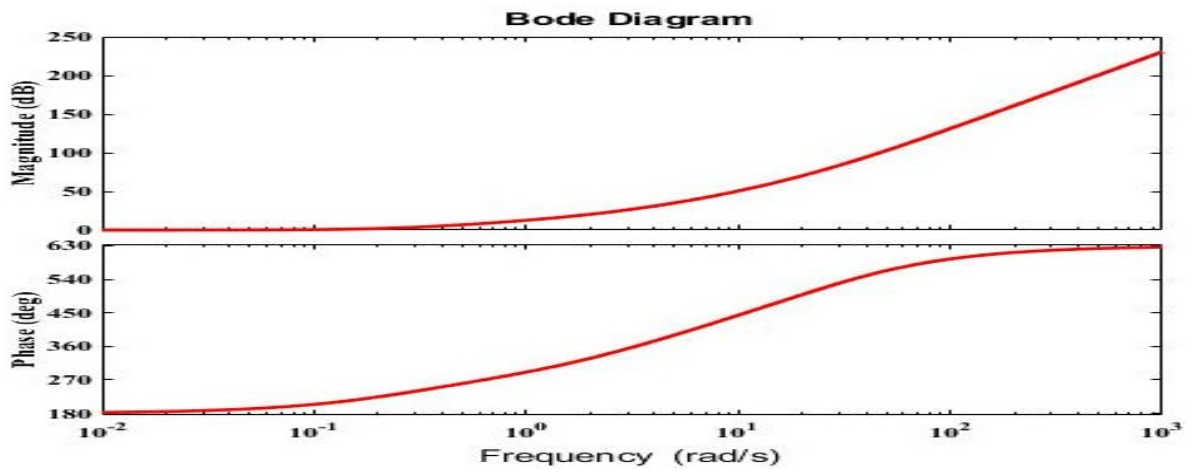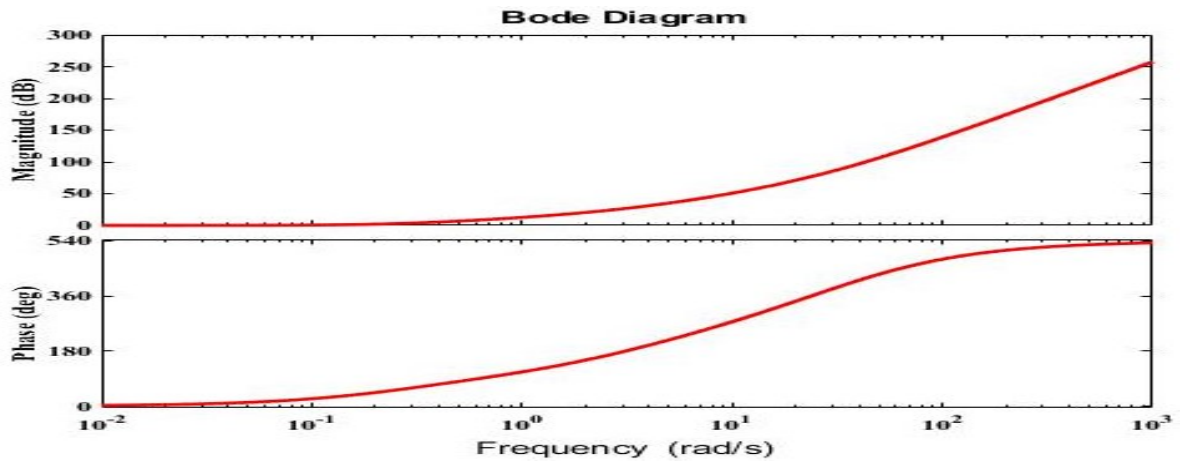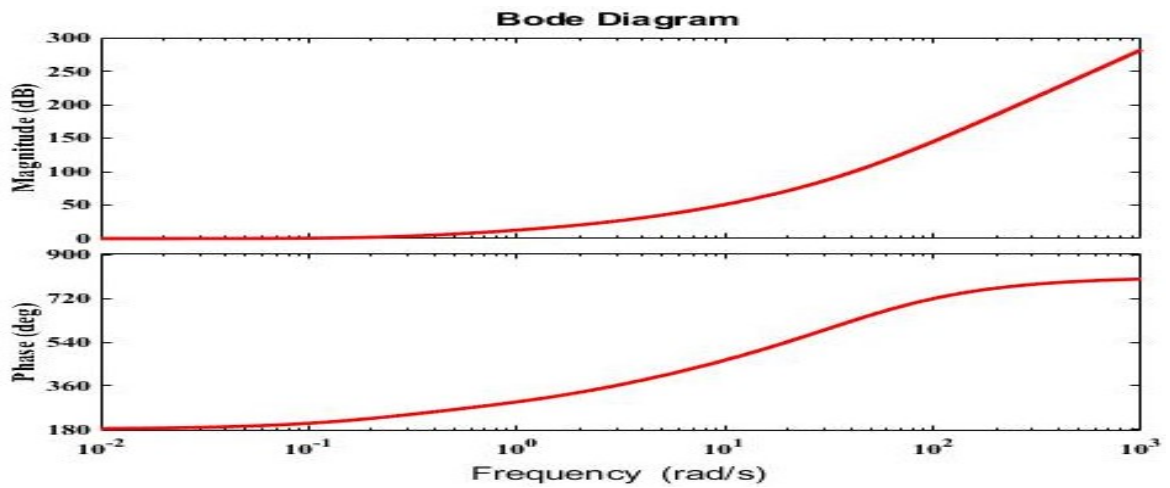
Figure 24: Bode plots for the inverse problem with different number of terms used in the transfer function: (a) 3, (b) 4, (c) 5, (d) 6, (e) 7.

Figure 24 shows that as the number of terms in the transfer function increases, both the magnitude and the phase start to increase at an earlier value of frequency and reach higher values as well. A suitable number of terms for the inverse problem has been chosen to achieve an acceptable degree of ill-posedness in the inverse problem. The degree of ill-posedness always plays a major factor in the inverse problem solutions. This is why the results in Figure 24 are important because they give us a simple way of evaluating the degree of ill-posedness of an inverse problem using the number of terms as a factor.

4.4 Two-layer Plate Results:

In this section, we will study a plate of two layers dissimilar instead of the single-layer plate. This was done as a preliminary study of multilayer plates.

4.4.1 Bode plot results:

We simulate based on the transfer functions from Equations (3.51) and (3.52) for different values of plate thickness (0.01, 0.02, 0.03, 0.04, and 0.05) m, and we obtain the Bode diagram for these values for thickness.

The simulations were done for a two-layer, one of aluminum and the other of aluminum alloy 2024 T6 with the following properties:

$$k_1 = 237 \ \left(\frac{W}{m.K}\right) \qquad and \quad \propto_1 = 9.715e^{-5} \ (\frac{m^2}{sec})$$

$$k_2 = 177 \ \left(\frac{W}{m.K}\right) \qquad and \quad \propto_2 = 7.3e^{-5} \ (\frac{m^2}{sec})$$
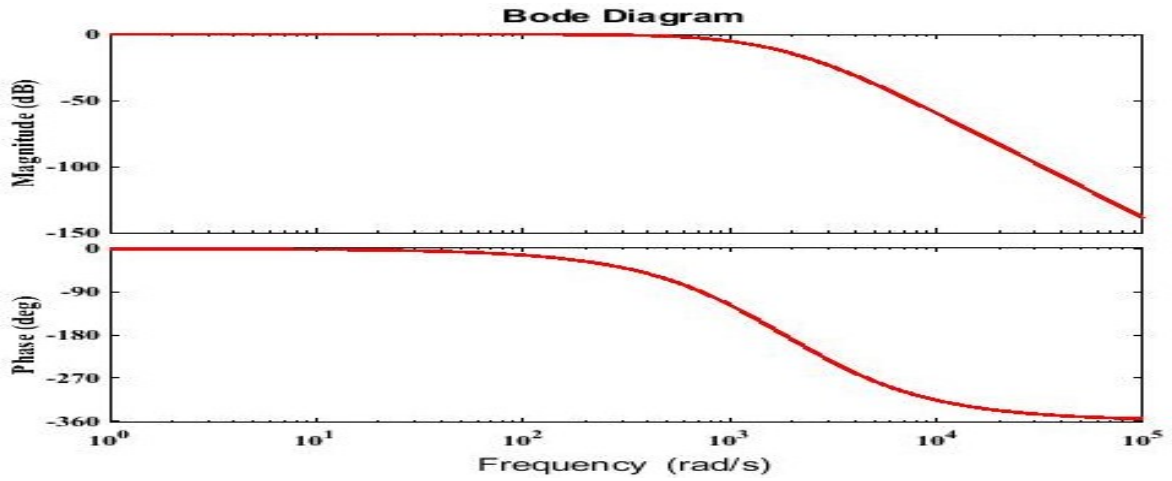
Figure 25: Bode plot for the open-loop with M=4, N=8, and L=0.01 m.
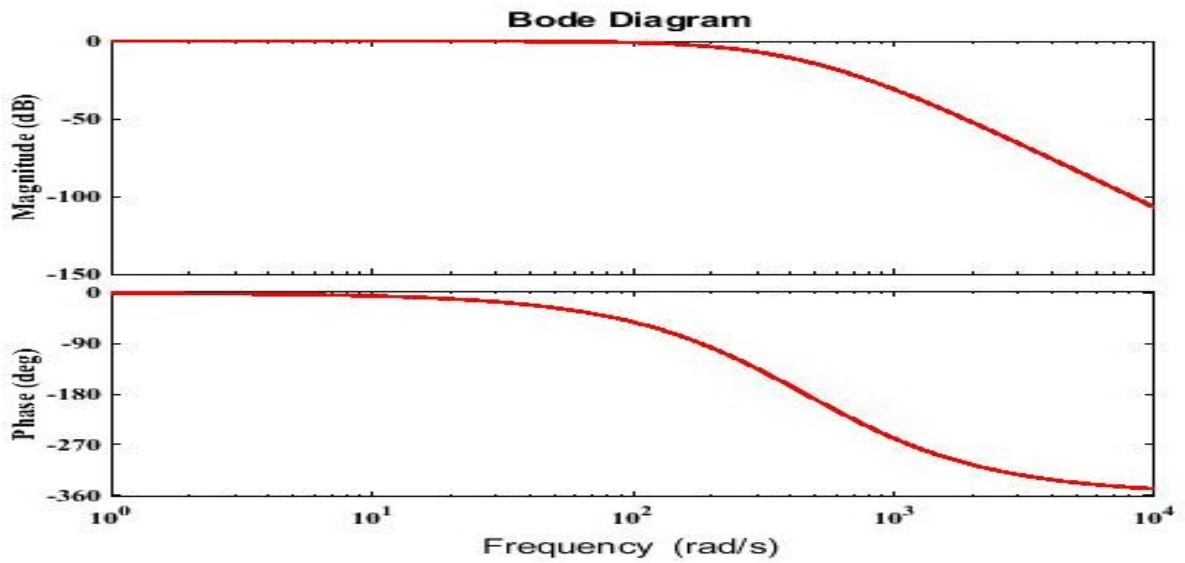
Figure 26: Bode plot for the open-loop with M=4, N=8, and L=0.02 m.
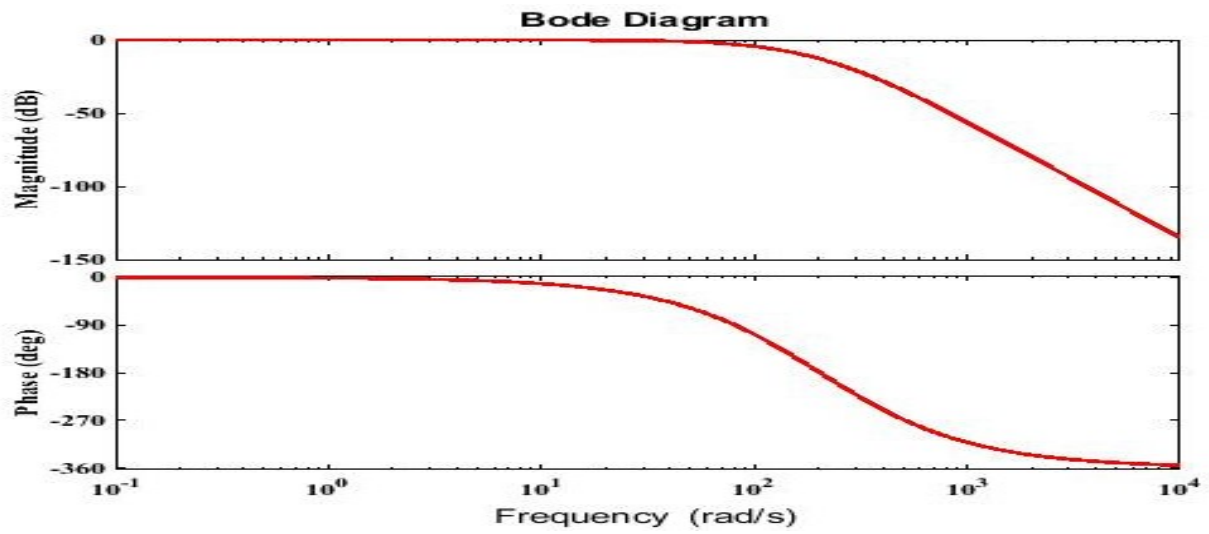
Figure 27: Bode plot for the open-loop with M=4, N=8, and L=0.03 m.
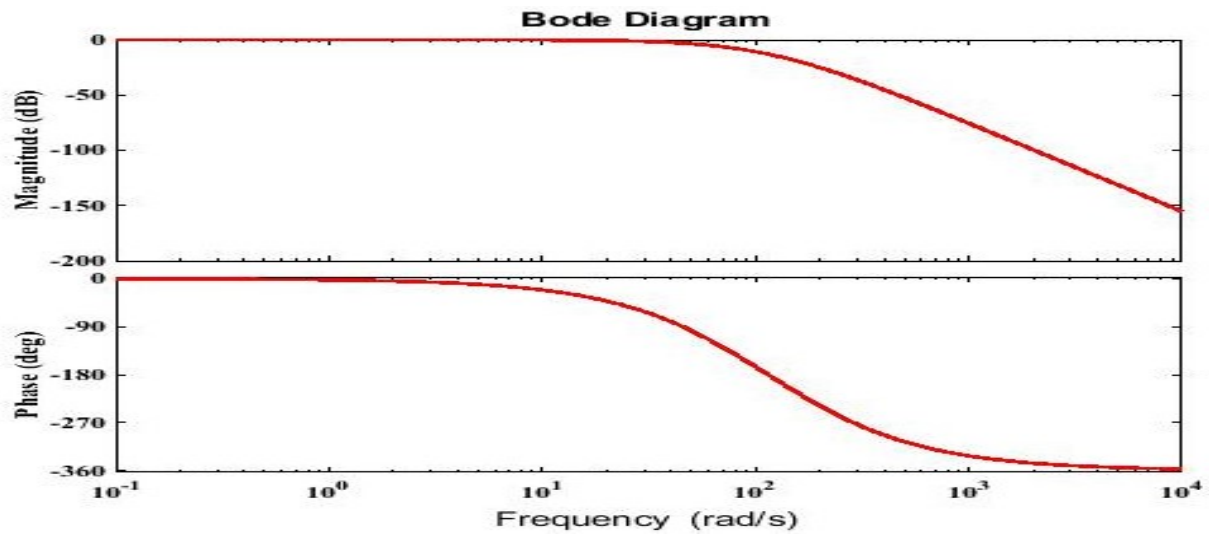
Figure 28: Bode plot for the open-loop with M=4, N=8, and L=0.04 m.
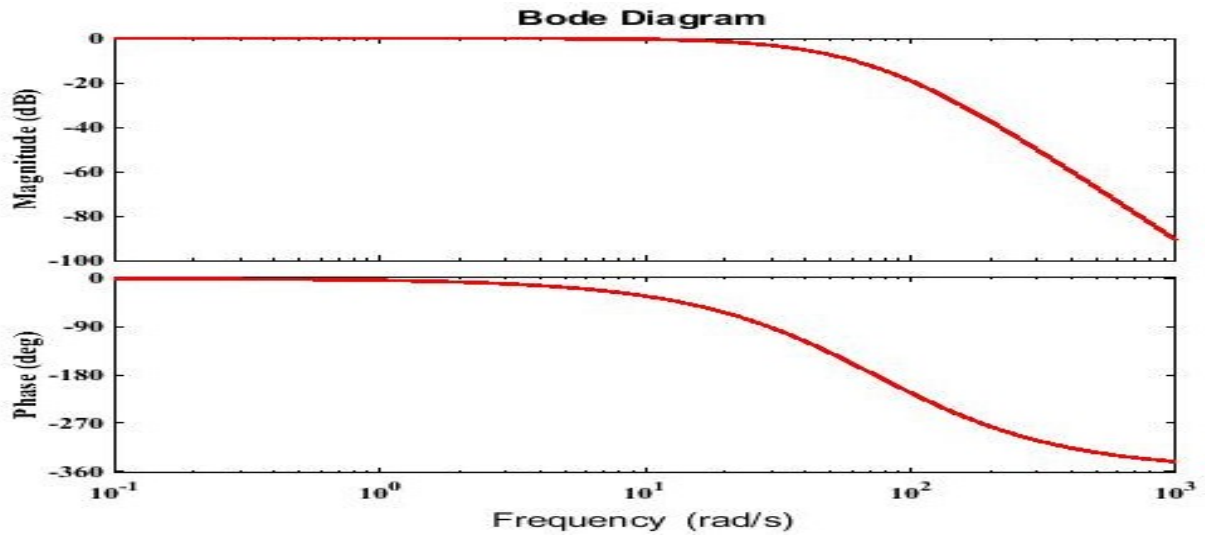
Figure 29: Bode plot for the open-loop with M=4, N=8, and L=0.05 m.

From the above Figures (25 – 29), we see that the bandwidth decreases significantly with the increase of plate thickness L.

Next are presented the results of the simulations for the open-loop and closed-loop cases when using the inverse problem transfer function.

4.4.2 Open Loop Case

We use L = 0.03 (m), M=4 terms, and N=8 terms where M is the number of terms in the inverse problem transfer function, while N is the number of terms in the direct problem transfer function. The results of the open-loop control approach are shown in Figure 30.

a

b

c

d

e

f

g
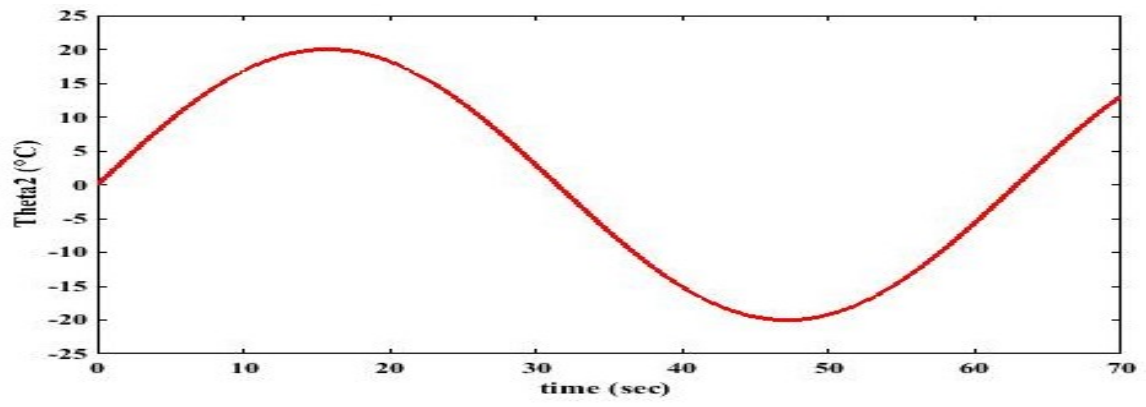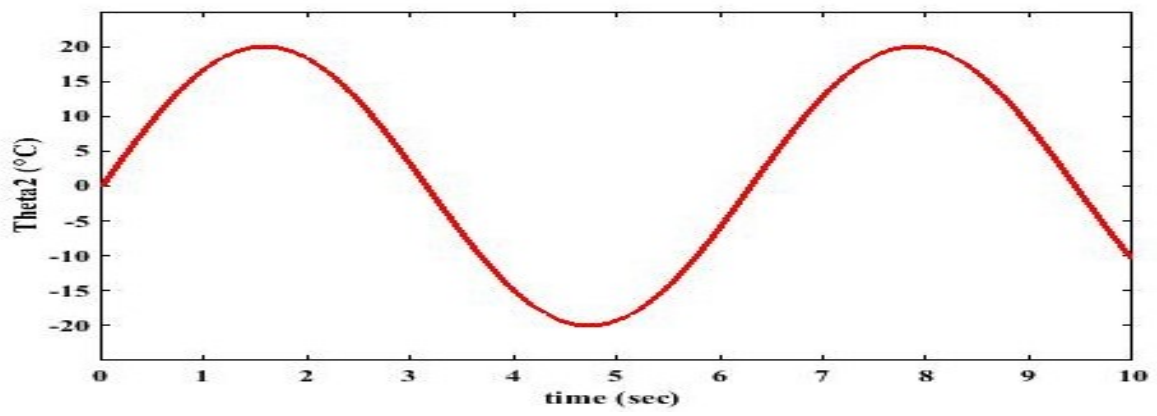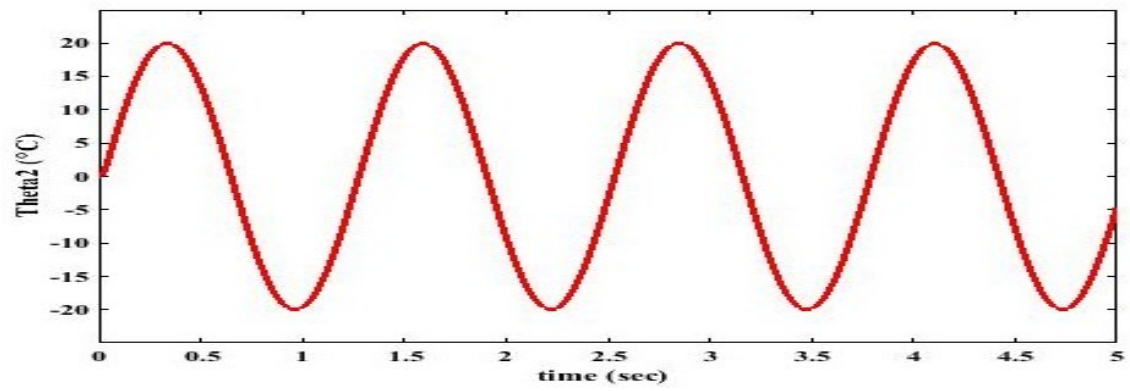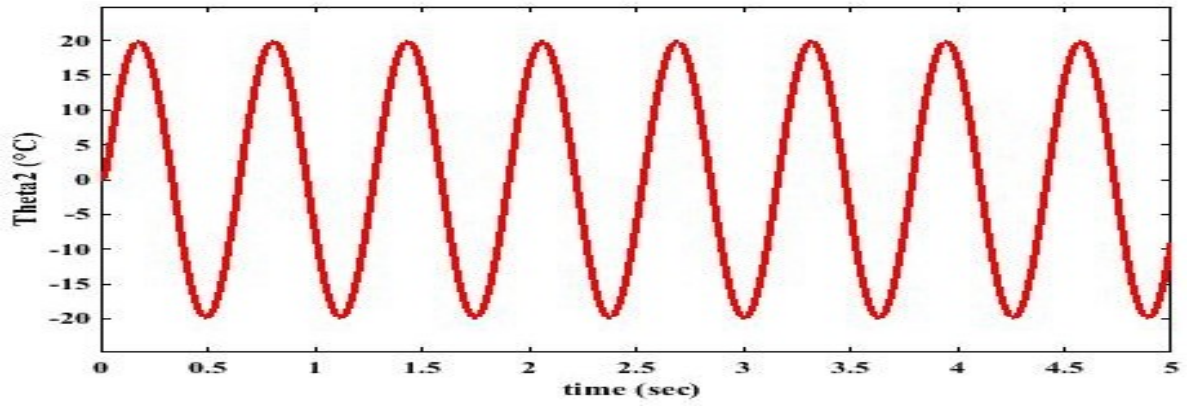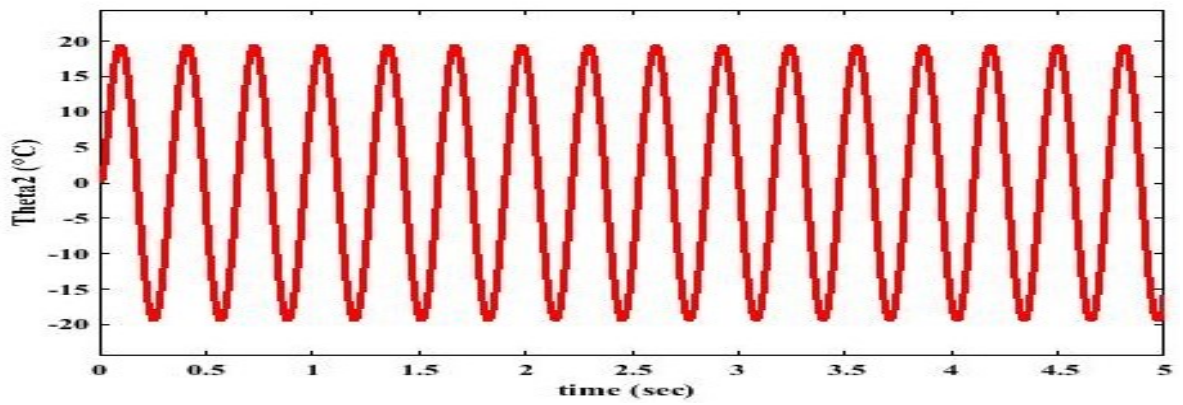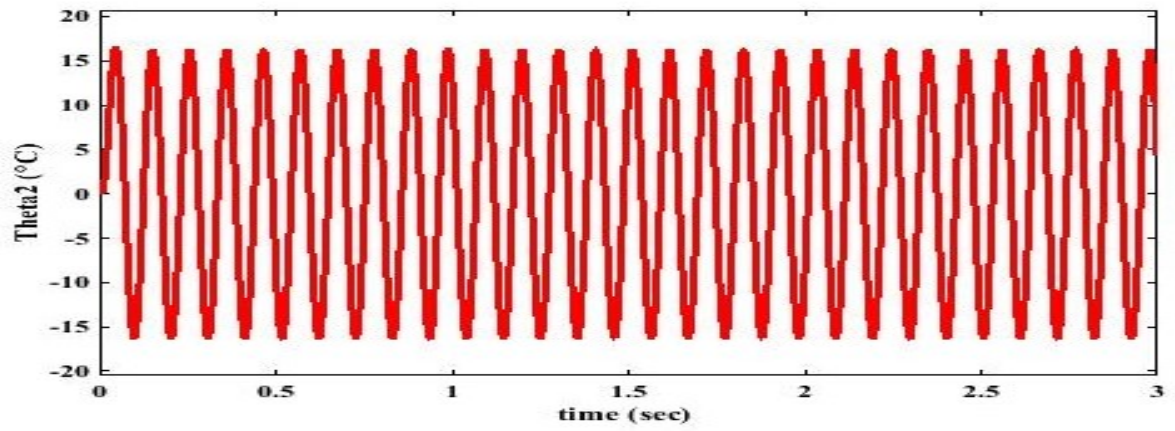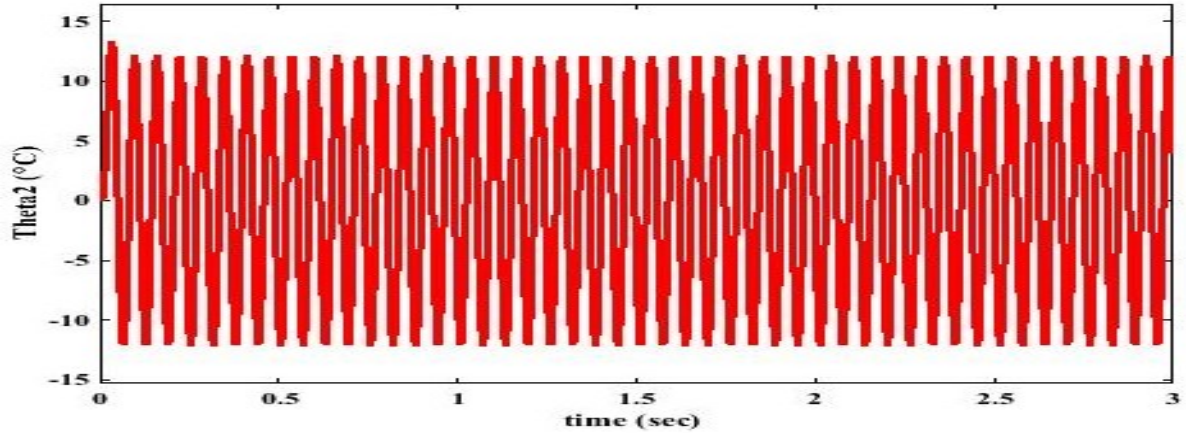
Figure 30: Relative temperature (θ_2) for the open-loop M=4, N=8 and frequency of a) 0.1, b) 1, c) 5, d) 10, e) 20, f) 60, g) 100 (rad/sec).

From Figure 30 (a-e), we see that the open-loop response is almost the same as the desired value where the frequency is less than 20 rad/sec, while from Figure 30 (e-f), we see that the response starts to decrease for higher frequency. In fact, as in the case of a single layer plate, the results for 20, 60, and 100 rad/sec can be obtained only with very high values of the temperature (θ_1), the command generated by the inverse problem transfer function.

4.4.3 Closed Loop Case

For L= 0.03 (m), M=4, and N=6, the results for the closed-loop case are shown in Figure 31.
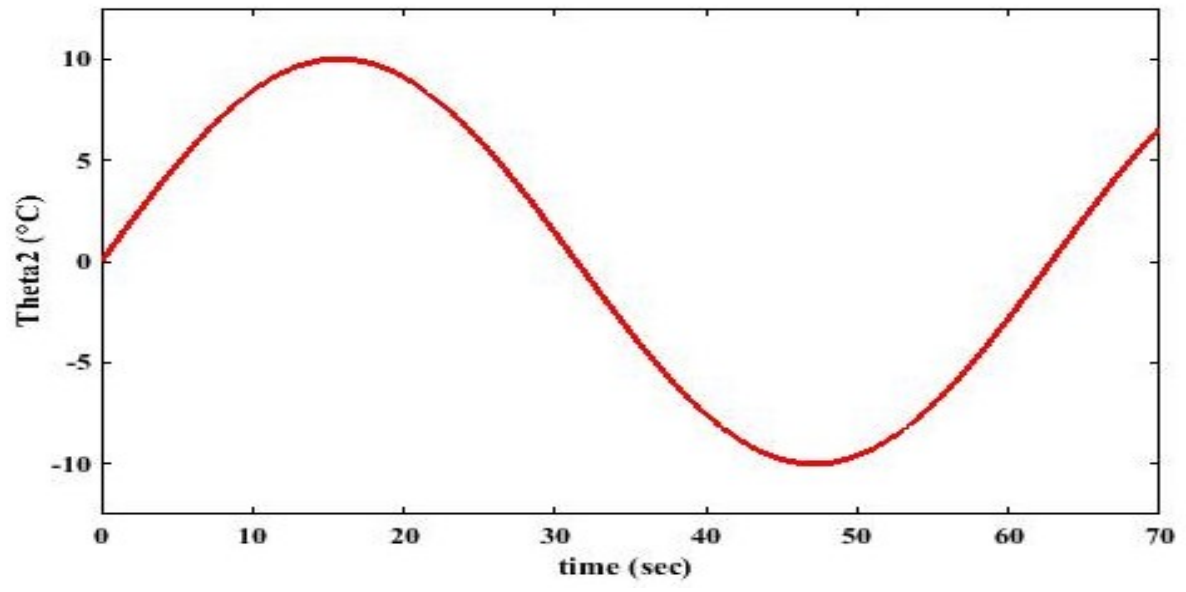
a
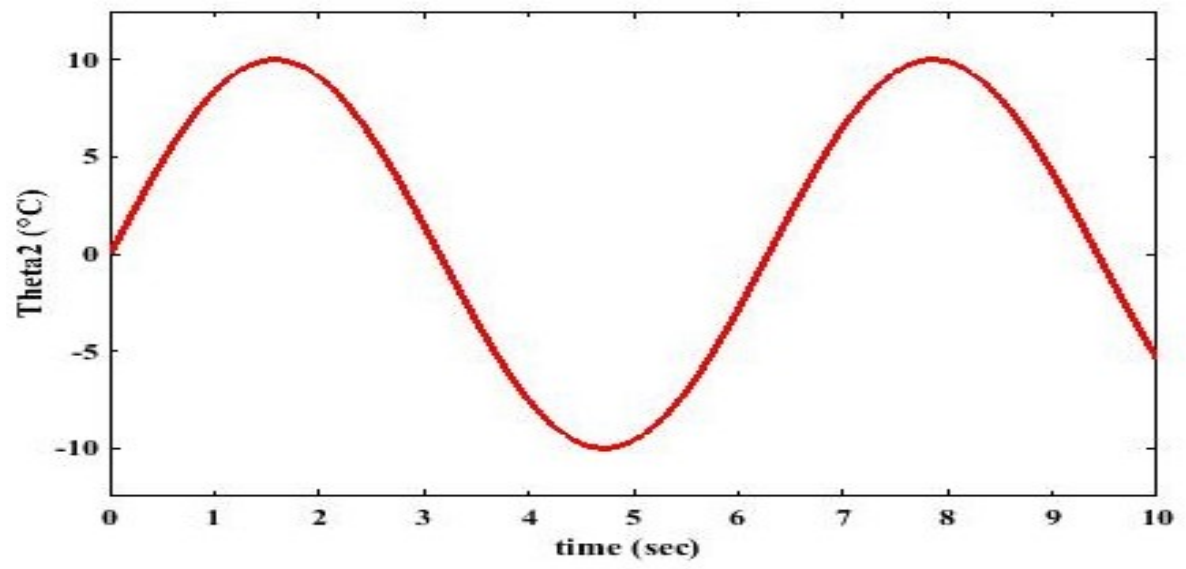
b
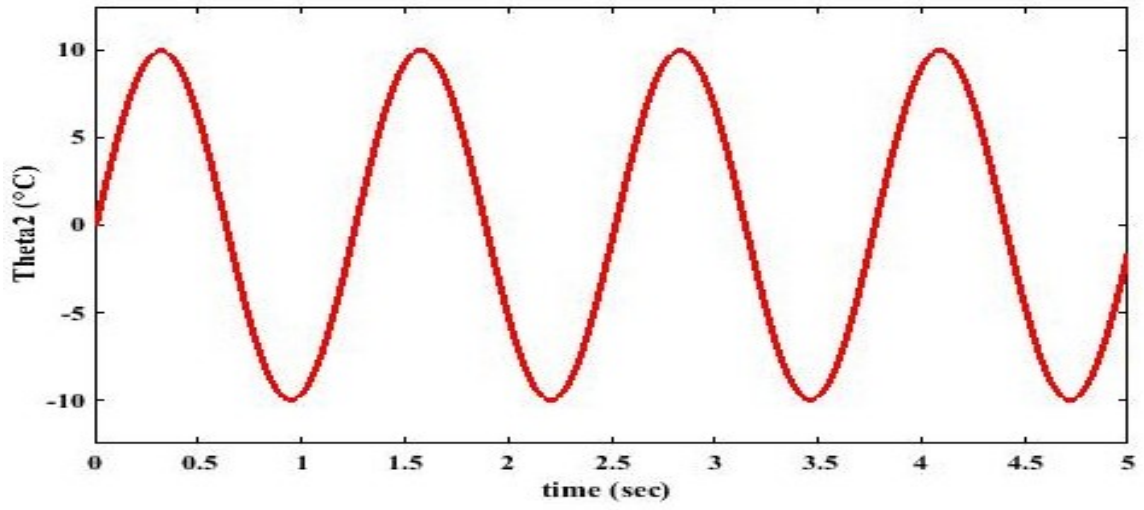
c
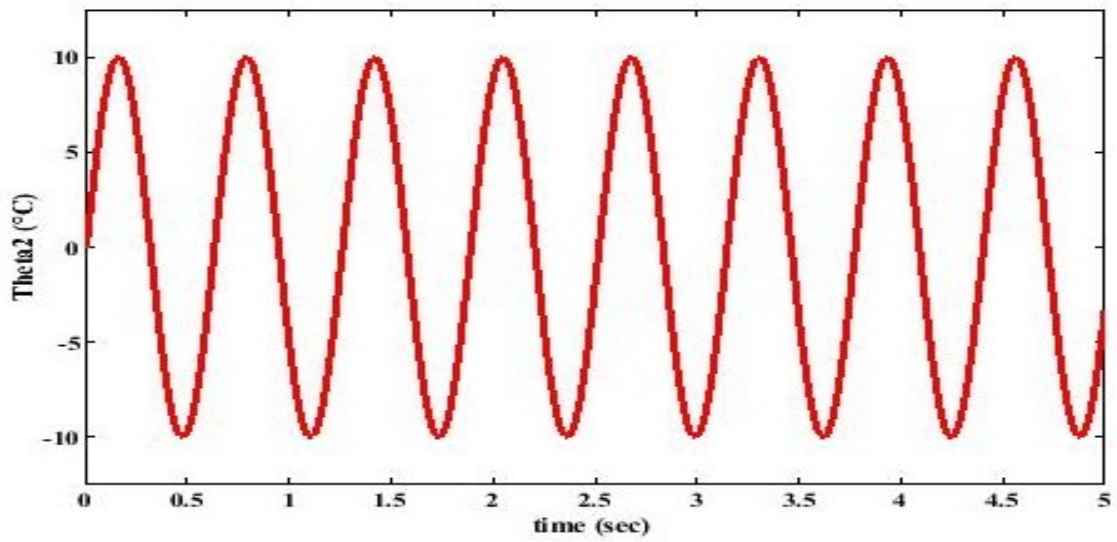
d
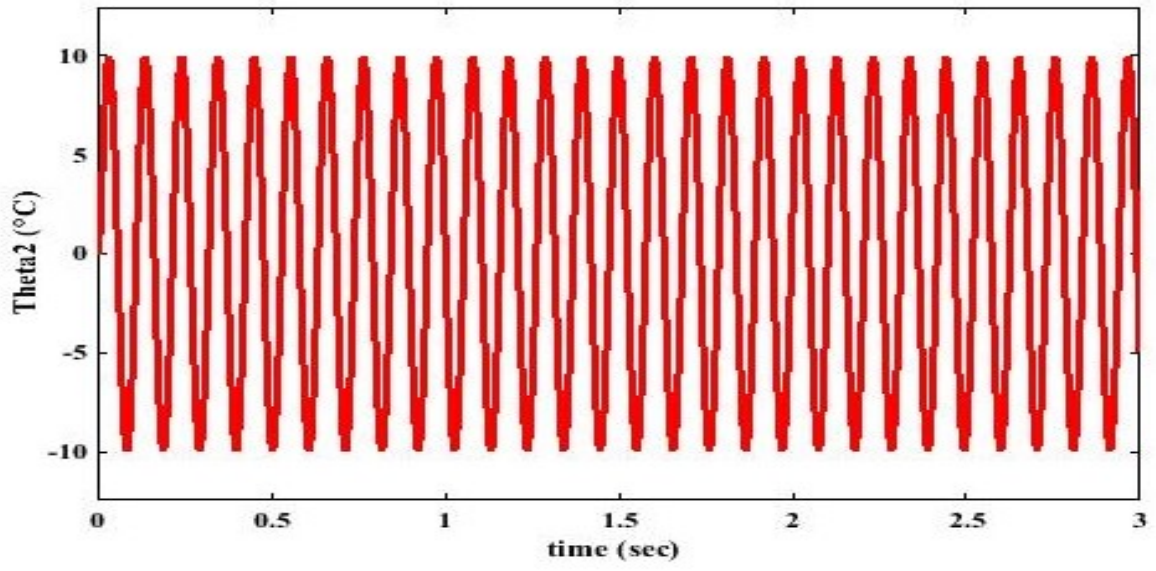
e
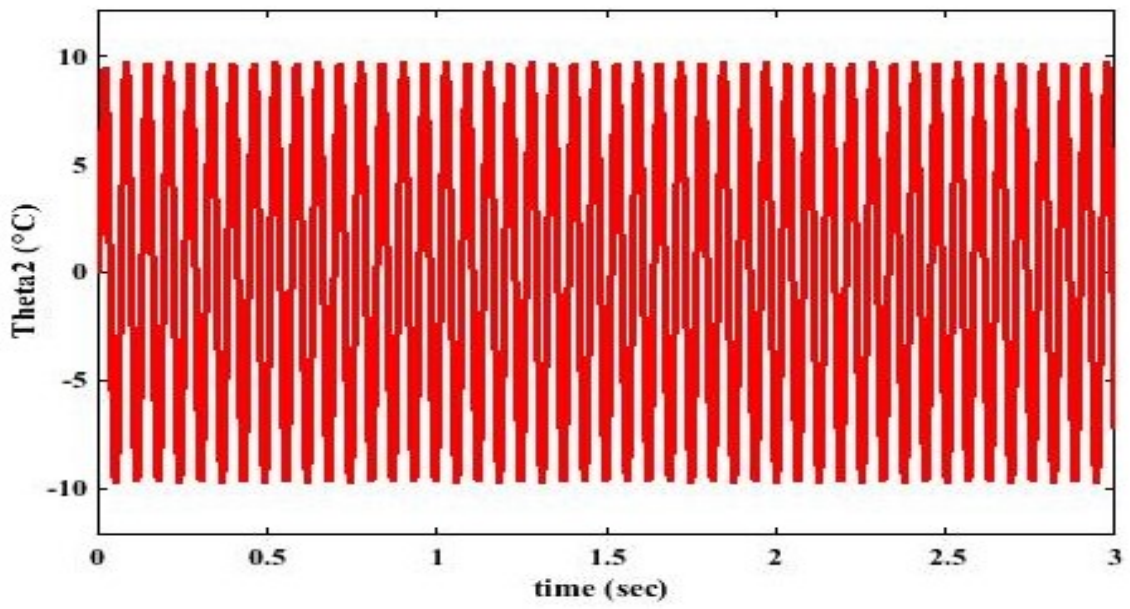
f
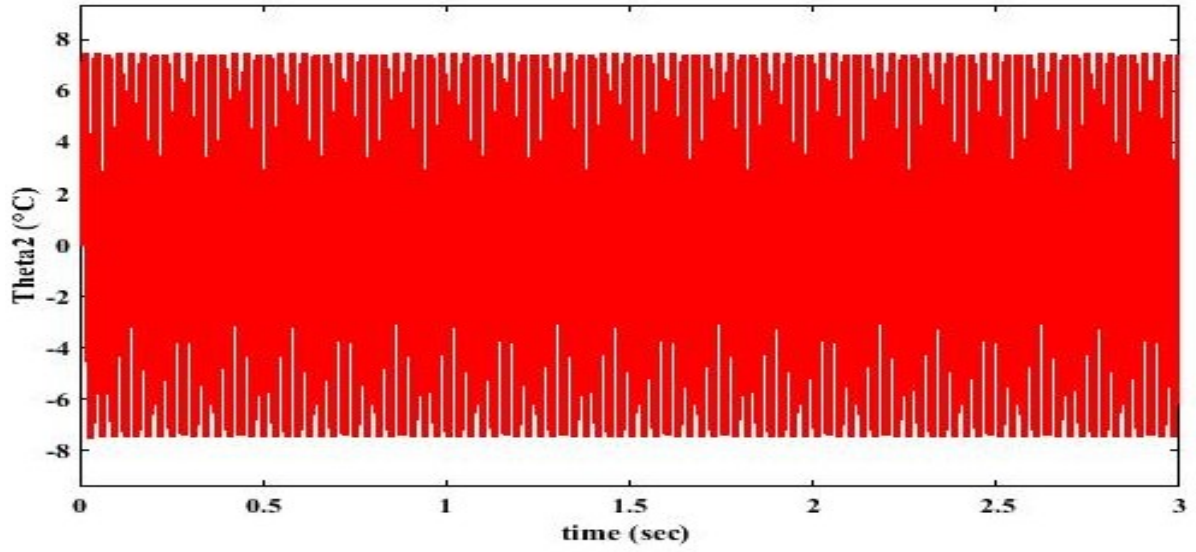
g
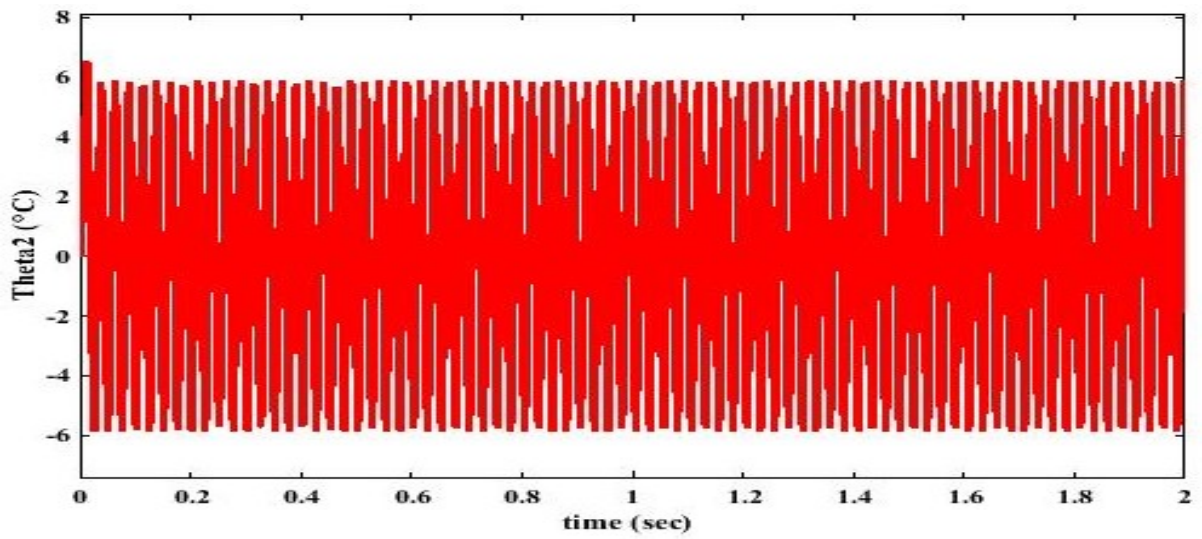
h

Figure 31: Relative temperature (θ_2) for the closed loop M=4, N=6, gain G_c =1, and frequency of a) 0.1, b) 1, c) 5, d) 10, e) 60, f) 100, g) 200, h) 250 (rad/sec).

a

b

c

d

e

f

85
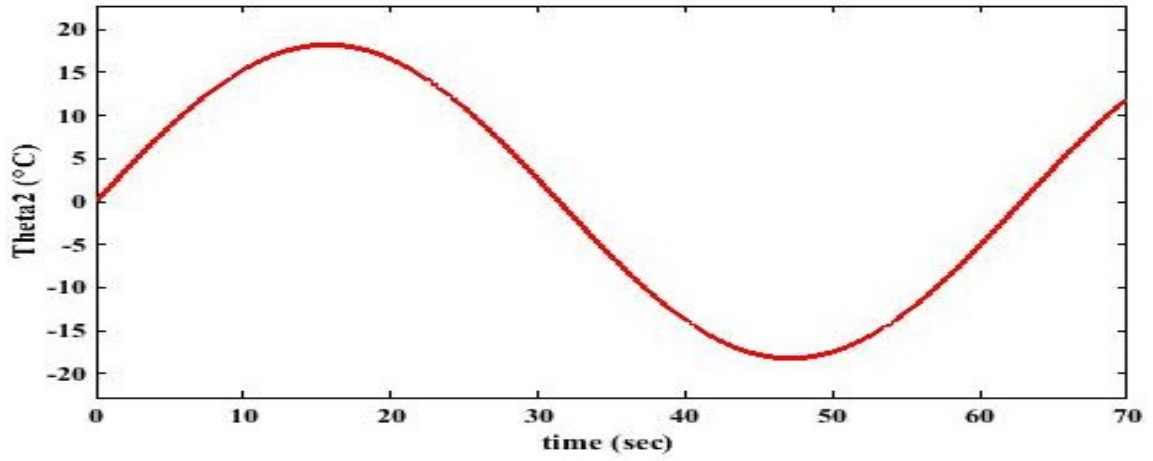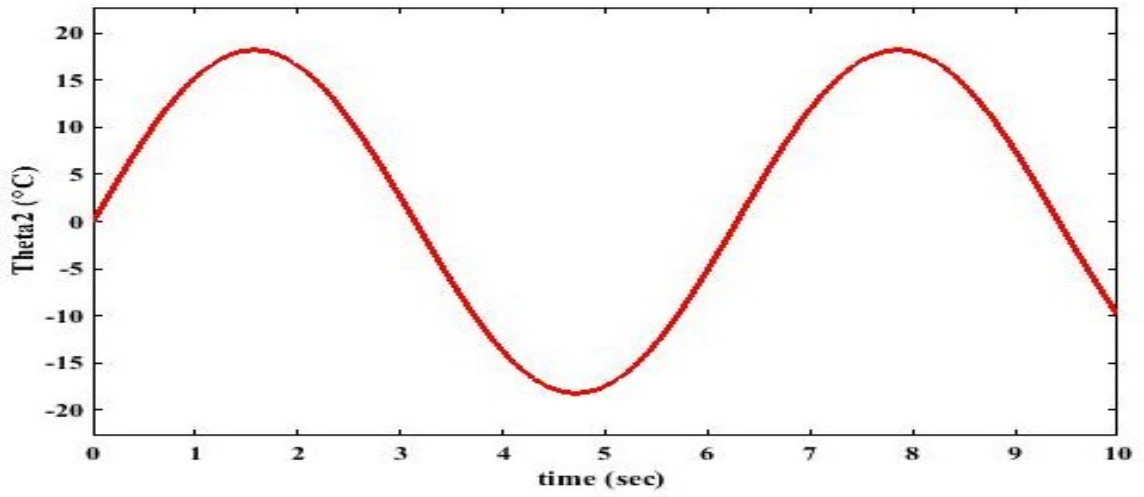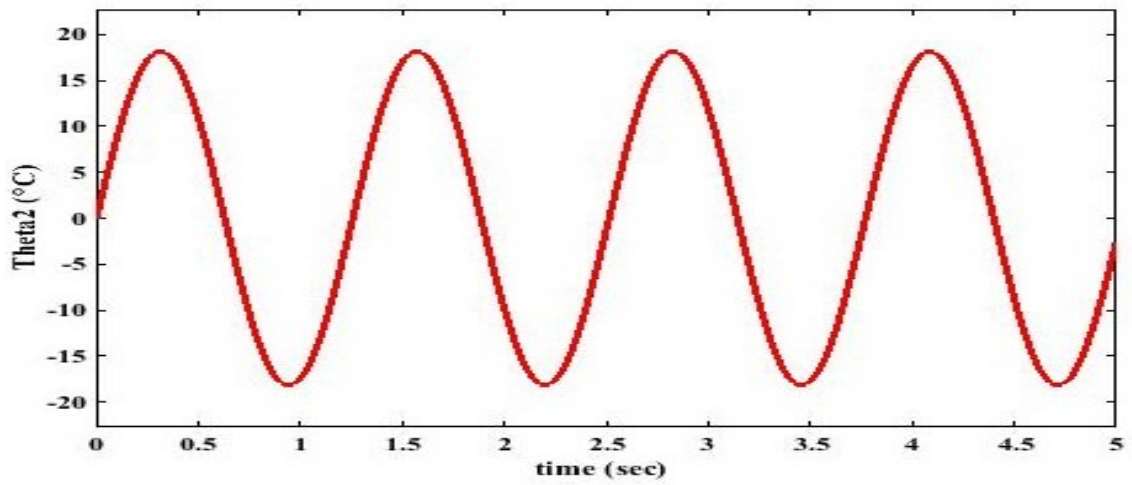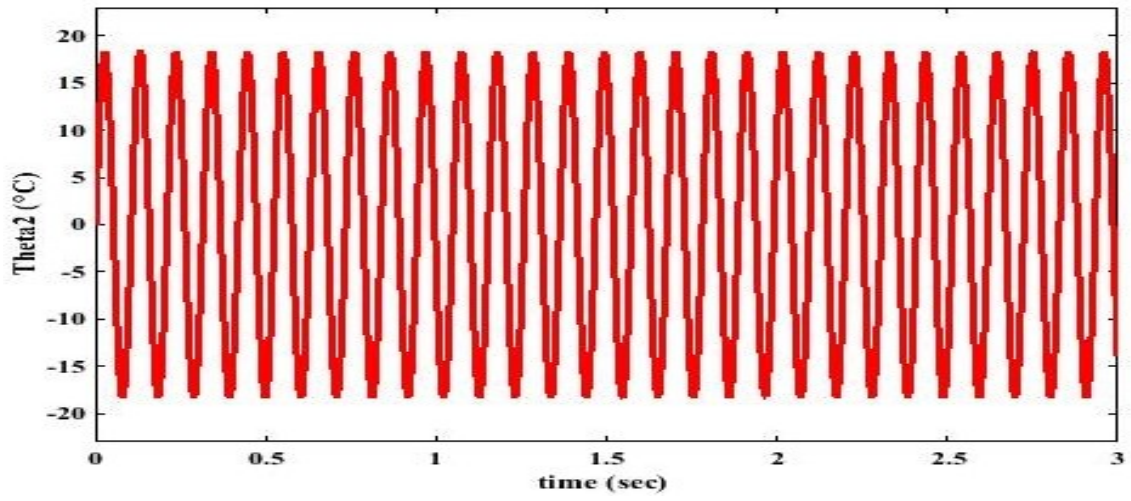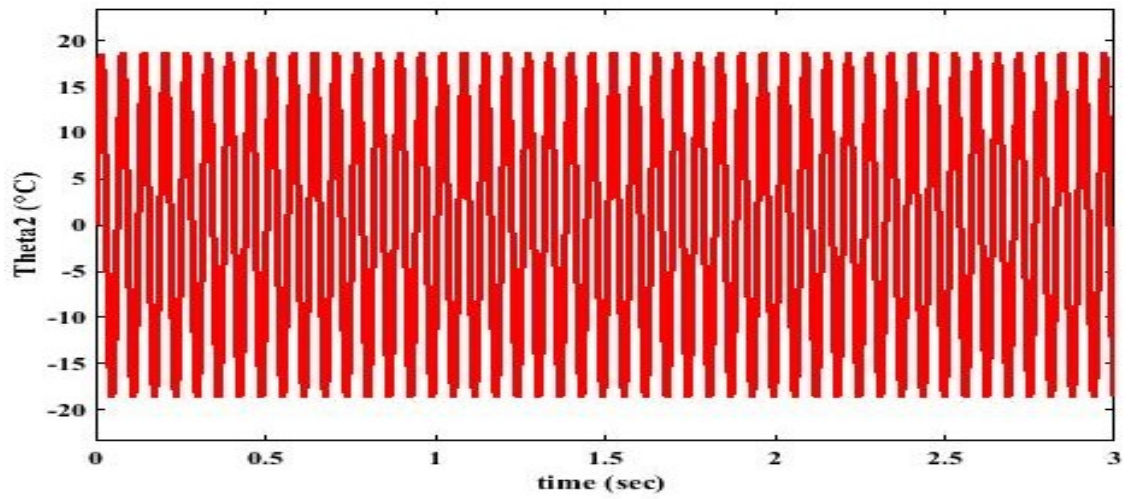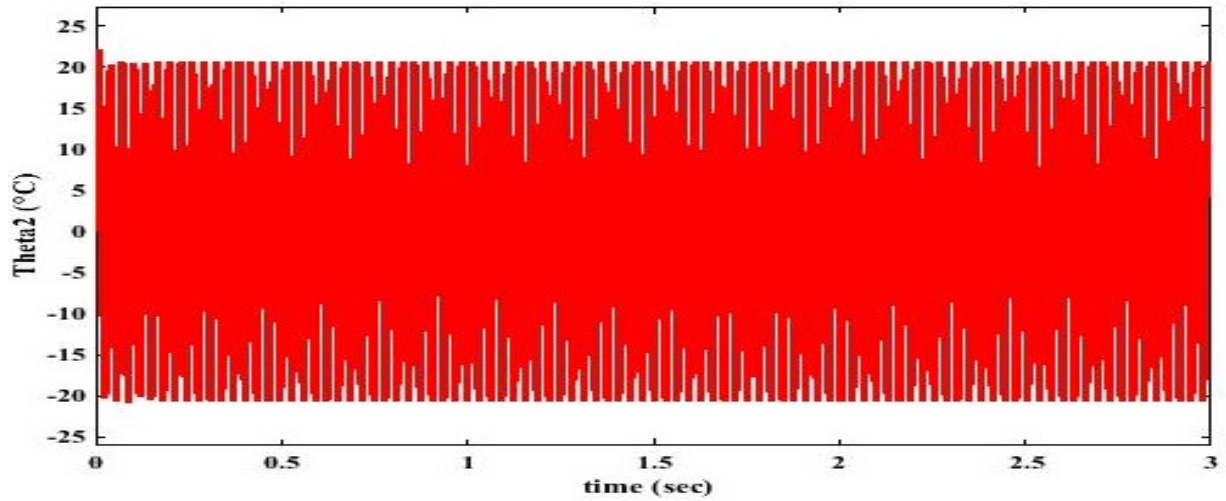
g
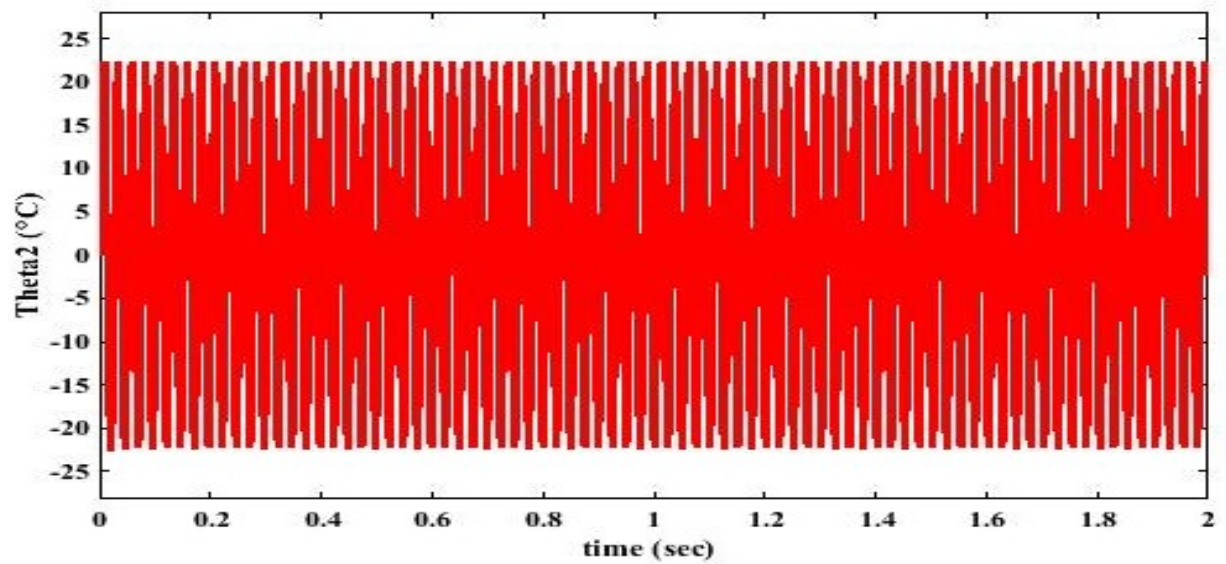
h

Figure 32: Relative temperature (θ_2) for the closed loop M=4, N=6, gain G_c =10, and frequency of a) 0.1, b) 1, c) 5, d) 10, e) 60, f) 100, g) 200, h) 250 (rad/sec).

Similar to the single-layer case from Figure 18 for k=1, in Figure 31 (a-f) for $Gc = 1$ we see that the closed-loop response is half of the desired value due to the gain value of one and frequency less than 100 (rad/sec). In Figure 31 (g-h), the response starts to decrease due

to a higher value of frequency. Similar to the single-layer case from Figure 19 for k=10, in Figure 32 (a-h), the gain k=10 we see that the closed-loop response is almost the same as the desired value due the gain value of ten for all frequencies used. These frequencies were used for simulations study to poof the control action of the controller for higher frequencies bandwidth and, again these frequencies cannot be achieved physically.

Next, are presented Bode diagram results.
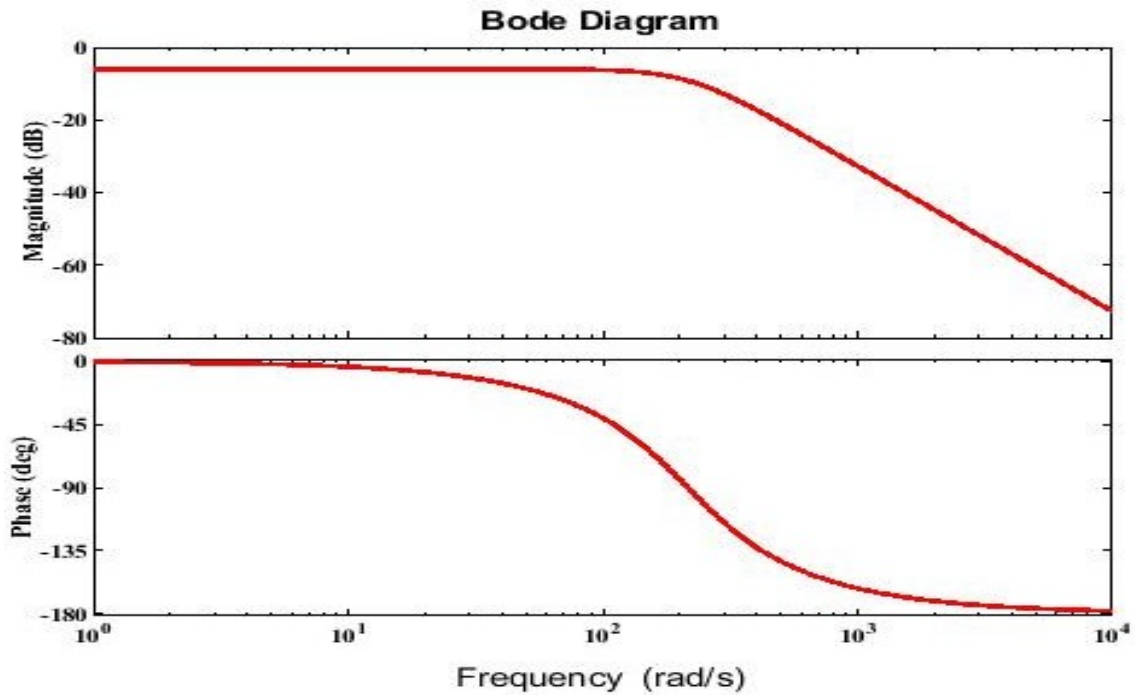
a
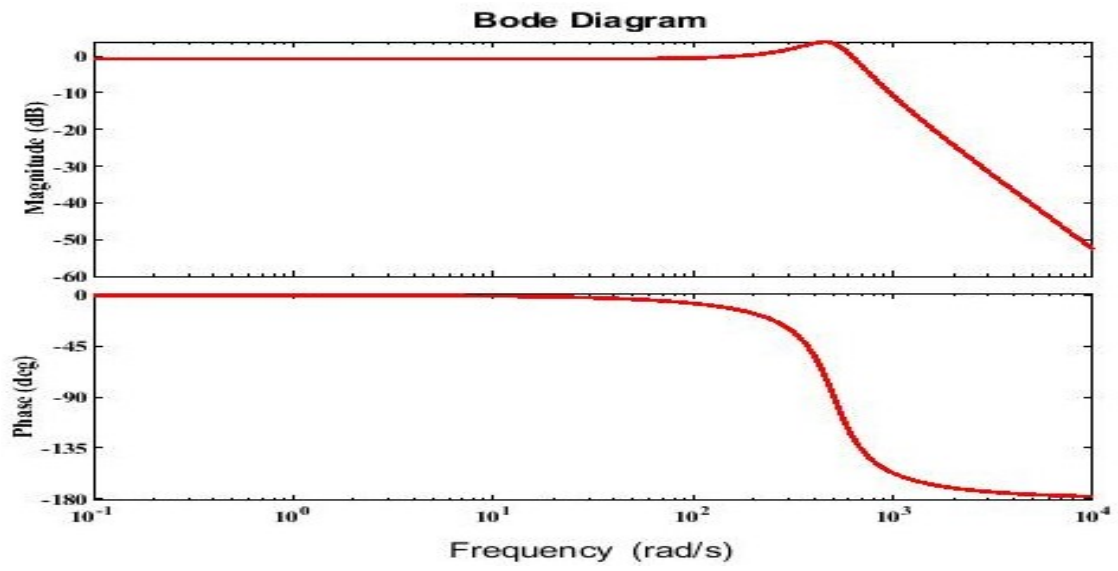
b
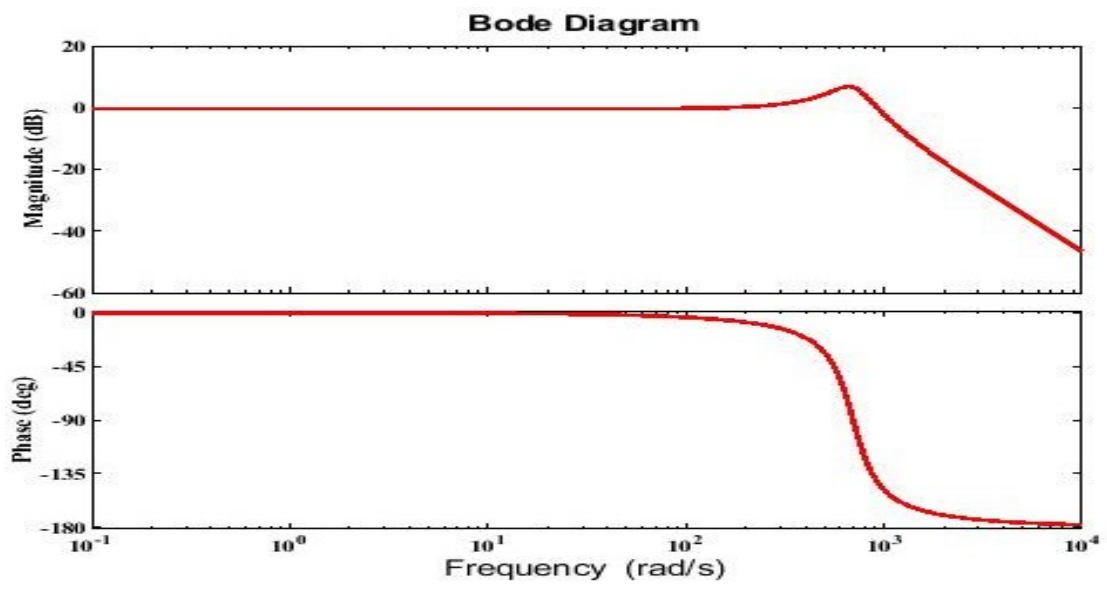
c
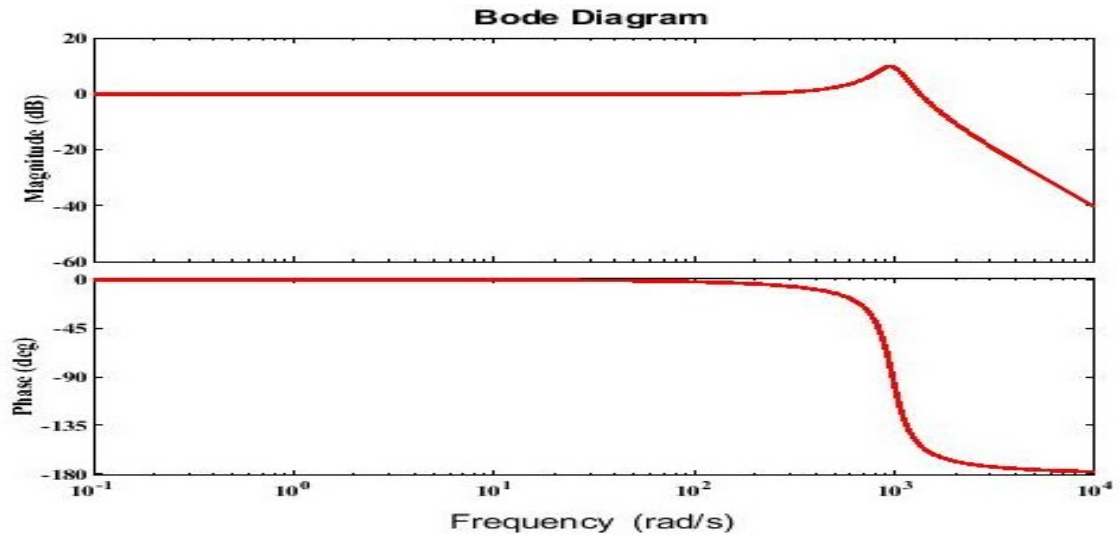
d
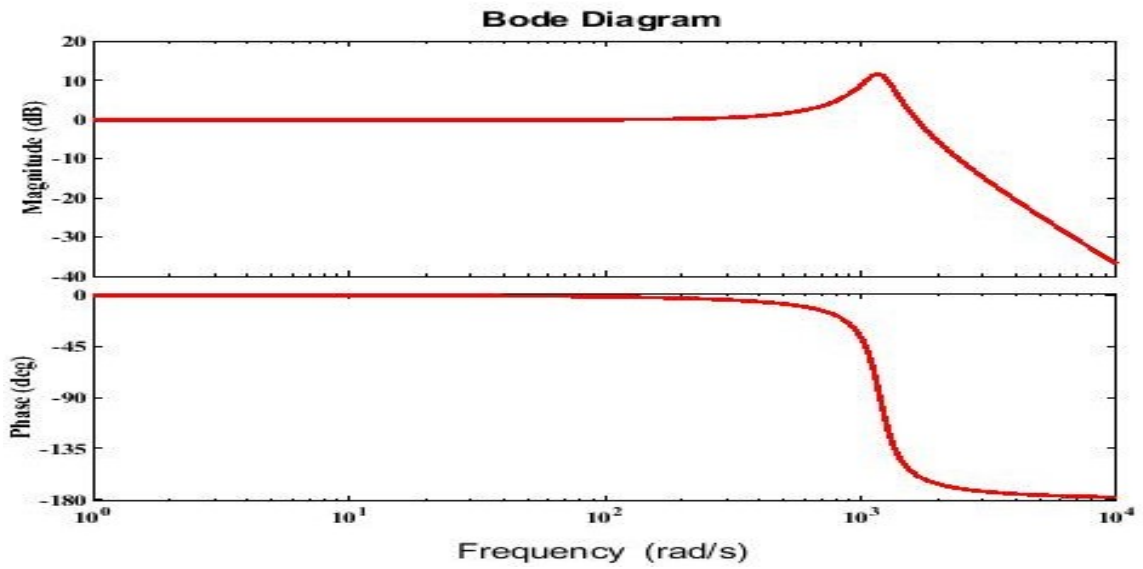
e
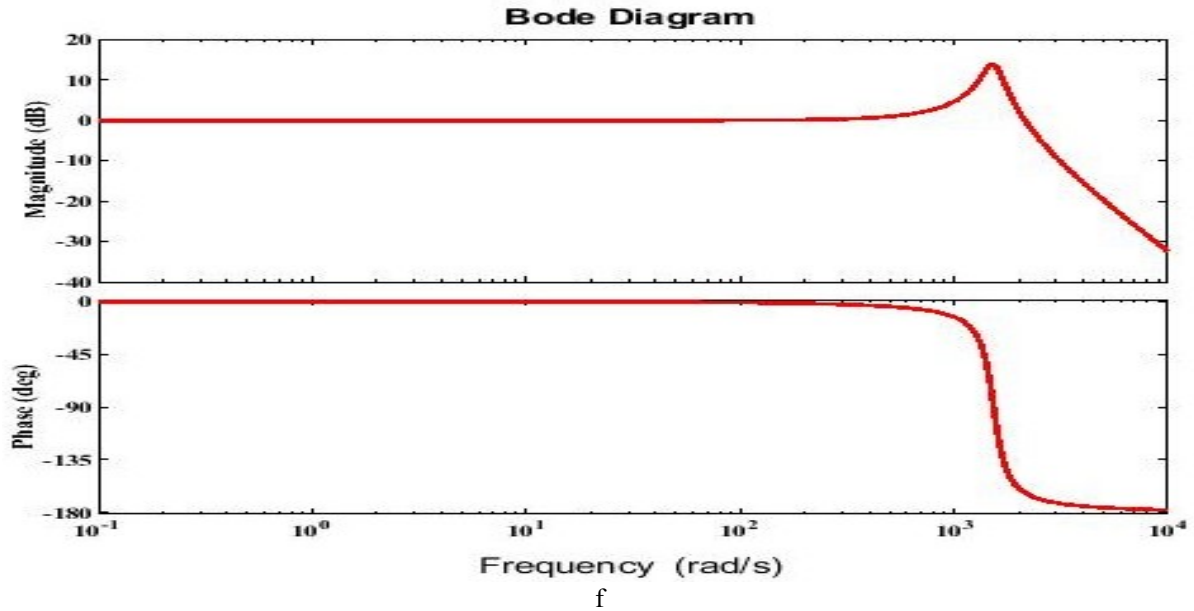
Figure 33: Bode plot for the closed loop L = 0.03 (m), and gain: a) 1, b) 10, c) 20, d) 40, e) 60, and f) 100.

From the Bode plots in Figure 33 (a-f), we see that for the same plate thickness and different gain values, the magnitude and the phase remain constant for a wider range of frequency, and this range increases; while increasing the gain value, the magnitude starts to have sudden local increase at higher frequencies, and this range increases; while increasing the gain value, the magnitude starts to have sudden local increase at higher frequencies. Achieving experiments for k larger than 10 can be constrained by resulting too high commands of this proportional controller.

In fact, simulation results in time and frequency domain for a frequency of 0.1 rad/s are valid for any lower frequency, including much lower frequencies used in experiments.

Chapter Five: Experimental Approach and Results

In this chapter, we will present the experimental setup and the experimental results for the inverse problem control approach.

5.1 Experimental Setup

Controlling the temperature of metal used in industry to a precise, desired value is required to maintain a longer functionality without affecting the final product. In this chapter, we present the experimental study for the closed-loop approach, using a two-stage experimental setup shown in Figure 34. The first part on the left is a PC, which computes the inverse problem, the control law, and the signal processing, while the second part on the right consists of a physical system corresponding to the direct problem components: the plate, thermocouples, signal amplifiers, and the power supply. Simulations were carried out for closed-loop control schemes for different values of input frequency and the input sinusoidal relative temperature amplitude of 10^0C above the initial relative temperature; the initial relative temperature is 60^0C above the environment temperature, this initial relative temperature was chosen to be physically achievable. The use of high initial relative temperature cannot be achievable with the current resources we have. The input was $\theta_2(0, t) = 10\sin(wt) = \theta_2^d(t)$. The simulations in the previous chapters were done for a sine amplitude of 20^0C, while in experiments we have to minimize the sine amplitude to 10^0C. This was done because we have to match the amplitude variations experimentally using the silicone rubber heater, and due to the heater limitations we have to drop the sine amplitude.

Figure 34 is the schematic diagram of the closed-loop experimental setup used to run the experiments. For these experiments, we use the same inverse problem as in the simulation setup with M=4 terms, the physical parts were the aluminum plate mentioned in the simulation; a 500-watt silicon rubber heater was used in the experiments with low-frequency values to give us a good heating period; while for the cooling we use a fan with different speeds.

In the experimental setup, we use the LABVIEW software to link the inverse problem with the direct problem (physical problem) using NI-DAQ USB-6259. Experiments were carried out for different values of input frequency and different gain values. Figure (34) shows the experimental setup used to run the experiments, the inverse problem, and the controller represented in the PC, while the direct problem is replaced by the physical plate. The inverse problem and the controller are computed in the PC are shown on the left-hand side, while the direct problem consists of the physical part shown on the right-hand side.
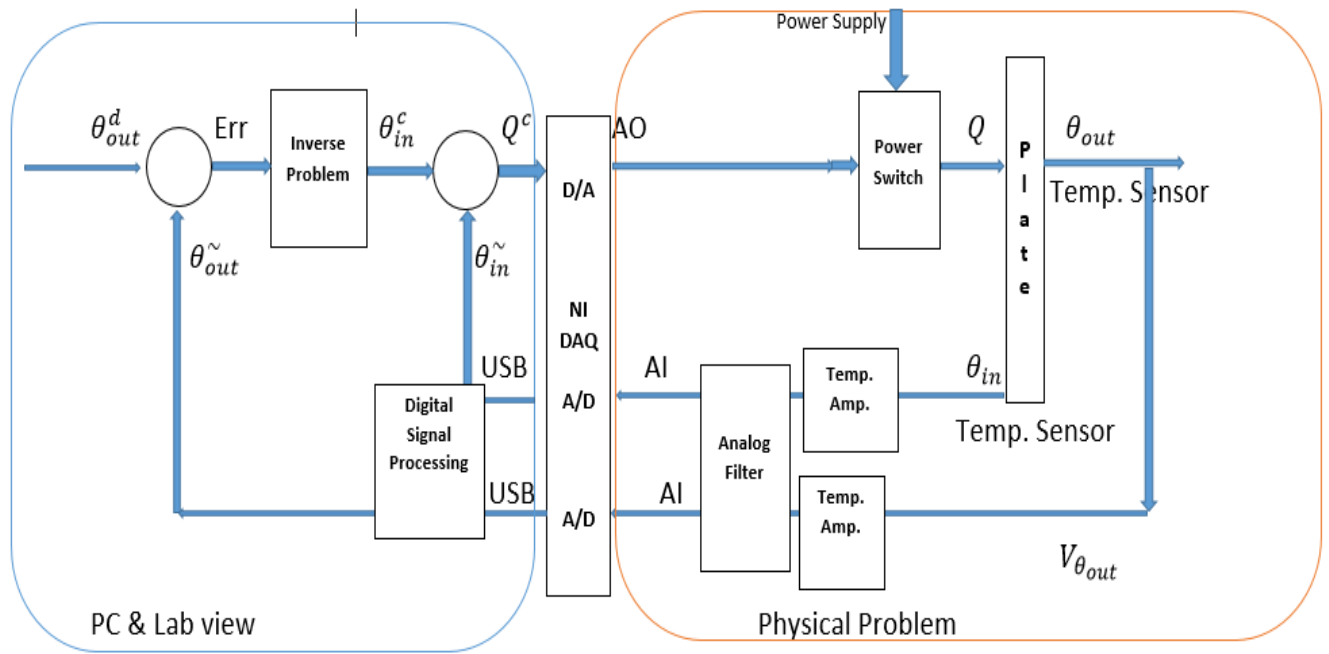
Figure 34: Experimental setup for the closed-loop approach.

5.2 Results and Discussion

Figures (35 to 37) show comparatively the simulation experimental results for a gain of k=1 and different frequencies when using inverse problem control.

.
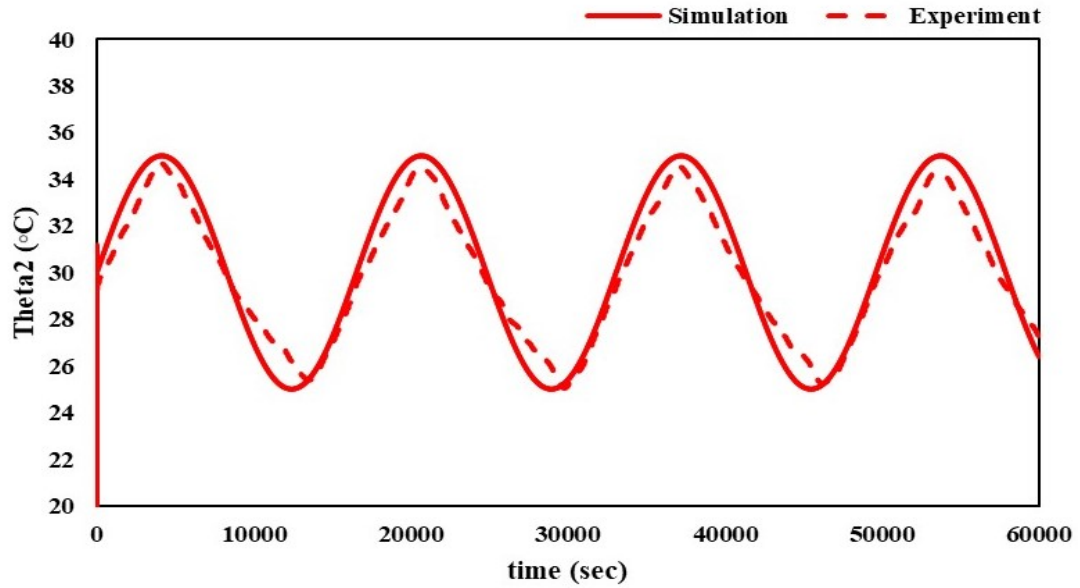
Figure 35: Relative temperature results for frequency of 0.00038 (rad/sec) and a control gain k = 1. a) Solid line is simulation result, b) Dashed line is the experimental result.
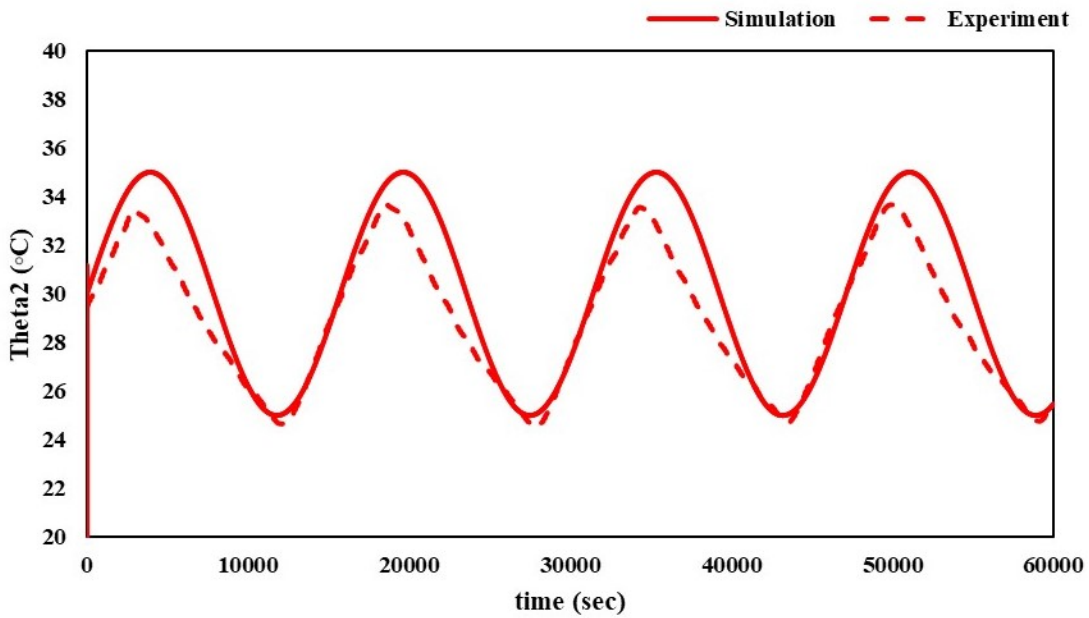
Figure 36: Relative temperature results for frequency of 0.0004 (rad/sec) and a control gain k = 1. a) Solid line is simulation result, b) Dashed line is the experimental result.
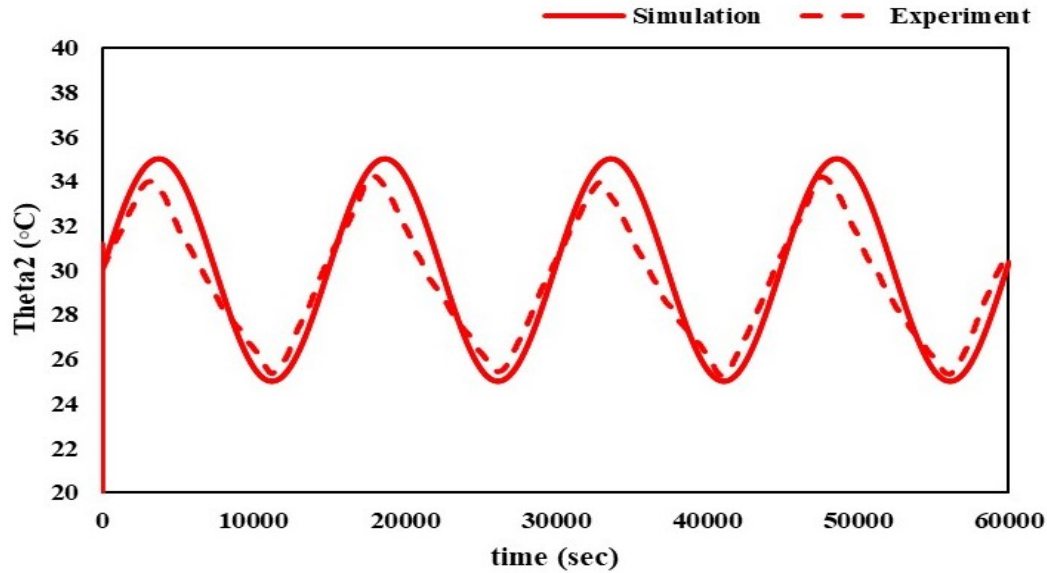
Figure 37: Relative temperature results for frequency of 0.00042 (rad/sec) and a control gain of k = 1. a) Solid line is simulation result, b) Dashed line is the experimental result.

The results shown in Figures (35 to 37) for the gain k=1 and frequencies of 0.00038, 0.0004, and 0.00042 (rad/sec) respectively show that the temperature oscillation in simulation results and the experimental results differ by only 1.5^0C. The average temperature is, however, about 30^0C; i.e., about half of the average desired temperature of 60^0C, as in Ch.4.2, due to the closed-loop output for $G_2^{-1} = G_1$ resulting in $\frac{1}{1+1} = 0.5$. This difference can be reduced by increasing the gain k.

The results in Figures (38 to 40) were obtained for a gain of k=5 and different frequencies.

Figure 38 refers in (a) to the simulation results for a frequency of 0.00038 (rad/sec) and in (b) the experimental results for the same gain value and frequency. From these two figures, we see that the output for both is matching within $1.5 - 2^0$ C.

Figures 39 and 40 indicate the same time variation as in Figure 38, for the same gain k=5 and frequencies of 0.0004 and 0.00042 (rad/sec), respectively. In this case, the average temperature is about 50^0C, i.e. much closer to the average desired temperature of 60^0C. Further improvements can be obtained by a suitable controller design.
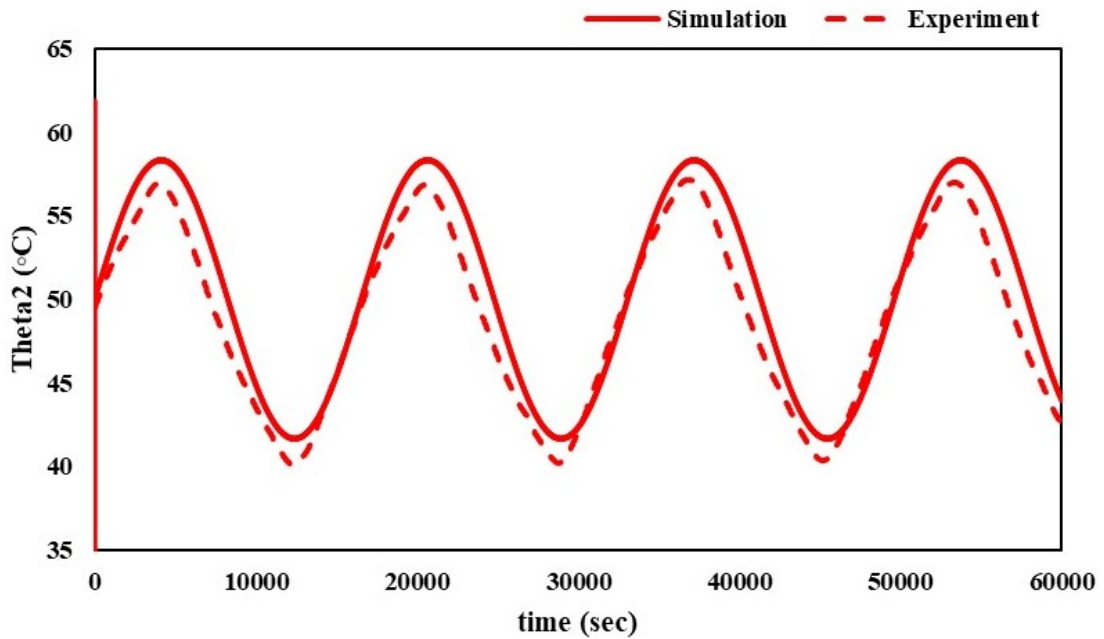
Figure 38: Relative temperature results for frequency of 0.00038 (rad/sec) and a control gain k = 5. a) Solid line is simulation result, b) Dashed line is the experimental result.
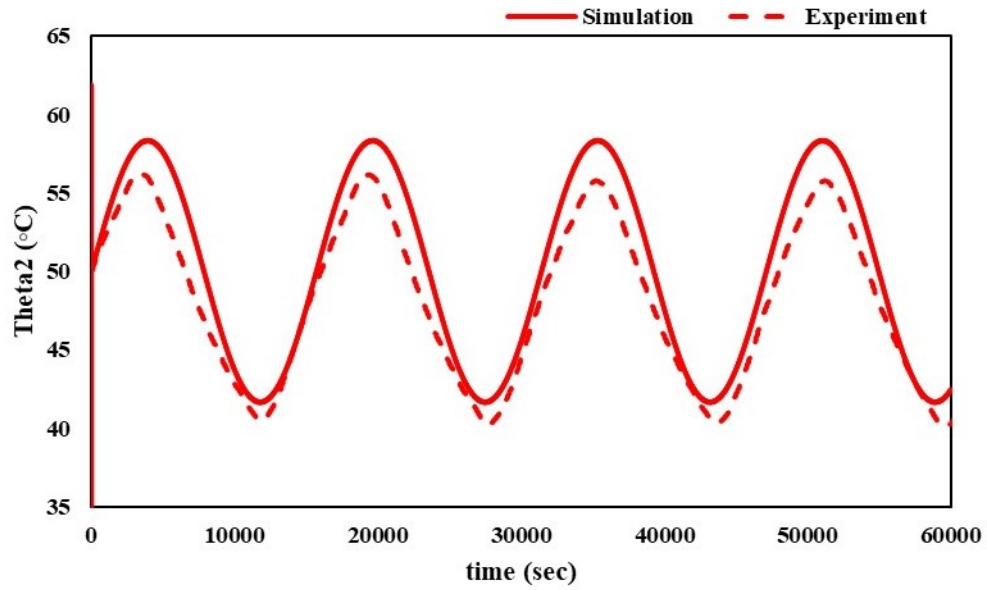
Figure 39: Relative temperature results for frequency of 0.00040 (rad/sec) and a control gain k = 5. a) Solid line is simulation result, b) Dashed line is the experimental result.
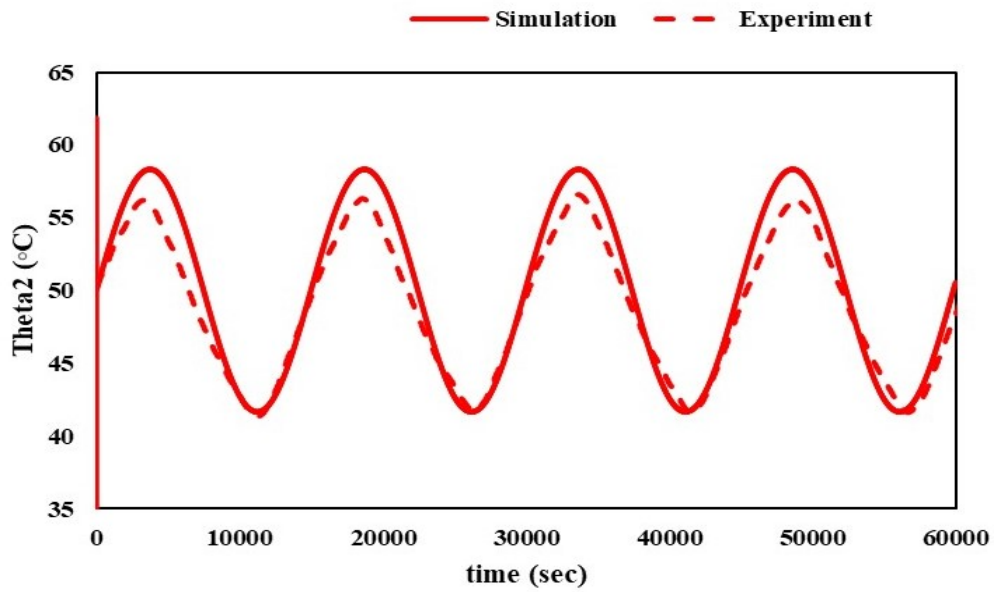
Figure 40: Relative temperature results for frequency of 0.00042 (rad/sec) and a control gain k = 5. a) Solid line is simulation result, b) Dashed line is the experimental result.

From the above simulations and experimental results, it can be seen that for both gain k values of 1 and 5, the sinusoidal response match within small difference, and this confirms that surface temperature oscillations of a thin plate can be successfully controlled using this approach and the desired temperature can be achieved for higher control gains k.

All experiments reach the required response after running for 4-5 hours; this required some adjustments for the time scales to be consistent with the simulation results for a period of 60000 (sec). The starting time of each experiment was modified to start the sine signal as in the simulation, which means the starting time of the signal varies for each experiment.

Chapter Six: Fractional Order Controller Design

In the current chapter, we will focus on the fractional-order controller approach, and it is the design process.

6.1 Controller Equation

In this section, we will design different types of fractional controllers to control the metal plate, and we derive the control equation based on the design method introduced by Monje et al book published in 2010 [39].

6.1.1 Fractional Proportional Integral Controller

The first controller is the Fractional Order Proportional Integral controller (FOPI$^\lambda$). The fractional-order PI controller formula is [43]:

$$C(j\omega)=k_p[1+ k_i(j\omega)^{-\lambda}] \tag{6.1}$$

$$C(j\omega)=k_p[1+k_i(\omega)^{-\lambda} \cos\left(\frac{\mu\pi}{2}\right)+jk_i(\omega)^{-\lambda} \sin\left(\frac{\mu\pi}{2}\right) \tag{6.2}$$

$$\text{Arg}[C(j\omega)]=\tan^{-1}[\frac{k_i(\omega)^{-\lambda} \sin\left(\frac{\mu\pi}{2}\right)}{1+ k_i(\omega)^{-\lambda} \cos\left(\frac{\mu\pi}{2}\right)}] \tag{6.3}$$

$$|C(j\omega)|=K_p\sqrt{[1+ k_i(\omega)^{-\lambda} \cos\left(\frac{\mu\pi}{2}\right)]^2+[k_I(\omega)^{-\lambda} \sin\left(\frac{\mu\pi}{2}\right)]^2} \tag{6.4}$$

The open-loop transfer function is:

$$L(j\omega) = C(j\omega) \, G(j\omega)$$

We want to satisfy three conditions to solve for the three variables of the controller:

1 - Robustness:

$$\left.\frac{d(Arg[L(j\omega)]}{d\omega}\right|_{\omega=\omega_{cg}}=0$$

2 - Gain crossover frequency:

$$|L(j\omega)|_{dB}=0$$

3 - Phase Margin:

$$Arg[L(j\omega)]|_{\omega=\omega_{cg}} = -\pi + \varphi_m$$

From condition (3), we get:

$$\tan^{-1}\left[\frac{k_I(\omega_{cg})^{-\lambda}\sin\left(\frac{\mu\pi}{2}\right)}{1+k_I(\omega_{cg})^{-\lambda}\cos\left(\frac{\mu\pi}{2}\right)}\right] - \tan^{-1}\left[\frac{2\zeta\omega_{cg}\omega_n}{\omega_n^2-\omega_{cg}^2}\right] = -\pi + \varphi_m \tag{6.5}$$

From condition (2), we get:

$$\frac{K_p\sqrt{[1+k_i(\omega_{cg})^{-\lambda}\cos\left(\frac{\mu\pi}{2}\right)]^2+[k_i(\omega_{cg})^{-\lambda}\sin\left(\frac{\mu\pi}{2}\right)]^2}}{\sqrt{(1-\frac{\omega_{cg}^2}{\omega_n^2})^2+4\zeta^2\omega_{cg}^2/\omega_n^2}}=1 \tag{6.6}$$

From condition (1), we get:

$$K_i = \frac{-B\pm\sqrt{B^2-4A[A\omega_{cg}^{-2\lambda}+\lambda(\omega_{cg})^{-2\lambda-1}]}}{2[A\omega_{cg}^{-2\lambda}+\lambda(\omega_{cg})^{-2\lambda-1}]} \tag{6.7}$$

Where

$$A= \frac{2\zeta\omega_n\left(\omega_n^2- \omega_{cg}{}^2\right)+4\zeta\omega_n\omega_{cg}{}^2}{(\omega_n^2- \omega_{cg}{}^2)^2+(2\zeta\omega_n\omega_{cg})^2}$$

And

$$B= 2A\omega_{cg}^{-\lambda} \cos\left[\frac{\lambda\pi}{2}\right]+\lambda\omega_{cg}^{-\lambda-1}\cos\left[\frac{\lambda\pi}{2}\right]$$

6.1.2 Fractional Proportional Derivative Controller

The second controller is the Fractional Order Derivative Controller (FOPD$^\mu$).

The system transfer function formula is [38]:

$$G= \frac{\omega_n^2}{s^2+2\zeta\omega_n s+\omega_n^2} \tag{6.8}$$

We get:

$$|G(j\omega)|=\frac{1}{\sqrt{(1-\frac{\omega^2}{\omega_n^2})^2+ 4\zeta^2\omega^2/\omega_n^2}} \tag{6.9}$$

$$Arg[G(j\omega)]=- \tan^{-1}\left[\frac{2\zeta\omega\omega_n}{\omega_n^2- \omega^2}\right] \tag{6.10}$$

The fractional order PD controller formula is [40][45]:

$$C(j\omega)=k_p[1+ k_d(j\omega)^\mu] \tag{6.11}$$

$$C(j\omega)=k_p[1+ k_d(\omega)^\mu \cos\left(\frac{\mu\pi}{2}\right) +jk_d(\omega)^\mu \sin\left(\frac{\mu\pi}{2}\right)] \tag{6.12}$$

$$Arg[C(j\omega)]=\tan^{-1}[\frac{\sin\left[\frac{(1-\mu)\pi}{2}\right]+k_d(\omega)^\mu}{\cos\left[\frac{(1-\mu)\pi}{2}\right]}]- \frac{(1-\mu)\pi}{2} \tag{6.13}$$

$$|c(j\omega)| = K_p \sqrt{(1 + K_d\omega^\mu \cos\left(\frac{\mu\pi}{2}\right))^2 + (1 + K_d\omega^\mu \sin\left(\frac{\mu\pi}{2}\right))^2} \qquad (6.14)$$

Where:

K_p is the proportional gain.

K_d is the derivative gain.

The open-loop transfer function is:

$$L\,(j\omega) = C\,(j\omega)\,G\,(j\omega)$$

We want to satisfy three conditions to solve for the three variables of the controller:

1 - Robustness:

$$\left.\frac{d(Arg[L(j\omega)]}{d\omega}\right|_{\omega=\omega_{cg}} = 0$$

2 - Gain crossover frequency:

$$|L(j\omega)|_{dB} = 0$$

3 - Phase Margin:

$$Arg[L(j\omega)]|_{\omega=\omega_{cg}} = -\pi + \varphi_m$$

From condition (3), we get:

$$\tan^{-1}\left[\frac{\sin\left[\frac{(1-\mu)\pi}{2}\right] + k_d(\omega_{cg})^\mu}{\cos\left[\frac{(1-\mu)\pi}{2}\right]}\right] - \frac{(1-\mu)\pi}{2} - \tan^{-1}\left[\frac{2\zeta\omega_{cg}\omega_n}{\omega_n^2 - \omega_{cg}^2}\right] = -\pi + \varphi_m \qquad (6.15)$$

From condition (2), we get:

$$\frac{K_p\sqrt{[1 + K_d\omega_{cg}^\mu\cos(\frac{\mu\pi}{2})]^2 + [K_d\omega_{cg}^\mu\sin(\frac{\mu\pi}{2})]^2}}{\sqrt{(1-\frac{\omega^2}{\omega_n^2})^2 + 4\zeta^2\frac{\omega^2}{\omega_n^2}}} = 1 \qquad (6.16)$$

From condition (1), we get:

$$\frac{\mu K_d \omega_{cg}^{\mu-1} \cos\left[\frac{(1-\mu)\pi}{2}\right]}{\cos^2\frac{(1-\mu)\pi}{2}+[\sin\frac{(1-\mu)\pi}{2}+K_d\omega_{cg}^{\mu}]^2} - \frac{2\zeta\omega_n\left(\omega_n^2-\omega_{cg}^2\right)+4\zeta\omega_n\omega_{cg}^2}{(\omega_n^2-\omega_{cg}^2)^2+(2\zeta\omega_n\omega_{cg})^2}=0 \tag{6.17}$$

From criteria (3), we can get a relation between K_d and μ as follows:

$$K_d= \frac{-B\pm\sqrt{B^2-4A^2\omega_{cg}^{2\mu}}}{2A\omega_{cg}^{2\mu}} \tag{6.18}$$

Where:

$$A= \frac{2\zeta\omega_n\left(\omega_n^2-\omega_{cg}^2\right)+4\zeta\omega_n\omega_{cg}^2}{(\omega_n^2-\omega_{cg}^2)^2+(2\zeta\omega_n\omega_{cg})^2}$$

$$B= 2A\omega_{cg}^{\mu}\sin\left[\frac{(1-\mu)\pi}{2}\right]-\mu\omega_{cg}^{\mu-1}\cos\left[\frac{(1-\mu)\pi}{2}\right]$$

6.1.3 Fractional Proportional Integral with Fractional Controller

The third controller is the Fractional Order Proportional Derivative Controller (FOPID$^{\mu}$).

The fractional-order PID controller formula is[44] [45]:

$$C(s)=k_p[1+\frac{k_i}{(s)^\lambda}+k_d(s)^\mu] \tag{6.19}$$

For the current controller we have $\lambda = 1$, we get:

$$C(j\omega) = k_p\{1 +k_d(\omega)^\mu \cos\left(\frac{\mu\pi}{2}\right)+j\left[-k_i\omega^{-1}+k_d(\omega)^\mu\sin\left(\frac{\mu\pi}{2}\right)\right]\} \tag{6.20}$$

Let

$$P(\omega)=1 +k_d(\omega)^\mu \cos\left(\frac{\mu\pi}{2}\right)$$

And

$$Q(\omega)=-k_i\omega^{-1}+k_d(\omega)^\mu\sin\left(\frac{\mu\pi}{2}\right)$$

Then

$$\text{Arg}[C(j\omega)]=\tan^{-1}\left[\frac{Q(\omega)}{P(\omega)}\right] \tag{6.21}$$

$$|C(j\omega)| = k_p\sqrt{P^2(\omega) + Q^2(\omega)} \tag{6.22}$$

We want to satisfy the four conditions to solve for the four variables of the controller:

1 - Robustness:

$$\left.\frac{d(\text{Arg}[L(j\omega)]}{d\omega}\right|_{\omega=\omega_{cg}}=0$$

2 - Gain crossover frequency:

$$|L(j\omega)|_{dB}=0$$

3 - Phase Margin:

$$\text{Arg}[L(j\omega)]|_{\omega=\omega_{cg}}= -\pi+ \varphi_m$$

4 - Noise rejection:

$$\left|T(j\omega)=\frac{C(j\omega)G(j\omega)}{1+C(j\omega)G(j\omega)}\right|_{dB}\leq A \text{ dB}$$

Where A is a designed value.

According to condition (2), we get:

$$\frac{k_p\sqrt{P^2(\omega)+Q^2(\omega)}}{\sqrt{(1-\frac{\omega_{cg}^2}{\omega_n^2})^2+4\zeta^2\omega_{cg}^2/\omega_n^2}}=1 \qquad (6\text{-}23)$$

From condition (3), we get:

$$\tan^{-1}\left[\frac{Q(\omega)}{P(\omega)}\right]-\tan^{-1}\left[\frac{2\zeta\omega\omega_n}{\omega_n^2-\omega^2}\right]=-\pi+\varphi_m \qquad (6\text{-}24)$$

From condition (1), we get:

$$\frac{P(\omega)*aa-Q(\omega)*pp}{P(\omega)^2+Q(\omega)^2}-\frac{2\zeta\omega_n(\omega_n^2-\omega_{cg}^2)+4\zeta\omega_n\omega_{cg}^2}{(\omega_n^2-\omega_{cg}^2)^2+(2\zeta\omega_n\omega_{cg})^2}=0 \qquad (6\text{-}25)$$

From condition (4), we get:

$$\frac{|C(j\omega)G(j\omega)|}{|1+C(j\omega)G(j\omega)|}=\frac{\sqrt{P^2(\omega)+Q^2(\omega)}}{\sqrt{[\frac{(1-\frac{\omega_{cg}^2}{\omega_n^2})^2}{K_p}+P(w)]^2+[Q(w)+2\zeta\frac{\omega_{cg}}{\omega_n K_p}]^2}}\leq A \qquad (6\text{-}26)$$

6.2 Results and Discussion

For the design purpose, the crossover frequency was set to be 20 (rad/sec), and the phase margin is set to be 65 degrees; all results had a one-second time step to see a clear step response away from Y-axis.

After we solve Equations (6.5, 6.6, and 6.7) for the fractional-order PI controller parameters, we get a controller formula as follows:

$$\text{FOPI}=1.3862+25.993(s)^{-1.486}$$

From Figure 41, we see that the system reaches the desired response after 1.5 seconds, but it has an overshoot of 20%.

After we solve Equations (6.16, 6.17, and 6.18) for the fractional-order PD controller parameters, we get a controller formula as follows:

$$FOPD= 1.5622 + 0.0086842(s)^{1.832}$$
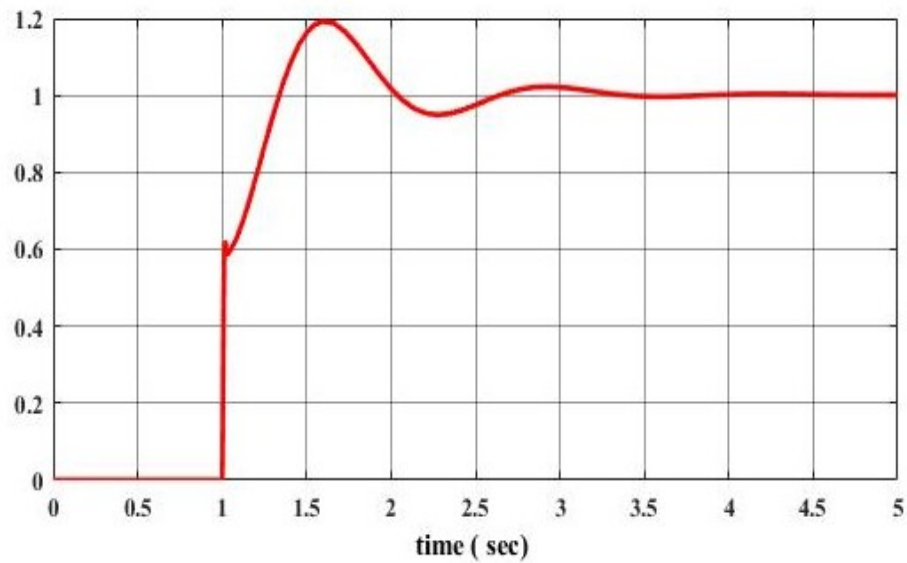
Figure 41: Step response for direct transfer function G_1 using fractional order proportional controller ($FOPI^\lambda$).
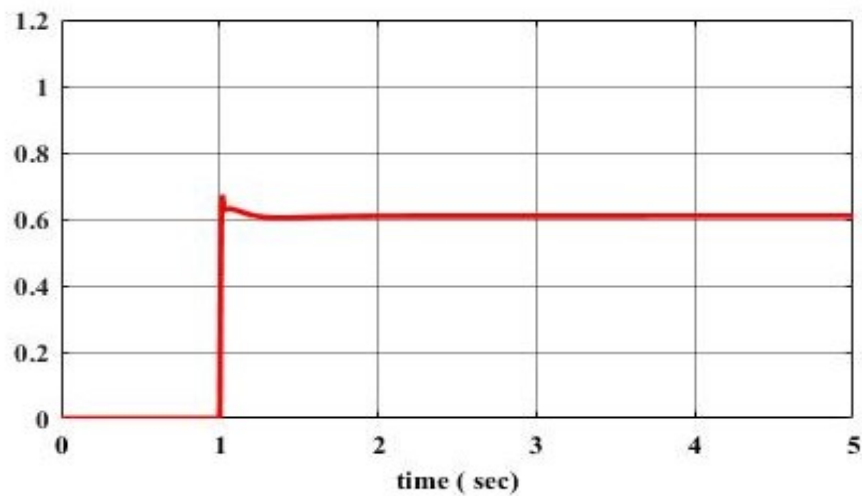
Figure 42: Step response for direct transfer function G using fractional order proportional derivative controller ($FOPD^\mu$).

From Figure 42, we can see that the controller can't reach the desired steady-state value no matter how long the time we give the system.

After we solve Equations (6.23, 6.24, 6.25 and 6.26) for the fractional order PID controller parameter, we get the controller formula as follows:

$$\text{FOPID} = 0.9639 + \frac{2.9379}{s} - 0.0862(s)^{0.713}$$

From Figure 43, we can see that the system reaches the desired response after 2.5 seconds, also with no overshoot.

From Figures 41, 42, and 43, we see that the best controller is the Fractional Order Proportional Derivative Controller (FOPID$^{\mu}$) since it achieves the desired response without overshoot and with zero steady-state error.

Now we compare the results with the Integer Order Controller (IOPID). From Figure 44, we can see that the response is slower with an overshoot of about 8%, and this favours the Fractional Order Proportional Derivative Controller (FOPID$^{\mu}$) over all other controllers. This is because this controller has four parameters to change, which gives it a better design over all the other controllers, where only three parameters are available to change. The results for the integer-order controller were obtained by using Automatic Tuning Criteria in Matlab$^{\text{TM}}$.
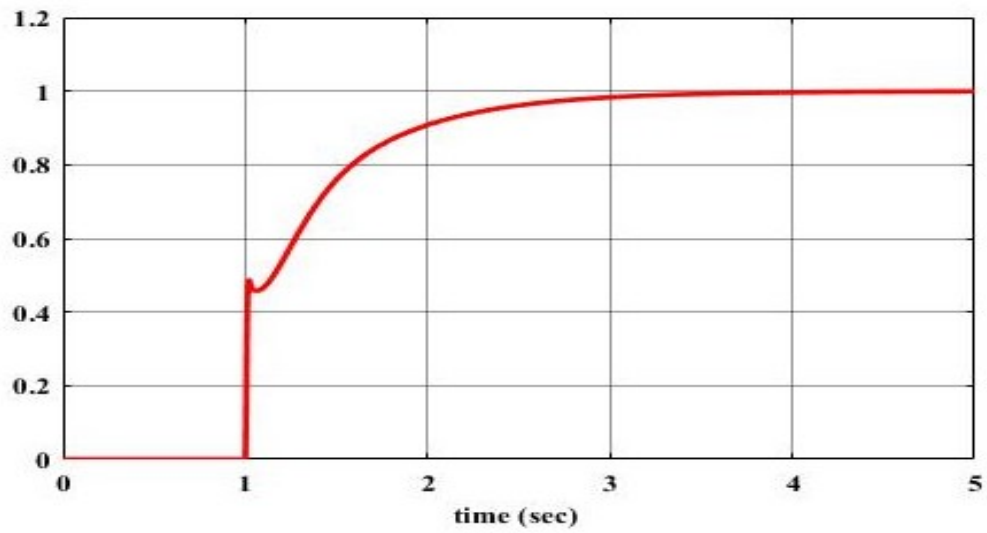
Figure 43: Step response for direct transfer function G using fractional order proportional derivative controller (FOPID$^{\mu}$).
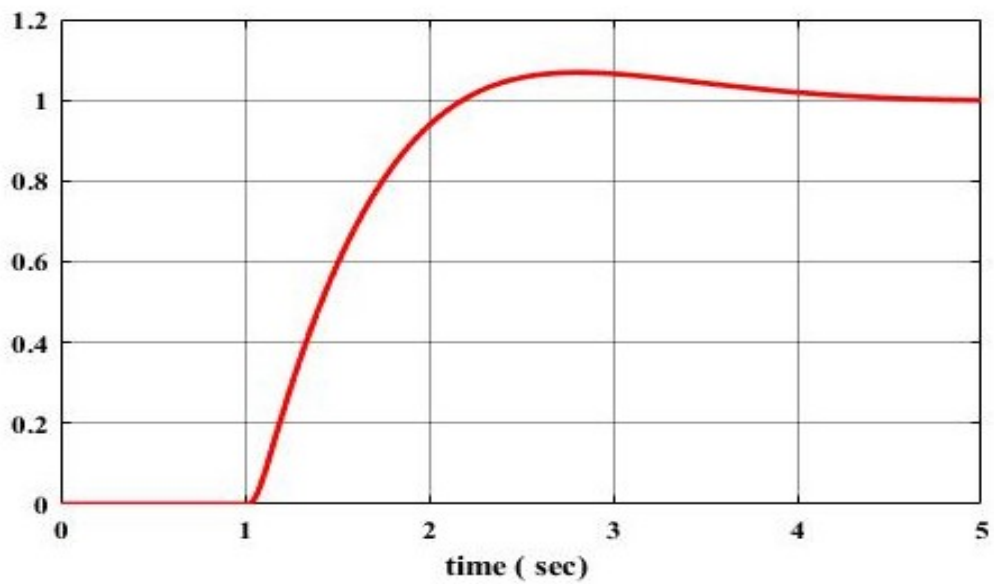
Figure 44: Step response for direct transfer function G using integer order proportional derivative controller (IOPID).

Chapter Seven: Fractional Proportional Integral Derivative Controller

In the current chapter, we will investigate the design procedure for the Fractional Order Proportional Integral Derivative (FOPID) controller. Also, we will present simulation results and experimental results.

7.1 Fractional Proportional Integral Derivative Controller Design

Figure 45 shows the closed-loop block diagram used for the designing purpose of fractional-order PID controller.
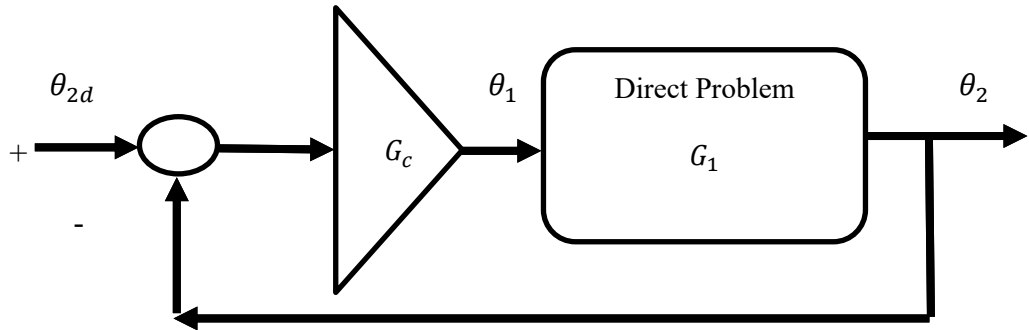
Figure 45: Closed loop control block diagram.

The resulted transfer functions for the direct were obtained after a Zero-Pole approximation was used for the resulted hyperbolic transfer functions are for M=0 and N=6:

$$G_1 = \frac{5.169*10^8}{(s+1.056)(s+ 9.054)(s+ 26.4)(s+ 85.54)(s+ 127.8)(s+ 178.5)} \tag{7.1}$$

The fractional-order PID controller formula is [40][41]:

$$G_c(s) = k_p[1 + \frac{k_i}{(s)^\lambda} + k_d(s)^\mu] \tag{7.2}$$

$$G_c(j\omega) = k_p\{1 + k_i\omega^{-\lambda}\left[\cos\left(\frac{\lambda\pi}{2}\right) + j\sin\left(\frac{-\lambda\pi}{2}\right)\right] + k_d\left(\omega\right)^\mu\left[\cos\left(\frac{\mu\pi}{2}\right) + j\sin\left(\frac{\mu\pi}{2}\right)\right]\} \tag{7.3}$$

$$G_c(j\omega) = k_p\{1 + k_i\omega^{-\lambda}\cos\left(\frac{\lambda\pi}{2}\right) + k_d(\omega)^\mu\cos\left(\frac{\mu\pi}{2}\right)$$

$$j\left[k_i\omega^{-\lambda}\sin\left(\frac{-\lambda\pi}{2}\right) + k_d(\omega)^\mu\sin\left(\frac{\mu\pi}{2}\right)\right]\} \tag{7.4}$$

Let:

$$P(\omega) = 1 + k_i\omega^{-\lambda}\cos\left(\frac{\lambda\pi}{2}\right) + k_d(\omega)^\mu\cos\left(\frac{\mu\pi}{2}\right) \tag{7.5}$$

And

$$Q(\omega) = -k_i\omega^{-\lambda}\sin\left(\frac{\lambda\pi}{2}\right) + k_d(\omega)^\mu\sin\left(\frac{\mu\pi}{2}\right) \tag{7.6}$$

Then

$$Arg[G_c(j\omega)] = tan^{-1}[\frac{Q(\omega)}{P(\omega)}] \tag{7.7}$$

$$|G_c(j\omega)| = k_p\sqrt{P(\omega)^2 + Q(\omega)^2} \tag{7.8}$$

The open-loop transfer function is:

$$L(j\omega) = G_c(j\omega)\,G(j\omega) \tag{7.9}$$

Fractional-order PID controller design must satisfy the five conditions to solve for the controller parameters [40]:

1 - Robustness:

$$\frac{d(Arg[L(j\omega)])}{d\omega}\Big|_{\omega=\omega_{cg}} = 0 \tag{7.10}$$

2 - Gain crossover frequency:

$$|L(j\omega)|_{dB} = 0 \tag{7.11}$$

3 - Phase Margin:

$$Arg[L(j\omega)]|_{\omega=\omega_{cg}} = -\pi + \varphi_m \tag{7.12}$$

4 - Noise rejection:

$$\left|T(j\omega) = \frac{C(j\omega)G(j\omega)}{1+C(j\omega)G(j\omega)}\right|_{dB} \leq A\ dB \tag{7.13}$$

Where A is a designed value.

5 - Disturbance rejection:

$$\left|S(j\omega) = \frac{1}{1+C(j\omega)G(j\omega)}\right|_{dB} \leq B\ dB \tag{7.14}$$

Where B is a designed value.

According to condition (1) we get:

$$\frac{p(\omega)aa-Q(\omega)bb}{p^2(\omega)+Q^2(\omega)} - \frac{0.947}{0.897\omega^2+1} - \frac{0.1052}{1.1067e^{-3}\omega^2+1} - \frac{0.03788}{1.4349e^{-3}\omega^2+1}$$

$$- \frac{0.01169}{1.366e^{-4}\omega^2+1} - \frac{0.007825}{6.1231e^{-5}\omega^2+1} - \frac{0.005602}{3.138e^{-5}\omega^2+1} = 0 \tag{7.15}$$

From condition (2) we get:

$$\frac{5.1689e^8 k_p\sqrt{P^2(\omega)+Q^2(\omega)}}{\sqrt{\omega^{12}+5.63e^4\omega^{10}+9.169e^8\omega^8+4.5e^{12}\omega^6+3.058e^{15}\omega^4+2.431e^{17}\omega^2+2.673e^{17}}} = 1 \tag{7.16}$$

From condition (3) we get:

$$Tan^{-1}\left[\frac{Q(\omega)}{P(\omega)}\right] - \tan^{-1}[0.947\omega] - \tan^{-1}[0.1052\omega] - \tan^{-1}[0.03788\omega] -$$

$$\tan^{-1}[0.01169\omega] - \tan^{-1}[0.007825\omega] - \tan^{-1}[0.005602\omega] = -\pi + \varphi_m \tag{7.17}$$

From condition (4) we get:

$$\frac{5.1689e^8 k_p \sqrt{p^2(\omega)+Q^2(\omega)}}{\sqrt{[5.1689e^8 k_p P(\omega)+5.17e^8-\omega^6+6.378e^4\omega^4-8.638e^7\omega^2]^2+[5.1689e^8 k_p Q(\omega)+428.8\omega^5-3.786e^6\omega^3+5.766e^8\omega]^2}} \leq A \quad (7.18)$$

Finally, from condition (5) we get:

$$\frac{\sqrt{\omega^{12}+5.63e^4\omega^{10}+9.169e^8\omega^8+4.5e^{12}\omega^6+3.058e^{15}\omega^4+2.431e^{17}\omega^2+2.673e^{17}}}{\sqrt{[5.1689e^8 k_p P(\omega)+5.17e^8-\omega^6+6.378e^4\omega^4-8.638e^7\omega^2]^2+[5.1689e^8 k_p Q(\omega)+428.8\omega^5-3.786e^6\omega^3+5.766e^8\omega]^2}} \leq B \quad (7\text{-}19)$$
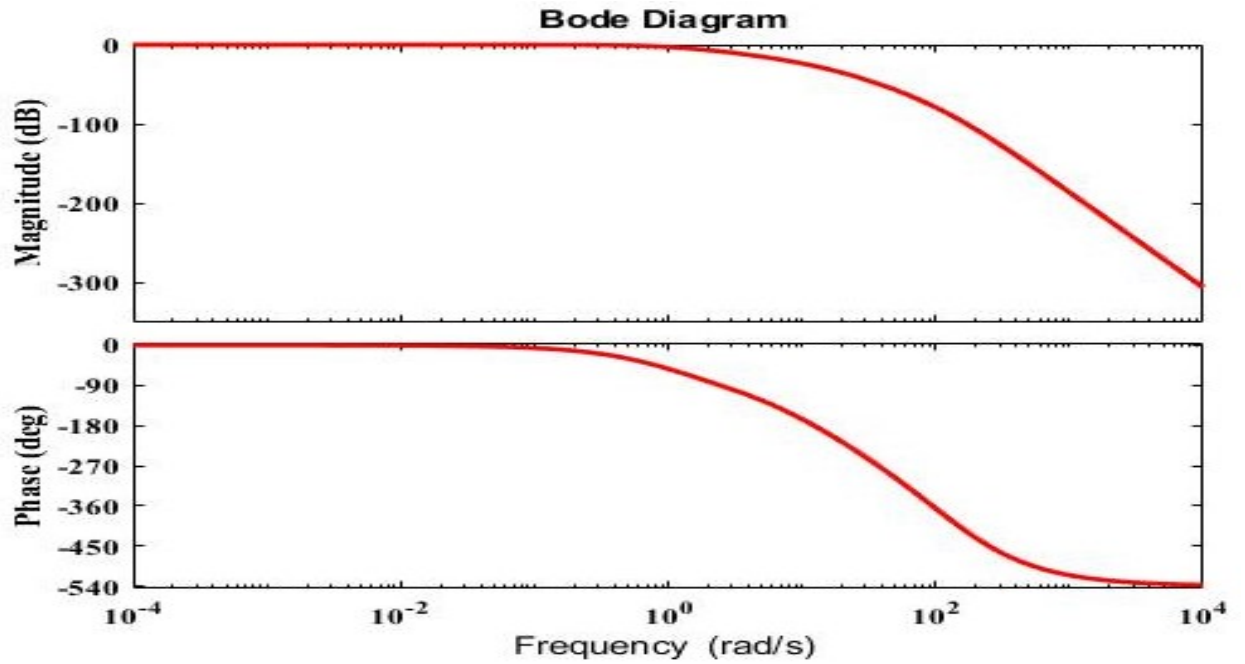
Figure 46: Bode plot diagram for the direct transfer function.

To get the FOPID controller parameters, we have solved Equations (7.15 through 7.19)

using the phase margin (-44.9∘) and the gain crossover frequency (0.8 rad/sec) from Figure

112

46, which is the Bode plot for the direct transfer function, A and B are chosen to be 20 dB; this was done using Nonlinear Optimization toolbox and Fsolve functions from MATLAB[TM].

The resulted FOPID is:

$$G_{FOPID}(s) = 1.0818 + \frac{0.265}{s^{0.9511}} + 0.549s^{0.9159}$$
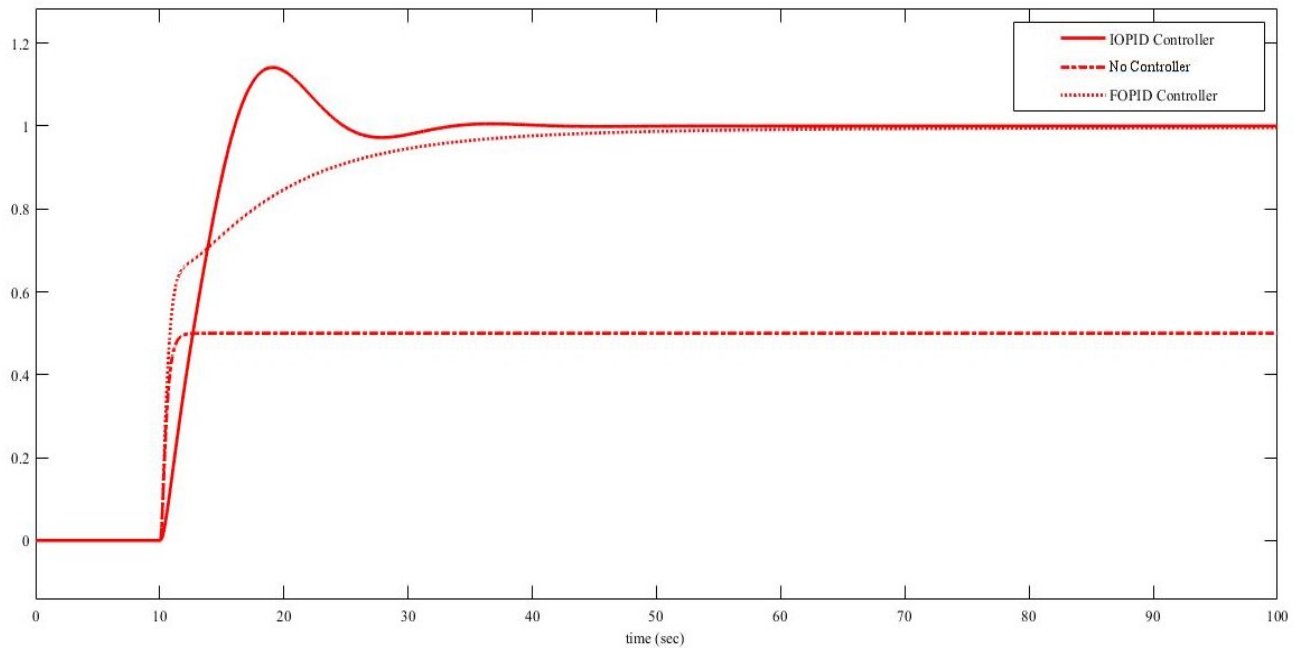
Figure 47: Step response results for direct transfer function G_1 using FOPID controller, IOPID controller, and No controller.

From Figure 47, we see that the FOPID controller produces the best step response with no overshoot, while the IOPID controller produces about 18% overshoot, the input was a unit step shifted on the x-axis to be away from the y-axis to see a clear response. Step response simulations permitted to find out which performance is advantageous. The result for the IOPID controller design was obtained using the first three conditions applied in the FOPID controller

113

design because we have only three parameters that needed to be found. The resulted IOPID controller was:

$$G_{IOPID}(\text{s}) = 0.1 + \frac{0.45572}{s} + 0.71194s$$

In Table 2, we show the step response properties for both the IOPID controller and the FOPID controller. From these results, we see that the FOPID controller performs better with regards to overshoot. On the other hand, we see that the IOPID controller has a lower Rise, and Settling time.

For our study, we decided that the critical criterion to be considered is the overshoot. This is because the heat conduction problem is a very slow process.

Table 2: Comparison of FOPID controller and IOPID controller step response properties.

Properties	IOPID	FOPID
Overshoot	14.1215	0
Rise Time	4.4376	13.3697
Settling Time	29.9342	39.9558

Next are the resulted response of the plant due to sinusoidal input of frequency of $\{40 + 10\sin(0.1\omega t)°C\}$. As shown in Figure 48 (a, b, and c), we see that the case of no controller response is half of the input signal, while both IOPID controller and FOPID

controller responses are practically the same as the input. The only concern is for the case of

the IOPID controller, we see the effect of the overshoot at the start of the simulation results.
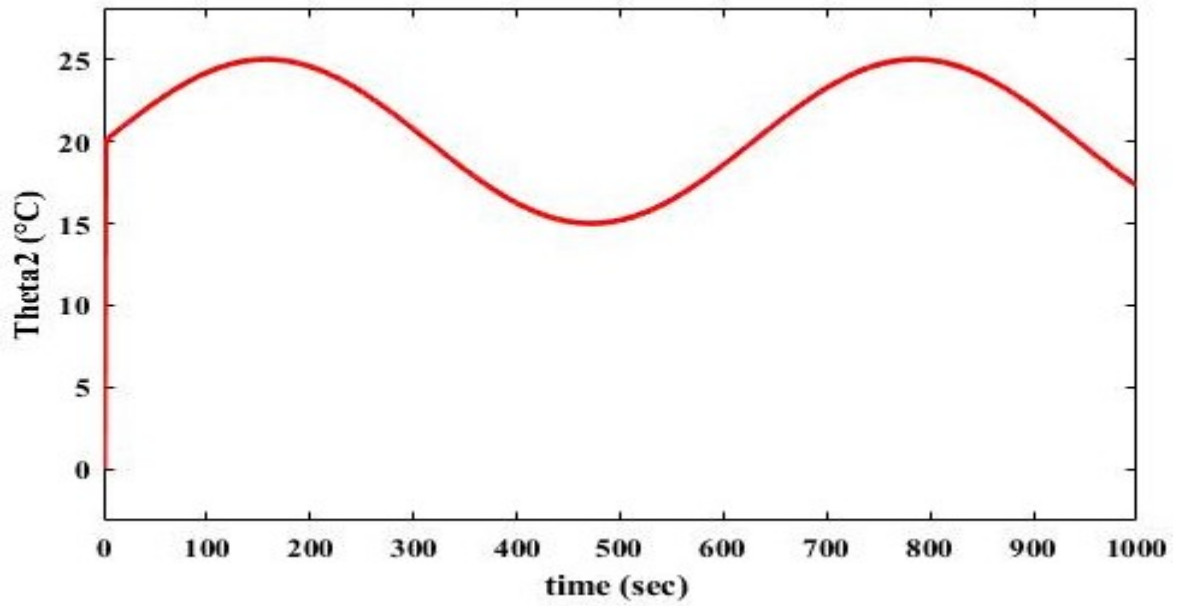
a
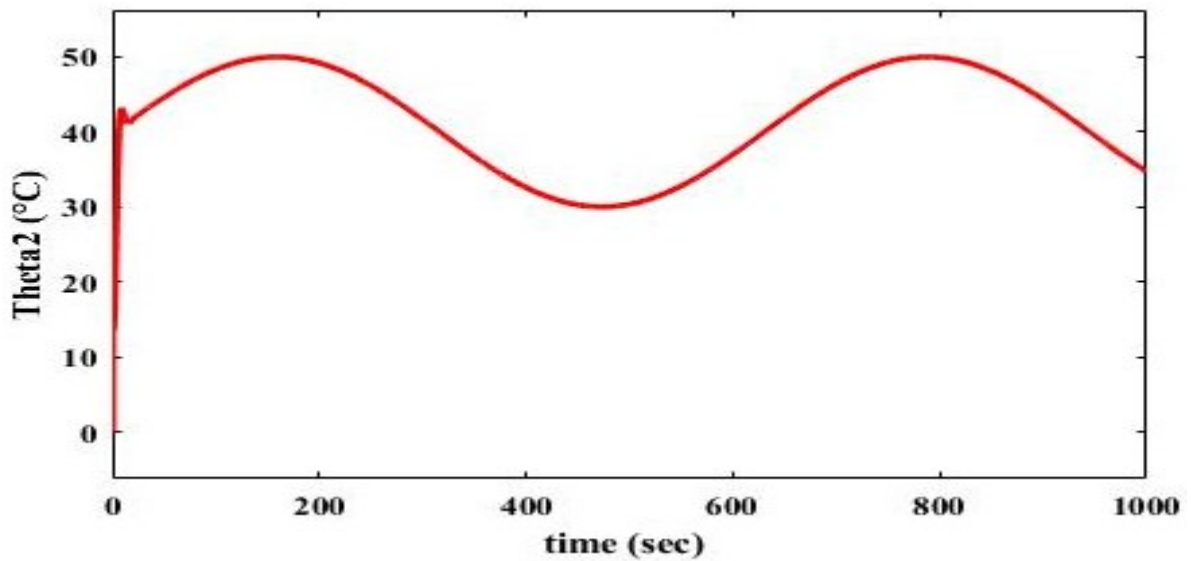
b
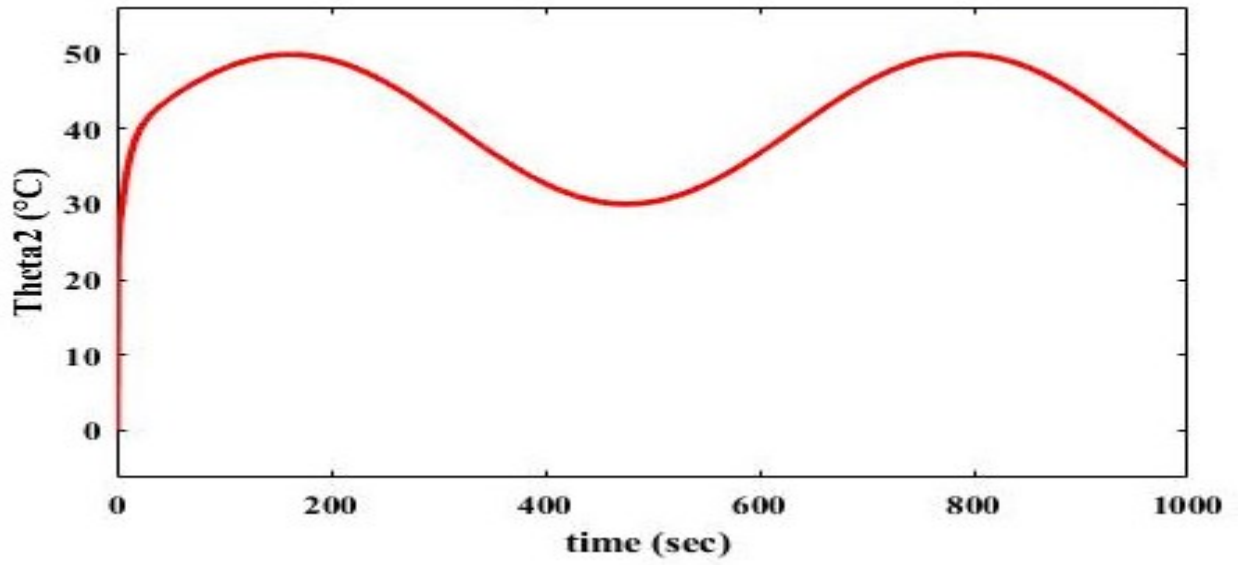
c

Figure (48): Comparison of plant response with a) No controller, b) IOPID controller, c) FOPID controller.
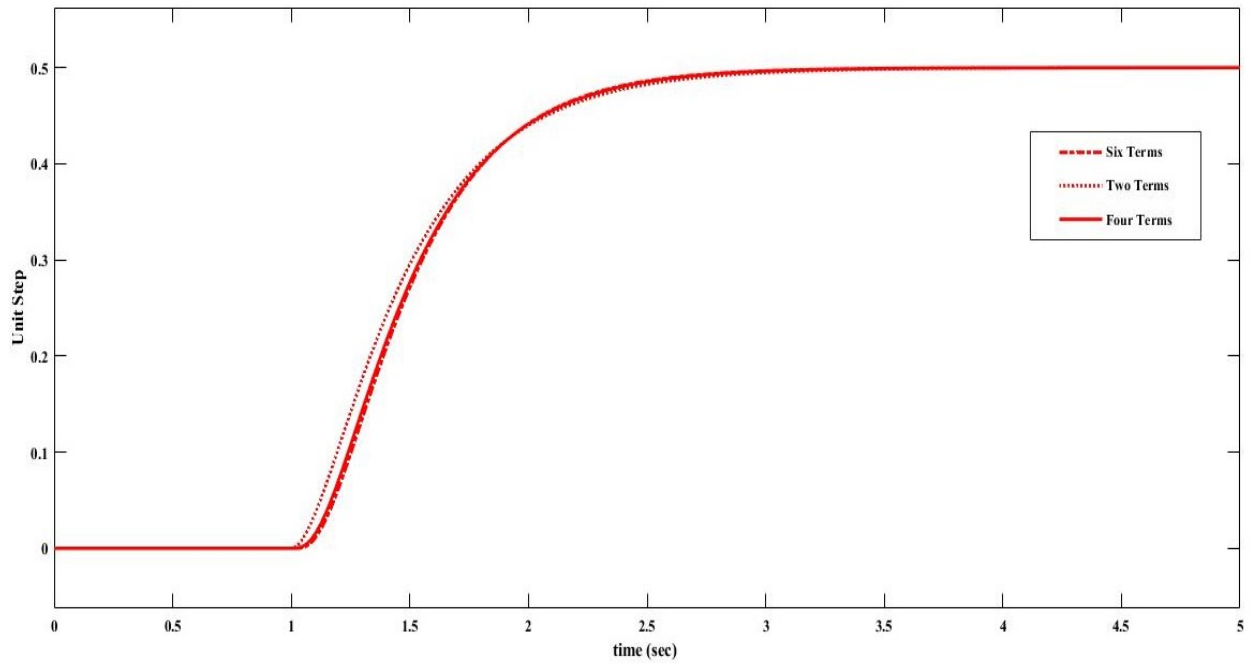
Figure (49): Step response comparison of two, four, and six terms used for approximation.

A different number of terms from Zero-Pole expansion was used to approximate the plant transfer function. The step response results are shown in Figure 49 and Figure 50. Results show that with a small number of terms, we could still get a good approximation. The case of two terms only results in slight changes than for three or more terms, while four, six, and eight terms cases are identical. We choose six terms to be the transfer function of interest.
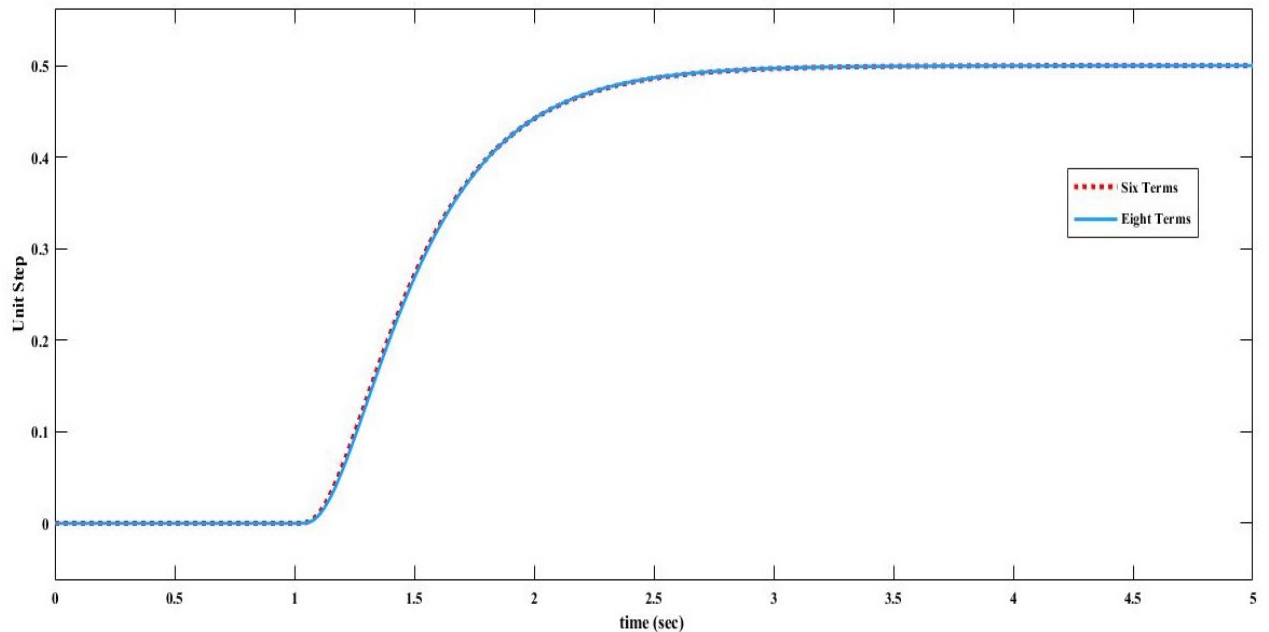
Figure (50): Step response comparison of six, and eight terms used for approximation.

7.2 Why Fractional Order Controller

The investigation in section (7.1) shows that both the IOPID controller and FOPID controller response are similar, except for the better performance of the FOPID controller with regard to the overshoot.

There are, however, other advantages of using the fractional-order controller. To do this, we will investigate the ability of the fractional-order controller to reduce noises compared

to the integer-order controller. To study the effect of using the FOPID on the measurement noises, we simulate the closed-loop scheme consisting of FOPID controller, the plant, and the random white noise of amplitude 1 in the feedback loop. The results are compared to the same closed-loop scheme for the IOPID controller. From the results shown in Figures (51 and 52), we see that for the FOPID controller results in (a) Figures have a significant ability to reduce noises are clear, while the IOPID controller results in (b) Figures show that almost there is no ability to reduce noises.

From this simulation study, we see that the FOPID controller can reduce noise. While for the IOPID controller it is shown that the ability to reduce noise is zero. We study this because noises always present in such a system, it comes from the plant or the measuring devices. In our case, that is the thermocouples used to measure temperatures.
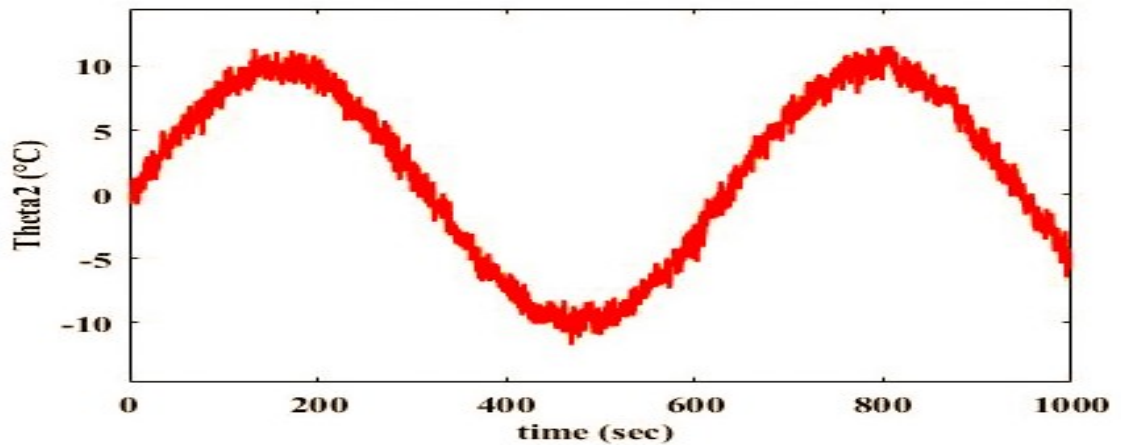
a
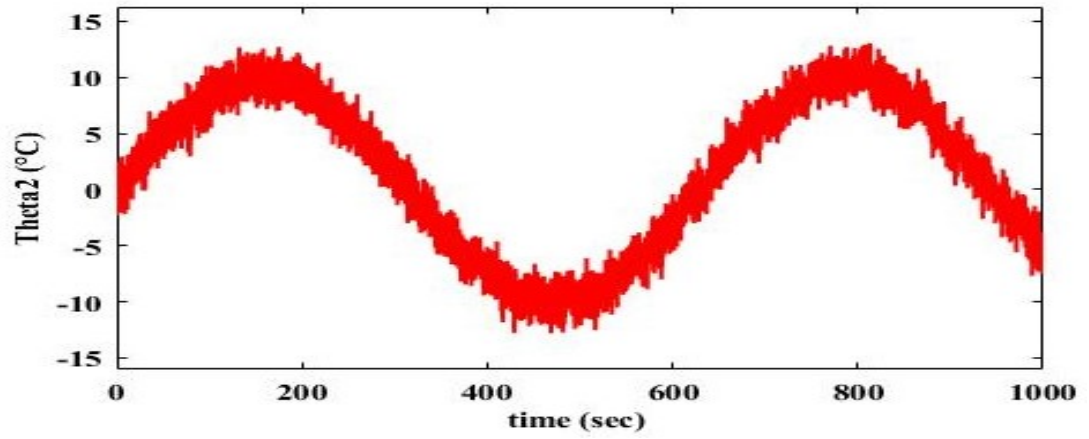
b

Figure 51: Theta2 response for frequency of 0.01 (rad/sec), a) FOPID controller, b) IOPID controller.

a

119
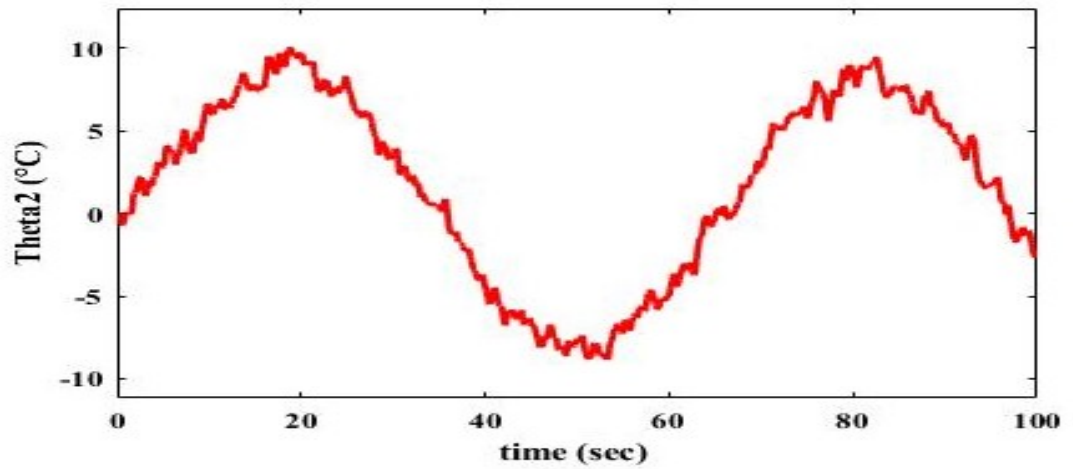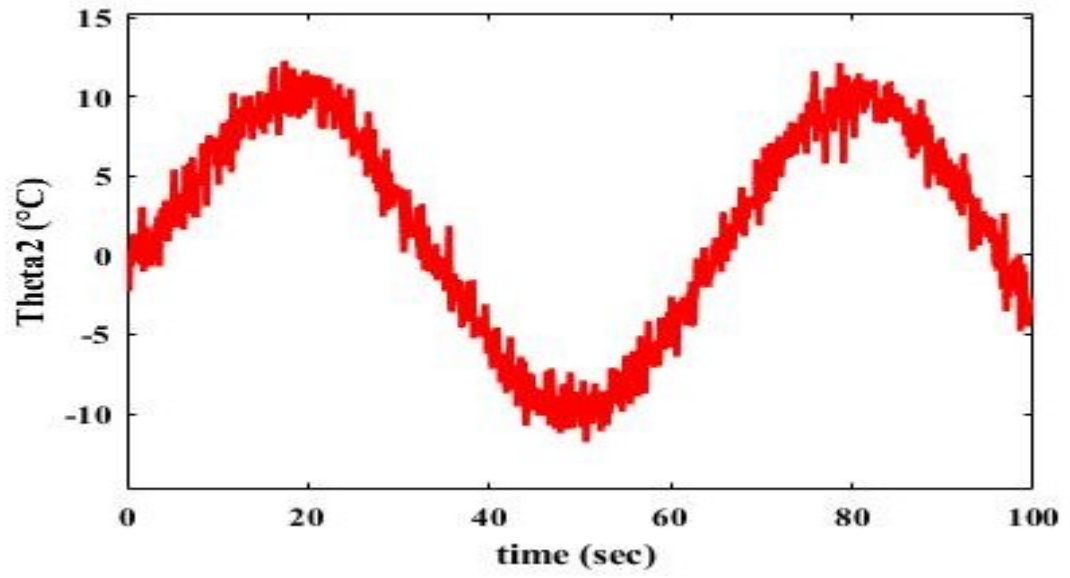
b

Figure 52: Theta2 response for frequency of 0.1 (rad/sec), a) FOPID controller, b) IOPID controller.

7.3 Results and Discussion

Experiments were carried out to verify the conclusions obtained using simulation results obtained for the above fractional order controller. Experiments were done for a very low frequency (0.0024, 0.0026, 0.0028 rad/sec). To physically achieve this frequency, silicone rubber heaters produced by OMEGA were used; while for the cooling, we use a fan with different values of the speeds. We control the speed of the fan to control the forced convection cooling rate following a sine wave. Both heating and cooling are controlled by the fractional order controller following the input sine wave. The cooling, however, is affected by the thermodynamics of the air between the fan and the plate. For these experiments, we used a heater of 500 watts, and to exactly give the required heat for each frequency, we used a variable AC input power supply for the heater. Experiments were done for 10^0C desired input temperature of (10sin(wt)) above the initial relative temperature of 40^0C and LABVIEW$^{\text{TM}}$ were used to run and record the results. The temperatures were measured using a K-type thermocouple produced by OMEGA.

Figures 53, 54, and 55 show that the experimental results almost produce the same simulated results. If we want to be more specific, we see that there is a lower end in the experimental results by 1^0C. The fractional-order controller shows very good results in the case of surface temperature control of a plate from both the simulated results and the experimental results. In experiments, the noise is present due to the use of the measurement devices. We face a lot of variations in the results: specifically the output signal of the controller. To overcome these difficulties, we have to add a low pass filter of 0.5 (rad/sec) cut-off frequency to filter out the signal and remove the high-frequency noise from the signal. The filter was used to get a smooth output signal, as we see in the experimental results.
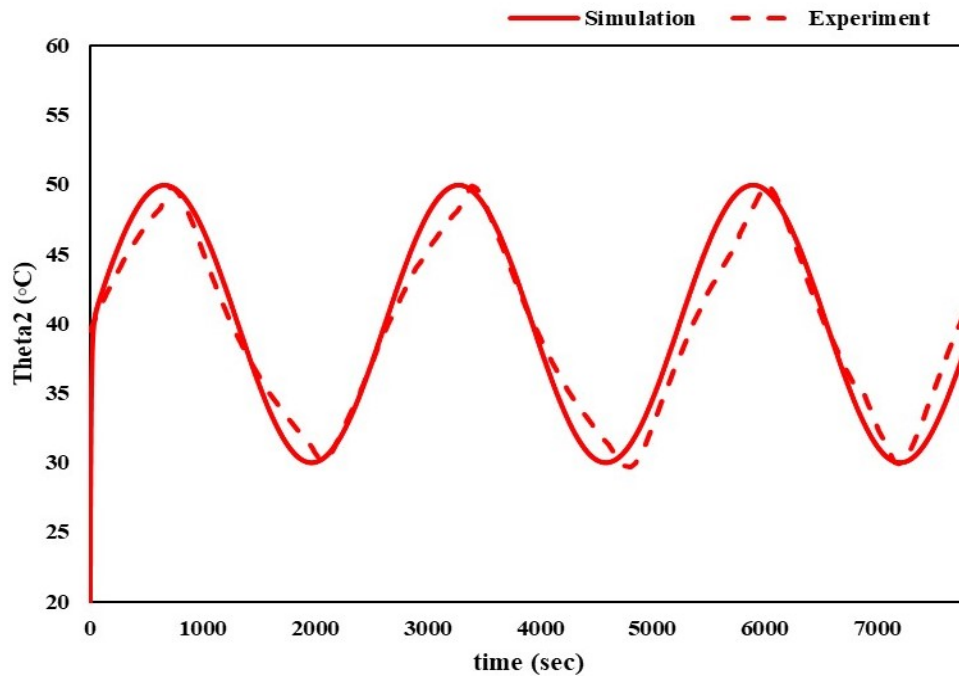
Figure 53: Relative temperature results for frequency of 0.0024 (rad/sec). a) The solid line is simulation result, b) Dashed line is an experimental result.
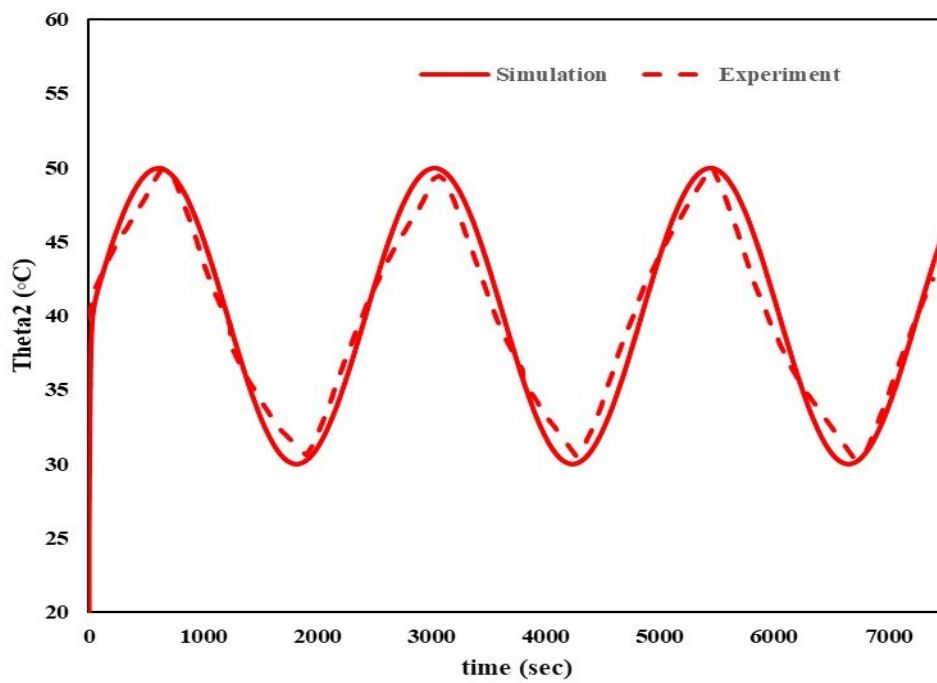
Figure 54: Relative temperature results for frequency of 0.0026 (rad/sec). a) The solid line is simulation result, b) Dashed line is an experimental result.
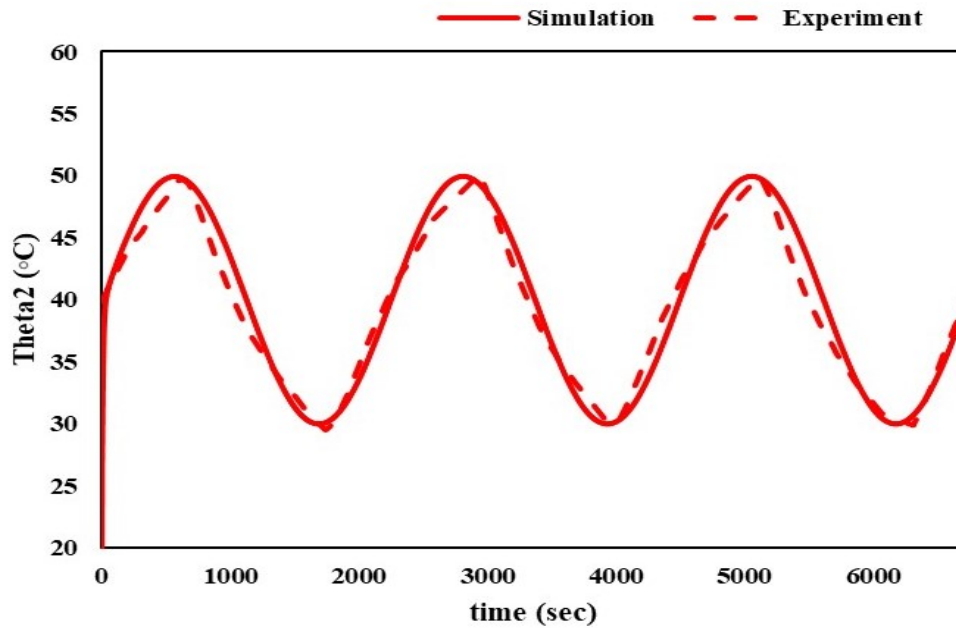
Figure 55: Relative temperature results for frequency of 0.0028 (rad/sec). a) The solid line is simulation result, b) Dashed line is an experimental result.

For the above experimental results, previous comments regarding the switch from heating to cooling are the same.

The results show that using a FOPID controller for the current system produces better results compared to an IOPID controller; this is why we proposed to use the fractional controller in a fractional-order system, as it is the case in our original system where the fractional-order was (0.5).

Chapter Eight: Conclusion and Future Work

8.1 Future Work

More study is needed for the multi-layer metal plates frequently used in the industry. This could start with extending this research study to a two-dimensional and three-dimensional case.

The fractional-order controller needs to be designed using a different design method, and the resulting controllers need to be compared to evaluate the benefits of each design.

Deferent types of boundary conditions need to be investigated. Temperature distribution through the plate thickness needs to be studied.

Multi heat-input in 1-D, 2- D and 3-D parts require distributed parameters heat transfer models and temperature controllers have to be developed.

8.2 Conclusions

The investigation concerns with achieving the desired temperature on one side surface of a plate controlled by a time-varying heat input on the other side. Simulations required the numerical calculation of high order transfer functions derivation, and the results show that the number of terms used in the approximation has a significant influence on the ill-posedness of the inverse problem. The simulation study verified that the temperature can be controlled for a wide range of frequency input.

The inverse problem approach, used in the first part of this study, shows that surface temperature can be efficiently controlled to the desired value. Experiments carried out to verify this approach show encouraging results, but only the low frequency can be achieved physically due to low-frequency bandwidth of plate heat transfer, and this range is up to 3 (rad/sec) maximum.

The fractional-order controller investigated as a second approach gives better results compared to the integer-order controller with regards to the overshoot. Different types of fractional order controllers were designed. Results show an improvement, depending on the number of parameters needed for each controller type. Such that when the number of controller parameters increases, the response of the controller becomes significantly better, but the performance saturates at a high number of parameters.

The fractional-order controller was investigated to find out its advantages over the integer-order controller, in particular with regard to the overshoot. Fractional order controller results show that response without overshoot can be achieved. The fractional-order controller design was experimentally investigated and verified. Results show that the fractional-order controller behaves better, which is proved by both experimental results and simulation results.

Fractional order systems can be controlled using both integer order controller and fractional-order controllers. The results were encouraging, but to be implemented for all fractional-order systems, they need to be further investigated.

The fractional-order controller shows good results in noise rejection produced by measuring devices compared to the integer-order controller. This is why we used the fractional controller with fractional-order systems.

Finally, during this study, we have done the following:

1- Designed the FOPID controller for a plate surface temperature control using multi-criteria applied to transient response.

2 - Simulation study and real-time experimental tests of the advantages of the proposed plate surface temperature Fractional Order - compared to Integer Order – PID.

3 – Multi-step control of a plate surface temperature control using an inverse problem approach under the constraint of ill-posedness.

4- Control of fractional-order heat conduction for a multi-layer plate.

5- Prove that the proposed Zero-Pole expansion is better than Taylor's expansion for the current research study.

References

[1] A. A. Dastjerdi, B. M. Vinagre, Y. Q. Chen, and S. H. HosseinNia, "Linear Fractional rder ontrollers; A urvey in the requency omain," *Annu. Rev. Control*, vol. 47, pp. 51–70, 2019.

[2] Milton Abramowitz and Irene A. Stegun., Handbook of Mathematical Functions with formulas, graphs, and mathematical tables, New York: Wiley, 1972.

[2] R. E. Gutiérrez, J. M. Rosário, and J. Tenreiro MacHado, Fractional Order Calculus: Basic Concepts and Engineering Applications, *Math. Prob. in Eng.*, vol. 2010, pp. 1-19 web, 2010.

[3] G. Stolz, Numerical Solutions to an Inverse Problem of Heat Conduction for Simple Shapes, *J. Heat Transfer* 82 (1), pp. 20-25, 1960.

[4] K. Miller and G. Viano, On the Necessity of Nearly-Best Possible Methods for Analytic Continuation of Scattering Data, *J. Math. Phys.,* vol. 14, no. 8, pp. 1037-1048, 1973.

[5] A. N. Tikhonov and V. Y. Arsenin, Solution of Ill-Posed Problems*, V. H. Winston & Sons,* Washington, DC, 1977.

[6] D. A. Murio, The Mollification Method and the Numerical Solution of an Inverse Heat Conduction Problem, *SIAM J. Stat. Comp.,* vol. 2, no. I, pp. 17-34, 1981.

[7] J. V. Beck, Nonlinear Estimation Applied to the Nonlinear Inverse Heat Conduction Problem, *Int. J. Heat Mass Transfer,* vol. 13, pp. 703-716, 1970.

[8] F. Scarpa and G. Milano, Kalman Smoothing Technique Applied to the Inverse Heat Conduction Problem, *Numerical Heat Transfer*, Part B, 28 pp. 79-96, 1995.

[9] Ching-yu Yangy and Chao-Kuang Chen, The Boundary Estimation in Two-Dimensional Inverse Heat Conduction Problems, *J. Phys. D: Appl. Phys*. vol. 29, pp. 333–339, 1996.

[10] M. Monde, Analytical Method in Inverse Heat Transfer Problem using Laplace Transform Technique, *International Journal of Heat and Mass Transfer,* vol. 43, pp. 3965-3975, 2000.

[11] I.N. Dul'kin and G.I. Garas'ko, Analytical Solutions of the 1-D Heat Conduction Problem for a Single Fin with Temperature Dependent Heat Transfer Coefficient – II. Recurrent Direct Solution, *International Journal of Heat and Mass Transfer,* vol. 45, pp. 1905–1914, 2002.

[12] J. R. Shenefelt, R. Luck, R. P. Talyor and J. T. Berry, Solution to Inverse Heat Conduction Problems Employing Singular Value Decomposition and Model-Reduction, *International Journal of Heat and Mass Transfer*, vol. 45, pp. 67-74, 2002.

[13] D. Necsulescu, Advanced Mechatronics: Monitoring and Control of Spatially Distributed Systems. *Singapore: World Scientific Company*, 2009.

[14] K. Woodbury, Inverse Engineering Handbook. *Boca Raton: CRC Press,* 2003.

[15] M. Ozisik and H. Orlande, Inverse Heat Transfer: Fundamentals and Applications, *New York ; Taylor & Francis,* 2000.

[16] J. Beck, B. Blackwell and JR Charles, Inverse Heat Conduction: Ill posed Problems. New York; *John Willey & Sons,* 1985.

[17] D. Maillet, S. Andre, J. Batsale, A. Degiovanni, and C. Moyne, Thermal Quadrupoles: Solving the Heat Equation Through Integral Transforms. Chichester ; *John Willey & Sons,* 2000.

[18] L. Torsten, A. Mhamdi, and W. Marquardt, Design, Formulation, and Solution of Multidimensional Inverse Heat Conduction Problems, *Numerical Heat Transfer,* Part B, vol. 47, pp. 111 - 133, 2005.

[19] X. Lu, and P. Tervola, Transient Heat Conduction in the Composite Slab-Analytical Method, *Journal of Physics A: Mathematical and General,* vol. 38, pp. 81 - 96, 2005.

[20] P. L. Woodfield, M. Monde, and Y. Mitsutake, Improved Analytical Solution for Inverse heat Conduction Problems on Thermally Thick and Semi-Infinite Solids, *International Journal of Heat and Mass Transfer,* vol. 49, pp. 2864 - 2876, 2006.

[21] R. Pourgholi, and M. Rostamian, A Numerical Technique for Solving IHCPs using Tikhonov Regularization Method, *Applied Mathematical Modelling,* vol. 34, pp. 2102 - 2110, 2010.

[22] Z. C. Feng, J. K. Chen, and Y. Zhang, Real-Time Solution of Heat Conduction in a Finite Slab for Inverse Analysis, *International Journal of Thermal Sciences,* vol. 49, pp. 762 - 768 ,2010.

[23] J. Zhou, Y. Zhang, J. K. Chen, and Z. C. Feng, Inverse Estimation of Surface Heating Condition in a Finite Slab with Temperature-Dependent Thermophysical Properties, *Heat Transfer Engineering,* vol. 32 No. 10, pp. 861 - 875, 2011.

[24] Z. C. Feng, J. K. Chen, Y. Zhang, and J. L. Griggs, Estimation of Front Surface Temperature and Heat Flux of a Locally Heated Plate from Distributed Sensor Data on the Back Surface, *International Journal of Heat and Mass Transfer*, vol. 54, pp. 3431 - 3439, 2011.

[25] Y. Ren, Y. Zhang, J. K. Chen, and Z. C. Feng, Inverse Estimation of the Front Surface Temperature of a 3D Finite Slab Based on the Back Surface Temperature Measured at Coarse Grids, *Numerical Heat Transfer,* part B, vol. 67, pp. 1 - 17, 2013.

[26] J. Pailhes, C. Pradere, J. L. Battaglia, J. Toutain, A. Kusiak, Aregba A. W., and Batsale J. C., Thermal Quadrupole Method with Internal Heat Sources, *International Journal of Thermal Sciences,* vol. 53, pp. 49-55, 2012.

[27] J.-C. Krapez and E. Dohou, Thermal Quadrupole Approaches Applied to Improve Heat Transfer Computations in Multilayered Materials with Internal Heat Sources, *International Journal of Thermal Sciences,* vol. 81, pp. 38-51, 2014.

[28] H. Najafi, K. A. Woodbury, and J. V. Beck, Real Time Solution for Inverse Heat Conduction Problems in a Two-Dimensional Plate with Multiple Heat Fluxes at the Surface, *International Journal of Heat and Mass Transfer*, vol. 91, pp. 1148 - 1156, 2015.

[29] S. Kukla and U. Siedlecka, Laplace Transform Solution of the Problem of Time-Fractional Heat Conduction in a Two-Layer Slab, *Journal of Applied Mathematics and Computational Mechanics,* vol. 14(4), pp. 105-113, 2015.

[30] C. Fan, F. Sun, and L. Yang, "A Simple Method for Inverse Estimation of Surface Temperature Distribution on a Flat Plate," Inverse Problems in Science and Engineering, Vol. 17, No. 7, pp. 885-899, 2009.

[31] Z. Feng, J. Chen, Y. Zhang and S. Montgomery-Smith, "Temperature and Heat Flux Estimation from Sampled Transient Sensor Measurements," International Journal of Thermal Sciences, vol. 49, pp. 2385-2390, 2010.

[32] S. Danaila, and A. Chira, Mathematical and Numerical Modeling of Inverse Heat Conduction Problem, *INCAS BULLETIN*, vol. 6, Issue, pp. 23 – 39, 2014.

[33] M. Ivanchov, and N. Kinash, Inverse Problem for the Heat-Conduction Equation in a Rectangular Domain, *Ukrainian Mathematical Journal,* vol. 69, no. 12, May 2018.

[34] H. Chen, I. Jay, J. Frankel, and M. Keyhani, Nonlinear Inverse Heat Conduction Problem of Surface Temperature Estimation by Calibration Integral Equation Method, Numerical Heat Transfer, Part B, vol. 73, no. 5, pp. 263–291, 2018.

[35] C. Chang, C. Liu, and C. Wang, Review of Computational Schemes in Inverse Heat Conduction Problems, *Journal of Smart Science*, vol. 6, no. 1, pp. 94–103, 2018.

[36] B. Gebhart, Heat Transfer, *McGraw Hill Inc*. USA, 2nd edition, 1971.

[37] K. Ogata, Modern Control Engineering. *5th ed. Upper Saddle River, New Jersey: Prentice-Hall,* 2010.

[38] D. Maillet, A. Andre, B. Batsale, Degiovanni A., and Moyne C., Thermal Quadrupoles: Solving the Heat Equation Through Integral Transforms. *John Willey & Sons*. Chichester, 1st edition, 2000.

[39] C. Monje, Y. Chen, B. Vinagre, D. Xue, and V. Feliu, Fractional-order Systems and Controls: Fundamentals and Applications. *Springer-Verlag*. New York, 1st edition. Ch. 5, 6, and 7, 2010.

[40] V. Shekher, V. Gupta, and S. Saroha, Analysis of Fractional Order PID Controller for Ceramic Infrared Heater, *International Journal of Engineering Development and Research*. vol. 4, issue 1, pp. 43-52, 2016.

[41] W. Zheng, Y. Lou, Y. Chen, Y. Pi, and W. Yu, An Improved Frequency-Domain Method for the Fractional Order $PI^{\lambda}D^{\mu}$ Controller Optimal Design, *International Federation of Automatic control.*, 51-4, pp. 681-686, 2018.

[42] E. Cokmez, S. Atic, F. Peker, and I. Kaya, Fractional-order PI Controller Design for Integrating Process Based on Gain and Phase Margin Specifications, *International Federation of Automatic Control*. 51-4, pp. 751-756, 2018.

[43] H. Li, Y. Lou, and Y. Chen, A Fractional Order Proportional and Derivative (FOPD) Controller: Tuning Rule and Experiments, *IEEE Transactions on Control Systems Technology*. vol. 18, no. 2, pp. 516-520, 2010.

[44] HongSheng Li and YangQuan Chen, A Fractional Order Proportional and Derivative (FOPD) Controller Tuning Algorithm, 2008 Chinese Control and Decision Conference, Yantai, Shandong, 2008, pp. 4059-4063.

[45] V. Batlle, R. Perez, and F. Garcia, Simple Fractional Order Controller Combined with a Smith Predictor for Temperature Control in a Steel Slab Reheating Furnace, *International Journal of Control, Automation, and Systems*. Vol. 11(3), pp. 533-544, 2013.

[46] C. Muresan, S. Folea, G. Mois, and E. Dulf, Development and Implementation of an FPGA Based Fractional Order Controller for a DC Motor, *Mechatronics*., vol. 23, Issue 7, pp. 798-804, 2013.

[47] C. Flores, V. Milanés and F. Nashashibi, Using Fractional Calculus for Cooperative Car-Following Control, *2016 IEEE 19th International Conference on Intelligent Transportation Systems (ITSC), Rio de Janeiro,* 2016*, pp. 907-912.*

[48] N. Tan, A. Yuce, and F. Deniz, Teaching Fractional Order Control Systems Using Interactive Tools, *International Conference on Education in Mathematics, Science & Technology (ICEMST)*. Vol. 4, pp. 554-563, Bodrum, Turkey, May 2016.

[49] R. Maurya and M. Bhandari, "Design of Optimal PID [FOPID] Controller for Linear System," *2016 International Conference on Micro-Electronics and Telecommunication Engineering (ICMETE), Ghaziabad,* 2016, *pp. 439-443.*

[50] D. Saptarshi, S. Suman, D. Shantanu, and G. Amitava, On the Selection of Tuning Methodology of FOPID Controllers for the Control of Higher Order Processes, *ISA Transactions,* vol. 50, issue 3, pp.376-388, July 2011.

[51] S. Jesus Isabel, and J. A. Machado Tenreiro, Fractional Control of Heat Diffusion Systems, *Journal of Nonlinear Dynamic*, vol. 54, pp. 263-282, 2008.

[52] R. Rapaic Milan, and D. Jelicic Zoran, Optimal Control of a Class of Fractional Heat Diffusion Systems, *Journal of Nonlinear dynamic*, vol. 62, pp. 39-51, 2010.

[53] R. El-khazali, Fractional-Order $PI^\lambda D^\mu$ Controller Design, *Computers and Mathematics with Applications*, vol. 66, pp. 639-646, 2013.

[54] W. Zheng, Y. Lou, X. Wang, Y. Pi, and Y. Chen, Fractional Order $PI^\lambda D^\mu$ Controller Design for Satisfying Time and Frequency Domain Specifications Simultaneously, *ISA Transactions*, vol. 68, pp. 212-222, 2017.

[55] M. Tavakoli-Kakhki, and M. Haeri, Temperature Control of a Cutting Process Using Fractional Order Proportional-Integral-Derivative Controller, *Journal of Dynamic Systems, Measurement, and Control*, Vol. 133, 2011.

[56] I. S. Jesus, R. S. Barbosa, J. A. T. Machado and J. B. Cunha, Strategies for the Control of Heat Diffusion Systems Based on Fractional Calculus, *2006 IEEE International Conference on Computational Cybernetics, Budapest, 2006, pp. 1-6.*

[57] V. Mehra, S. Srivastava, and P. Varshney, "Fractional-Order PID Controller Design for Speed Control of DC Motor," *2010 3rd International Conference on Emerging Trends in Engineering and Technology, Goa, 2010, pp. 422-425.*

[58] V. Ranjan, S. Jadhav and M. Patil, Design of Integer and Fractional order PID Controller using Dominant Pole Placement Method, *IJCA Proceedings on International Conference and Workshop on Emerging Trends in Technology 2014* ICWET 2014(2):19-24, May 2013.

[59] **U.** Al-Saggaf, I. Mehedi, M. Bettayeb, and R. Mansouri**,** Fractional-Order Controller Design for a Heat Flow Process, *Journal of Systems and Control Engineering*, Vol. 230(7), pp. 680–691, 2016.

[60] M. Bongulwar, and B. Patre, Design of FOPID Controller for Fractional-Order Plants with Experimental Verification, *International Journal of Dynamic Control*, vol. 6, pp. 213–223, 2018.

[61] R. Mettu, and R. Ganta, Design of Fractional Order $PI^\lambda D^\mu$ Controller for Liquid Level Control of a Spherical Tank Modeled As a Fractional Order System, *Int. Journal of Engineering Research and Applications,* Vol. 3, Issue 6, pp.438-443, 2013.

[62] I. Jesus, J. Machado, and R. Barbosa, Control of a Heat Diffusion System through a Fractional Order Nonlinear Algorithm, *Journal of Computers and Mathematics with Applications,* vol. 59, pp. 1687-1694, 2010.

[63] J. Viola, L. Angel and J. M. Sebastian, Design and Robust Performance Evaluation of a Fractional Order PID Controller Applied to a DC Motor, *in IEEE/CAA Journal of Automatica Sinica, vol. 4, no. 2, pp. 304-314, April 2017.*

[64] E. Edet and R. Katebi, Design and Tuning of Fractional-Order PID Controllers for Time-Delayed Processes, *2016 UKACC 11th International Conference on Control (CONTROL), Belfast, 2016, pp. 1-6.*

[65] R. Caponetto, G. Dongola, L. Fortuna, and A. Gallo, New Results on the Synthesis of FO-PID Controllers, *Communications in Nonlinear Science and Numerical Simulation*, vol. 15, pp. 997–1007, 2010.

[66] S. Dormido, E. Pisoni, and A. Visioli, Interactive Tools for Designing Fractional-Order PID Controllers, *International Journal of Innovative Computing, Information and Control,* vol. 8, no. 7(A), pp. 4579-4590, July 2012.

[67] F. Zhang, C. Yang, X. Zhou, and W. Gui, Fractional-Order PID Controller Tuning using Continuous State Transition Algorithm, *Neural Computing & Applications*, vol. 29, pp. 795–804, 2018.

[68] M. Vajta, Fractional Order Model and Controller of a Heat Process, *IFAC Proceedings Volumes*, vol. 45, Issue 2, 2012, pp. 587-592, 2012.

[69] A. Yüce, N. Tan, and D. Atherton, Fractional Order PI Controller Design for Time Delay Systems, *IFAC- (International Federation of Automatic Control)*, vol. 49, issue 10, pp. 94–99, 2016.

[70] Z. Yakoub, M. Chetoui, M. Amairi, and M. Aoun, Model-Based Fractional Order Controller Design, *IFAC- (International Federation of Automatic Control),* vol. 50, issue 1, pp. 10431–10436, 2017.

[71] D. Sierociuk, and M. Wiraszka, A New Variable Fractional-Order PI Algorithm, *IFAC-(International Federation of Automatic Control),* vol. 51, issue 4, pp. 745–750, 2018.

[72] C. Yin, S. Zhong, and W. Chen, Design of Sliding Mode Controller for a Class of Fractional-Order Chaotic Systems, *Communications in Nonlinear Science and Numerical Simulation*, vol. 17, pp. 356–366, 2012.

[73] L. Angel and J. Viola, Design and Statistical Robustness Analysis of FOPID, IOPID and SIMC PID Controllers Applied to a Motor-Generator System, *in IEEE Latin America Transactions, vol. 13, no. 12, pp. 3724-3734, Dec. 2015.*

[74] M. Aghababa, Optimal Design of Fractional-Order PID Controller for Five Bar Linkage Robot using a New Particle Swarm Optimization Algorithm, *Soft Computing*, vol. 20, issue 10, pp. 4055-4067, 2016.

[75] A. Zamani, S. Barakati, and S. Yousofi-Darmian, Design of a Fractional Order PID Controller using GBMO Algorithm for Load-Frequency Control with Governor Saturation Consideration, *ISA Transactions*, vol. 64, pp. 56–66, 2016.

[76] L. Ouhsaine, Y. Boukal, M. El-Ganaoui, M. Darouach, M. Zasadzinski, A. Mimet, and N. Radhy, A General Fractional-Order Heat Transfer Model for Photovoltaic/Thermal Hybrid Systems and Its Observer Design, *Energy Procedia,* vol. 139, pp. 49-54, 2017.

[77] M. Bongulwar, and B. Patre, Design of $PI^\lambda D^\mu$ controller for Global Power Control of Pressurized Heavy Water Reactor, *ISA Transactions*, vol. 69, pp.234–241, 2017.

[78] S. Swain, D. Sain, S. Mishra, and S. Ghosh, Real Time Implementation of Fractional Order PID Controllers for a Magnetic Levitation Plant, *International Journal of Electronics and Communications*, vol. 78, pp. 141–156, 2017.

[79] K. Gherfia, A. Charef, and H. Abbassi, Proportional Integral-Fractional Filter Controller Design for First Order Lag Plus Time delay System, *International Journal of Systems Science*, vol. 49, no. 8, pp. 1654–1673, 2018.

[80] R. Sumathi, and P. Umasankar, Optimal Design of Fractional Order PID Controller for Time-Delay Systems: an IWLQR Technique, *International Journal of General Systems*, vol. 47, no. 7, pp. 714–730, 2018.

[81] T. Zhan, and S. Ma, The Controller Design for Singular Fractional-Order Systems with Fractional Order $0 < \alpha < 1$, *ANZIAM Journal*, vol. 60, pp. 230–248, 2018.

[82] A. Maddahi, N. Sepehri, and W. Kinsner, Fractional-Order Control of Hydraulically Powered Actuators: Controller Design and Experimental Validation, *IEEE/ASME Transaction on Mechatronics*, vol. 24, no. 2, April 2019.

[83] A. Chevalier, C. Francis, C. Copot, C. Ionescu, and R. De Keyser, Fractional-Order PID Design: Towards Transition from State-of-Art to State-of-Use, *ISA Transactions*, vol. 84, pp. 178–186, 2019.

[84] M. Jain, A. Rani, N. Pachauri, V. Singh, and A. Mittal, Design of Fractional Order 2-DOF PI Controller for Real-Time Control of Heat Flow Experiment, *International Journal of Engineering Science and Technology*, vol. 22, pp. 215–228, 2019.

[85] Liu, L., F. Pan, and D. Xue, Fractional-Order Controller Design for Oscillatory Fractional Time-Delay Systems Based on the Numerical Inverse Laplace Transform Algorithms. *Mathematical Problems in Engineering 2015 (2015): 1–10. Web.*

[86] C. Wang, W. Fu, and Y. Shi, Tuning Fractional Order Proportional Integral Differentiation Controller for Fractional Order System, *Proceedings of the 32nd Chinese Control Conference, Xi'an, 2013, pp. 552-555.*

[87] S. Elmetennani, I. N'Doye, K. N. Salama and T. Laleg-Kirati, Performance Analysis of Fractional-Order PID Controller for a Parabolic Distributed Solar Collector, *2017 IEEE AFRICON, Cape Town, 2017, pp. 440-445.*

[88] C. Wang, X. Liu, H. Shi, R. Xin and X. Xu, Design and Implementation of Fractional PID Controller for Rotary Inverted Pendulum, *2018 Chinese Control And Decision Conference (CCDC), Shenyang, 2018, pp. 6730-6735.*

[89] Barbosa, Ramiro & Silva, Manuel & Tenreiro Machado, José & Galhano, Alexandra & Jesus, Isabel & Reis, Cecília & Marcos, Maria. (2010). Some Applications of Fractional Calculus in Engineering. *Mathematical Problems in Engineering 2010.* *https://doi.org/10.1155/2010/639801*.

[90] P. Shah, and S. Agashe, Review of Fractional PID Controller, *Mechatronics*, vol. 38, pp. 29–41, 2016.

[91] Junyi, C., and C. Binggang, Fractional-Order Control of Pneumatic Position Servosystems, *Mathematical Problems in Engineering 2011.* https://doi.org/10.1155/2011/287565.

[92] P. Kumar, S. Chatterjee, D. Shah, U. Saha, and S. Chatterjee, On Comparison of Tuning Method of FOPID Controller for Controlling Field Controlled DC Servo Motor, *Cogent Engineering*, vol. 4.1, 2017. https://doi.org/10.1080/23311916.2017.1357875.

[93] A. V. Panteleev, T. A. Letova, and E. A. Pomazueva, Parametric Design of Optimal in Average Fractional-Order PID Controller in Flight Control Problem, *Automation and Remote Control,* 2018, Vol. 79, No. 1, pp. 153–166.

[94] **K.** Ranjbaran, and M. Tabatabaei, Fractional Order [PI], [PD] and [PI][PD] Controller Design using Bode's Integrals, *International Journal of Dynamic and Control*, vol. 6, pp. 200–212, 2018.

[95] Y. Tang, X. Zhang, D. Zhang, G. Zhao, and X. Guan, Fractional Order Sliding Mode Controller Design for Antilock Braking Systems, *Neurocomputing*, vol. 111, pp. 122–130, 2013.

Appendices

All appendices follow Procedure from Monje et al Book [39].

A: FOPID Controller Design

The Zero-Pole approximated plate direct transfer function is:

$$G_1 = \frac{5.169*10^8}{(s+1.056)(s+9.054)(s+26.4)(s+85.54)(s+127.8)(s+178.5)} \tag{A.1}$$

The magnitude of the direct transfer function is:

$$|G_1(j\omega)| = \frac{5.1689e^8}{\sqrt{\omega^{12}+5.63e^4\omega^{10}+9.169e^8\omega^8+4.5e^{12}\omega^6+3.058e^{15}\omega^4+2.431e^{17}\omega^2+2.673e^{17}}} \tag{A.2}$$

The phase of the direct transfer function is:

$$Arg[G_c(j\omega)] =$$
$$-tan^{-1}(\tfrac{\omega}{1.056})-tan^{-1}(\tfrac{\omega}{9.504})-tan^{-1}(\tfrac{\omega}{26.4})-tan^{-1}(\tfrac{\omega}{85.54})-tan^{-1}(\tfrac{\omega}{127.8})-tan^{-1}(\tfrac{\omega}{178.5}) \tag{A.3}$$

The FOPID controller formula is:

$$G_c(s) = k_p[1 + \frac{k_i}{(s)^\lambda} + k_d(s)^\mu] \tag{A.4}$$

Which can be rewritten as:

$$G_c(j\omega) = k_p\{1 + k_i\omega^{-\lambda}\left[\cos\left(\tfrac{\lambda\pi}{2}\right)+jsin\left(\tfrac{-\lambda\pi}{2}\right)\right] + k_d\left(\omega\right)^\mu\left[\cos\left(\tfrac{\mu\pi}{2}\right)+j\sin\left(\tfrac{\mu\pi}{2}\right)\right]\} \tag{A.5}$$

$$G_c(j\omega) = k_p\{1 + k_i\omega^{-\lambda}\cos\left(\frac{\lambda\pi}{2}\right) + k_d(\omega)^\mu\cos\left(\frac{\mu\pi}{2}\right)$$

$$+j\left[k_i\omega^{-\lambda}\sin\left(\frac{-\lambda\pi}{2}\right) + k_d(\omega)^\mu\sin\left(\frac{\mu\pi}{2}\right)\right]\} \tag{A.6}$$

We denote:

$$P(\omega) = 1 + k_i\omega^{-\lambda}\cos\left(\frac{\lambda\pi}{2}\right) + k_d(\omega)^\mu\cos\left(\frac{\mu\pi}{2}\right) \tag{A.7}$$

And

$$Q(\omega) = -k_i\omega^{-\lambda}\sin\left(\frac{\lambda\pi}{2}\right) + k_d(\omega)^\mu\sin\left(\frac{\mu\pi}{2}\right) \tag{A.8}$$

Then the phase angle of the FOPID controller transfer function is:

$$Arg[G_c(j\omega)] = tan^{-1}\left[\frac{Q(\omega)}{P(\omega)}\right] \tag{A.9}$$

And the magnitude of the FOPID controller transfer function is:

$$|G_c(j\omega)| = k_p\sqrt{P(\omega)^2 + Q(\omega)^2} \tag{A.10}$$

The open loop transfer function is:

$$L\ (j\omega) = G_c(j\omega)\ G\ j\omega) \tag{A.11}$$

Fractional order PID controller design must satisfy five conditions to solve for the controller parameters [34]:

1- Robustness:

$$\frac{d(Arg[L(j\omega)]}{d\omega}\Bigg|_{\omega=\omega_{cg}} = 0$$

2 - Gain crossover frequency:

$$|L(j\omega)|_{dB} = 0$$

3 - Phase Margin:

$$Arg[L(j\omega)]|_{\omega=\omega_{cg}} = -\pi + \varphi_m$$

4 - Noise rejection:

$$\left|T(j\omega) = \frac{C(j\omega)G(j\omega)}{1+C(j\omega)G(j\omega)}\right|_{dB} \leq A \ dB$$

Where A is a designed value.

5 - Disturbance rejection:

$$\left|S(j\omega) = \frac{1}{1+C(j\omega)G(j\omega)}\right|_{dB} \leq B \ dB$$

Where B is a designed value.

According to condition (1), we have:

$$\frac{d(Arg[L(j\omega)]}{d\omega}\Bigg|_{\omega=\omega_{cg}} = 0$$

$$Arg[L(j\omega)] =$$
$$tan^{-1}[\frac{Q(\omega)}{P(\omega)}] - tan^{-1}(\frac{\omega}{1.056}) - tan^{-1}(\frac{\omega}{9.504}) - tan^{-1}(\frac{\omega}{26.4}) - tan^{-1}(\frac{\omega}{85.54}) - tan^{-1}(\frac{\omega}{127.8}) - tan^{-1}(\frac{\omega}{178.5}) \quad (A.12)$$

To get the derivative of $\dfrac{d(tan^{-1}[\frac{Q(\omega)}{P(\omega)}])}{d\omega}$

Let $\quad y_2 = tan^{-1}\left[\frac{Q(\omega)}{P(\omega)}\right]$

Then $\quad tan(y_2) = \left[\frac{Q(\omega)}{P(\omega)}\right]$

$$\frac{1}{\cos^2 y_2} \frac{dy_2}{d\omega} = \frac{P(\omega) * aa - Q(\omega) * pp}{P^2(\omega)}$$

Where

$$aa = \lambda k_i\, \omega^{-\lambda-1} \sin\left(\frac{\lambda\pi}{2}\right) + \mu k_d \omega^{\mu-1} \sin\left(\frac{\lambda\pi}{2}\right)$$

And

$$pp = -\lambda k_i\, \omega^{-\lambda-1} \cos\left(\frac{\lambda\pi}{2}\right) + \mu k_d \omega^{\mu-1} \cos\left(\frac{\lambda\pi}{2}\right)$$

From the above, we get:

$$\frac{dy_2}{d\omega} = \frac{P(\omega) * aa - Q(\omega) * pp}{P^2(\omega)} \frac{\cos^2 y_2}{\cos^2 y_2 + \sin^2 y_2}$$

$$\frac{\cos^2 y_2 + \sin^2 y_2}{\cos^2 y_2} = tan^2 y_2 + 1$$

Using $\tan(y_2) = \left[\frac{Q(\omega)}{P(\omega)}\right]$ we get

$$\frac{\cos^2 y_2 + \sin^2 y_2}{\cos^2 y_2} = \frac{Q^2(\omega) + P^2(\omega)}{P^2(\omega)}$$

And

$$\frac{dy_2}{d\omega} = \frac{P(\omega) * aa - Q(\omega) * pp}{P^2(\omega) + Q^2(\omega)}$$

Now to get

146

$$\frac{d(tan^{-1}[0.947\omega])}{d\omega}$$

Let

$$y_1 = tan^{-1}(0.947\omega)$$

$$tan(y_1) = (0.947\omega)$$

$$\frac{1}{cos^2 y_1}\frac{dy_1}{d\omega} = 0.947$$

$$\frac{dy_1}{d\omega} = 0.947\frac{cos^2 y_1}{cos^2 y_1 + sin^2 y_1}$$

$$\frac{cos^2 y_1 + sin^2 y_1}{cos^2 y_1} = tan^2 y_1 + 1$$

$$\frac{dy_1}{d\omega} = \frac{d(tan^{-1}[0.947\omega])}{d\omega} = \frac{0.947}{0.897\omega^2 + 1}$$

Similarly,

$$\frac{d(tan^{-1}[0.1052\omega])}{d\omega} = \frac{0.1052}{0.011067\omega^2 + 1}$$

$$\frac{d(tan^{-1}[0.0.03788\omega])}{d\omega} = \frac{0.03788}{0.0014349\omega^2 + 1}$$

$$\frac{d(tan^{-1}[0.001169\omega])}{d\omega} = \frac{0.01169}{1.3666e^{-4}\omega^2 + 1}$$

$$\frac{d(tan^{-1}[0.0.007825\omega])}{d\omega} = \frac{0.007825}{6.1231e^{-5}\omega^2 + 1}$$

$$\frac{d(tan^{-1}[0.005602\omega])}{d\omega} = \frac{0.0.00562}{3.138e^{-5}\omega^2 + 1}$$

Finally, from condition (1), we get:

$$\frac{p(\omega)aa - Q(\omega)bb}{p^2(\omega) + Q^2(\omega)} - \frac{0.947}{0.897\omega^2+1} - \frac{0.1052}{1.1067e^{-3}\omega^2+1} - \frac{0.03788}{1.4349e^{-3}\omega^2+1} - \frac{0.01169}{1.366e^{-4}\omega^2+1}$$

$$-\frac{0.007825}{6.1231e^{-5}\omega^2+1} - \frac{0.005602}{3.138e^{-5}\omega^2+1} = 0 \tag{A.13}$$

From condition (2), we get:

$$\frac{5.1689e^8 k_p\sqrt{P^2(\omega)+Q^2(\omega)}}{\sqrt{\omega^{12}+5.63e^4\omega^{10}+9.169e^8\omega^8+4.5e^{12}\omega^6+3.058e^{15}\omega^4+2.431e^{17}\omega^2+2.673e^{17}}} = 1 \tag{A.14}$$

From condition (3), we get:

$$\text{Tan}^{-1}\left[\frac{Q(\omega)}{P(\omega)}\right] - tan^{-1}[0.947\omega] - tan^{-1}[0.1052\omega] - tan^{-1}[0.03788\omega] - tan^{-1}[0.01169\omega] -$$

$$tan^{-1}[0.007825\omega] - tan^{-1}[0.005602\omega] = -\pi + \varphi_m \tag{A.15}$$

From condition (4), we have:

$$\left|\frac{C(j\omega)G(j\omega)}{1+C(j\omega)G(j\omega)}\right|_{dB} \le A\ dB \tag{A.16}$$

$$\left|\frac{C(j\omega)G(j\omega)}{1+C(j\omega)G(j\omega)}\right| = \frac{|C(j\omega)G(j\omega)|}{|1+C(j\omega)G(j\omega)|}$$

$$|C(j\omega)G(j\omega)| = \frac{5.1689e^8 k_p\sqrt{P^2(\omega)+Q^2(\omega)}}{\sqrt{\omega^{12}+5.63e^4\omega^{10}+9.169e^8\omega^8+4.5e^{12}\omega^6+3.058e^{15}\omega^4+2.431e^{17}\omega^2+2.673e^{17}}}$$

$$|1+C(j\omega)G(j\omega)| = \left|1+\frac{5.1689e^8 k_p(P(\omega)+jQ(\omega))}{(j\omega+1.056)(j\omega+9.504)(j\omega+26.4)(j\omega+85.54)(j\omega+127.8)(j\omega+178.5)}\right|$$

$$|1+C(j\omega)G(j\omega)| = \left|\frac{5.1689e^8 k_p(P(\omega)+jQ(\omega))+(j\omega+1.056)(j\omega+9.504)(j\omega+26.4)(j\omega+85.54)(j\omega+127.8)(j\omega+178.5)}{(j\omega+1.056)(j\omega+9.504)(j\omega+26.4)(j\omega+85.54)(j\omega+127.8)(j\omega+178.5)}\right|$$

$$\begin{aligned}&|1+C(j\omega)G(j\omega)|\\&= \frac{\sqrt{[5.1689e^8 k_p P(\omega)+5.17e^8-\omega^6+6.378e^4\omega^4-8.638e^7\omega^2]^2+[5.1689e^8 k_p Q(\omega)+428.8\omega^5-3.786e^6\omega^3+5.766e^8\omega]^2}}{\sqrt{\omega^{12}+5.63e^4\omega^{10}+9.169e^8\omega^8+4.5e^{12}\omega^6+3.058e^{15}\omega^4+2.431e^{17}\omega^2+2.673e^{17}}}\end{aligned}$$

$$\frac{5.1689e^8 k_p\sqrt{P^2(\omega)+Q^2(\omega)}}{\sqrt{[5.1689e^8 k_p P(\omega)+5.17e^8-\omega^6+6.378e^4\omega^4-8.638e^7\omega^2]^2+[5.1689e^8 k_p Q(\omega)+428.8\omega^5-3.786e^6\omega^3+5.766e^8\omega]^2}} \le A$$

Finally, from condition (5), we have:

$$\left|\frac{1}{1+C(j\omega)G(j\omega)}\right|_{dB} \le B \ dB \tag{A.17}$$

$$\left|\frac{1}{1+C(j\omega)G(j\omega)}\right| = \frac{|1|}{|1+C(j\omega)G(j\omega)|}$$

$$|1+C(j\omega)G(j\omega)| = \frac{\sqrt{[5.1689e^8 k_p P(\omega)+5.17e^8-\omega^6+6.378e^4\omega^4-8.638e^7\omega^2]^2+[5.1689e^8 k_p Q(\omega)+428.8\omega^5-3.786e^6\omega^3+5.766e^8\omega]^2}}{\sqrt{\omega^{12}+5.63e^4\omega^{10}+9.169e^8\omega^8+4.5e^{12}\omega^6+3.058e^{15}\omega^4+2.431e^{17}\omega^2+2.673e^{17}}}$$

From the above, we get:

$$\frac{\sqrt{\omega^{12}+5.63e^4\omega^{10}+9.169e^8\omega^8+4.5e^{12}\omega^6+3.058e^{15}\omega^4+2.431e^{17}\omega^2+2.673e^{17}}}{\sqrt{[5.1689e^8k_pP(\omega)+5.17e^8-\omega^6+6.378e^4\omega^4-8.638e^7\omega^2]^2+[5.1689e^8k_pQ(\omega)+428.8\omega^5-3.786e^6\omega^3+5.766e^8\omega]^2}} \leq B$$
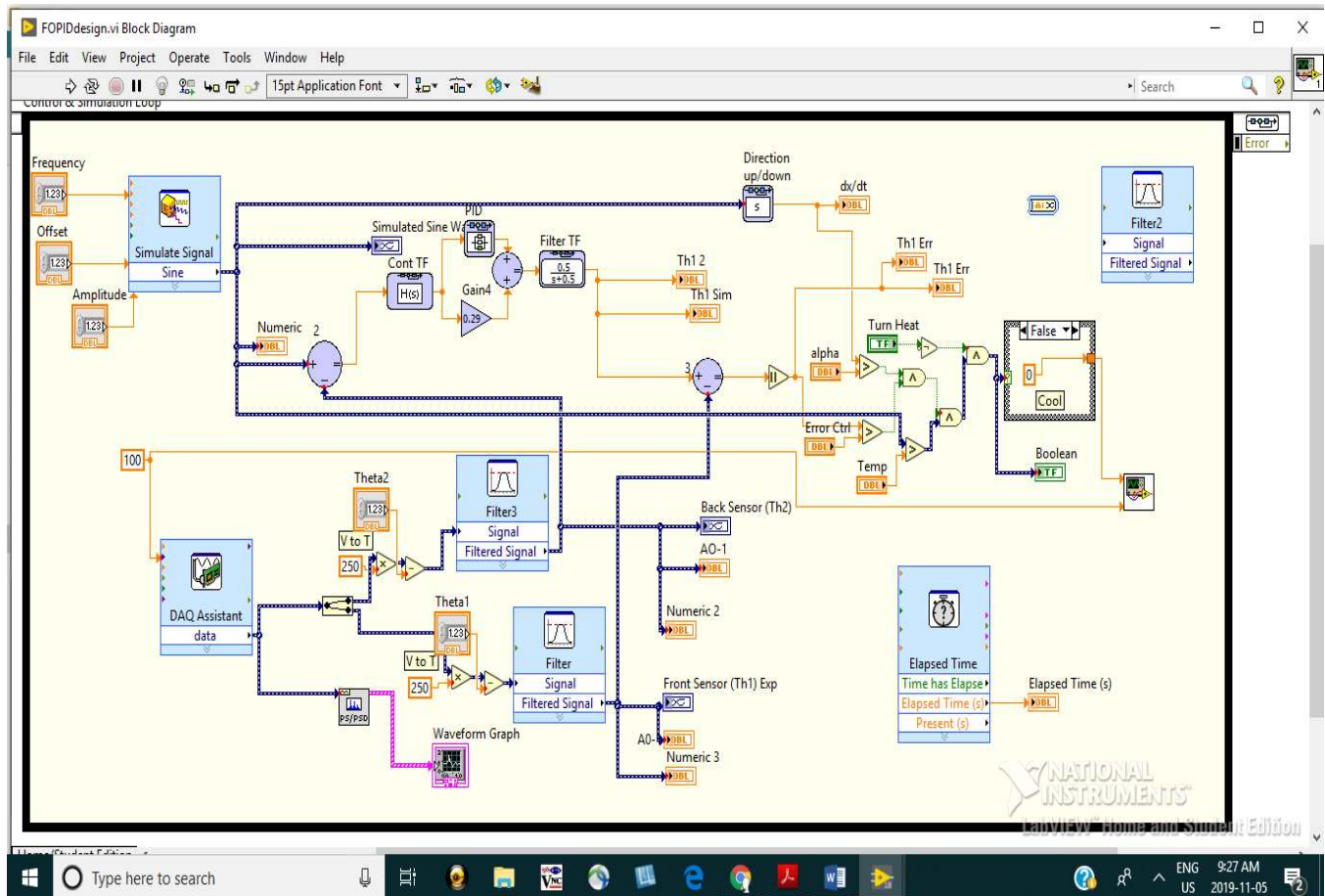
Screenshot of experimental work using Labview™

The following is the Matlab program used to obtain approximated transfer functions.

```
%This is the programme to obtained the approximated transfer
function
%This programme obtained both direct and invers transfer
function
clear all
clc
%function G1= derict()
%Transfer function
```

```matlab
%G1=Direct problem
%G2=Inverse problem
L = (0.5*25.4)/1000;
%Al Thermal properties
a1=6.9031e-5;
k1=167;
rho=2700;
cp=896;
bbb=k1/(rho*cp);
L1=L/2;
% Al Alloy 2024 T6 Thermal properties
a2=a1;%7.3-5;
L2=L/2;
k2=k1;%177;% AL Alloy 2024 T 6
%%%%%%%%%%%%%%%%%%%%%%%%%%%%%%%%%%%%%%%%%%%
b=[sqrt(a1)*k2]/[sqrt(a2)*k1];
y=[L]/([sqrt(a1)]);
x=[L]/([sqrt(a1)]);
%%%%%%%%%%%%%%%%%%%%%%%%%%%%%%%%%%%%%

%%%%%%%%%%%%%%s = zpk('s');
s = tf('s');
%syms s A w
%G2=A*(w/((s^2) +(w^2)));
Px1 = -[(pi/2)*(1)*(1/(x))]^2;
Px2 = -[(pi/2)*(3)*(1/(x))]^2;
Px3 = -[(pi/2)*(5)*(1/(x))]^2;
Px4 = -[(pi/2)*(9)*(1/(x))]^2;
Px5 = -[(pi/2)*(11)*(1/(x))]^2;
Px6 = -[(pi/2)*(13)*(1/(x))]^2;
Px7 = -[(pi/2)*(15)*(1/(x))]^2;
Px8 = -[(pi/2)*(17)*(1/(x))]^2;
%%%%%%%%%%%%%%%%%%%%%%%%%%%%%%%%%%%%

Py1 = -[(pi/2)*(1)*(1/(y))]^2;
%bw = ureal('bw',5,'Percentage',10)
Py11 = ureal('Py1',Py1,'Percentage',10);
Py2 = -[(pi/2)*(3)*(1/(y))]^2;
Py12 = ureal('Py2',Py2,'Percentage',10);
Py3 = -[(pi/2)*(5)*(1/(y))]^2;
Py13 = ureal('Py3',Py3,'Percentage',10);
Py4 = -[(pi/2)*(9)*(1/(y))]^2;
Py14 = ureal('Py4',Py4,'Percentage',10);
Py5 = -[(pi/2)*(11)*(1/(y))]^2;
Py15 = ureal('Py5',Py5,'Percentage',10);
Py6 = -[(pi/2)*(13)*(1/(y))]^2;
Py16 = ureal('Py6',Py6,'Percentage',10);
```

```matlab
Py7 = -[(pi/2)*(15)*(1/(y))]^2;
Py8 = -[(pi/2)*(17)*(1/(y))]^2;
%a1 = (P1*P2*P3*P4*P5*P6)/[(P1-P2)*(P1-P4)*(P1-P3)*(P1-
P5)*(P1-P6)];
%a2 = (P1*P2*P3*P4*P5*P6)/[(P2-P1)*(P2-P4)*(P2-P3)*(P2-
P5)*(P2-P6)];
%a3 = (P1*P2*P3*P4*P5*P6)/[(P3-P2)*(P3-P4)*(P3-P1)*(P3-
P5)*(P3-P6)];
%a4 = (P1*P2*P3*P4*P5*P6)/[(P4-P2)*(P4-P1)*(P4-P3)*(P4-
P5)*(P4-P6)];
%a5 = (P1*P2*P3*P4*P5*P6)/[(P5-P2)*(P5-P4)*(P5-P3)*(P5-
P1)*(P5-P6)];
%a6 = (P1*P2*P3*P4*P5*P6)/[(P6-P2)*(P6-P4)*(P6-P3)*(P6-
P5)*(P6-P1)];




%%%%%%%%%%%%%%%%%%%%%%%%%%%%%%%%%%%%%%%%%%%%%%%%%%%%%%%%%%%%
GcoshD1=[(1/2)+(b/2)]*[(Px1*Px2*Px3*Px4*Px5*Px6)/[(s-Px1)*(s-
Px2)*(s-Px3)*(s-Px4)*(s-Px5)*(s-Px6)]];
%GcoshD1=[(1/2)+(b/2)]*[(Px1*Px2)/[(s-Px1)*(s-Px2)]];

GcoshI1=[(1/2)+(b/2)]*[(Py11*Py12*Py13*Py14)/[(s-Py11)*(s-
Py12)*(s-Py13)*(s-Py14)]];
 GcoshI1=[(1/2)+(b/2)]*[(Py1*Py2*Py3*Py4)/[(s-Py1)*(s-Py2)*(s-
Py3)*(s-Py4)]];

%%%%%%%%%%%%%%%%%%%%%%%%%%%%%%%%%%%%%%%%%%%%%%%%%%%%%%%%%%%%%%%%
Gdirect=(GcoshD1);%+(GcoshD2);%+(Gcosh2+Gcosh22)
Ginverse=(1)/(GcoshI1);% + GcoshI2);
Gopen=[Ginverse]*[Gdirect];
Gopenr = minreal(Gopen);
%[z,p,k] = tf2zpk(Gdirect)
%w = logspace(-0.0001,10,100);
%w = linspace(0.1,100*pi,1000);
%opt = bodeoptions;
%opt.PhaseMatching = 'on';
%bode(Gdirect);
%%%%Gopen.NominalValue
%%%%get(Gopen)
%%%%Gopen.Uncertainty
%margin (Gopen);
%step(Gopen);
%hold on
%Gc=1;
%GG=Gc*Gopen/(1+Gc*Gopen);
```

```matlab
%step(GG);
%hold on
%step (Gdirect);
%grid on
%GGG=((1/22805)*s^2 +(306.2/22805)*s+1)

%pole(Gopenr);
```

The following are the two functions used for Matlab optimization tools

```matlab
function f = omar(x)
%KK=22804.74;
%Wn=sqrt(KK);
%FF=306.2;%2zetaWn
%Zeta=FF/(2*Wn);
%T1=5.5;T2=6.5;
%x(3)<=[1];
Kp=x(1);
Ki=x(2);
lam=x(3);
Kd=x(4);%x(4)=4;
mu=x(5);
%Kd=-0.5;
%x(5)=[0,1];
Wcg=0.8; %%%%(rad/sec)
Phim=(pi*(180-44.9)/180); %%%(degree)
P=1+Ki*((Wcg)^-lam)*cos(pi*lam/2)+Kd*((Wcg)^mu)*cos(pi*mu/2);
Q=-Ki*((Wcg)^-lam)*sin(pi*lam/2)+Kd*((Wcg)^mu)*sin(pi*mu/2);
aa=lam*Ki*(Wcg^(-lam-1))*sin(lam*pi/2)+mu*Kd*(Wcg^(mu-
1))*sin(mu*pi/2);
bb=-lam*Ki*(Wcg^(-lam-1))*cos(lam*pi/2)+mu*Kd*(Wcg^(mu-
1))*cos(pi*mu/2);
f =
5.1689e8*(Kp*(P^2+Q^2))/sqrt(Wcg^12+5.63e4*Wcg^10+9.169e8*Wcg^
8+...
    4.5e12*Wcg^6+3.058e15*Wcg^4+2.431e17*Wcg^2+2.673e17)-1;




function [ceq,c] = moham(x)
%KK=22804.74;
```

```matlab
%Wn=sqrt(KK);
%FF=306.2;%2zetaWn
%Zeta=FF/(2*Wn);
Kp=x(1);
Ki=x(2);
lam=x(3);
Kd=x(4);%x(4)=4;
mu=x(5);
%Kd=;
%x(5)=[0,1];
Wcg=0.8; %%%(rad/sec)
Phim=(pi*(180-44.9)/180); %%%(degree)
P=1+Ki*((Wcg)^-lam)*cos(pi*lam/2)+Kd*((Wcg)^mu)*cos(pi*mu/2);
Q=-Ki*((Wcg)^-lam)*sin(pi*lam/2)+Kd*((Wcg)^mu)*sin(pi*mu/2);
aa=lam*Ki*(Wcg^(-lam-1))*sin(lam*pi/2)+mu*Kd*(Wcg^(mu-
1))*sin(mu*pi/2);
bb=-lam*Ki*(Wcg^(-lam-1))*cos(lam*pi/2)+mu*Kd*(Wcg^(mu-
1))*cos(pi*mu/2);
ceq(1) =atan(Q/P)-
(atan(0.947*Wcg)+atan(0.1052*Wcg)+atan(0.03788*Wcg)+...

atan(0.01169*Wcg)+atan(0.007825*Wcg)+atan(0.005602*Wcg))+pi-
Phim;
ceq(2) =((P*aa-Q*bb)/(P^2+Q^2))-
((0.947/(0.897*(Wcg^2)+1))+(0.1052/(0.0011067*(Wcg^2)+1))...
    +(0.03788/(0.0014349*(Wcg^2)+1))+(0.001169/(1.3666e-
6*(Wcg^2)+1))+...
    (0.007825/(6.1231e-5*(Wcg^2)+1))+(0.005602/(3.138e-
5*(Wcg^2)+1)));
%c1eq = [ ];
c(2)
=sqrt(Wcg^12+5.63e4*Wcg^10+9.169e8*Wcg^8+4.5e12*Wcg^6+3.058e15
*Wcg^4+...
    2.431e17*Wcg^2+2.673e17)/(sqrt([5.1689e8*x(1)*P+5.17e8-
Wcg^6+6.378e4*Wcg^4-...
    8.638e7*Wcg^2]^2+[5.1689e8*x(1)*Q+5.766e8*Wcg+428.8*Wcg^5-
3.876e6*Wcg^3]^2))+20;

c(1)
=5.1689e8*x(1)*sqrt(P^2+Q^2)/(sqrt([5.1689e8*x(1)*P+5.17e8-
Wcg^6+...
    6.378e4*Wcg^4-
8.638e7*Wcg^2]^2+[5.1689e8*x(1)*Q+5.766e8*Wcg+428.8*Wcg^5-
3.876e6*Wcg^3]^2))+20;
%c2eq = [ ];
%ceq =
%c3eq = [ ];
```

```
%c = sqrt(P^2+Q^2)/sqrt([P+(1/x(1))*(1-
Wcg^2/Wn^2)]^2+[Q+2*Zeta*Wcg/x(1)*Wn]^2)+20;
%ceq = [ ];
```

The following is the Matlab function used in the Fsolve from Matlab:

```
function F = rootFOPID(x)

%KK=22804.74;
%Wn=sqrt(KK);
%FF=306.2;%2zetaWn
%Zeta=FF/(2*Wn);
%T1=5.5;T2=6.5;
Wcg=0.8; %%%(rad/sec)
Phim=(pi*(180-44.9)/180); %%%(degree)
Kp=x(1);
Ki=x(2);
lam=x(3);
Kd=x(4);%x(4)=4;
mu=x(5);
P=1+Ki*((Wcg)^-lam)*cos(pi*lam/2)+Kd*((Wcg)^mu)*cos(pi*mu/2);
Q=-Ki*((Wcg)^-lam)*sin(pi*lam/2)+Kd*((Wcg)^mu)*sin(pi*mu/2);
aa=lam*Ki*(Wcg^(-lam-1))*sin(lam*pi/2)+mu*Kd*(Wcg^(mu-
1))*sin(mu*pi/2);
bb=-lam*Ki*(Wcg^(-lam-1))*cos(lam*pi/2)+mu*Kd*(Wcg^(mu-
1))*cos(pi*mu/2);
%end
F = [((P*aa-Q*bb)/(P^2+Q^2))-
((0.947/(0.897*(Wcg^2)+1))+(0.1052/(0.0011067*(Wcg^2)+1))...
    +(0.03788/(0.0014349*(Wcg^2)+1))+(0.001169/(1.3666e-
6*(Wcg^2)+1))+...
    (0.007825/(6.1231e-5*(Wcg^2)+1))+(0.005602/(3.138e-
5*(Wcg^2)+1)));
    atan(Q/P)-
[atan(0.947*Wcg)+atan(0.1052*Wcg)+atan(0.03788*Wcg)+...
    atan(0.01169*Wcg)+atan(0.007825*Wcg)+atan(0.005602*Wcg)]-
Phim+pi;
5.1689e8*(Kp*(P^2+Q^2))/sqrt(Wcg^12+5.63e4*Wcg^10+9.169e8*Wcg^
8+...
    4.5e12*Wcg^6+3.058e15*Wcg^4+2.431e17*Wcg^2+2.673e17)-1;
     5.1689e8*Kp*sqrt(P^2+Q^2)/(sqrt([5.1689e8*Kp*P+5.17e8-
Wcg^6+...
    6.378e4*Wcg^4-
8.638e7*Wcg^2]^2+[5.1689e8*Kp*Q+5.766e8*Wcg+428.8*Wcg^5-
3.876e6*Wcg^3]^2))+0;

sqrt(Wcg^12+5.63e4*Wcg^10+9.169e8*Wcg^8+4.5e12*Wcg^6+3.058e15*
Wcg^4+...
```

```
    2.431e17*Wcg^2+2.673e17)/(sqrt([5.1689e8*Kp*P+5.17e8-
Wcg^6+6.378e4*Wcg^4-...
     8.638e7*Wcg^2]^2+[5.1689e8*Kp*Q+5.766e8*Wcg+428.8*Wcg^5-
3.876e6*Wcg^3]^2))+0];
%Feq = [ ];
```

B: Fractional Proportional Integer Integral Fractional Derivative Controller Design

The resulted transfer functions for both direct and inverse problems were obtained after a Zero-Pole approximation was used for the resulted hyperbolic transfer functions are:

$$G_1 = \frac{5.169*10^8}{s^6+428.7s^5+6.337*10^4s^4+3.785*10^6s^3+8.63610^7s^2+5.764*10^8s+5.169*10^8} \qquad \text{(B.1)}$$

$$G_2 = \frac{s^4+122.5s^3+3450s^2+2.497*10^4s+2.267*10^4}{2.267*10^4} \qquad \text{(B.2)}$$

From the above two transfer functions, we get our plant transfer function as their product, then we simplify the results in the form of Zero-Pole transfer function we get the following:

$$G = G_2 * G_1 = \frac{22804.75}{s^2+306.2s+22804.75} \qquad \text{(B.3)}$$

$$G = \frac{\omega_n^2}{s^2+2\zeta\omega_n s+\omega_n^2} \qquad \text{(B.4)}$$

From reference [38] we get:

$$|G(j\omega)| = \frac{1}{\sqrt{(1-\frac{\omega^2}{\omega_n^2})^2+ 4\zeta^2\omega^2/\omega_n^2}} \qquad \text{(B.5)}$$

$$Arg[G(j\omega)] = - tan^{-1}\left[\frac{2\zeta\omega\omega_n}{\omega_n^2- \omega^2}\right] \qquad \text{(B.6)}$$

The fractional-order PID controller formula is:

$$C(s) = k_p[1 + \frac{k_i}{(s)^\lambda} + k_d(s)^\mu]$$ (B.7)

$$C(j\omega) = k_p\{1 + k_i\omega^{-\lambda}\left[\cos\left(\frac{\lambda\pi}{2}\right) + j\sin\left(\frac{-\lambda\pi}{2}\right)\right] + k_d\left(\omega\right)^\mu\left[\cos\left(\frac{\mu\pi}{2}\right) + j\sin\left(\frac{\mu\pi}{2}\right)\right]\}$$

For the current controller, we have $\lambda = 1$,

$$C(j\omega) = k_p\{1 + k_i\omega^{-1}\cos\left(\frac{\pi}{2}\right) + k_d(\omega)^\mu\cos\left(\frac{\mu\pi}{2}\right)$$
$$+j\left[k_i\omega^{-1}\sin\left(\frac{-\pi}{2}\right) + k_d(\omega)^\mu\sin\left(\frac{\mu\pi}{2}\right)\right]\}$$ (B.8)

$$C(j\omega) = k_p\{1 + k_d(\omega)^\mu\cos\left(\frac{\mu\pi}{2}\right) + j\left[-k_i\omega^{-1} + k_d(\omega)^\mu\sin\left(\frac{\mu\pi}{2}\right)\right]\}$$ (B.9)

Let:

$$P(\omega) = 1 + k_d(\omega)^\mu\cos\left(\frac{\mu\pi}{2}\right)$$ (B.10)

And

$$Q(\omega) = -k_i\omega^{-1} + k_d(\omega)^\mu\sin\left(\frac{\mu\pi}{2}\right)$$ (B.11)

Then

$$Arg[C(j\omega)] = \tan^{-1}\left[\frac{Q(\omega)}{P(\omega)}\right]$$ (B.12)

$$|C(j\omega)| = k_p\sqrt{P^2(\omega) + Q^2(\omega)}$$ (B.13)

The open loop transfer function is:

$$L(j\omega) = C(j\omega)\,G(j\omega)$$ (B.14)

We want to satisfy five conditions to solve for variables:

1 - Robustness:

$$\frac{d(Arg[L(j\omega)])}{d\omega}\bigg|_{\omega=\omega_{cg}} = 0$$

158

2 - Gain crossover frequency:

$$|L(j\omega)|_{dB} = 0$$

3 - Phase Margin:

$$Arg[L(j\omega)]|_{\omega=\omega_{cg}} = -\pi + \varphi_m$$

4 - Noise rejection:

$$\left|T(j\omega) = \frac{C(j\omega)G(j\omega)}{1 + C(j\omega)G(j\omega)}\right|_{dB} \leq A\ dB$$

Where A is a designed value.

5 - Disturbance rejection:

$$\left|S(j\omega) = \frac{1}{1+C(j\omega)G(j\omega)}\right|_{dB} \leq B\ dB$$

Where B is a designed value.

According to condition (2) we get:

$$\frac{k_p\sqrt{P^2(\omega)+Q^2(\omega)}}{\sqrt{(1-\frac{\omega^2}{\omega_n^2})^2 + 4\zeta^2\omega^2/\omega_n^2}} = 1 \tag{B.15}$$

From condition (3) we get:

$$Arg[L(j\omega)]|_{\omega=\omega_{cg}} = -\pi + \varphi_m \tag{B.16}$$

$$tan^{-1}\left[\frac{Q(\omega)}{P(\omega)}\right] - tan^{-1}\left[\frac{2\zeta\omega\omega_n}{\omega_n^2- \omega^2}\right] = -\pi + \varphi_m \tag{B.17}$$

From condition (1) we get:

$$\frac{d(Arg[L(j\omega)]}{d\omega}\bigg|_{\omega=\omega_{cg}} = 0$$

$$Arg[L(j\omega)]|_{\omega=\omega_{cg}} = tan^{-1}\left[\frac{Q(\omega)}{P(\omega)}\right] - tan^{-1}\left[\frac{2\zeta\omega/\omega_n}{\omega_n^2- \omega^2}\right] \tag{B.18}$$

To get the derivative of

$$\frac{d\left(tan^{-1}\left[\frac{2\zeta\omega\omega_n}{\omega_n^2 - \omega^2}\right]\right)}{d\omega}$$

We assume:

$$y_1 = \ tan^{-1}\left[\frac{2\zeta\omega\omega_n}{\omega_n^2 - \omega^2}\right]$$

Then

$$\tan y_1 = \ \frac{2\zeta\omega\omega_n}{\omega_n^2 - \omega^2}$$

From it we find

$$\frac{d}{d\omega}[\tan y_1] = \frac{2\zeta(\omega_n^2 - \omega^2)\omega_n + 4\zeta\omega^2\omega_n}{(\omega_n^2 - \omega^2)^2}$$

Which is

$$\frac{1}{cos^2 y_1}\frac{dy_1}{d\omega} = \frac{2\zeta(\omega_n^2 - \omega^2)\omega_n + 4\zeta\omega^2\omega_n}{(\omega_n^2 - \omega^2)^2}$$

Then

$$\frac{dy_1}{d\omega} = \frac{2\zeta(\omega_n^2 - \omega^2)\omega_n + 4\zeta\omega^2\omega_n}{(\omega_n^2 - \omega^2)^2} \frac{cos^2 y_1}{cos^2 y_1 + sin^2 y_1}$$

And

$$\frac{dy_1}{d\omega} = \frac{2\zeta(\omega_n^2 - \omega_{cg}^2)\omega_n + 4\zeta\omega_{cg}^2\omega_n}{(\omega_n^2 - \omega_{cg}^2)^2} \frac{1}{[1 + (\frac{2\zeta\omega_{cg}\omega_n}{\omega_n^2 - \omega_{cg}^2})^2]}$$

Simplifying we get:

$$\frac{dy_1}{d\omega} = \frac{2\zeta\omega_n(\omega_n^2 - \omega_{cg}^2) + 4\zeta\omega_n\omega_{cg}^2}{(\omega_n^2 - \omega_{cg}^2)^2 + (2\zeta\omega_n\omega_{cg})^2}$$

To get the

$$\frac{d\left(tan^{-1}\left[\frac{Q(\omega)}{P(\omega)}\right]\right)}{d\omega}$$

We assume:

$$y_2 = \ tan^{-1}\left[\frac{Q(\omega)}{P(\omega)}\right]$$

Then

$$\tan y_2 = \frac{Q(\omega)}{P(\omega)}$$

$$\frac{1}{\cos^2 y_2}\frac{dy_2}{d\omega} = \frac{P(\omega)*aa - Q(\omega)*pp}{P(\omega)^2}$$

Where:

$$bb = \frac{dP}{d\omega} = \mu k_d(\omega)^{\mu-1}\cos\left(\frac{\mu\pi}{2}\right)$$

And

$$aa = \frac{dQ}{d\omega} = k_i\omega^{-2} + \mu k_d(\omega)^{\mu-1}\sin\left(\frac{\mu\pi}{2}\right)$$

$$\frac{dy_2}{d\omega} = \frac{P(\omega)*aa - Q(\omega)*pp}{P(\omega)^2}\frac{\cos^2 y_2}{\cos^2 y_2 + \sin^2 y_2}$$

$$\frac{dy_2}{d\omega} = \frac{P(\omega)*aa - Q(\omega)*pp}{P(\omega)^2}\frac{P(\omega)^2}{P(\omega)^2 + Q(\omega)^2}$$

$$\frac{dy_2}{d\omega} = \frac{P(\omega)*aa - Q(\omega)*pp}{P(\omega)^2 + Q(\omega)^2}$$

$$\frac{d(Arg[L(j\omega)])}{d\omega}\bigg|_{\omega=\omega_{cg}} = \frac{dy_2}{d\omega} - \frac{dy_1}{d\omega}$$

$$\frac{P(\omega)*aa - Q(\omega)*pp}{P(\omega)^2 + Q(\omega)^2} - \frac{2\zeta\omega_n(\omega_n^2 - \omega_{cg}^2) + 4\zeta\omega_n\omega_{cg}^2}{(\omega_n^2 - \omega_{cg}^2)^2 + (2\zeta\omega_n\omega_{cg})^2} = 0 \qquad (B.19)$$

From condition (4) we get:

$$\left|\frac{C(j\omega)G(j\omega)}{1 + C(j\omega)G(j\omega)}\right| \leq A\, dB_{dB}$$

$$\left|\frac{C(j\omega)G(j\omega)}{1+C(j\omega)G(j\omega)}\right| = \frac{|C(j\omega)G(j\omega)|}{|1+C(j\omega)G(j\omega)|} \qquad (B.20)$$

We have:

$$|C(j\omega)G(j\omega)| = \frac{k_p\sqrt{P^2(\omega) + Q^2(\omega)}}{\sqrt{(1-\frac{\omega^2}{\omega_n^2})^2 + 4\zeta^2\omega^2/\omega_n^2}}$$

161

And

$$|1 + C(j\omega)G(j\omega)| = \left|1 + Kp\{P(\omega) + jQ(\omega)\} * \frac{1}{1 - \frac{\omega^2}{\omega_n^2} + j2\zeta\frac{\omega}{\omega_n}}\right|$$

$$|1 + C(j\omega)G(j\omega)| = \frac{\left|1 - \frac{\omega^2}{\omega_n^2} + j2\zeta\frac{\omega}{\omega_n} + Kp\{P(\omega) + jQ(\omega)\}\right|}{\left|1 - \frac{\omega^2}{\omega_n^2} + j2\zeta\frac{\omega}{\omega_n}\right|}$$

$$|1 + C(j\omega)G(j\omega)| = K_p \frac{\sqrt{[\frac{(1 - \frac{\omega^2}{\omega_n^2})^2}{K_p} + P(w)]^2 + [Q(w) + 2\zeta\frac{\omega}{\omega_n K_p}]^2}}{\sqrt{(1 - \frac{\omega^2}{\omega_n^2})^2 + 4\zeta^2\omega^2/\omega_n^2}}$$

Then Equation B.20 becomes:

$$\frac{|C(j\omega)G(j\omega)|}{|1+C(j\omega)G(j\omega)|} = \frac{\sqrt{P^2(\omega)+Q^2(\omega)}}{\sqrt{[\frac{(1-\frac{\omega^2}{\omega_n^2})^2}{K_p}+P(w)]^2+[Q(w)+2\zeta\frac{\omega}{\omega_n K_p}]^2}} \leq A\ dB \qquad (B.21)$$

C: Fractional Proportional Derivative Controller Design

After we get the Transfer function to our plant:

$$G_1 =$$

$$\frac{5.169*10^8}{s^6+428.7s^5+6.337*10^4s^4+3.785*10^6s^3+8.63610^7s^2+5.764*10^8s+5.169*10^8} \quad (C.1)$$

$$G_2 = \frac{s^4+122.5s^3+3450s^2+2.497*10^4s+2.267*10^4}{2.267*10^4} \quad (C.2)$$

From the above two transfer functions, we get our plant transfer function as a product of both of them, then we simplify the results in the form of Zero-Pole transfer function we get the following:

$$G = G_2 * G_1 = \frac{22804.75}{s^2+306.2s+22804.75} \quad (C.3)$$

$$G = \frac{\omega_n^2}{s^2+2\zeta\omega_n s+\omega_n^2} \quad (C.4)$$

From reference [38] we get:

$$|G(j\omega)| = \frac{1}{\sqrt{(1-\frac{\omega^2}{\omega_n^2})^2+ 4\zeta^2\omega^2/\omega_n^2}} \quad (C.5)$$

And

$$Arg[G(j\omega)] = -tan^{-1}\left[\frac{2\zeta\omega\omega_n}{\omega_n^2- \omega^2}\right] \quad (C.6)$$

The fractional order PD controller formula is [44][45]:

$$C(j\omega) = k_p[1+ k_d(j\omega)^\mu] \quad (C.7)$$

$$C(j\omega) = k_p[\,1 + \, k_d(\omega)^\mu \cos\left(\frac{\mu\pi}{2}\right) + jk_d(\omega)^\mu \sin\left(\frac{\mu\pi}{2}\right)] \tag{C.8}$$

$$Arg[C(j\omega)] = tan^{-1}[\frac{\sin\left[\frac{(1-\mu)\pi}{2}\right]+k_d(\omega)^\mu}{\cos\left[\frac{(1-\mu)\pi}{2}\right]}] - \frac{(1-\mu)\pi}{2} \tag{C.9}$$

$$|C(j\omega)| = K_p \sqrt{[1 \, + K_d\omega^\mu\cos(\frac{\mu\pi}{2})]^2 + [K_d\omega^\mu\sin(\frac{\mu\pi}{2})]^2} \tag{C.10}$$

The open-loop transfer function is:

$$\text{L} \,(j\omega) = \text{C} \,(j\omega) \, \text{G} \,(j\omega) \tag{C.11}$$

We want to satisfy three conditions to solve for the controller variables:

1 - Robustness:

$$\frac{d(Arg[L(j\omega)]}{d\omega}\bigg|_{\omega=\omega_{cg}} = 0$$

2 - Gain crossover frequency:

$$|L(j\omega)|_{dB} = 0$$

3 - Phase Margin:

$$Arg[L(j\omega)]|_{\omega=\omega_{cg}} = -\pi + \, \varphi_m$$

From condition (3) we get:

$$tan^{-1}[\frac{\sin\left[\frac{(1-\mu)\pi}{2}\right]+k_d(\omega_{cg})^\mu}{\cos\left[\frac{(1-\mu)\pi}{2}\right]}] - \frac{(1-\mu)\pi}{2} - \, tan^{-1}\left[\frac{2\zeta\omega_{cg}\omega_n}{\omega_n^2-\omega_{cg}^2}\right] = -\pi + \, \varphi_m \tag{C.12}$$

From criteria (2) we get:

$$\frac{K_p \sqrt{[1 + K_d \omega_{cg}^{\mu} \cos(\frac{\mu\pi}{2})]^2 + [K_d \omega_{cg}{}^{\mu} \sin(\frac{\mu\pi}{2})]^2}}{\sqrt{(1-\frac{\omega^2}{\omega_n^2})^2 + 4\zeta^2 \omega^2/\omega_n^2}} = 1 \tag{C.13}$$

From condition (1) we get:

$$\frac{d(Arg[L(j\omega)])}{d\omega}\bigg|_{\omega=\omega_{cg}} = 0 \tag{C.14}$$

$$Arg[L(j\omega)] = tan^{-1}[\frac{\sin\left[\frac{(1-\mu)\pi}{2}\right] + k_d(\omega)^{\mu}}{\cos\left[\frac{(1-\mu)\pi}{2}\right]}] - \frac{(1-\mu)\pi}{2} - tan^{-1}\left[\frac{2\zeta\omega\omega_n}{\omega_n^2 - \omega^2}\right] \tag{C.15}$$

To get the derivative of $\dfrac{d(tan^{-1}\left[\frac{2\zeta\omega\omega_n}{\omega_n^2 - \omega^2}\right])}{d\omega}$ we assume:

$$y_1 = tan^{-1}\left[\frac{2\zeta\omega\omega_n}{\omega_n^2 - \omega^2}\right]$$

Then

$$\tan y_1 = \frac{2\zeta\omega\omega_n}{\omega_n^2 - \omega^2}$$

From it we find

$$\frac{d}{d\omega}[\tan y_1] = \frac{2\zeta(\omega_n^2 - \omega^2)\omega_n + 4\zeta\omega^2\omega_n}{(\omega_n^2 - \omega^2)^2}$$

Which is

$$\frac{1}{cos^2 y_1}\frac{dy_1}{d\omega} = \frac{2\zeta(\omega_n^2 - \omega^2)\omega_n + 4\zeta\omega^2\omega_n}{(\omega_n^2 - \omega^2)^2}$$

Then

$$\frac{dy_1}{d\omega} = \frac{2\zeta(\omega_n^2 - \omega^2)\omega_n + 4\zeta\omega^2\omega_n}{(\omega_n^2 - \omega^2)^2}\frac{cos^2 y_1}{cos^2 y_1 + sin^2 y_1}$$

And

$$\frac{dy_1}{d\omega} = \frac{2\zeta(\omega_n^2 - \omega_{cg}{}^2)\omega_n + 4\zeta\omega_{cg}{}^2\omega_n}{(\omega_n^2 - \omega_{cg}{}^2)^2}\frac{1}{[1 + (\frac{2\zeta\omega_{cg}\omega_n}{\omega_n^2 - \omega_{cg}{}^2})^2]}$$

Simplifying we get:

$$\frac{dy_1}{d\omega} = \frac{2\zeta\omega_n(\omega_n^2 - \omega_{cg}^2) + 4\zeta\omega_n\omega_{cg}^2}{(\omega_n^2 - \omega_{cg}^2)^2 + (2\zeta\omega_n\omega_{cg})^2}$$

We also get the derivative of

$$\frac{d\left(tan^{-1}\left[\frac{sin\left[\frac{(1-\mu)\pi}{2}\right]+k_d(\omega)^\mu}{cos\left[\frac{(1-\mu)\pi}{2}\right]}\right]\right)}{d\omega}$$

In the same manner:

Assume

$$y_2 = tan^{-1}\left[\frac{sin\left[\frac{(1-\mu)\pi}{2}\right]+k_d(\omega)^\mu}{cos\left[\frac{(1-\mu)\pi}{2}\right]}\right]$$

Then

$$tan\, y_2 = \left[\frac{sin\left[\frac{(1-\mu)\pi}{2}\right]+k_d(\omega)^\mu}{cos\left[\frac{(1-\mu)\pi}{2}\right]}\right]$$

From it we find

$$\frac{d}{d\omega}[tan\, y_2] = \frac{\mu k_d\omega^{\mu-1}}{cos\left[\frac{(1-\mu)\pi}{2}\right]}$$

Which is

$$\frac{1}{cos^2 y_2}\frac{dy_2}{d\omega} = \frac{\mu k_d\omega^{\mu-1}}{cos\left[\frac{(1-\mu)\pi}{2}\right]}$$

From it we get

$$\frac{dy_2}{d\omega} = \frac{\mu k_d\omega^{\mu-1}}{cos\left[\frac{(1-\mu)\pi}{2}\right]}\left[\frac{1}{1+tan^2 y_2}\right]$$

We have

$$tan^2 y_2 = \left[\frac{sin\left[\frac{(1-\mu)\pi}{2}\right]+k_d(\omega)^\mu}{cos\left[\frac{(1-\mu)\pi}{2}\right]}\right]^2$$

Which is can be rewritten as

$$tan^2 y_2 = \frac{[sin\left[\frac{(1-\mu)\pi}{2}\right]+k_d(\omega)^\mu]^2}{cos^2\left[\frac{(1-\mu)\pi}{2}\right]}$$

From the above we get

$$tan^2 y_2 + 1 = \frac{cos^2\left[\frac{(1-\mu)\pi}{2}\right] + [sin\left[\frac{(1-\mu)\pi}{2}\right] + k_d(\omega)^\mu]^2}{cos^2\left[\frac{(1-\mu)\pi}{2}\right]}$$

We use this to get

$$\frac{dy_2}{d\omega} = \frac{\mu k_d \omega^{\mu-1} cos\left[\frac{(1-\mu)\pi}{2}\right]}{cos^2\left[\frac{(1-\mu)\pi}{2}\right] + [sin\left[\frac{(1-\mu)\pi}{2}\right] + k_d(\omega)^\mu]^2}$$

Applying this obtained derivative in Equation C.14, we get:

$$\frac{\mu K_d \omega_{cg}^{\mu-1} cos\left[\frac{(1-\mu)\pi}{2}\right]}{cos^2\frac{(1-\mu)\pi}{2}+[sin\frac{(1-\mu)\pi}{2}+K_d\omega_{cg}^\mu]^2} - \frac{2\zeta\omega_n(\omega_n^2-\omega_{cg}^2)+4\zeta\omega_n\omega_{cg}^2}{(\omega_n^2-\omega_{cg}^2)^2+(2\zeta\omega_n\omega_{cg})^2} = 0 \qquad (C.16)$$

From Equation C.12, we can get a relation between K_d and μ as follows:

$$tan^{-1}[\frac{sin\left[\frac{(1-\mu)\pi}{2}\right]+k_d(\omega_{cg})^\mu}{cos\left[\frac{(1-\mu)\pi}{2}\right]}] = \frac{(1-\mu)\pi}{2} + tan^{-1}\left[\frac{2\zeta\omega_n\omega_{cg}}{\omega_n^2-\omega_{cg}^2}\right] - \pi + \varphi_m \qquad (C.17)$$

$$[\frac{sin\left[\frac{(1-\mu)\pi}{2}\right]+k_d(\omega_{cg})^\mu}{cos\left[\frac{(1-\mu)\pi}{2}\right]}] = tan\{\frac{(-\mu)\pi}{2} - \frac{\pi}{2} + tan^{-1}\left[\frac{2\zeta\omega_{cg}\omega_n}{\omega_n^2-\omega_{cg}^2}\right] + \varphi_m\} \qquad (C.18)$$

$$K_d = \frac{1}{\omega_{cg}^\mu}tan\left\{\frac{(-\mu)\pi}{2} - \frac{\pi}{2} + tan^{-1}\left[\frac{2\zeta\omega_{cg}\omega_n}{\omega_n^2-\omega_{cg}^2}\right] + \varphi_m\right\}cos\left[\frac{(1-\mu)\pi}{2}\right] - \frac{1}{\omega_{cg}^\mu}sin\left[\frac{(1-\mu)\pi}{2}\right] \qquad (C.19)$$

From Equation C.16, we can get a relation between K_d and μ as follows:

$$\frac{\mu K_d \omega_{cg}^{\mu-1} \cos\left[\frac{(1-\mu)\pi}{2}\right]}{\cos^2\frac{(1-\mu)\pi}{2} + sin^2\left[\frac{(1-\mu)\pi}{2}\right] + k_d^2 \omega_{cg}^{2\mu} + 2k_d \omega_{cg}^{\mu} \sin\left[\frac{(1-\mu)\pi}{2}\right]} -$$

$$\frac{2\zeta\omega_n(\omega_n^2 - \omega_{cg}{}^2) + 4\zeta\omega_n\omega_{cg}{}^2}{(\omega_n^2 - \omega_{cg}{}^2)^2 + (2\zeta\omega_n\omega_{cg})^2} = 0 \qquad\qquad \text{(C.20)}$$

$$\frac{\mu K_d \omega_{cg}^{\mu-1} \cos\left[\frac{(1-\mu)\pi}{2}\right]}{1 + k_d^2 \omega_{cg}^{2\mu} + 2k_d \omega_{cg}^{\mu} \sin\left[\frac{(1-\mu)\pi}{2}\right]} = \frac{2\zeta\omega_n(\omega_n^2 - \omega_{cg}{}^2) + 4\zeta\omega_n\omega_{cg}{}^2}{(\omega_n^2 - \omega_{cg}{}^2)^2 + (2\zeta\omega_n\omega_{cg})^2} \qquad \text{(C.21)}$$

Assume

$$A = \frac{2\zeta\omega_n(\omega_n^2 - \omega_{cg}{}^2) + 4\zeta\omega_n\omega_{cg}{}^2}{(\omega_n^2 - \omega_{cg}{}^2)^2 + (2\zeta\omega_n\omega_{cg})^2}$$

Then Equation C.21 becomes as follows:

$$\mu K_d \omega_{cg}^{\mu-1} \cos\left[\frac{(1-\mu)\pi}{2}\right] = A\{1 + k_d^2 \omega_{cg}^{2\mu} + 2k_d \omega_{cg}^{\mu} \sin\left[\frac{(1-\mu)\pi}{2}\right]\} \qquad \text{(C.22)}$$

Assume

$$B = 2A\omega_{cg}^{\mu} \sin\left[\frac{(1-\mu)\pi}{2}\right] - \mu\omega_{cg}^{\mu-1} \cos\left[\frac{(1-\mu)\pi}{2}\right]$$

Then Equation C.22 becomes as follows:

$$Ak_d^2\omega_{cg}^{2\mu} + Bk_d + A = 0 \qquad\qquad \text{(C.23)}$$

From Equation C.23, we can find a relation between K_d and μ as follows:

$$K_d = \frac{-B \pm \sqrt{B^2 - 4A^2\omega_{cg}^{2\mu}}}{2A\omega_{cg}^{2\mu}} \qquad\qquad \text{(C.24)}$$

D: Fractional Proportional Integral Controller Design

After we get the Transfer function to our plant:

$$G_1 = \frac{5.169 * 10^8}{s^6 + 428.7s^5 + 6.337 * 10^4 s^4 + 3.785 * 10^6 s^3 + 8.63610^7 s^2 + 5.764 * 10^8 s + 5.169 * 10^8} \tag{D.1}$$

$$G_2 = \frac{s^4 + 122.5s^3 + 3450s^2 + 2.497 * 10^4 s + 2.267 * 10^4}{2.267 * 10^4} \tag{D.2}$$

From the above two transfer functions, we get the plant transfer function as their product, then we simplify the results in the form of Zero-Pole transfer function we get the following:

$$G = G_2 * G_1 = \frac{22804.75}{s^2 + 306.2s + 22804.75} \tag{D.3}$$

$$G = \frac{\omega_n^2}{s^2 + 2\zeta\omega_n s + \omega_n^2} \tag{D.4}$$

From reference [38] we get:

$$|G(j\omega)| = \frac{1}{\sqrt{(1 - \frac{\omega^2}{\omega_n^2})^2 + 4\zeta^2\omega^2/\omega_n^2}} \tag{D.5}$$

And

$$Arg[G(j\omega)] = -tan^{-1}\left[\frac{2\zeta\omega\omega_n}{\omega_n^2 - \omega^2}\right] \tag{D.6}$$

The fractional-order PI controller formula is:

169

$$C(j\omega) = k_p[1 + k_I(j\omega)^{-\lambda}] \tag{D.7}$$

$$C(j\omega) = k_p[1 + k_I(\omega)^{-\lambda}\cos\left(\frac{\mu\pi}{2}\right) - jk_I(\omega)^{-\lambda}\sin\left(\frac{\mu\pi}{2}\right)] \tag{D.8}$$

$$Arg[C(j\omega)] = \tan^{-1}[\frac{k_I(\omega)^{-\lambda}\sin\left(\frac{\mu\pi}{2}\right)}{1 + k_I(\omega)^{-\lambda}\cos\left(\frac{\mu\pi}{2}\right)}] \tag{D.9}$$

$$|C(j\omega)| = K_p\sqrt{[1 + k_I(\omega)^{-\lambda}\cos\left(\frac{\mu\pi}{2}\right)]^2 + [k_I(\omega)^{-\lambda}\sin\left(\frac{\mu\pi}{2}\right)]^2} \tag{D.10}$$

The open-loop transfer function is:

$$L\ (j\omega) = C\ (j\omega)\ G\ (j\omega) \tag{D.11}$$

We want to satisfy three conditions to solve for the controller variables:

1 - Robustness:

$$\frac{d(Arg[L(j\omega)])}{d\omega}\bigg|_{\omega=\omega_{cg}} = 0$$

2 - Gain crossover frequency:

$$|L(j\omega)|_{dB} = 0$$

3 - Phase Margin:

$$Arg[L(j\omega)]|_{\omega=\omega_{cg}} = -\pi + \varphi_m$$

From condition (3) we get:

$$\tan^{-1}[\frac{k_I(\omega)^{-\lambda}\sin\left(\frac{\mu\pi}{2}\right)}{1 + k_I(\omega)^{-\lambda}\cos\left(\frac{\mu\pi}{2}\right)}] - \tan^{-1}\left[\frac{2\zeta\omega_{cg}\omega_n}{\omega_n^2 - \omega_{cg}^2}\right] = -\pi + \varphi_m \tag{D.12}$$

From condition (2) we get:

$$\frac{K_p\sqrt{[1 + k_I(\omega)^{-\lambda}\cos\left(\frac{\mu\pi}{2}\right)]^2 + [k_I(\omega)^{-\lambda}\sin\left(\frac{\mu\pi}{2}\right)]^2}}{\sqrt{(1 - \frac{\omega^2}{\omega_n^2})^2 + 4\zeta^2\omega^2/\omega_n^2}} = 1 \tag{D.13}$$

From condition (1) we get:

$$\frac{d(Arg[L(j\omega)]}{d\omega}\bigg|_{\omega=\omega_{cg}} = 0 \tag{D.14}$$

$$Arg[L(j\omega)] = tan^{-1}[\frac{k_I(\omega)^{-\lambda}\sin\left(\frac{\mu\pi}{2}\right)}{1+k_I(\omega)^{-\lambda}\cos\left(\frac{\mu\pi}{2}\right)}] - tan^{-1}\left[\frac{2\zeta\omega\omega_n}{\omega_n^2-\omega^2}\right] \tag{D.15}$$

To get the derivative of

$$\frac{d(tan^{-1}\left[\frac{2\zeta\omega\omega_n}{\omega_n^2-\omega^2}\right])}{d\omega}$$

We assume:

$$y_1 = tan^{-1}\left[\frac{2\zeta\omega\omega_n}{\omega_n^2-\omega^2}\right]$$

Then

$$\tan y_1 = \frac{2\zeta\omega\omega_n}{\omega_n^2-\omega^2}$$

From it we find

$$\frac{d}{d\omega}[\tan y_1] = \frac{2\zeta(\omega_n^2-\omega^2)\omega_n+4\zeta\omega^2\omega_n}{(\omega_n^2-\omega^2)^2}$$

Which is

$$\frac{1}{cos^2 y_1}\frac{dy_1}{d\omega} = \frac{2\zeta(\omega_n^2-\omega^2)\omega_n+4\zeta\omega^2\omega_n}{(\omega_n^2-\omega^2)^2}$$

Then

$$\frac{dy_1}{d\omega} = \frac{2\zeta(\omega_n^2-\omega^2)\omega_n+4\zeta\omega^2\omega_n}{(\omega_n^2-\omega^2)^2}\frac{cos^2 y_1}{cos^2 y_1+sin^2 y_1}$$

And

$$\frac{dy_1}{d\omega} = \frac{2\zeta(\omega_n^2-\omega_{cg}^2)\omega_n+4\zeta\omega_{cg}^2\omega_n}{(\omega_n^2-\omega_{cg}^2)^2}\frac{1}{[1+(\frac{2\zeta\omega_{cg}\omega_n}{\omega_n^2-\omega_{cg}^2})^2]}$$

Simplify, we get:

$$\frac{dy_1}{d\omega} = \frac{2\zeta\omega_n(\omega_n^2 - \omega_{cg}^2) + 4\zeta\omega_n\omega_{cg}^2}{(\omega_n^2 - \omega_{cg}^2)^2 + (2\zeta\omega_n\omega_{cg})^2}$$

We also get the derivative of

$$\frac{d(tan^{-1}[\frac{k_I(\omega)^{-\lambda}\sin(\frac{\mu\pi}{2})}{1+k_I(\omega)^{-\lambda}\cos(\frac{\mu\pi}{2})}])}{d\omega}$$

In the same manner:

Assume

$$y_2 = tan^{-1}[\frac{k_I(\omega)^{-\lambda}\sin(\frac{\mu\pi}{2})}{1+k_I(\omega)^{-\lambda}\cos(\frac{\mu\pi}{2})}]$$

Then

$$\tan y_2 = \left[\frac{k_I(\omega)^{-\lambda}\sin(\frac{\mu\pi}{2})}{1+k_I(\omega)^{-\lambda}\cos(\frac{\mu\pi}{2})}\right]$$

From it we find

$$\frac{d}{d\omega}[\tan y_2] = [\frac{[1+k_I(\omega)^{-\lambda}\cos(\frac{\lambda\pi}{2})][-\lambda k_I(\omega)^{(-\lambda-1)}\cos(\frac{\lambda\pi}{2})]-[k_I(\omega)^{-\lambda}\sin(\frac{\lambda\pi}{2})(\lambda k_I(\omega)^{(-\lambda-1)}\sin(\frac{\lambda\pi}{2})]}{[1+k_I(\omega)^{-\lambda}\cos(\frac{\lambda\pi}{2})]^2}]$$

Which is

$$\frac{1}{\cos^2 y_2}\frac{dy_2}{d\omega} = \frac{[-\lambda k_I(\omega)^{(-\lambda-1)}\cos(\frac{\lambda\pi}{2})]-[\lambda k_I^2(\omega)^{-2\lambda-1}][\sin^2(\frac{\lambda\pi}{2})+\cos^2(\frac{\lambda\pi}{2})]}{[1+k_I(\omega)^{-\lambda}\cos(\frac{\lambda\pi}{2})]^2}$$

From it we get

$$\frac{dy_2}{d\omega} = \frac{[-\lambda k_I(\omega)^{(-\lambda-1)}\cos(\frac{\lambda\pi}{2})]-[\lambda k_I^2(\omega)^{-2\lambda-1}]}{[1+k_I(\omega)^{-\lambda}\cos(\frac{\lambda\pi}{2})]^2}[\frac{1}{1+tan^2 y_2}]$$

We have

$$tan^2 y_2 = [\frac{k_I(\omega)^{-\lambda}\sin(\frac{\mu\pi}{2})}{1+k_I(\omega)^{-\lambda}\cos(\frac{\mu\pi}{2})}]^2$$

From the above we get

$$tan^2 y_2 + 1 = \frac{[1 + k_I(\omega)^{-\lambda} \cos\left(\frac{\mu\pi}{2}\right)]^2 + [k_I(\omega)^{-\lambda} \sin\left(\frac{\mu\pi}{2}\right)]^2}{[1 + k_I(\omega)^{-\lambda} \cos\left(\frac{\mu\pi}{2}\right)]^2}$$

We use this to get

$$\frac{dy_2}{d\omega} = \frac{[-\lambda k_I(\omega)^{(-\lambda-1)} \cos\left(\frac{\lambda\pi}{2}\right)] - [\lambda k_I^2(\omega)^{-2\lambda-1}]}{[1 + k_I(\omega)^{-\lambda} \cos\left(\frac{\mu\pi}{2}\right)]^2 + [k_I(\omega)^{-\lambda} \sin\left(\frac{\mu\pi}{2}\right)]^2}$$

Apply these obtained derivatives in Equation D.14, we get:

$$\frac{[-\lambda k_I(\omega)^{(-\lambda-1)} \cos\left(\frac{\lambda\pi}{2}\right)] - [\lambda k_I^2(\omega)^{-2\lambda-1}]}{[1 + k_I(\omega)^{-\lambda} \cos\left(\frac{\mu\pi}{2}\right)]^2 + [k_I(\omega)^{-\lambda} \sin\left(\frac{\mu\pi}{2}\right)]^2} - \frac{2\zeta\omega_n(\omega_n^2 - \omega_{cg}^2) + 4\zeta\omega_n\omega_{cg}^2}{(\omega_n^2 - \omega_{cg}^2)^2 + (2\zeta\omega_n\omega_{cg})^2} = 0 \qquad (D.16)$$

From Equation D.12, we can get a relation between K_I and λ as follows:

$$tan^{-1}\left[\frac{k_I(\omega_{cg})^{-\lambda} \sin\left(\frac{\mu\pi}{2}\right)}{1 + k_I(\omega_{cg})^{-\lambda} \cos\left(\frac{\mu\pi}{2}\right)}\right] = tan^{-1}\left[\frac{2\zeta\omega_n\omega_{cg}}{\omega_n^2 - \omega_{cg}^2}\right] - \pi + \varphi_m \qquad (D.17)$$

$$\left[\frac{k_I(\omega_{cg})^{-\lambda} \sin\left(\frac{\mu\pi}{2}\right)}{1 + k_I(\omega_{cg})^{-\lambda} \cos\left(\frac{\mu\pi}{2}\right)}\right] = tan\left\{-\pi + tan^{-1}\left[\frac{2\zeta\omega_{cg}\omega_n}{\omega_n^2 - \omega_{cg}^2}\right] + \varphi_m\right\} \qquad (D.18)$$

$$k_I(\omega_{cg})^{-\lambda} \sin\left(\frac{\mu\pi}{2}\right) = tan\left\{-\pi + tan^{-1}\left[\frac{2\zeta\omega_{cg}\omega_n}{\omega_n^2 - \omega_{cg}^2}\right] + \varphi_m\right\}[1 +$$
$$k_I(\omega_{cg})^{-\lambda} \cos\left(\frac{\mu\pi}{2}\right)] \qquad (D.19)$$

$$K_I = \frac{tan\left\{-\pi + tan^{-1}\left[\frac{2\zeta\omega_{cg}\omega_n}{\omega_n^2 - \omega_{cg}^2}\right] + \varphi_m\right\}}{-(\omega_{cg})^{-\lambda} \cos\left(\frac{\mu\pi}{2}\right) tan\left\{-\pi + tan^{-1}\left[\frac{2\zeta\omega_{cg}\omega_n}{\omega_n^2 - \omega_{cg}^2}\right] + \varphi_m\right\} + (\omega_{cg})^{-\lambda} \sin\left(\frac{\mu\pi}{2}\right)} \qquad (D.20)$$

From Equation D.16, we can get a relation between K_I and λ as follows:

$$\frac{[-\lambda k_I(\omega_{cg})^{(-\lambda-1)} \cos\left(\frac{\lambda\pi}{2}\right)] - [\lambda k_I^2(\omega_{cg})^{-2\lambda-1}]}{[1 + k_I(\omega_{cg})^{-\lambda} \cos\left(\frac{\mu\pi}{2}\right)]^2 + [k_I(\omega_{cg})^{-\lambda} \sin\left(\frac{\mu\pi}{2}\right)]^2} - \frac{2\zeta\omega_n(\omega_n^2 - \omega_{cg}^2) + 4\zeta\omega_n\omega_{cg}^2}{(\omega_n^2 - \omega_{cg}^2)^2 + (2\zeta\omega_n\omega_{cg})^2} = 0 \qquad (D.21)$$

$$\frac{[-\lambda k_I(\omega_{cg})^{(-\lambda-1)}\cos\left(\frac{\lambda\pi}{2}\right)]-[\lambda k_I^2(\omega_{cg})^{-2\lambda-1}]}{1+k_I^2\omega_{cg}^{-2\lambda}+2k_I\omega_{cg}^{-\lambda}\cos[\frac{\lambda\pi}{2}]} = \frac{2\zeta\omega_n(\omega_n^2-\omega_{cg}{}^2)+4\zeta\omega_n\omega_{cg}{}^2}{(\omega_n^2-\omega_{cg}{}^2)^2+(2\zeta\omega_n\omega_{cg})^2} \qquad \text{(D.22)}$$

Assume

$$A = \frac{2\zeta\omega_n(\omega_n^2-\omega_{cg}{}^2)+4\zeta\omega_n\omega_{cg}{}^2}{(\omega_n^2-\omega_{cg}{}^2)^2+(2\zeta\omega_n\omega_{cg})^2}$$

Then Equation D.22 becomes as follows:

$$[-\lambda k_I(\omega_{cg})^{(-\lambda-1)}\cos\left(\frac{\lambda\pi}{2}\right)] - [\lambda k_I^2(\omega_{cg})^{-2\lambda-1}] = A\{1 + k_I^2\omega_{cg}^{-2\lambda} + 2k_I\omega_{cg}^{-\lambda}\cos[\frac{\lambda\pi}{2}]\} \quad \text{(D.23)}$$

Assume

$$B = 2A\omega_{cg}^{-\lambda}\cos\left[\frac{\lambda\pi}{2}\right]+\lambda\omega_{cg}^{-\lambda-1}\cos\left[\frac{\lambda\pi}{2}\right]$$

Then Equation D.23 becomes as follows:

$$k_d^2[A\omega_{cg}^{2\mu} + \lambda(\omega_{cg})^{-2\lambda-1}] + Bk_d + A = 0 \qquad \text{(D.24)}$$

From Equation D.24, we can find the relation between K_I and λ as follows:

$$K_I = \frac{-B \pm \sqrt{B^2-4A[A\omega_{cg}^{-2\lambda}+\lambda(\omega_{cg})^{-2\lambda-1}]}}{2[A\omega_{cg}^{-2\lambda}+\lambda(\omega_{cg})^{-2\lambda-1}]} \qquad \text{(D.25)}$$

Publications

[1]   D. Necsulescu, B. Jarrah, and J. Sasiadek, "Closed - Loop control of plate temperature using inverse problem," in ICINCO 2016 - Proceedings of the 13th International Conference on Informatics in Control, Automation and Robotics, 2016, vol. 1, pp. 421–425.

[2]   D. Necsulescu and B. Jarrah, "Real-time temperature control of thin plates," in International Conference of Control, Dynamic Systems, and Robotics, 2016.

[3]   D. S. Necsulescu and B. A. Jarrah, "Real-Time Temperature Control of a One Dimensional Metal Plate," in Proceedings - 2017 21st International Conference on Control Systems and Computer, CSCS 2017, 2017, pp. 5–12.

[4]   D. S. Necsulescu, B. A. Jarrah, and J. Z. Sasiadek, "Experimental verification for closed loop control of thin plate surface temperature," in 2018 IEEE International Conference on Automation, Quality and Testing, Robotics, AQTR 2018 - THETA 21st Edition, Proceedings, 2018, pp. 1–6.

[5]   D. S. Necsulescu, B. A. Jarrah, and J. Z. Sasiadek, "Fractional controller for thin plate surface temperature control," in ICINCO 2019 - Proceedings of the 16th International Conference on Informatics in Control, Automation and Robotics, 2019, vol. 1, pp. 641–647.